# Subunit Organisation and Assembly of the 2-Oxoglutarate Dehydrogenase Multienzyme Complex (OGDC)

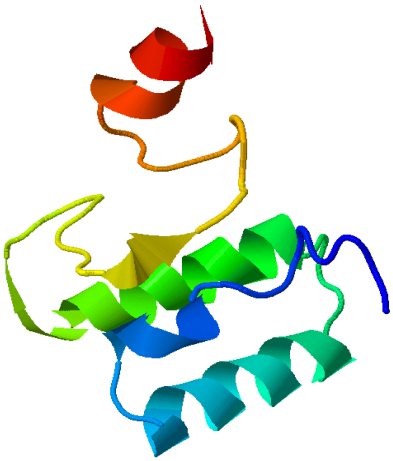


**ADEL IBRAHIM AHMAD AL-ALAWY**

*College of Medical, Veterinary and Life Sciences*
*University of Glasgow*


June 2013

A thesis submitted for award of the degree of
*Doctor of Philosophy*

*This thesis is dedicated to my parents*

*For their endless love, support & encouragement*

# Abstract

The family of mammalian 2-oxoacid dehydrogenase complexes (PDC, BCOADC and OGDC) are stable, high $M_r$ assemblies composed of multiple copies of 3 separate enzymes (E1, E2 and E3) that catalyse key stages in carbohydrate and amino acid metabolism. Their respective E1 and E2 enzymes are complex-specific while E3 is the identical gene product in all 3 complexes.

In general terms, the oligomeric E2 'cores' provide the structural and mechanistic framework to which their partner E1 and E3 enzymes are tethered tightly but non-covalently. However, the mode of E1 and E3 binding differs significantly from complex to complex. In the BCOADC, its cubic E2 core is composed of 24 identical subunits to which E1b and E3 bind stably in a mutually-exclusive fashion via multiple subunit binding domains (SBDs). In a variation of this theme, the icosahedral (60-meric) E2-PDC core comprises 2 types of subunit, E2 and an E2-related polypeptide, E3 binding protein (E3BP). In this case, E1p and E3 bind independently to specific SBDs located on E2 and E3BP, respectively. In contrast, OGDC differs significantly from its counterparts as its 24-meric E2 core does not contain any apparent SBDs. In addition, there is no equivalent to E3BP in this complex. Hence, how stable complex formation is achieved for the OGDC is still an area of active research, particularly in view of increasing evidence implicating OGDC deficiency as a major causative factor in a variety of neurodegenerative and oxidative stress disorders.

Previous subunit-specific proteolysis, enzymatic and immunological studies on native bovine OGDC in our laboratory have suggested that an intact E1o N-terminal region is vital for maintaining the structural integrity of the complex. In particular, a single cleavage of E1o at

Arg77 results in complete loss of OGDC function stemming from dissociation of both E3 and a large, active E1o species (E1') from the native E2 core assembly.

The principal aim of this thesis was to establish the location and precise nature of the domains responsible for protein-protein interactions between the constituent E1o, E2o and E3 enzymes of OGDC and their roles in assembly, taking into account our previous data and the unique domain organisation of E2. It was also a goal to produce a recombinant version of the human OGDC for future biomedical studies including genetic analysis of naturally-occurring mutant forms.

Initially, the cloning, expression and purification of a series of E1o N-terminal constructs (His-tag, GST or MBP fusion proteins: 60, 90 and 153 a.a.s in length) is described extending from Ser1 to Phe153 of mature human E1o. Access to 10-30 mg of highly-purified E1o N-terminal peptides was required to enable testing of the ability of this region to interact with E3 (and also E2) employing a range of biochemical and biophysical techniques. High-level expression of full-length E1o was also achieved; however, attempts to produce active E1o in soluble form proved unsuccessful. Recombinant human E2o and E3 were both produced as soluble active enzymes in high yield.

A preliminary structural characterisation of the E1o N-terminal region was also undertaken employing synthetic peptides, circular dichroism and a basic bio-informatics approach. These studies demonstrated that the N-terminal region had the potential to form 2 short α-helical segments linked by regions of unstructured and flexible polypeptide chain. Moreover, a 3D-structural prediction for mature, full-length human E1o confirmed that its N-termini were highly accessible, extending above the enzyme surface and situated in close proximity at one end

of the homodimer. Although there was no apparent sequence homology, our data also suggested that this region had several of the main structural features of the E3-SBD located on E3BP.

Direct evidence that the N-terminal region of E1 bound to E3 post-translationally was obtained using peptide array technology, alanine scanning, isothermal titration calorimetry (ITC), affinity chromatography and gel filtration (GFC). Interaction of E1o N-terminal peptides with E3 was salt-sensitive and reduced over the range 0-0.5M NaCl, i.e. similar to that required to promote E3 dissociation from intact OGDC. Only the longer E1o-90 and E1o-153 constructs complexed with E3 and evidence suggested that steric hindrance by the fusion partner blocked E3 binding to the short E1o-60 GST fragment.

As expected, in the absence of any obvious SBD on E2o, no direct interaction could be detected between E2o and E3 using ITC or GFC. In addition, no post-translation association occurred between our purified E1o constructs and fully-assembled, oligomeric E2o. In contrast, co-expression of E1o-90 and E1o-153 constructs with E2o (but not E1o-60) resulted in the formation of an E1o-90/E2o GST or E1o-153/E2o GST sub-complex. Moreover, these N-terminal E1o/E2o sub-complexes supported stable E3 binding as judged by affinity chromatography and GFC. Taken together, the data presented in this thesis have established that the E1o N-terminal region is pivotal for mediating formation of a stable multi-enzyme assembly by directing self-integration with the E2o core during or immediately after synthesis and subsequently promoting high-affinity E3 binding in a manner reminiscent of E3BP integration with the oligomeric E2-PDC core.

To test the functional importance of the putative E3-binding domain on E1o, the E1o constructs were employed as inhibitors of OGDC and PDC activity since it was anticipated that they should displace E3 from its normal binding site in the intact complexes. Incubation of OGDC or PDC with the E1o-90 and E1o-153 (but not E1o-60) constructs caused preferential inhibition of OGDC activity. Conversely, an E3BP-SBD construct was a more effective inhibitor of PDC suggesting that the mode of E3 interaction differs significantly in these 2 complexes.

In summary, our data have provided (a) new insights into the structure, organisation and mode of assembly of the mammalian OGDC; (b) suggested new approaches to producing a recombinant model OGDC as an important biological tool for future biomedical and genetic studies and (c) raised new questions concerning the subunit composition, architecture, and stoichiometry of its core assembly.

# Table of Contents

# List of Tables

**Chapter 1**



**Chapter 2**



**Chapter 3**



**Chapter 4**

# List of Figures

## Chapter 1



## Chapter 3

## Chapter 4

## Chapter 5

## Chapter 6



## Chapter 7

# Acknowledgements

I would like to express my profound gratitude to my supervisor, Professor Gordon Lindsay for his wise and instructive supervision and for his excellent guidance. Without his initiative and constructive advice, this study would not have been possible. I am also thankful for his endless patience and kindness. I would like to extend my gratitude to Professor William Cushley for his unlimited support and continuous encouragement. I am also grateful to Dr. Donna McGow for her great help and support.

Special and sincere thanks to Professor Alan Cooper and Dr. Margaret Nutley for their important contributions, collaboration and, in particular, their constructive scientific comments and advice on ITC experiments. I am also grateful to Dr. Sharon Kelly for collaborating on CD experiments and for advice on the interpretation of data. Special thanks to Dr. George Baillie for providing materials needed for peptide array experiments. I also gratefully thank to Dr. Brian Smith for his support and advice.

Many thanks to my close friends: Dr. Adel Al-Khedaide and Dr. Zafer Al-Shehri for unending support. Thanks are also given to Dr. Swetha Vijayakrishnan, Dr. Zhenbo Cao and Mr. Sourav Banerjee for their help and encouragement.

Finally, I am eternally grateful to my parents, my wonderful wife, my sisters and my brother, Eng. Mohammed, for their kindness, encouragement, support and endless patience. I am also thankful to my son, Hemo, for his inspiring smile and warm heart that enabled me to go through many difficulties. I send my very special thanks to my younger brother, Ahmad, in heaven.

# Author's Declaration

I hereby declare that the work presented in this thesis is my own, except where otherwise cited or acknowledged. No part of this thesis has been presented for any other degree.

**ADEL AL-ALAWY**

June, 2013

# Abbreviations

| | |
|---|---|
| Å | Angstrom |
| $A_{260}$ | Absorbance at 260 nm |
| $A_{280}$ | Absorbance at 280 nm |
| a.a. | Amino acid |
| Ab | Antibody |
| AD | Alzheimer's disease |
| AMA | Anti-mitochondrial antibodies |
| Amp | Ampicillin |
| Approx. | Approximately |
| APS | Ammonium persulphate |
| AUC | Analytical ultracentrifugation |
| BCOADC | Branched-chain 2-oxoacid dehydrogenase complex |
| BSA | Bovine serum albumin |
| CaM | Calmodulin |
| CAT | Chloramphenicol acetyltransferase |
| CBP | Calmodulin binding peptide |
| CD | Circular dichroism |
| cDNA | complementary DNA |
| Chl | Chloramphenicol |
| CoA | Coenzyme A |

| | |
|---|---|
| CTD | C-terminal catalytic domain |
| CV | Column volume |
| DMSO | Dimethyl sulfoxide |
| DTT | Dithiothreitol |
| E1 | 2-Oxoacid dehydrogenase |
| E1o | 2-Oxoglutarate dehydrogenase |
| E1p | Pyruvate dehydrogenase |
| E2 | Dihydrolipoamide acyltransferase |
| E2o | Dihydrolipoyl succinyltransferase |
| E2p | Dihydrolipoamide acetyltransferase |
| E3 | Dihydrolipoamide dehydrogenase |
| E3BP | E3-binding protein |
| ECL | Enhanced chemiluminescence |
| EDTA | Ethylene diamine tetra-acetic acid |
| ELISA | Enzyme-linked immuneabsorbent assay |
| EtBr | Ethidium bromide |
| FAD | Flavin adenine dinucleotide |
| GABA | γ-Aminobutyric acid |
| GCS | Glycine cleavage system |
| GdmCl | Guanidinium chloride |
| GFC | Gel filtration chromatography |
| GIP | General import pore |

| | |
|---|---|
| GSH | Glutathione |
| GST | Glutathione S-transferase |
| HNE | 4-Hydroxy-2-nonenal |
| H-protein | lipoic acid-containing protein |
| HRP | Horseradish peroxidase |
| IPTG | Isopropyl-β-D-thiogalactopyranoside |
| ITC | Isothermal titration calorimetry |
| Kan | Kanamycin |
| LB | Luria Broth |
| LD | Lipoyl domain |
| L-protein | Lipoamide dehydrogenase |
| LR | Linker region |
| $\Psi$ | Membrane potential |
| MBP | Maltose binding protein |
| MC | Metal chelate chromatography |
| MES | 2-(N-morpholino) ethane sulfonic |
| MOPS | 3-(N-morpholino) propane sulfonic acid |
| MPP | Mitochondrial matrix processing peptidase |
| MS | Molecular mass spectrum |
| MSF | Mitochondrial import stimulating factor |
| MTS | Mitochondrial targeting sequence |
| MWCO | Molecular weight cutoff |

| | |
|---|---|
| *N* | Binding stoichiometry |
| OGDC | 2-Oxogluturate dehydrogenase complex |
| PBC | Primary biliary cirrhosis |
| PBS | Phosphate buffered saline |
| PDC | Pyruvate dehydrogenase complex |
| PDK | Pyruvate dehydrogenase kinase |
| PDP | Pyruvate dehydrogenase phosphatase |
| PEG | Polyethelene glycol |
| $P_i$ | Inorganic phosphate |
| PMSF | Phenyl methane sulphonyl fluoride |
| P-protein | Glycine decarboxylase |
| Protein X | E3-binding protein |
| Prxs | Peroxiredoxins |
| ROS | Reactive oxygen species |
| SANS | Small angle neutron scattering |
| SAXS | Small angle X-ray scattering |
| SBD | Subunit binding domain |
| SDS | Sodium dodecyl sulfate |
| SOC | Super optimal broth with catabolite repression |
| SOD | Superoxide dismutase |
| TAE | Tris-acetate-EDTA |
| TCA | Trichloroacetic acid |

| | |
|---|---|
| TEMED | N, N, N', N'-tetramethyl ethylene diamine |
| ThDP | Thiamine diphosphate |
| TFE | 2,2,2,Trifluoroethanol |
| TIM | Translocase of inner mitochondrial membrane |
| TOM | Translocase of the outer mitochondrial membrane |
| T-protein | Tetrahydrofolate transferase |
| Tris | 2-Amino-2-(hydroxymethyl)-1, 3-propanol |
| $V_o$ | Void volume |
| v/v | Volume to volume |
| wt | Wild-type |
| w/v | Weight to volume |
| w/w | Weight to weight |

# Chapter 1

# Introduction to the 2-oxoacid dehydrogenase multienzyme complexes

## 1.1 The multienzyme complexes

Most metabolic pathways depend on adjacent enzymes to catalyze their individual reaction steps in a defined sequence. In many cases those enzymes associate and organize themselves into active complexes in which the individual enzymes can be linked covalently or noncovalently to increase the efficiency of the metabolic pathway. In particular, ordered arrays of enzymes can improve catalytic efficiency and protect unstable intermediates by direct transfer of metabolites or substrates from one enzyme to the next within the complexes without releasing metabolites into the bulk medium of the cell, thereby reducing diffusion time and increasing binding probability to the next enzyme. This mechanism, also termed 'substrate channeling', is a major topic in molecular biology (Easterby 1989; Perham 1991; Huang *et al.* 2001).

One of the primary examples of stable multienzyme complexes is the family of 2-oxoacid (alpha-keto acid) dehydrogenase complexes, which are large multimeric assemblies located in the mitochondrial matrix (Smith and Neidhardt 1983). These macromolecular ($M_r$ 4-10x$10^6$) structures serve as paradigms for understanding protein structure-function relationships, the biological significance of protein assemblies, molecular recognition phenomena and protein-protein interactions (Reed 1974). In addition, the 2-oxoacid dehydrogenase complexes are

amongst the largest and most complicated multienzyme complexes known at present and play a key regulatory role in carbohydrate and amino acid utilization (Yeaman 1986).

The 2-oxoacid dehydrogenase multienzyme complexes are fundamental to the energy providing mechanisms of cells in all aerobic organisms. As such they are distributed ubiquitously in nature where they carry out the irreversible oxidative decarboxylation of various 2-oxoacid substrates in carbohydrate metabolism and in the degradation of a select group of amino acids (Yeaman 1989; Reed and Hackert 1990).

The general mechanism of 2-oxoacid oxidation in animal tissues and microorganisms is detailed below:

$$\mathbf{RCOCO_2H + CoA\text{-}SH + NAD^+ \rightarrow RCO\text{-}S\text{-}CoA + CO_2 + NADH + H^+}$$

**Where R =** $-CH_3$ (pyruvate)
or $-CH_2CH_2COOH$ (2-oxoglutarate)
or $-CH(CH_3)_2$ (3-methyl-2-oxobutyric acid; a product of valine transamination)
or $-CH_2CH(CH_3)_2$ (4-methyl-2-oxopentanoic acid; a product of leucine transamination)
or $-CH(CH_3)CH_2CH_3$ (3-methyl-2-oxopentanoic acid; a product of isoleucine transamination)
or $-CH_2CH_3$ (2-oxobutyric acid; a product of threonine transamination)
or $-CH_2CH_2SCH_3$ (4-methylthio-2-oxobutyric acid; a product of methionine transamination)

This reaction represents a general overview of the oxidative decarboxylation of 2-oxoacid substrates linked to nicotinamide adenine dinucleotide ($NAD^+$) and coenzyme A (CoA), which occurs in the mitochondrial matrix of eukaryotic cells (Hackert *et al.* 1983; Randle 1983; Yeaman 1986).

Acetyl Coenzyme A (acetyl CoA), the main reaction product of the pyruvate dehydrogenase complex, is a key intermediate in the biosynthesis of fatty acids, ketone bodies and cholesterol in addition to its role in oxidative energy generation (Fig. 1.1). Oxidative decarboxylation of pyruvate, 2-oxoglutarate, and branched-chain 2-oxoacids occurs via a sequence of reactions involving acyl group transfer via a covalently-linked lipoic acid cofactor (Schwartz and Reed 1970; Reed 2001).

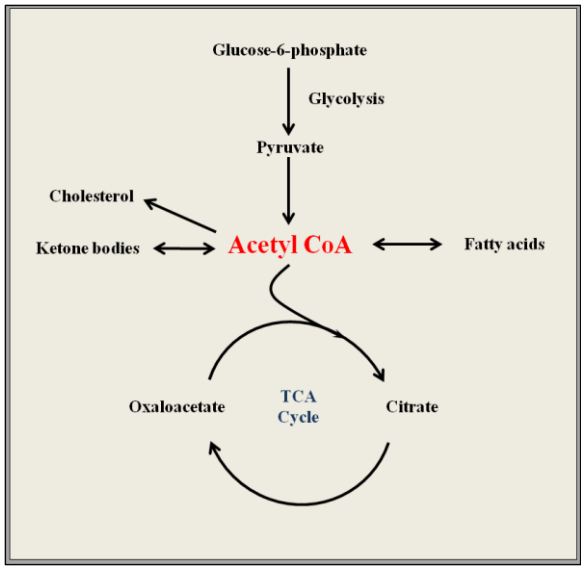


**Figure 1.1: The role of acetyl CoA in glycolysis and the citric acid cycle**

Interestingly, three major structurally and mechanistically analogous 2-oxoacid dehydrogenase multienzyme complexes have been characterized to date. These are as follows: the pyruvate dehydrogenase complex (PDC) that is specific for pyruvate; the 2-oxogluturate dehydrogenase complex (OGDC) that is specific for 2-oxoglutarate, and a third branched-chain 2-oxoacid dehydrogenase complex (BCOADC) that is involved in the oxidative decarboxylation of 2-oxoacids derived from the breakdown of leucine, isoleucine, valine, threonine and also methionine (Yeaman 1986; Perham 1991; Perham 2000).

These three multi-enzyme complexes control pivotal steps linking glycolysis to the citric acid cycle, a key step within the citric acid cycle itself and in the degradation of the keto-acid derivatives of the branched-chain amino acids feeding into the cycle. Additionally, these multienzyme complexes are members of the thiamine diphosphate (ThDP)-requiring 2-oxoacid dehydrogenase complex family, while also sharing a common protein component dihydrolipoamide dehydrogenase (E3) utilizing the coenzymes lipoamide, flavin adenine dinucleotide (FAD) and $NAD^+$ (Mattevi *et al.* 1992a; Jordan *et al.* 2000). The products of the catalytic reactions of the 2-oxoacid complexes are acetyl CoA in the case of PDC, succinyl CoA in the case of OGDC, and several branched-chain acyl CoAs in the case of BCOADC (Patel and Roche 1990; Harris *et al.* 1997) (Fig. 1.2).

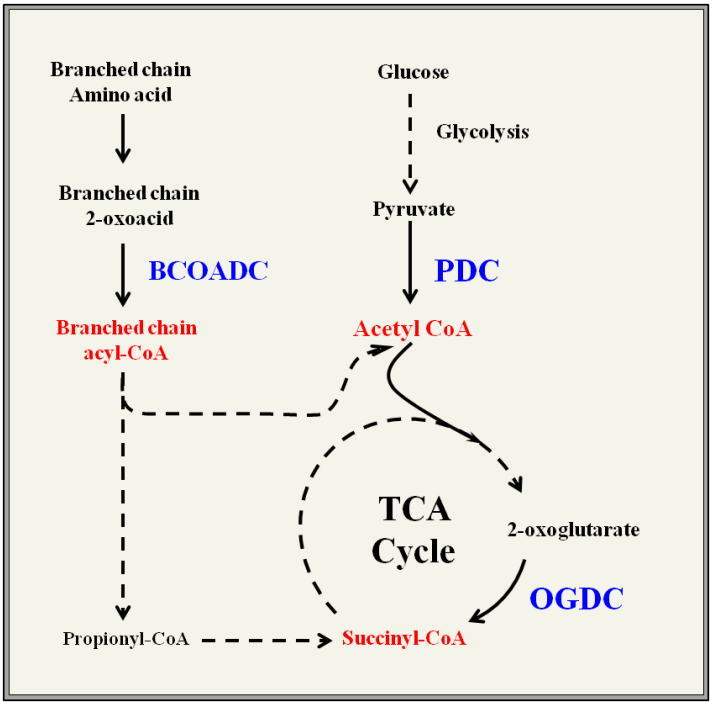


**Figure 1.2: Flowchart representation of the role of 2-oxoacid dehydrogenase complexes in cellular metabolism**
Enzymes are shown in blue and their products in red.

All of those complexes have distinctive general morphologies involving large non-covalent assembles comprising multiple copies of three separate enzymes: 2-oxoacid dehydrogenase (E1), dihydrolipoamide acyltransferase (E2), and dihydrolipoamide dehydrogenase (E3). The E3 enzyme is common to PDC, OGDC and BCOADC in mammals and is involved in reoxidation of the dihydrolipoamide group and the transfer of electrons via FAD to $NAD^+$ (Jones *et al.* 2000; Reed 2001). Furthermore, the complex-specific E1 and E2 enzymes are referred to as (E1p, E2p, E1o, E2o, E1b, E2b) in PDC, OGDC and BCOADC, respectively.

## 1.2 Reaction mechanism of the 2-oxoacid dehydrogenase complexes

It is clear that the oxidative decarboxylation of pyruvate and 2-oxoglutarate undergo a parallel sequence of reactions to give rise to acetyl CoA and succinyl CoA. The reactions are detailed below (Reed 1974; Bunik 2003).

$RCOCO_2H$ + ThDP-**E1** → [RCH(OH)- ThDP]-**E1** + $CO_2$

[RCH(OH)- ThDP]-**E1** + $LipS_2$-**E2** → ThDP-**E1** + [RCO-S-LipSH]-**E2**

[RCO-S-LipSH]-**E2** + HS-CoA → RCO-S-CoA + $[Lip(SH)_2]$-**E2**

$[Lip(SH)_2]$-**E2** + **E3**-FAD → $LipS_2$-**E2** + Reduced **E3**-FAD

Reduced **E3**-FAD + $NAD^+$ → **E3**-FAD + NADH + $H^+$

**Where R =** $-CH_3$ (pyruvate)
or $-CH_2CH_2COOH$ (2-oxoglutarate)
or $-CH(CH_3)_2$ (3-methyl-2-oxobutyric acid; a product of valine transamination)
or $-CH_2CH(CH_3)_2$ (4-methyl-2-oxopentanoic acid; a product of leucine transamination)
or $-CH(CH_3)CH_2CH_3$ (3-methyl-2-oxopentanoic acid; a product of isoleucine transamination)
or $-CH_2CH_3$ (2-oxobutyric acid; a product of threonine transamination)
or $-CH_2CH_2SCH_3$ (4-methylthio-2-oxobutyric acid; a product of methionine transamination)
ThDP (Thiamine diphosphate).
$LipS_2$ and $Lip(SH)_2$ (Lipoamide and its reduced form).

In each case, the catalytic process involves significant coupling between the various enzymes (E1, E2 and E3). Thus, while OGDC catalyses the conversion of 2-oxoglutarate, CoA, and $NAD^+$ into succinyl-CoA, NADH, and $CO_2$ with the aid of its FAD and thiamine diphosphate (ThDP) cofactors (Mattevi *et al.* 1992a; Sheu and Blass 1999a), mitochondrial PDC catalyzes the parallel conversion of pyruvate to acetyl-CoA (Reed 2001; Ciszak *et al.* 2006).

E1 is responsible for the decarboxylation of substrate (pyruvate in the case of PDC or 2-oxoglutarate in the case of OGDC) and the subsequent reductive acylation of the lipoamide prosthetic group on E2 via its cofactor ThDP (Mattevi *et al.* 1992a; Jordan *et al.* 2000; Perham *et al.* 2002). The interaction of pyruvate or 2-oxoglutarate with ThDP on E1 promotes the formation of a nucleophilic carbanion on the coenzyme in the presence of $Mg^{2+}$ facilitating the release of $CO_2$ (Sheu and Blass 1999a; Perham *et al.* 2002). Subsequently, E2 transfers the acetyl group (succinyl group in the case of OGDC) from the lipoamide cofactor to CoA (Tanaka *et al.* 1974).

Finally, the dihydrolipoamide group of E2 is reoxidised by E3 by electron transfer from the E2-linked $S^6$,$S^8$-acetyldihydrolipoamide moiety initially to FAD and then to $NAD^+$ as the final electron acceptor (Koike *et al.* 1974; Danson *et al.* 1978; Milne *et al.* 2002) (Fig. 1.3).

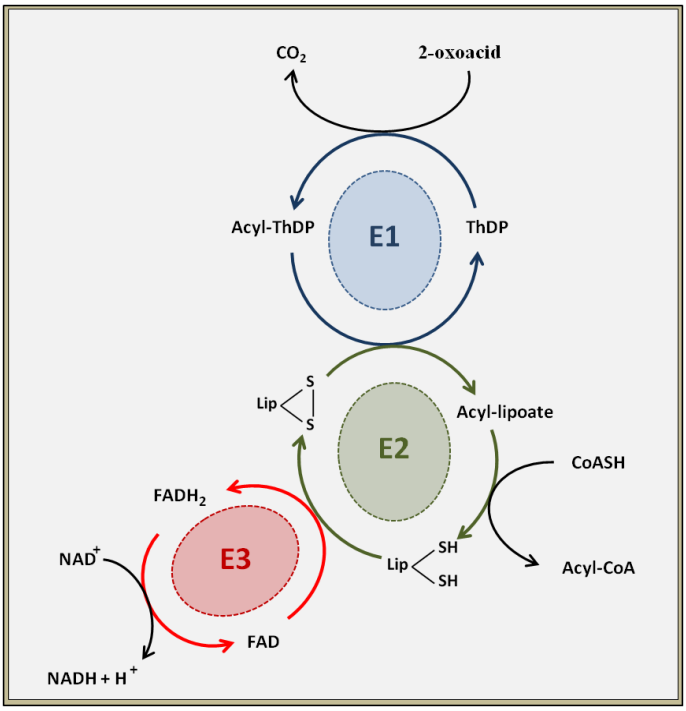


**Figure 1.3: Reaction sequence of the 2-oxoacid dehydrogenase complexes**
E1, 2-oxoacid dehydrogenase; E2, dihydrolipoamide acyltransferase, and E3, dihydrolipoamide dehydrogenase. 2-oxoacid (2-oxoglutarate or pyruvate). ThDP (Thiamine diphosphate). $LipS_2$ and $Lip(SH)_2$ (Lipoamide and its reduced form).

## 1.3 OGDC and PDC complexes: organization and structural information

The mammalian 2-oxoglutarate dehydrogenase complex (OGDC), also referred to as α-ketoglutarate dehydrogenase, is an enzyme complex most commonly known for its key role in the citric acid cycle (Lyubarev and Kurganov 1989). OGDC is located in close proximity to the mitochondrial inner membrane where it is involved in the conversion of 2-oxoglutarate to succinyl-CoA and $CO_2$ (Mattevi *et al.* 1992a; McCartney *et al.* 1998). It consists of multiple copies of three components (E1o, E2o and E3) (Jones *et al.* 2000). The first component,

2-oxoglutarate dehydrogenase (E1o) (EC 1.2.4.2), catalyses the initial rate-limiting decarboxylation step. Dihydrolipoyl succinyltransferase (E2o) (EC 2.3.1.61) then transfers the succinyl group to CoA. Finally, dihydrolipoyl dehydrogenase (E3) (EC 1.8.1.4) is required for reoxidation of the lipoamide on E2o (Tanaka *et al.* 1974; Spencer *et al.* 1984). The E3 component is identical in most 2-oxoacid dehydrogenase complexes excluding a number of prokaryotes such as *Thermus thermophilus* where various complex-specific E3s have been detected (Nakai *et al.* 2008).

Mitochondrial PDC from all known organisms contains three enzymes namely, pyruvate dehydrogenase (E1p, EC 1.2.4.1), dihydrolipoamide acetyltransferase (E2p, EC 2.3.1.1) and E3 (Graham and Perham 1990). In addition to its vital role in regulation, E2p provides the structural and mechanistic framework for the complex (Reed 2001). Eukaryotic PDC contains an additional component called E3-binding protein (E3BP), originally referred to as protein X (De Marcucci and Lindsay 1985b). E3BP, an E2-related polypeptide, is tightly integrated into the E2p core assembly via its C-terminal region and supports the overall reaction of the complex by promoting the tight binding of E3 (Hiromasa *et al.* 2004).

OGDC and PDC are stable, organized, high molecular mass assemblies (4-10 x $10^6$ Da) with E2 forming an oligomeric core to which components E1 and E3 bound tightly, yet non-covalently (Burns *et al.* 1988; Perham 2000).

OGDC has been characterized in human, plants, animals, bacteria, and fungi (Ishikawa *et al.* 1966; Reed and Oliver 1968; Meixner-Monori *et al.* 1985; Mareck *et al.* 1986; Patel and Harris 1995; Millar *et al.* 1999). It is thought that the basic organisation of OGDC resembles PDC (from Gram-negative bacteria such as *Escherichia coli* and *Azotobacter vinelandii*) and

BCOADC, with 24 E2o subunits forming a cubic core exhibiting octahedral (point group 432) symmetry (Reed and Hackert 1990; Perham 1991; Wallis *et al.* 1996; Sanderson *et al.* 1996a; Knapp *et al.* 1998; Frank *et al.* 2005). Furthermore, electron microscopic studies on mammalian OGDC suggest that the diameter of the complex is about 26nm (Markiewicz and Strumiło 1995). In contrast, E2p in higher eukaryotes and Gram-positive bacteria such as *Bacillus stearothermophilus*, is organised as a 60-meric pentagonal dodecahedron with icosahedral (532) symmetry (Oliver and Reed 1982; Wagenknecht *et al.* 1990; Perham 2000).

Human E2o has a distinctive structure consisting of only two domains; an N-terminal lipoyl domain (LD), and a C-terminal catalytic domain (CTD); hence, unlike PDC and BCOADC, no obvious subunit binding domain (SBD) is apparent to promote E1o and/or E3 binding (Bradford *et al.* 1987; Nakano *et al.* 1994). However, bacterial E2o, prokaryotic E2p, and E2b exhibit a similar multi-domain organisation comprising three domains (LD, SBD and CTD) (Packman and Perham 1987; Griffin *et al.* 1988; Thekkumkara *et al.* 1988; Reed and Hackert 1990; Perham 1991; Robien *et al.* 1992; Mattevi *et al.* 1992a; Nakai *et al.* 2008).

OGDC activity is controlled by feedback inhibition via its end products. Thus, NADH and succinyl CoA inhibit E1o activity (Roche and Lawlis 1982; Panov and Scarpa 1996; Qi *et al.* 2011). In contrast, mammalian PDC activity is primarily controlled by two regulatory components; pyruvate dehydrogenase kinase (PDK, EC 2.7.1.99) and pyruvate dehydrogenase phosphatase (PDP, EC 3.1.3.43) via a phosphorylation-dephosphorylation mechanism with phosphorylation of the rate-limiting E1p enzyme causing total inactivation (Ciszak *et al.* 2006).

### 1.3.1 2-oxoacid dehydrogenase (E1)

The E1o component of OGDC is a complex-specific homodimer ($\alpha_2$) with a subunit mass of approx. 100,000 Da (Lindsay 1989; Perham 1991). In eukaryotic PDC and BCOADC, E1 is a heterotetramer ($\alpha_2\beta_2$) composed of subunits with molecular masses of approx. 41,000 Da and 36,000 Da, respectively (Burns *et al.* 1988; Hawkins *et al.* 1990; Perham 1991; Ciszak *et al.* 2001). In contrast, E1p in Gram-negative bacteria is again present as an $\alpha_2$ homodimer with a subunit $M_r$ of 100,000 (Stephens *et al.* 1983; Matuda *et al.* 1991; Perham 1991).

Each E1o subunit contains a $Mg^{2+}$ ion and ThDP in the active site (Fig. 1.4). Twelve copies of E1o are thought to bind to the edges of the 24-meric cubic E2o core (Perham 1991; Mattevi *et al.* 1992a). It has been reported that $Mg^{2+}$ is required for OGDC activity by increasing the affinity of binding between ThDP and E1o (Zavala *et al.* 2000). Furthermore, a highly conserved motif sequence (approx. 30 amino acids) constitutes the binding site for ThDP and this motif is present in yeast, *E. coli* and human complexes (Hawkins *et al.* 1989). Recently, it has been reported that histidine residues (H260, H298, and H729) located near the ThDP binding site interact with the 2-oxoglutarate substrate to promote the decarboxylation process (Shim *et al.* 2011).

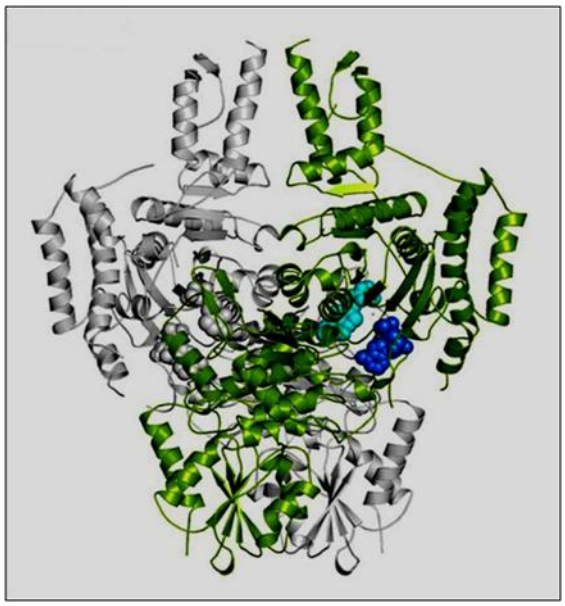

**Figure 1.4: Crystal structure of E1o of the *E. coli* 2-oxoglutarate dehydrogenase complex (OGDC)**
E1o consists of two subunits as shown in green and grey. Each subunit contains a $Mg^{2+}$ and ThDP in the active site (cyan spheres). AMP is bound in a separate binding pocket (blue spheres). The image was adapted from Frank *et al.* (2007).

Pyruvate dehydrogenase (E1p), also a ThDP-requiring enzyme, promotes the decarboxylation of pyruvate and the subsequent transfer of an acetyl group from ThDP to the prosthetic group of the E2p lipoyl domain (Kern *et al.* 1997; Berg *et al.* 1998). Moreover, X-ray crystallographic studies on E1b from *Pseudomonas putida*, E1p from *E.coli*, as well as mammalian E1p indicate a high degree of structural similarity (Ævarsson *et al.* 1999; Ciszak *et al.* 2001; Arjunan *et al.* 2002; Ciszak *et al.* 2003). The crystal structure of human E1p at 1.95Å resolution confirms the heterotetrameric arrangement of the E1α and E1β subunits (α, α`, β, β`) (Fig. 1.5) (Ciszak *et al.* 2003). Its ThDP cofactor is located at the end of a 20 Å long hydrophobic channel close to the active site that interacts with the lipoyl-lysine of the lipoyl domain (Ciszak *et al.* 2003).

While, the E1β subunits are responsible for binding E1p to the E2p core non-covently, the catalytic domain of E1α includes the ThDP binding site (Hawkins *et al.* 1989; Lessard and Perham 1995; Seyda *et al.* 2000). Despite, the fact that the two active sites are chemically equivalent, they are dynamically non-equivalent. While, one active site catalyses the decarboxylation step, the other active site is involved in the simultaneous reductive acetylation of the E2p-bound lipoamide. As a result, either pyruvate or the lipoyl-lysine moiety is allowed access to ThDP (at any given time), giving rise to a flip-flop enzymatic mechanism (Ciszak *et al.* 2003). The crystal structure of *B. stearothermophilus* E1p reveals a 20 Å tunnel (proton wire) of acidic residues connecting the two active sites. This proton wire facilitates proton shuttling between two active sites without any obvious conformational changes in the structure of the two subunits (Frank *et al.* 2004).

**Figure 1.5: Crystal structure of the E1p component of the human pyruvate dehydrogenase complex (PDC)**
Crystal structure of the $\alpha_2\beta_2$ E1p of PDC. The α, and, α' subunits are shown in magenta and grey, while β and, β' are shown in white and red respectively. ThDP cofactors are denoted in cyan. The image was adapted from Frank *et al.* (2007).

Protein-protein interaction studies by NMR on *B. stearothermophilus* PDC revealed that the interface region between the E1α and E1β subunits houses the binding site for the lipoyl domain of E2p (Howard *et al.* 2000), while the E1β subunits are responsible for binding E1p to the E2p core.

In *E. coli* OGDC, the *sucA* gene encoding E1o is located very close to the genes encoding other TCA cycle enzymes (Hull *et al.* 1983; Darlison *et al.* 1984). The *kgd1* gene encoding E1o has also been cloned from *Yarrowia lipolytica* (Holz *et al.* 2011) and *Saccharomyces cerevisiae* (Repetto and Tzagoloff 1989). Human liver cDNA (*OGDH* gene) encoding E1o has been characterised and its location assigned to chromosome arm 7p at p13-p14 (Szabo *et al.* 1994; Koike 1995; Koike 1998).

Specific proteolysis of bovine OGDC with low levels of trypsin induced cleavage at a single site in the E1o N-terminal region (located at Arg77) resulting in loss of overall complex activity indicating the vital role of this region (Fig. 1.6) (Frank *et al.* 2007). Loss of activity was caused by dissociation of a large catalytically-active E1 fragment (E1') and E3 from the E2o core assembly highlighting its pivotal role in ensuring overall complex stability (Kresze *et al.* 1981; Rice *et al.* 1992; McCartney *et al.* 1998). These studies suggest that the E1o N-terminus is important for maintaining the structural integrity of the complex. It may also be involved directly in E3 binding (Rice *et al.* 1992). Interestingly, immunological analysis has also shown that E1o antiserum cross-reacts weakly with E3BP of PDC while anti-E3BP specific serum is also able to recognize E1o (Rice *et al.* 1992; McCartney *et al.* 1998).

Previous studies on mammalian OGDC have reported tight binding of E1o to the E2o core in comparison to E3 (Reed and Hackert 1990).

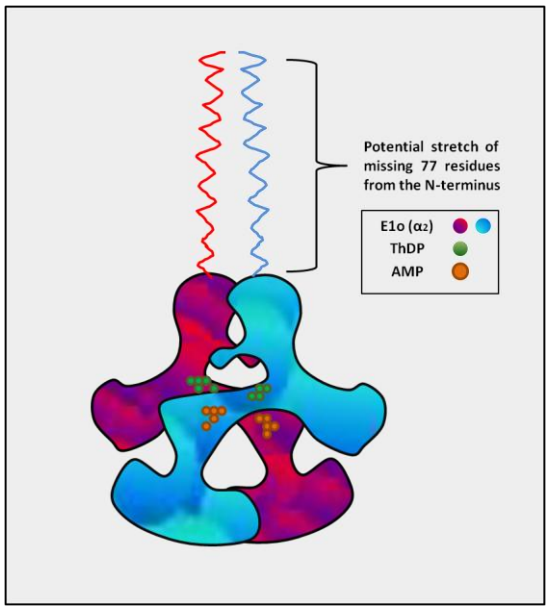


**Figure 1.6: Simplified model representing the general structure of E1 of 2-oxoglutarate dehydrogenase complex (OGDC) from *E. coli***
E1o consists of two subunits as shown in red and blue. Each subunit contains an $Mg^{2+}$ and ThDP in the active site (green spheres). AMP is bound in a separate binding pocket (orange spheres). The N-terminal residues (77 a.a.) of E1o were removed by limited digestion with trypsin before crystallization (Frank *et al.* 2007).

A recent X-ray crystallographic study of a bacterial E1o has indicated that it cannot be crystallized unless its N-terminal region (77a.a. in length) (Fig. 1.6), which appears to be natively-disordered, is removed (Frank *et al.* 2007). These studies are in agreement with earlier reports demonstrating the highly immunogenic nature of this region and its extreme sensitivity to proteolysis (Rice *et al.* 1992).

Amino acid sequence comparison of E1o from different sources including yeast, gram negative bacteria (*E. coli*), porcine and human tissue have indicated that human E1o has 37% and 40% sequence identity with the *E. coli* E1o and yeast E1o respectively (Koike *et al.* 1992; Koike 1998). Furthermore, this study reveals that human E1o has high sequence identity (93%) with porcine E1o and produces an mRNA of similar size (Koike *et al.* 1992).

Different isoforms of mammalian E1o have been identified. These isoforms may have different modes of regulation, and appear to be produced in a tissue-specific manner. The human *OGDH* gene located on chromosome 7 encoding E1o is known as the E1o heart isoform (OGDH-H) while different alternative forms has been isolated (Szabo *et al.* 1994; Koike 1995; Koike 1998). There are two main additional isoforms: human brain E1o isoform (OGDH-L) protein (Bunik and Fernie 2009) and a mitochondrial hypothetical protein (DHTKD1) (Bunik and Degtyarev 2008a).

OGDH-L was discovered in 2008 during the purification of OGDC from brain tissue (Bunik and Degtyarev 2008a; Bunik *et al.* 2008b). The *OGDH-L* gene was isolated from brain cDNA libraries and is located on chromosome 10 (Nagase *et al.* 1999; Team 2002; Bunik and Degtyarev 2008a). Amino acid sequence alignment of human heart OGDH-H and human brain OGDH-L isoforms have shown that the OGDH-L isoform conserves all the structural features and domain organization of the OGDH-H and has a high degree of the sequence similarity (approx. 85% overall similarity to OGDH-H), although the highest similarity is observed within their catalytic domains (Bunik and Degtyarev 2008a).

Mitochondrial hypothetical isoform (DHTKD1) exemplifies an additional putative 2-oxoglutarate dehydrogenase-like protein. The corresponding gene encoding DHTKD1 is localised to the small arm of human chromosome 10 (Nagase *et al.* 2001; Team 2002; Bunik and Degtyarev 2008a). Sequence comparison of DHTKD1 with OGDH-H predicted approx. 51% similarity. It displays lower sequence similarity to OGDH-L compared to OGDH-H. However, the N-terminal region of DHTKD1 appears to be non-conserved owing to a deletion such that DHTKD1 N-terminal is about 60 amino acid shorter than the corresponding OGDH-H N-terminal (Bunik and Degtyarev 2008a; Bunik *et al.* 2008b). This deletion in the N-terminal region of DHTKD1 isoform may affect the interaction with E3 and/or E2o (Rice *et al.* 1992; McCartney *et al.* 1998; Bunik and Degtyarev 2008a; Bunik *et al.* 2008b). A recent study has established that DHTKD1 is involved in the decarboxylation of 2-oxoadipate to glutaryl-CoA, a key reaction in the lysine degradation pathway. Deficiencies of DHTKD1 activity caused by mutation results in elevated levels of 2-oxoaminoadipate and 2-oxoadipate (Danhauser *et al.* 2012). 2-oxoadipic aciduria is an inherited disturbance of lysine, tryptophan, and hydroxyl-lysine catabolism. It is a neurological disease characterised by accumulation of 2-oxoadipic acid and 2-aminoadipic acid in body fluids leading to ataxia, muscular hypotonia and epilepsy.

OGDC activity is mediated by changes in the mitochondrial concentration of free $Ca^{2+}$ (Lawlis and Roche 1981; Rutter and Denton 1989; Panov and Scarpa 1996). The effect of $Ca^{2+}$ on OGDC is achieved via direct binding to the complex leading to the allosteric activation of E1o and simultaneous lowering of the $K_m$ for its 2-oxoglutarate substrate (Roche and Lawlis 1982; Rutter and Denton 1989; Scaduto 1994).

$Ca^{2+}$ induced activation is generally mediated by direct binding to a specific $Ca^{2+}$-binding motif or indirectly via $Ca^{2+}$-binding proteins e.g. calmodulin (CaM) that lead to conformational changes enabling the regulation of function by $Ca^{2+}$ (Zhou *et al.* 2006). Major $Ca^{2+}$-binding motifs are the helix-loop-helix structure, referred to as an EF-hand (Rigden and Galperin 2004; Zhou *et al.* 2006) and the related EF-hand-like domains (helix-loop-strand) in bacterial proteins such as the galactose-binding protein of *Salmonella typhimurium* (Drake *et al.* 1997; Zhou *et al.* 2006). In addition, $Ca^{2+}$ binding sites found in many major protein families are widely implicated in numerous biological processes including $Ca^{2+}$ signaling and homeostasis.

Interestingly, sequence and structural comparison of the OGDC has identified a number of potential $Ca^{2+}$-binding sites within the N- and C-terminal regions of E1o (Bunik and Degtyarev 2008a). Bunik and Degtyarev (2008a) have described three possible $Ca^{2+}$ binding motifs; ExDxDx and DxDxDx within the N-terminal region and NDDxDx within the conserved catalytic domain of E1o supporting the important role that this divalent cation in E1o regulation.

### 1.3.2 Dihydrolipoamide acyltransferase (E2) core organisation

In general terms, E2 forms the central catalytic and structural framework of all three 2-oxoacid dehydrogenase complexes, to which multiple copies of E1 and E3 bind non-covalently. Crystal structures of several cubic OGDC cores have been solved: truncated *E. coli* (tE2o) at low resolution (15 - 18 Å) (Derosier *et al.* 1971); porcine untruncated E2o at 7.0 Å resolution (Suzuki *et al.* 2002) and the truncated cubic core of *E. coli* tE2o at 3.0 Å resolution (Knapp *et*

*al.* 1998). The *E. coli* 24-meric core assembly has a diameter of 149 ± 15 Å displaying octahedral (432) symmetry (Derosier *et al.* 1971).

PDC core assemblies comprising E2p subunits (Patel and Roche 1990) exhibit different morphologies and symmetries depending on the organism. In higher eukaryotes and Gram-positive bacteria such as *B. stearothermophilus,* the E2p core is organised as a 60-meric pentagonal dodecahedron with icosahedral (532) symmetry (Fig. 1.7). In prokaryotes, 60 copies of E1p or 60 copies of E3 can bind to the E2p core in a mutually exclusive fashion, while in mammalian PDC, the E2p/E3BP core binds 20-30 copies of E1p and 6-12 copies of E3 (Oliver and Reed 1982; Wagenknecht *et al.* 1990; Perham 2000).

In contrast, the E2p core of PDC of Gram-negative bacteria such as *E. coli* and *A. vinelandii* forms a 24-meric structure with octahedral (432) symmetry (Fig. 1.7) (Yang *et al.* 1985; Mattevi *et al.* 1992c).

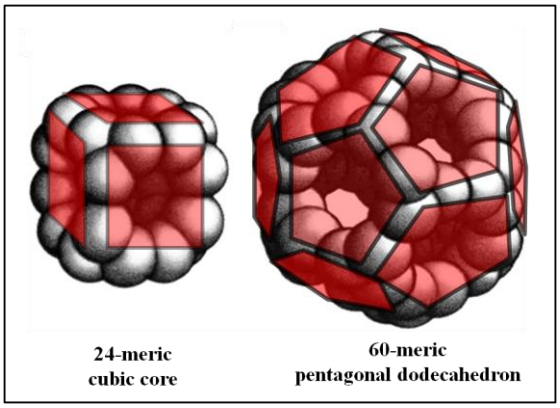


**Figure 1.7: Simplified models representing structures of the E2 cores of the 2-oxoacid dehydrogenase complexes**
The E2 core structure can be pictured as 24-meric cubic (OGDC, BCOADC, and PDC of *E. coli* and *A. vinelandii*) or a 60-meric pentagonal dodecahedron (PDC of *B. stearothermophilus* and mammals).

Interestingly, two models of mammalian PDC core formation have been proposed: the 'addition' model (60 copies of E2p plus 12 copies of E3BP) based on a cryo-electron microscopy study (Stoops *et al.* 1997) and the 'substitution' model (48 copies of E2p plus 12 copies of E3BP) by means of small angle X-ray scattering (SAXS) and analytical ultracentrifugation (AUC) (Hiromasa *et al.* 2004). However, a recent SAXS and small angle neutron scattering (SANS) study on the PDC core (rE2p/E3BP), truncated PDC core (tE2p/E3BP) and native bovine heart PDC core (bE2p/E3BP) has shown that all of the PDC core assemblies have open (unoccupied) pentagonal faces supporting the 'substitution' model with 12 copies of E3BP replaced an equivalent number of E2ps within the 60-meric core (Vijayakrishnan *et al.* 2010). In addition, owing to variation in the composition between bovine and recombinant PDC cores, in which number of E3BPs can range from 0 to 20 depending on the availability of E3BP, a 'variable E3BP substitution model' has been proposed incorporating 40 copies of E2p plus 20 copies of E3BP at maximal occupancy (Vijayakrishnan *et al.* 2010).

The organization of the bacterial E2o core has also been determined by electron microscopy and X-ray crystallography (Reed 1974; Oliver and Reed 1982). Moreover, an electron cryotomography study of *E. coli* OGDC has shown that the E1o and E3 subunits bind flexibly approximately 11 nm away from the E2o core surface (Murphy and Jensen 2005).

In *E. coli,* the OGDC core structure is organised as a cube with the E2o trimers occupying each of the 8 vertices (Fig. 1.8). Each E2o trimer is capable of binding E1o and/or E3 (Reed *et al.* 1975; Najdi *et al.* 2010). In mammalian OGDC, E1o binds more tightly to the E2o core than its E3 counterpart (Reed and Hackert 1990).

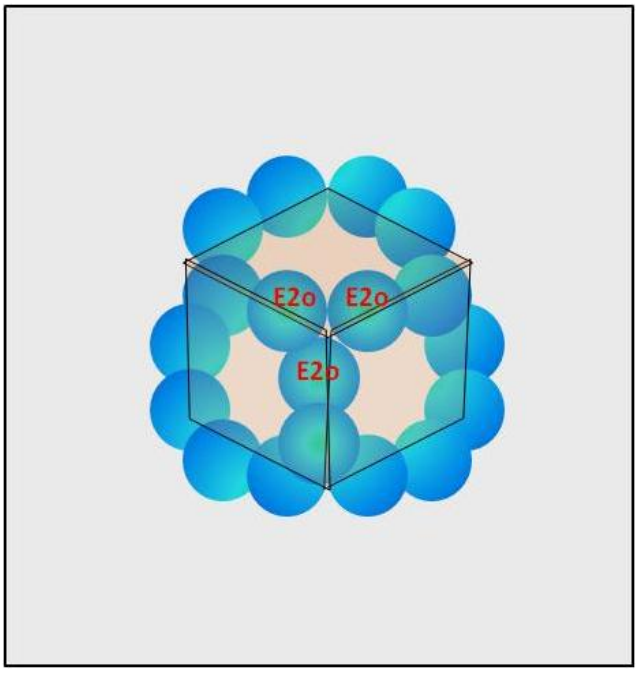


**Figure 1.8: Simplified model of the E2o core structure of the 2-oxoglutarate dehydrogenase complex**
The OGDC core structure can be pictured as a cube with a trimer of E2o occupying each vertex.

E2p ($M_r$ 59,600) comprises three types of domain (Fig. 1.9). Firstly, there is an N-terminal lipoyl domain ($M_r$. 9,000) that acts as a 'swinging arm' visiting all three active sites within the complex and varying in number according to the organism (Reed and Hackert 1990). While, only one LD exists in yeast and gram positive bacterial PDC (60-meric, icosahedral), there are two or three LDs in the icosahedral mammalian and 24-meric, octahedral gram negative bacterial PDCs, respectively (Perham 1991; Perham 2000).

The LD is followed by a SBD ($M_r$ 4,000), to which E1p binds tightly but noncovalently (Spector *et al.* 1998). Both E1p and E3 bind to E2p in bacterial PDC, while specific binding occurs between E1p:E2p and E3:E3BP in mammalian PDC. Finally, the SBD is followed by a 300 amino acid CTD that assembles to form the octahedral (24-meric) or icosahedral (60-meric) inner core depending on the source (Izard *et al.* 1999; Zhou *et al.* 2001; Milne *et al.* 2002). Furthermore, all these domains are joined by flexible and extended linker regions (LR) (20-30 amino acid residues) rich in alanine, proline and other charged amino acid residues (Reed 1974; Hackert *et al.* 1983; Westphal and de Kok 1990; Green *et al.* 1992; Perham 2000; Milne *et al.* 2002).

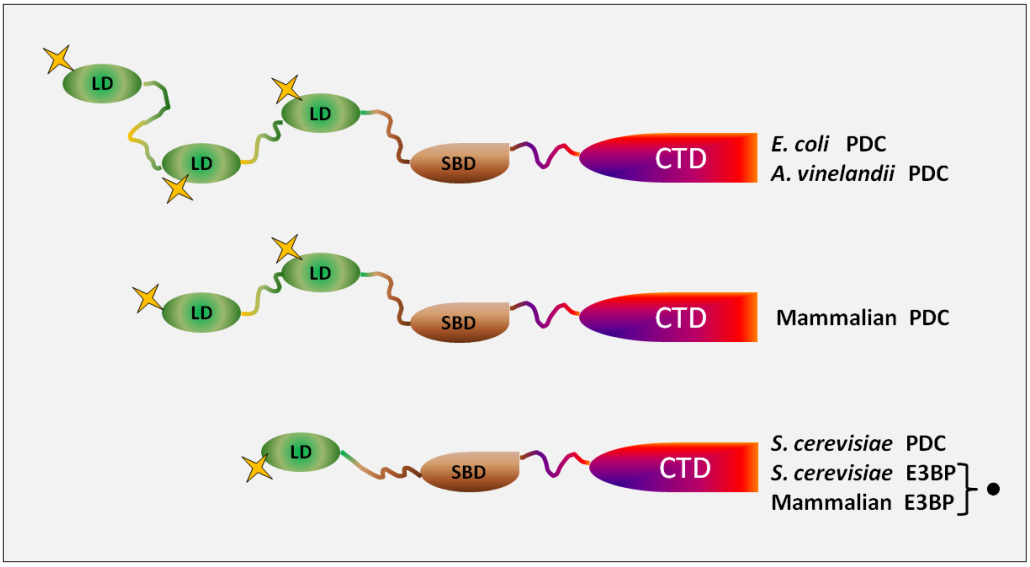


**Figure 1.9: Schematic representation of the domains and linker regions of the E2p and E3BP from various sources**

The domains are separated by long, flexible linker regions. Lipoyl domain (LD), Subunit binding domain (SBD) and C-terminal domain (CTD) are also shown. Lipoyl groups are indicated by a yellow star.

**(•)** E3BP has no acetyltransferase activity.

Mammalian E2o has subunit mass of approx. 48,000 Da (Lindsay 1989) and differs significantly from E2s of its companion 2-oxoacid dehydrogenase complexes (PDC and BCOADC), as it does not contain an E1o or E3-SBD as judged by the cDNA sequence analysis (Fig. 1.10). Hence, human E2o has a unique structure comprising only two domains (LD and CTD) (Bradford *et al.* 1987; Packman and Perham 1987; Wagenknecht *et al.* 1990; Nakano *et al.* 1994). It is postulated that the exon encoding the putative E1o-SBD or E3-SBD might have been lost during gene evolution (Lawlis and Roche 1981; Spencer *et al.* 1984; Bradford *et al.* 1987; Reed and Hackert 1990; Westphal and de Kok 1990; Nakano *et al.* 1994; Koike *et al.* 2000).

In contrast, NMR studies, sequence analysis and selective proteolysis of E2o of *E. coli* and *A. vinelandii* OGDC have shown that a 50 amino acid domain exists between the LD and CTD, which serves as a binding site for E3 (Fig. 1.10); hence, specific proteolysis at a single site located between the bacterial LD and CTD results in dissociation of E3 from the E2o core assembly (Packman and Perham 1986; Guest 1987; Robien *et al.* 1992; Mattevi *et al.* 1992a). Furthermore, recent X-ray crystallography studies have determined the structure of the equivalent *T. thermophilus* SBD (approx. 35 residues) in association with its E3 partner (Nakai *et al.* 2008).

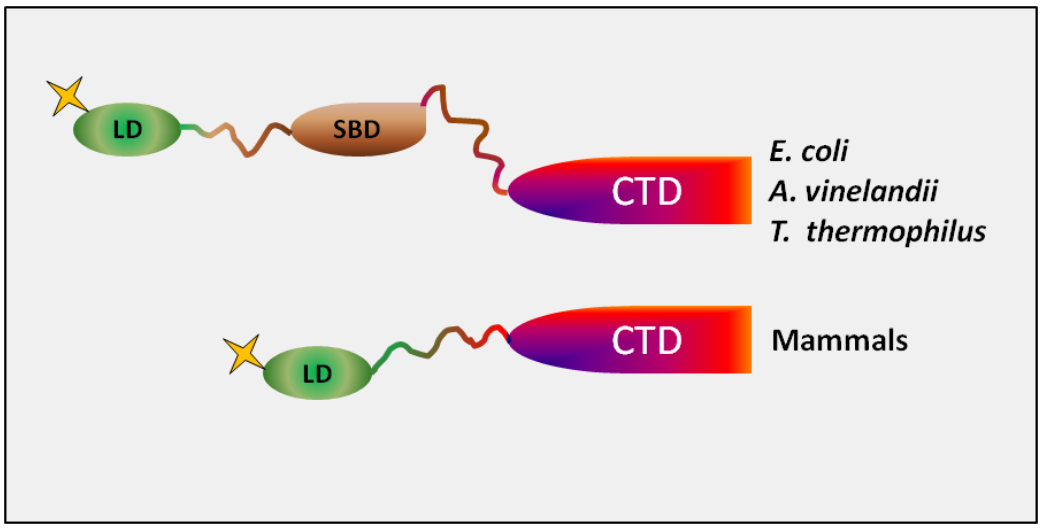


**Figure 1.10: Schematic representation of the domains and linker regions of the E2o chains of 2-oxoglutarate dehydrogenase complexes (OGDC)**
The domains are separated by long, flexible linker regions. Lipoyl domain (LD), Subunit binding domain (SBD) and C-terminal domain (CTD) are also shown. Lipoyl groups are indicated by a yellow star.

Interestingly, bacterial and mammalian E2o exhibits greater sequence conservation than their corresponding E2b or E2p counterparts (Russell and Guest 1991; Matuda *et al.* 1992); therefore, *E. coli* E2o and mammalian E2o are likely to exhibit similar quaternary structures (Tanaka *et al.* 1972; Bunik *et al.* 2000). In *E. coli*, E2o is encoded by the *sucB* gene which is close to *sucA*, the gene encoding E1o (Stephens *et al.* 1983; Spencer *et al.* 1984; Guest 1987; Park *et al.* 1997).

Human fibroblast cDNA encoding E2o has been characterised and the *DLST* gene assigned to chromosome 14q at q24.2-q24.3 (Nakano *et al.* 1993; Patel and Harris 1995; Bunik and Fernie 2009). Moreover, the sequence of the human gene showed 97% similarity to that of rat E2o (Nakano *et al.* 1991; Nakano *et al.* 1993). The basic architectural, design and structural features of the bacterial octahedral E2o, mammalian E2b (Griffin *et al.* 1988; Hakozaki *et al.* 2002) and

*E. coli* E2p are similar as predicted from inspection of their amino acid sequences (except that E2o contains only one LD) (Packman and Perham 1987; Graham *et al.* 1989). Interestingly, several studies have established a reduction in OGDC activity linked to Alzheimer's disease (AD) and in some AD cases are linked to polymorphism of the *DLST* gene (Nakano *et al.* 1997; Sheu *et al.* 1999b).

The general structural features of bacterial OGDC have been studied by electron microscopy and electron cryotomography (Murphy and Jensen 2005; Najdi *et al.* 2010). The E1o and E3 subunits are located above the surface of the E2o core and frequently separated by a gap (3-5 nm), although a thin strand of density is sometimes apparent perhaps suggesting the presence of the SBD and linker sequences in this region. Moreover, cryo-electron microscopy of *E. coli* OGDC demonstrated that the linker gap in E2o-E3 sub-complexes was more easily pictured than in the E2o-E1o sub-complexes suggesting that the bridge between the E2o-E1o sub-complexes contains more mass than the E2o-E3 bridges (Wagenknecht *et al.* 1990).

The primary function of E2 in 2-oxoacid dehydrogenase complexes is in the transfer of the acyl group to CoA via a dihydrolipoyl group covalently attached to a specific lysine residue in the LD (Howard *et al.* 2000; Milne *et al.* 2002). Owing to the flexibility of the LRs, the LDs have sufficient mobility to interact with all three active sites within the complex, the so-called lipoyl 'swinging arm' (Radford *et al.* 1989; Perham 2000). Amino acid sequence comparison has confirmed that the LR (31 amino acids) of *A. vinelandii* E2o at the end of its single LD is similar to that existing at the end of all three LDs of *E. coli* PDC (Westphal and de Kok 1990).

### 1.3.2.1 The lipoyl domain (LD)

The LDs of human E2 play a key role in the overall reaction. They are about 80 amino acid residues in length with a molecular mass of approx. 8 kDa (Perham 2000; Reed 2001; Murphy and Jensen 2005). Lipoyl domains house the essential lipoic acid cofactor that is linked to a specific lysine residue of the LD by a lipoyl ligase (Wallis *et al.* 1996). In the intact complex, lipoamide serves as a substrate for E1 , E2, and E3, although E1 requires it to be attached to a folded domain for measurable activity (Graham *et al.* 1989).

Protein lipoylation in mammals is a two-step enzymatic process: the first step is catalysed by the lipoate activating enzyme that promotes the formation of lipoyl-AMP, followed by the transfer of lipoate onto the LD by the lipoyl-AMP:$N^6$-lysine lipoyl transferase (Fujiwara *et al.* 1996). In contrast, protein lipoylation in bacteria is a one-step enzymatic process catalysed by lipoate-protein ligase A that promotes covalent attachment of the lipoic acid cofactor to the folded apo-protein via activation/ transfer of lipoate (Morris *et al.* 1994; Zhao *et al.* 2003).

The structures of the LDs of PDC and OGDC from various organisms have been determined by NMR. Three-dimensional structures have been solved for the E2o LD from *E. coli* (Ricaud *et al.* 1996) and *A. vinelandii* (Berg *et al.* 1995) and display close structural similarity. Moreover, 3D structures have been solved for the E2p-LDs of *E. coli*, *A. vinelandii* and human which are also extremely similar with no major variations observed (Wallis *et al.* 1996). The typical LD forms a flattened β-barrel comprising two antiparallel β-sheets: each of them contains four strands with a two-fold quasi-symmetry axis (Ricaud *et al.* 1996). The lysine residue, to be lipoylated is

situated on a prominent loop at the tip of a type I β-turn (Fig. 1.11) (Dardel *et al.* 1993; Wallis and Perham 1994).

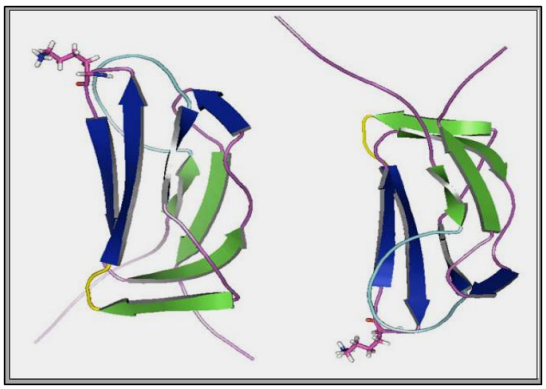

**Figure 1.11: Atomic structure of the lipoyl domain (LD)**
The two β-sheets are shown in green and blue. The lysine residue is drawn in stick representation. The surface loops involved in E1 binding are shown in cyan and yellow, respectively (Dardel *et al.* 1993).

The N-terminal and C-terminal residues are neighbours in one β-sheet (Ricaud *et al.* 1996). Moreover, NMR and secondary structure assignments have indicated that the *A. vinelandii* E2o LD exhibits high structural similarity to the E2p LD (Berg *et al.* 1995). Nevertheless, *E. coli* E1o exhibits a high degree of specificity for its cognate E2o LD whereas *E. coli* E1o does not interact with the corresponding E2p LD (Graham *et al.* 1989).

### 1.3.2.2 The subunit binding domain (SBD)

In the bacterial OGDC and PDC, the E1 and E3 subunits appear to bind to the SBD and the inner core-catalytic domain (Packman and Perham 1986; Packman and Perham 1987; Robien *et al.* 1992; Mattevi *et al.* 1992a; Nakano *et al.* 1993; Spector *et al.* 1998).

The SBD is responsible for binding E1o and/or E3 to the bacterial E2o core. It is the smallest folded, stable domain known to date (35 amino acid residues, approx. 4 kDa) (Perham 1991; Hipps *et al.* 1994; Lessard and Perham 1995; Murphy and Jensen 2005). Surprisingly, no equivalent SBD involved in E1o and/or E3 binding is apparent in mammalian OGDC. In *B. stearothermophilus* both E1p and E3 compete to bind to the E2p-SBD (Frank *et al.* 2005), while, in mammalian PDC, E1p specifically binds to E2p-SBD and E3 binds to the E2-related E3BP-SBD (Perham 2000). A three-dimensional solution NMR structure of a synthetic peptide comprising the *E. coli* SBD-E2o (Robien *et al.* 1992) and a recent crystal structure of E3-SBD-E2o sub-complex from *T. thermophilus* (Nakai *et al.* 2008) have shown similar structures comprising two parallel α-helices (H1 and H2), separated by a short $3^{10}$-helix or β-turn and two irregular loops (L1 and L2). The irregular loops along with the α-helices appear to form the domain core (Fig. 1.12). Moreover, conserved hydrophobic residues provide stability to the core (Robien *et al.* 1992; Nakai *et al.* 2008). It is also apparent that the basic SBD structure is similar to the other known SBDs of PDC and BCOADC (Kalia *et al.* 1993).

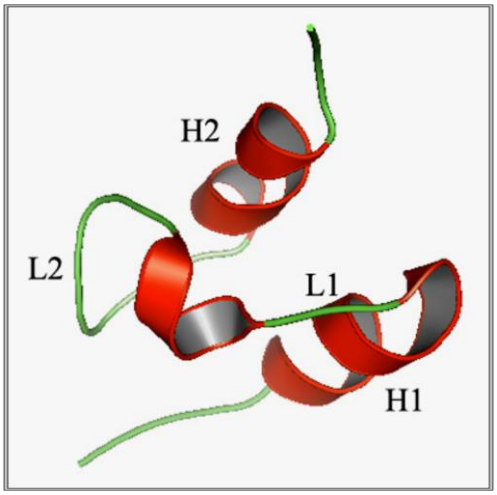


**Figure 1.12: Atomic structure of the E2p-SBD of *B. stearothermophilus***
Two short parallel α-helices (H1 & H2) shown in red are attached to a $3^{10}$-helix via two loops (L1 & L2) denoted in green.

### 1.3.2.3 The C-terminal domain (CTD)

The CTD of OGDC, (approx. 300 a.a.s; ~26 kDa) assembles to form its octahedral (24-meric) inner core by association of trimeric intermediates located at each vertex (Reed *et al.* 1975; Robien *et al.* 1992; Murphy and Jensen 2005). The CTD of E2p assembles to form an octahedral (24-meric) or icosahedral (60-meric) inner core depending on the organism (Izard *et al.* 1999; Zhou *et al.* 2001; Milne *et al.* 2002). The tE2o-CTD crystal structure from *E. coli* has been solved to 3.0 Å resolution (Knapp *et al.* 2000). No major differences in protein-protein contacts and overall CTD organization have been observed between eukaryotic E2o and E2b (Knapp *et al.* 1998; Kato *et al.* 2006). Moreover, Koike and his colleagues (Koike *et al.* 2000) have established that the porcine E2o C-terminal residues, Leu383, Leu384, and Leu385 are involved in the trimer–trimer interactions and important for cubic core formation as deletion of these residues leads to a failure of core formation.

The E2o CTD contains the trans-succinylase active site (Westphal and de Kok 1990) with a 30Å long channel at the interface between adjacent E2o subunits forming the entrance for lipoamide and CoA. The E2p CTD possesses the active site motif (DHRXXDG) required for the acetyltransferase activity of the complex (Radford *et al.* 1987; Stoops *et al.* 1992). Interestingly, chloramphenicol acetyltransferase (CAT), a naturally-occurring trimer in bacteria, has limited structural homology to E2-CTD (Leslie *et al.* 1988). Moreover, its conserved C-terminal active-site histidines have a catalytic function similar to the C-terminal proton acceptor residues (His375-E2o, His602-E2p, and His391-E2b) located at the centres of the E2 active sites (Spencer *et al.* 1984; Guest 1987; Kato *et al.* 2006).

### 1.3.3 Dihydrolipoamide dehydrogenase (E3)

E3 is a FAD containing flavoprotein. It serves as a common component for all three 2-oxoacid dehydrogenase multienzyme complexes (OGDC, PDC and BCOADC) and in most organisms is encoded by a single gene. Nevertheless, in prokaryotes such as *T. thermophilus* and in plants such as pea (*Pisum sativum*) multiple E3s have been detected (Conner *et al.* 1996; Nakai *et al.* 2008). In addition, in some cases, E3s are encoded for different complexes (Nakai *et al.* 2008). E3 always consists of two identical subunits forming a homodimer ($M_r$ 106,000) with one FAD molecule noncovalently bound per subunit (Patel and Harris 1995; Harris *et al.* 1997; Lindsay *et al.* 2000).

The primary function of E3 is to reoxidise the reduced lipoamide moiety of the E2 polypeptide via electron transfer from the dihydrolipoamide moiety to FAD and $NAD^+$ (Carothers *et al.* 1989; Mande *et al.* 1996).

As stated previously, a novel E3BP polypeptide is responsible for binding E3 to the mammalian E2p core while in prokaryotes such as gram positive bacteria, E3 competes with E1p for binding to the E2p core (De Marcucci and Lindsay 1985b; Behal *et al.* 1989; Sanderson *et al.* 1996a; Sanderson *et al.* 1996b; McCartney *et al.* 1998). However, the stability of the bacterial E3-E2p sub-complex is considerably greater than the equivalent E3-E2o sub-complex (Poulsen and Wedding 1970; Bunik *et al.* 2000). In the BCOADC, E3 also appears to bind weakly to the intact assembly (Clarkson and Lindsay 1991).

E3BP is tightly bound to the dihydrolipoamide acetyltransferase core and cannot be removed from the core except under denaturing conditions (Gopalakrishnan *et al.* 1989; Rahmatullah *et al.* 1989; McCartney *et al.* 1997). Previous stoichiometry studies showed that E3BP and E3 formed a stable 2:1 complex (Smolle *et al.* 2006). While one LD of this complex is docked into E3, the other is peripherally extended away from the E3 dimer suggesting the presence of a possible dynamic 'flip-flop' enzymatic mechanism, as in the case of E1p. However, a crystal structure of the E3BP-SBD/E3 sub-complex indicates a 1:1 stoichiometry (Ciszak *et al.* 2006). Electron microscopy studies suggest that E3 is located a about 60 Å above the surface of the *S. cerevisiae* oligomeric E2p assembly (Stoops *et al.* 1997).

In mammalian PDC, 20-30 copies of E1p are specifically bound to the E2p core (Reed 1974; Stoops *et al.* 1997), while, 6-12 copies of E3 associate with E3BP (Sanderson *et al.* 1996a). Furthermore, the mammalian E2p:E3BP core is thought to comprise 12 copies of E3BP and 48 copies of E2p (Hiromasa *et al.* 2004). As stated previously, a 'variable E3BP substitution model' has also been proposed where 40 copies of E2p bind 20 copies of E3BP incorporated at maximal occupancy (Vijayakrishnan *et al.* 2010).

X-ray crystallography of E3 from *A. vinelandii*, *P. putida*, *Pseudomonas fluorescens*, *B. stearothermophilus, S. cerevisiae*, pig heart and human has provided detailed information regarding its overall structure (Takenaka *et al.* 1988; Schierbeek *et al.* 1989; Mattevi *et al.* 1991; Mattevi *et al.* 1992b; Mattevi *et al.* 1993; Mande *et al.* 1996; Toyoda *et al.* 1998; Brautigam *et al.* 2005). It is clear that the main E3 structural features are similar between eukaryotes and prokaryotes. Alignment of human liver E3 has also shown 96% sequence identity with pig heart

E3 (Sanderson *et al.* 1996a). E3 comprises four principal functional domains: a FAD binding domain, $NAD^+$ binding domain, interface domain and central domain (Fig. 1.13) (Lindsay *et al.* 2000; Ciszak *et al.* 2006).

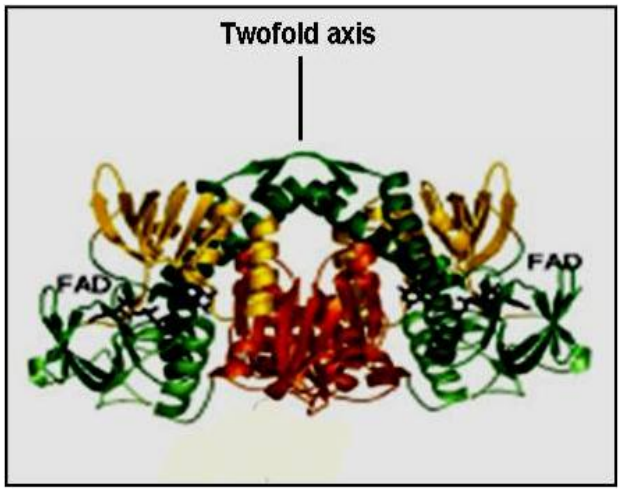


**Figure 1.13: Crystal structure of the dihydrolipoamide dehydrogenase (E3)**
The various domains namely, FAD binding domain (green), $NAD^+$ binding domain (yellow), interface domain (light green) and central domain (orange) are denoted. The FAD cofactors are shown. The image was taken from Ciszak et al (2006).

### 1.3.3.1 Glycine cleavage system (GCS)

Another mitochondrial multienzyme complex also containing a similar lipoamide dehydrogenase is the glycine cleavage system. The glycine decarboxylase complex, also known as the GCS is composed of four different components: glycine decarboxylase (P-protein, $M_r$ 210,000), a lipoic acid-containing protein (H-protein, $M_r$ 14,000), tetrahydrofolate transferase (T-protein, 45,000 Da) and lipoamide dehydrogenase (L-protein, $M_r$ 100,000).

When these four components were isolated from bacterial sources, they were referred to as P1, P2, P3, and P4 respectively (Freudenberg and Andreesen 1989; Douce *et al.* 2001; Hasse *et al.* 2009). The GCS is located in the inner mitochondrial membrane and catalyses the irreversible oxidation of glycine to yield carbon dioxide and ammonia, with the reduction of $NAD^+$ to NADH (Hasse *et al.* 2009).

The reaction mechanism involves a cycle of reactions including the initial decarboxylation step, transfer of an amino methyl group to the lipoyl group of H-protein (catalysed by the P-protein), methylamine transfer (catalysed by the T-protein) and electron transfer (catalysed by the L-protein) (Douce *et al.* 2001). The H-protein plays a central role in carrying reaction intermediates and, in essence, acting as a substrate for the three component enzymes during the enzymatic reaction.

Interestingly, GCS exhibits a significant degree of similarity to the various 2-oxoacid dehydrogenase complexes (OGDC, PDC, and BCOADC) as the H-protein is analogous to an E2 lipoyl domain. Its lipoyl group is covalently bound to a lysine residue and serves as the structural heart of the GCS (Faure *et al.* 2000). Moreover, the L-protein (E3) is also a component of the OGDC, PDC, and BCOADC in plants (Faure *et al.* 2000; Douce *et al.* 2001).

The GCS does not form a stable complex as an integrated assembly has never been isolated. Precipitation and fractionation experiments have shown that the components of GCS dissociate easily into independent species suggesting that all components involved in the GCS interact very

weakly (Walker and Oliver 1986). In addition, a large excess of the H protein is found free in cell extracts (Douce *et al.* 2001).

Stoichiometry studies using ultracentrifugation and quantitative ELISA of the matrix of pea mitochondria have shown that the GCS components are present in the ratio 4 P-protein: 27 H-protein: 9 T-protein: 2 L-protein (Oliver *et al.* 1990; Douce *et al.* 2001). Moreover, X-ray crystallography and small angle X-ray scattering experiments on solutions containing a mixture of H-protein and L-protein have failed to detect any significant interaction between the two components (Faure *et al.* 2000; Neuburger *et al.* 2000). Interestingly, specific recognition by T and H proteins to form a 1:1 complex has been characterized by small X-ray angle scattering (Cohen-Addad *et al.* 1997). However, the precise physical structure and organization of the GCS has not been completely resolved to date.

### *1.3.4 Mitochondrial targeting and assembly of the 2-oxoacid dehydrogenase complexes*

Mitochondria are membrane-enclosed organelles present in most eukaryotic cells. They are responsible for the chemical reactions involved in oxidative phosphorylation. Mitochondrial DNA encodes 13 essential subunits of the 4 major inner membrane complexes involved in the respiratory chain and ATP production (Takenaka *et al.* 1988; Wang *et al.* 2002).

Most mitochondrial proteins (800-1000) are encoded by nuclear genes and translated in the cytoplasm as cytosolic precursors that are often characterized by the presence of N-terminal matrix-targeting sequences allowing the nascent unfolded polypeptide chains to pass through mitochondrial membranes post-translationally (Pfanner and Truscott 2002a; Pfanner and Wiedemann 2002b). Cytosolic precursors are generally cleaved by a specific protease during polypeptide translocation into the mitochondrial matrix (Douglas *et al.* 1986).

Mitochondrial presequences are rich in hydroxylated amino acids (threonine and serine) and positively charged amino acids such as arginine and lysine, and usually display an absence of acidic residues (Hurt *et al.* 1986; Roise and Schatz 1988; Mukhopadhyay *et al.* 2007). Although, lacking any sequence similarity, matrix-targeting sequences tend to form amphipathic α-helices that are recognised by the main mitochondrial import receptor, MOM 70. In addition, cytosolic chaperones recognize mitochondrial precursors during targeting of pre-proteins to the mitochondria maintaining them in an 'unfolded', translocation-competent state (Roise and Schatz 1988; Neupert 1997).

The delivery of proteins to mitochondria (Fig. 1.14) and import process are mediated by molecular chaperones that also assist the folding and assembly of proteins. To import proteins through translocation pores of mitochondrial membranes, they must be unfolded. Thus, during translation on cytosolic ribosomes chaperones Hsp70 and Hsp40 bind to nascent precursor chains in order to prevent premature folding (Beddoe and Lithgow 2002). Cytosolic Hsp70 and Hsp40 are members of a heat shock protein family involved in protein folding while also preventing aggregation during or immediately after translation (Flaherty *et al.* 1990). Besides

these two major classes, several special types of heat shock proteins exist (Hsp60s and Hsp90s) that have important functions in protein folding and assembly and are named according to their molecular weight size (Neupert 1997; Voos and Rottgers 2002).

Mitochondrial import stimulating factor (MSF) generally recognizes mitochondrial precursors and facilitates their import into mitochondria (Neupert 1997). The MSF aids in the transfer of precursors to the translocase receptor (TOM complex) situated on the mitochondrial outer membrane (Hulett *et al.* 2008). The TOM complex comprises 7 different integral membrane proteins forming a general import pore (GIP) representing the entry gate into mitochondria (Fig. 1.14) (Pfanner and Truscott 2002a; Pfanner and Wiedemann 2002b). After passage through the GIP, the precursor is transferred to the translocase of inner mitochondrial membrane (TIM complex) which forms a channel across the inner mitochondrial membrane (Schleyer *et al.* 1982; Pfanner and Wiedemann 2002b). However, translocation across the outer and inner membranes is driven by electrostatic interactions of positively charged presequence and by chemical energy (ATP), membrane potential ($\psi$) and the mitochondrial Hsp70, which all appear to act cooperatively to pull the precursor protein into the matrix (Gakh *et al.* 2002).

Once the presequence is imported into the matrix, it is no longer necessary and cleaved by the mitochondrial matrix processing peptidase (MPP). After release of mature protein, it undergoes folding and maturation assisted by a matrix-located Hsp60 chaperone system analogous to the bacterial GroEL/ES complex (Douglas *et al.* 1986; Omura 1998; Pfanner and Truscott 2002a; Pfanner and Wiedemann 2002b).

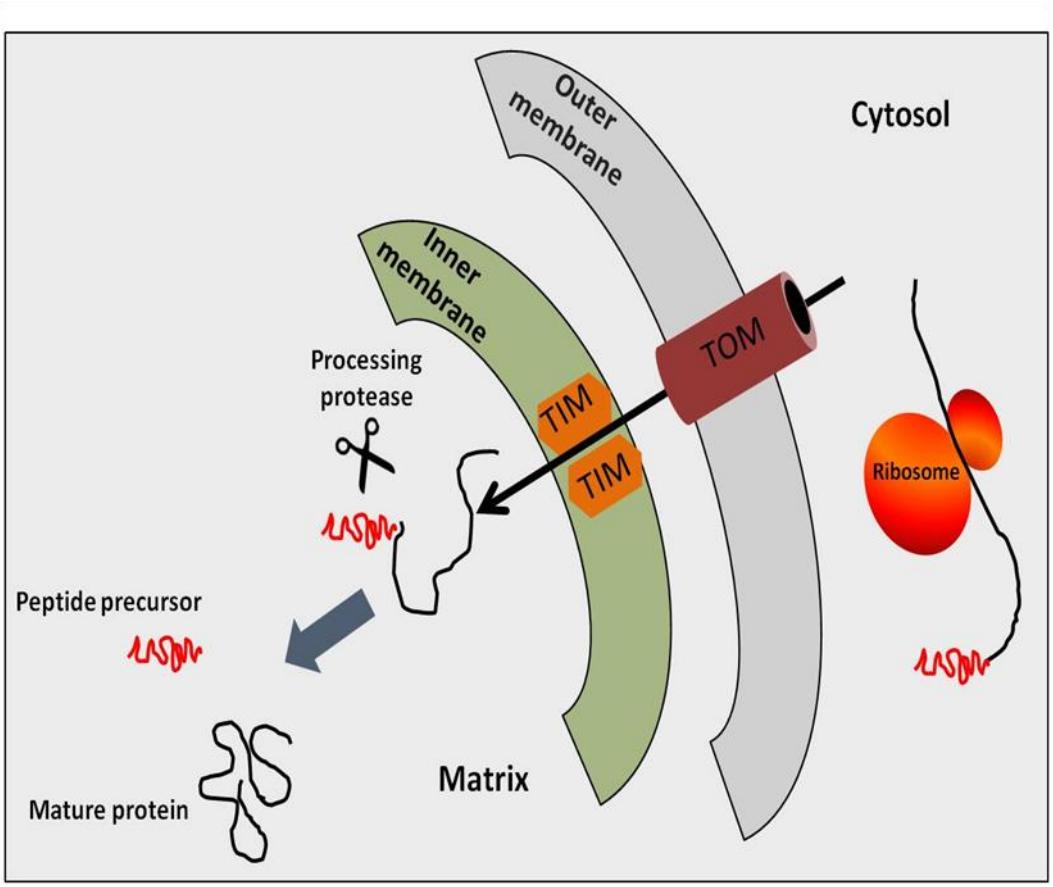


**Figure 1.14: Protein translocation into mitochondrial matrix**
The precursor protein is recognized by the TOM complex of the mitochondrial outer membrane. Then precursors are transported across the intermembrane space to the translocase complex (TIM) of the mitochondrial inner membrane and enter the mitochondrial matrix where the MTS is cleaved off by the mitochondrial processing peptidase.

In the case of the OGDC, PDC, and BCOADC, all their constituent polypeptides are encoded by the nuclear genome and are individually transported post-translationally to mitochondria prior to assembly (Thekkumkara *et al.* 1988; Maas and Bisswanger 1990; Wang *et al.* 2002). Once inside the mitochondria the E2 precursor is cleaved to induce self-assembly before association with E1 and E3 to form a stable complex (Milne *et al.* 2006).

Previous immune-precipitation studies have shown that the molecular mass of the cytoplasmic E1o precursor is approx. 1500-3000 kDa greater than the mitochondrial mature E1o form (Hunter and Lindsay 1986). Subsequent isolation of the gene encoding E1o indicated the presequence of a 40 a.a. signal sequence required for mitochondrial targeting which is removed on entry into the organelle (Thekkumkara *et al.* 1988; Wang *et al.* 2002; Pfanner and Wiedemann 2002b). The signal peptides of OGDC subunits are listed in (Table 1.1).

| OGDC subunits | Protein | Mature peptide | Signal peptide | Signal sequence |
|---|---|---|---|---|
| E1o | 1-1002 | 41-1002 | 1-40 | MFHLRTCAAKLRPLTASQTVKTFSQNRPAAARTFQQIRCY |
| E2o | 1-453 | 47-453 | 1-46 | MLSRSRCVSRAFSAPLSAFQKGNCPLGRRSLPGVSLCQGPGYPNSR |
| E3 | 1-511 | 43-511 | 1-42 | MQSWSRVYCSLAKRGHFNRISHGLQGLSAVPLRTYADQPIDA |

**Table 1.1: OGDC subunit signal peptide precursors**
E1o, E2o, and E3 presequences are shown (Feigenbaum and Robinson 1993; Nakano *et al.* 1993; Koike 1995).

The basic organisation of the OGDC is directed by the self-assembly of its cubic core. To this E2o core approximately 12 E1o dimers bind non-covalently (Hunter and Lindsay 1986; Nakano *et al.* 1991). Moreover, 6 copies of dihydrolipoamide dehydrogenase (E3) are also suggested to bind to the six faces of this complex at maximal occupancy (Reed 1974; Robien *et al.* 1992).

Interestingly, an *in vivo* assembly study of the yeast OGDC core has reported that an appropriate expression balance between E1o and E2o is essential; thus, over-expression of E2o might cause ineffective complex assembly resulting in sub-optimal activity (Repetto and Tzagoloff 1991).

## 1.4 Regulation of the 2-oxoacid dehydrogenase complexes

The major 2-oxoacid dehydrogenase complexes (PDC, OGDC) play a vital role in glucose metabolism by catalyzing the oxidative decarboxylation of pyruvate or 2-oxoglutarate to acetyl-CoA or succinyl-CoA, respectively. It has been documented that PDC and OGDC have similar structural organization (Packman and Perham 1986; Yeaman 1989; Perham 1991), however, there are major differences in regulation and catalysis between the complexes.

OGDC plays a key role in the regulation of 2-oxoglutarate levels. The regulation of OGDC is subjected to feedback inhibition by its end products, NADH and succinyl CoA that inhibit the E1o enzyme (Lawlis and Roche 1981; Panov and Scarpa 1996). OGDC activity is also mediated by changes in the mitochondrial concentration of free $Ca^{2+}$ and is stimulated by $Ca^{2+}$ mobilizing hormones such as vasopressin and glucagon (Panov and Scarpa 1996).

Several studies have demonstrated that free $Ca^{2+}$ (µM range) regulates mammalian OGDC (Rashed *et al.* 1988; Zavala *et al.* 2000). The effect of $Ca^{2+}$ on OGDC is achieved via direct binding to the complex leading to the allosteric activation of E1o and simultaneous lowering of the $K_m$ for its 2-oxoglutarate substrate (Roche and Lawlis 1982; Scaduto 1994). Moreover, $Mg^{2+}$ also stimulates OGDC activity in the presence of ThDP by increasing the binding affinity of ThDP for E1o (Zavala *et al.* 2000; Qi *et al.* 2011). Interestingly, ThDP itself has a positive allosteric effect on OGDC which increases the affinity of OGDC for its substrate by causing conformational changes in the complex (Strumito *et al.* 2002). In addition, $NAD^+$, CoA, 2-oxoglutarate and ADP stimulate OGDC activity whereas these effectors are antagonized by ATP and NADH (Rashed *et al.* 1988; Zavala *et al.* 2000). Previous studies have demonstrated

that inorganic phosphate (Pi) at physiological concentrations is also a positive effector activating OGDC significantly (Roche and Lawlis 1982; Chinopoulos *et al.* 1999).

Many studies have shown that the OGDC is inhibited by oxidative stress and, in particular, by reactive oxygen species such as hydrogen peroxide and superoxide (Halliwell and Gutteridge 1985; Siesjo *et al.* 1995; Chinopoulos *et al.* 1999; Tretter and Adam-Vizi 2000; Sweetlove *et al.* 2002). Furthermore, the cytotoxic lipid peroxidation product 4-hydroxy-2-nonenal (HNE) reduced OGDC activity via reacting with the E2o-LD (Humphries and Szweda 1998). In addition, powerful oxidants such as peroxynitrite ($ONOO^-$) formed by the reaction of superoxide with the free radical nitric oxide, inactivated OGDC whereas incubation with glutathione (GSH) restored activity (Shi *et al.* 2011).

Normal brain function depends on oxidation of glucose via glycolysis and the TCA cycle. As OGDC is the key regulatory enzyme in the cycle, oxidative decarboxylation of 2-oxoglutarate has an impact on the synthesis of glutamate in neurons which can be further converted to γ-aminobutyric acid (GABA) neurotransmitters. Thus decreases in OGDC activity have been linked to a wide range of neurodegenerative diseases (Gibson *et al.* 2000). In brain tissue, OGDC defects can lead to accumulation of toxic levels of neurotransmitters such as glutamate that is catabolised by OGDC after its transamination to form 2-oxoglutarate (Shoffner 1997).

In mammalian PDC, two principal types of regulatory mechanism are found. The first of these is end product inhibition by metabolites like NADH and acetyl-CoA, while the second involves covalent modification of the complex by a phosphorylation/dephosphorylation mechanism. PDC is regulated by specific pyruvate dehydrogenase kinases (PDKs, EC 2.7.1.99) that deactivate the complex and pyruvate dehydrogenase phosphatases (PDPs, EC 3.1.3.43), that activate it (Fig. 1.15) (Linn *et al.* 1969; Behal *et al.* 1993; Harris *et al.* 2002).

PDK is exists as a dimer and has four tissue-specific isoforms namely PDK1, PDK2, PDK3 and PDK4. Moreover, these isoforms vary in their kinetic parameters, mode of regulation, and phosphorylation site specificity (Popov 1997; Sugden and Holness 2003). PDKs phosphorylate three serine residues (Ser264, Ser271, and Ser203) of human PDC E1α (Yeaman *et al.* 1978; Sale and Randle 1981; Kolobova *et al.* 2001). While, PDK1 can phosphorylate all three serine residues, the other three isoenzymes can only act on sites 1 and 2 and do so at different rates (Wieland 1983; Dahl *et al.* 1987). Interestingly, phosphorylation at any single site leads to complete inactivation of the rate-limiting E1 enzyme (Kolobova *et al.* 2001).

PDK is activated by NADH and acetyl-CoA, providing an alternative means of PDC inhibition by these two major end products of the reaction. PDK activation involves interaction with E2p via changes in the oxidation and acetylation state of the lipoamide moiety induced by NADH and acetyl-CoA (Patel and Korotchkina 2001; Roche *et al.* 2003). Moreover, a limited number of PDK molecules (1-3) per complex are found to be adequate to inactivate PDC (Yeaman 1989).

Dephosphorylation of E1p by PDPs reactivate the enzyme (Huang *et al.* 1998). Two tissue-specific PDP heterodimeric isoforms have been identified in mammalian tissues designated as PDP1 and PDP2 (Huang *et al.* 1998; Maj *et al.* 2006). PDP1 is expressed predominantly in muscle tissue whereas PDP2 is found in adipose tissue, heart, kidney, and liver (Huang *et al.* 1998). Furthermore, dephosphorylation of E1p by PDPs is $Mg^{2+}$ and $Ca^{2+}$ dependent. In addition, during starvation, while PDK concentrations increase PDP expression decreases leading to PDC inhibition in various tissues (Linn *et al.* 1969; Roche and Cate 1976; Damuni and Reed 1987; Huang *et al.* 1998; Huang *et al.* 2003).

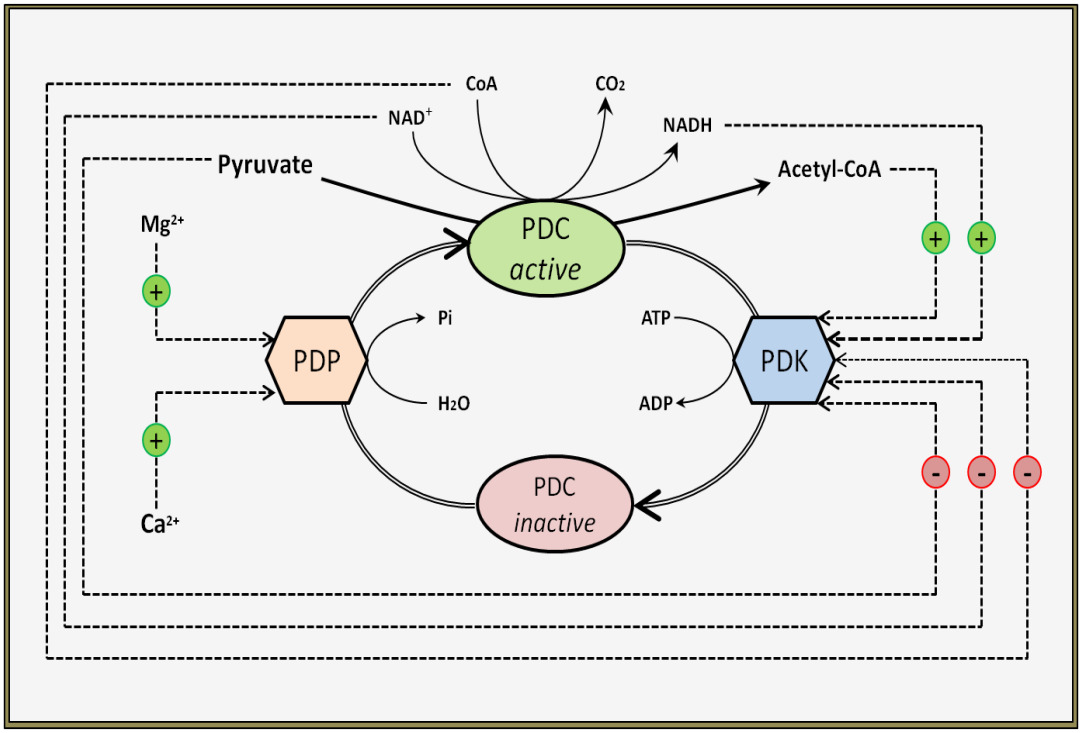


**Figure 1.15: Regulatory mechanism of PDC**

The regulatory enzymes (PDK and PDP) mediating PDC conversion between its active (dephosphorylated) and inactive (phosphorylated) forms. The $Mg^{2+}$ and $Ca^{2+}$ ions stimulate dephosphorylation of PDC.

## 1.5 The 2-oxoacid dehydrogenase multienzyme complexes and disease

PDC and OGDC deficiencies are associated with a wide range of genetic, metabolic and autoimmune disorders such as metabolic lactic acidosis, diabetes and primary biliary cirrhosis (PBC) (Fussey *et al.* 1988; Joplin and Gershwin 1997; Huang *et al.* 2003; Mayers *et al.* 2003; Patel *et al.* 2011) . Furthermore, PDC and OGDC deficiencies have been widely implicated in the aetiology of the major neurodegenerative disorders including Alzheimer's disease (AD) (Sheu *et al.* 1994; Blass 1999; Bubber *et al.* 2005; Shi *et al.* 2005).

### *1.5.1 Oxidative stress and Alzheimer's disease (AD)*

An imbalance in the production and removal of redox-active species gives rise to oxidative stress. The main targets of oxidative damage are the key macromolecules of the cell, namely proteins, lipids and nucleic acids that can contribute to tissue injury following irradiation and hyperoxia (Bellomo 1991; Nath *et al.* 1991). Oxidative stress arises owing to an enhanced production of reactive oxygen species (ROS) and/or the diminished/abolished ability of the biological system to detoxify the reactive intermediates or repair the resulting damage. However, disturbances in the normal redox state can result in the excess production of peroxides and free oxygen radicals that damage cell components and produce toxic effects (Hammond and Hess 1985; Kirkinezos and Moraes 2001).

Oxidative stress is implicated as a causative factor in many diseases like atherosclerosis, heart failure, myocardial infarction, and neurodegenerative disorders (Floyd 1999; Finkel 2000). When the oxidation potential is not significantly increased, the cell has the ability to overcome these small perturbations and regain its original state (Gutteridge 1994). However, moderate oxidative stress can lead to apoptosis, while severe stress can lead to necrosis (Lennon *et al.* 1991).

There are three major ROS, superoxide anions ($O_2^{\cdot -}$), hydrogen peroxide ($H_2O_2$) and hydroxyl radicals ($^{\cdot}OH$) (Turrens 1997; Cabiscol *et al.* 2000). They are generated by all aerobic organisms during normal cellular metabolism (Valko *et al.* 2005). When ROS levels are significantly high, organisms utilise a series of defence systems involving several antioxidant enzymes, such as superoxide dismutase (SOD), catalase, glutathione peroxidase and the thioredoxin-dependent peroxiredoxins (Prxs) (Fridovich 1995; Cao *et al.* 2005).

Mammalian PDC and OGDC are major targets for oxidative stress as their components (E1, E2, and E3) contain several thiol groups involved in catalysis. Exposure of E2 (PDC and OGDC) from *S. cerevisiae* and *E. coli* to hydrogen peroxide and superoxide anions have established these complexes to be a major target of oxidative stress (Tamarit *et al.* 1998; Cabiscol *et al.* 2000). In many disorders linked to mitochondrial and cell damage, a high level of ROS has been observed. It has been demonstrated that in certain conditions e.g. accumulation of NADH, the OGDC itself can be a major source of ROS production in mitochondria in addition to electron leakage from complexes I and III of mitochondrial electron transport chain (Bunik and Sievers 2002; Bunik 2003; Starkov *et al.* 2004).

Studies have shown that 5-15% of the world's population over the age of 65 is affected by AD (Katzman 1986). AD is a progressive neurodegenerative disorder characterized by the development of senile plaques and neurofibrillary tangles correlated with memory loss, cognition and communication defects (Waldemar *et al.* 2007). Mitochondrial defects including diminished OGDC and PDC function are characteristic of many neurodegenerative diseases and could be responsible for increased oxidative brain damage in AD induced by oxidative stress (Gibson *et al.* 2000; Sims *et al.* 2000; Shi *et al.* 2005).

The cause and progression of AD is not well understood. Studies have shown the activity of the PDC to be reduced by 50% in patients with AD (Gibson *et al.* 1998). Furthermore, a link between reduced OGDC activity and the development and progression of AD has also been demonstrated (Hoyer 2000; Gibson *et al.* 2005; Shi *et al.* 2005). As stated previously, in brain tissue, OGDC inhibition can lead to accumulation of toxic amounts of glutamate that is normally catabolised by OGDC after its transamination to form 2-oxoglutarate (Shoffner 1997). Moreover, OGDC and PDC deficiency in brain tissues can affect cell viability due to energy shortages as a result of a lack of production of acetyl-CoA and succinyl-CoA (Klivenyi *et al.* 2004; Tretter and Adam-Vizi 2005; Szutowicz *et al.* 2006).

The human *DLST* gene encoding E2o have been characterised and assigned to chromosome 14 (Nakano *et al.* 1993; Patel and Harris 1995; Bunik and Fernie 2009). Interestingly, several neurodegenerative diseases including AD have been found to be linked to a locus on chromosome 14 (Schellenberg *et al.* 1992; Sheu *et al.* 1999b). Genotyping studies have demonstrated that AD risk is associated with polymorphism of the *DLST* gene and possession of

the apolipoprotein E4 *(APOE4)* allele (Nakano *et al.* 1997; Sheu *et al.* 1999b). APOE4 is a variant of apolipoprotein E that is essential for the normal catabolism of lipids. In contrast, conflicting reports have concluded that the there is no association between *DLST* gene and AD (Matsushita *et al.* 2001; Prince *et al.* 2001).

### *1.5.2 Primary Biliary Cirrhosis (PBC)*

Primary biliary cirrhosis (PBC) is an autoimmune disease of the liver characterized by the accumulation of bile within the liver (cholestasis) owing to destruction of the small bile ducts leading to liver tissue damage, scarring, fibrosis and cirrhosis (Culp *et al.* 1982; Yeaman *et al.* 2000). PBC is a disease that is typically found in middle-aged woman between 40-60 years of age. There is increasing evidence that a number of immune disease related genes are linked to the X chromosome (Zinn 2001; Long *et al.* 2002; Jones 2003).

LDs and their lipoamide cofactors, in particular, are major self-antigens in primary biliary cirrhosis (PBC). Studies have shown that up to 95% of PBC patient produce autoantibodies against E2p (Fussey *et al.* 1988; Yeaman *et al.* 1988) and often produce antibodies against other lipoic acid containing proteins including E3BP (Palmer *et al.* 1999; Yeaman *et al.* 2000). Gershwin and colleagues (Gershwin *et al.* 1987) have also demonstrated that most patients with PBC possess anti-mitochondrial antibodies (AMAs) against E2p. Moreover, specific serum IgM AMA levels are commonly elevated (Nishio *et al.* 2001).

Recently, it has been reported that the X chromosome monosomy in white blood cells is increased in female PBC patients and increases with age (Invernizzi *et al.* 2004; Invernizzi *et al.* 2005).

Initially, assignment of the main M2"a" antigen ($M_r$ ~ 68-80 kDa) in PBC patients was carried out by isolating a rat liver cDNA clone using patient AMA (Gershwin *et al.* 1987). Subsequently, the protein expressed was identified as E2p (Yeaman *et al.* 1988). In addition, E3BP was classified as the M2"c" antigen ($M_r$ ~ 50-56 kDa) when purified bovine PDC was probed with the PBC patient sera (Yeaman *et al.* 1988).

According to Moteki and colleagues (Moteki *et al.* 1996); E2p is the major autoantigen of PBC, with sera from 80% - 90% PBC patients containing E2p specific AMA, while 60% of PBC patients are reactive to the E2b and 30% to 80% reactive to E2o. Furthermore, autoantibodies have also been detected against E1α and E1β subunits of PDC (Fussey *et al.* 1989). However, AMA have been also detected against E2o, E2b and E3BP in some patients (Yeaman *et al.* 1988; Surh *et al.* 1989; Fussey *et al.* 1991). The exact mechanism of breakdown of self-tolerance towards these ubiquitous mitochondrial antigens remains unclear.

As it is not within the remit of this thesis, the reader is referred to the following reviews dealing with recent theories to account for the aetiology of PBC (Yeaman *et al.* 2000; Lindor *et al.* 2009; Poupon 2010).

## 1.6 Project Aims

Human 2-oxoacid dehydrogenase complexes (PDC, OGDC and BCOADC) are composed of 3 distinct enzymes (E1, E2 and E3). In addition, mammalian PDC has a fourth accessory component, termed E3BP, which supports the overall reaction of the PDC by promoting the tight binding of E3 to the E2p core. Human OGDC differs significantly from PDC/BCOADC, as it does not contain any SBD for E1o or E3 and there is no equivalent to E3BP in this complex. Hence, human E2o has a unique structure comprising only two domains (LD and CTD), unlike the E2p and E2b. Since human OGDC has unique subunit organisation and E3 is a common component of the 3 complexes, the principal area of research in this project relates to an investigation of interactions between human OGDC subunits (E1o, E2o and E3) in order to understand complex organisation, stability and assembly.

Previous selective proteolysis and immunological analysis in our laboratory have suggested that the N-terminal region of mammalian E1o is important for maintaining the structural integrity of the entire complex and may be involved in interacting with both E2o and E3 (Rice *et al.* 1992; McCartney *et al.* 1998). Therefore, the objectives of this thesis were to determine initially if the N-terminal region of human E1o has the ability to interact with E3 and/or E2o and, if confirmed, to map the region of E1o involved in subunit binding and thereby establish its role in maintaining OGDC integrity.

Initial research (chapter 3) was directed towards the cloning and expression of 9 short N-terminal human E1o constructs (60 a.a., 90 a.a. and 153 a.a.) in various forms (His-tag, MBP and GST fusion proteins) and cloning/expression of mature human E1o in an *E. coli* BL21 host system. In addition, both His-tagged E2o and E3 were over-expressed and purified.

A crystallography study of *E. coli* E1o has indicated that it cannot be crystallized unless its N-terminal region (77 a.a.), which appears to be highly-flexible and natively-disordered is removed (Frank *et al.* 2007). In chapter 4, a preliminary structural characterization of the N-terminal region of human E1o was performed using synthetic peptides, circular dichroism (CD) and a basic bio-informatics approach to determine if this region has a tendency to assume a stable 3-D conformation similar to the SBDs of E2p, E2b and E3BP. In addition, sequence comparison and alignment analysis of the main E1o isoforms was investigated.

The main aim of chapter 4 was to investigate a potential interaction between N-terminal E1o and E3. To achieve this goal, a range of biochemical and biophysical approaches were applied including; peptide array analysis, ala-scanning, native-PAGE, ITC, gel filtration and GST affinity chromatography. A similar series of experiments using N-terminal E1o constructs to test their ability to interact with E2o were described in chapter 5. This chapter also includes a co-expression and interaction study of N-terminal E1o and native E2o to check the possibility that the E1o N-terminus co-integrates with E2o in a similar fashion to the way in which E3BP is integrated with E2p during or immediately after synthesis.

As a corollary to the main aims of the thesis, inhibition studies (chapter 6) on native bovine OGDC/PDC were conducted using N-terminal E1o constructs in order to establish the functional significance of the E1o N-terminus in tethering E3 to the native OGDC. A similar study was performed using the E3BP-SBD to determine if it had an inhibitory effect on PDC and OGDC activity by selective displacement of complex bound E3.

# Chapter 2

# Materials and Methods

## 2.1 Chemicals, enzymes and standard materials

All routine materials, chemicals, reagents, cells, antibodies, and enzymes used in this study were purchased from different suppliers as listed in Table 2.1, Table 2.2 and Table 2.3.

| Chemicals / Reagents | Supplier |
|---|---|
| Bacto-tryptone, bacto-yeast extract, and bacto-agar | Formedium Ltd, UK |
| Sodium chloride, di-sodium hydrogen phosphate anhydrous, ethanol, potassium di-hydrogen phosphate, di-potassium hydrogen phosphate, sodium acetate anhydrous, imidazole, magnesium chloride, trichloroacetic acid (TCA), sodium dodecyl sulfate (SDS), and acetic acid | VWR (BDH Ltd), UK |
| Tris base, sodium hydroxide, EDTA, 40% (w/v) acrylamide, methanol, acetone, and sucrose | Fisher chemicals, UK |
| Lipoic acid, ethidium bromide, Tween®20, chloramphenicol, ampicillin, kanamycin, nicotinamide adenine dinucleotide ($NAD^+$, oxidized form), nicotinamide adenine dinucleotide (NADH, reduced form), pyruvic acid, 2-oxoglutaric acid, Ponceau S dye, glycerol, rubidium chloride, Coenzyme A trilithium salt, calcium chloride, 3-(N-morpholino) propane sulfonic acid (MOPS), L-glutathione reduced, L-cysteine, thiamine diphosphate chloride (ThDP), Ficoll, potassium acetate, Coomassie Brilliant Blue G250, phenyl methane sulphonyl fluoride (PMSF), N, N, N', N'-tetramethyl ethylene diamine (TEMED), maltose, hydrochloric acid, ammonium persulphate (APS), oligonucleotide primers, and bovine serum albumin (BSA) | Sigma, UK |
| Xylene cyanol FF, and sodium azide ($NaN_3$) | Fluka, UK |
| 20 MC metal chelate resin | Amersham, USA |
| Protease inhibitor EDTA-free, complete protease inhibitor Mini tablets, and agarose | Roche, UK |
| Bradford reagent | BioRad, UK |
| Dithiothreitol (DTT) and isopropyl-β-D-thiogalactopyranoside (IPTG) | Melford Laboratories Ltd. UK |
| Thrombin and low molecular mass SDS marker | GE Healthcare, UK |

**Table 2.1: Chemicals and reagents used in this study**

| Kits/ Columns | Supplier |
|---|---|
| HiPrep 16/60 Sephacryl S-300 High Resolution column<br>Glutathione Sepharose 4B column<br>MBP Trap HP column<br>ECL western blotting detection kit<br>HRP Conjugate kit | GE Healthcare, UK |
| Amicon ultra concentrators (membrane cutoffs of 10 kDa and 30 kDa) | Fisher chemicals, UK |
| 1KDa cutoff (2ml) tubes<br>Nitrocellulose membrane (ECL Hybond) | Amersham, USA |
| QIAquick gel extraction kit, Blocking kit | Qiagen, UK |
| Quick Ligation Kit | New England Biolabs (NEB), UK |
| Wizard SV DNA Minipreps Kit, restriction enzymes, Calf intestinal alkaline phosphatase, Taq polymerase, dNTP and 1kb DNA ladder | Promega, USA |
| Expand high fidelity PCR system kit | Roche, UK |
| Dialysis cassettes/dialysis tubing of various cut off sizes | Pierce, USA |
| TOPO/ TA kits | Invitrogen, UK |

**Table 2.2: Kits and columns used in this study**

| Antibodies/Cells | Supplier |
|---|---|
| Anti- His tag antibody | Qiagen, UK |
| Anti-rabbit IgG secondary antibody | Sigma, UK |
| Anti-GST Antibody | GE Healthcare, UK |
| Polyclonal E3 and E1o antisera (rabbit anti-bovine sera). | Animal-house, University of Glasgow. |
| *E. coli* DH5α component cells | Stratagene, USA |
| *E. coli* BL21 (DE3) pLysS strain<br>*E. coli* BL21 Star (DE3) pLysS strain<br>*E. coli* TOP10 competent cells | Invitrogen, UK |

**Table 2.3: Antibodies and cells used in this study**

# 2.2 Molecular Biology

## 2.2.1 Synthetic oligonucleotide primers

Oligonucleotides for gene amplification by the Polymerase Chain Reaction (PCR) were designed in the laboratory to be compatible with the sequence to be inserted and the chosen vector. All PCR primers were ordered from Sigma, UK on the 25 mmol scale (see chapter 3). The 3' and 5' termini of the primers were typically designed to start with a CG clamp to increase binding efficiency. The CG composition, melting temperatures and secondary structures were checked before ordering.

## 2.2.2 Plasmid vectors

**pET-14b**: (4671bp) bacterial (*E. coli*) expression vector for the production of His-tagged recombinant fusion proteins. It contains the gene for ampicillin (*Amp*) resistance, the T7 promoter and encodes a six histidine (*His*) sequence at its 5' terminus followed by a thrombin cleavage site, three cloning sites and T7 terminator. The vector was purchased from Novagen (Appendix 1).

**pET-28b**: (5368bp) bacterial (*E. coli*) expression vector for the production of His-tagged recombinant fusion proteins. It contains the gene for kanamycin (*KanA*) resistance, the T7 promoter, N-terminal histidine sequence, thrombin cleavage site, multiple cloning sites and T7 terminator. The pET-28b vector housing the E2o construct was already available in the laboratory (Appendix 2).

**pET-30a**: (5422bp) bacterial (*E. coli*) expression vector for the production of His-tagged recombinant fusion proteins. It is ampicillin resistant, carries the T7 promoter, thrombin cleavage site, T7 terminator and N- and C-terminal poly histidine sequences. The maltose binding protein (MBP) cloned into the pET-30a vector was kindly gifted by Dr. Brian Smith, Glasgow University (Appendix 3).

**pGEX-2T**: (4900bp) an *E. coli* expression vector (ampicillin resistant) for production of glutathione S-transferase recombinant fusion proteins containing the *tac* promoter. The pGEX-2T vector was purchased from Pharmacia (Appendix 4).

**pCR®2.1 TOPO®**: (3900bp): an *E.coli* expression vector supplied linearized with single 3'-thymidine (T) overhangs for TA Cloning with topoisomerase I covalently bound to the vector. The pCR®2.1 TOPO® vector was purchased from Invitrogen (Appendix 5).

### 2.2.3 Plasmid propagation and purification

Recombinant plasmid and vector DNA amplified in *E. coli* DH5α cells were purified using the Wizard® Plus SV Minipreps DNA Purification System (Promega, USA) according to manufacturer's instructions. Briefly, a single colony was picked using a sterile pipette tip, added to a 5ml LB overnight culture (see section 2.2.6) and grown with the appropriate antibiotic at 37$^{o}$C for 16 h with shaking. The cultures were then centrifuged at 10,000xg for 10 min. The pellets were re-suspended in Tris-based buffer (10mM EDTA, 100μg /ml RNAse A,

50mM Tris-HCl, pH 7.8). Cell lysis solution (0.2M NaOH) containing 1% (w/v) SDS was added and mixed well to lyse the cells. The mixture was incubated for 5 min in the presence of alkaline protease. Neutralising buffer (2.12M acetic acid, 4.09M GdmCl, 0.759M potassium acetate) was then added and mixed well to neutralise the solution. The mixture was centrifuged at 13,000xg for 10 min in a bench-top centrifuge to pellet out the insoluble material. The DNA containing supernatant was applied to a DNA binding column and centrifuged as before. The column was washed with 10mM Tris-HCl, pH 7.8, 60% (v/v) ethanol, 60mM potassium acetate to remove contaminants before the DNA was eluted using 100µl nuclease free water. Purified plasmid was stored at -20$^{o}$C. The quality and quantity of the plasmids was analysed by agarose gel electrophoresis. Plasmids used in this study are listed in Table 2.4.

| Plasmid Name | Vector | Insert | Source |
|---|---|---|---|
| E3 His-14b | pET-14b | Human E3, aa 1 - 509 | A. Brown (2002) |
| E2o His-14b | pET-14b | Human E2o, aa 1 - 407 | A. Brown (2002) |
| E2o His-28b | pET-28b | Human E2o, aa 1 - 407 | G. Singh (2008) |
| E2p - GST - XSBD | pGEX-2T | Human E2p, aa 166 - 230 | A. Brown (2002) |
| E1o - 60 - His | pET-14b | Human E1o, aa 11 - 70 | A. Al-Alawy |
| E1o - 60 - GST | pGEX-2T | Human E1o, aa 11 - 70 | A. Al-Alawy |
| E1o - 60 - MBP | pET-30a | Human E1o, aa 11 - 70 | A. Al-Alawy |
| E1o - 90 - His | pET-14b | Human E1o, aa 1 - 90 | A. Al-Alawy |
| E1o - 90 - GST | pGEX-2T | Human E1o, aa 1 - 90 | A. Al-Alawy |
| E1o - 90 - MBP | pET-30a | Human E1o, aa 1 - 90 | A. Al-Alawy |
| E1o - 153 - His | pET-14b | Human E1o, aa 1 - 153 | A. Al-Alawy |
| E1o - 153 - GST | pGEX-2T | Human E1o, aa 1 - 153 | A. Al-Alawy |
| E1o - 153 - MBP | pET-30a | Human E1o, aa 1 - 153 | A. Al-Alawy |
| Full-length E1o | pET-14b | Human E1o, aa 1 - 962 | A. Al-Alawy |

**Table 2.4: Plasmids used in this study**

### 2.2.4 Agarose gel electrophoresis

Plasmid DNA and PCR products were analysed by agarose gel electrophoresis as described by Maniatis and colleagues (Maniatis *et al.* 1987a). Typically, (0.8% - 2%) (w/v) agarose was dissolved in TAE buffer (1mM EDTA, 40mM glacial acetic acid, 40mM Tris-HCl, pH 7.5). The gel was placed in an electrophoresis tank. DNA fragment size was determined by use of a DNA ladder (Promega, USA) run in parallel to the unknown sample. In general, 5µl DNA samples were diluted by adding 2µl loading buffer (15% (w/v) Ficoll, 0.25% (w/v) bromophenol blue, 0.25% (v/v) Xylene Cyanol FF). Gel electrophoresis was run at 100 volts (V) and 250mA for 50 min to 1 h. Agarose gels were stained for 30 min with ethidium bromide (EtBr) in distilled water (1µg/ml in $dH_2O$). DNA samples were visualised under 320nm UV light and photographed with a Polaroid DS34 direct screen-imaging camera.

### 2.2.5 DNA extraction and purification from agarose

Digested plasmid DNA and PCR products were subjected to gel electrophoresis (see section 2.2.4), then the linear DNA fragments were excised from the gel using a scalpel under UV light and purified using a Qiagen gel extraction kit (QIAgen, UK) according to the manufacturer's instructions. DNA was eluted in 50µl of elution buffer (10mM Tris-HCl, pH 8.5) and its quality and quantity viewed by agarose gel electrophoresis before storing at -20°C.

## 2.2.6 Polymerase chain reaction (PCR)

A putative clone of human E1o cDNA (IMAGE ID 100004510-OCAA-22-D1) obtained from Source Bioscience Ltd, UK (100ng) was used as the PCR template to amplify and clone the human full-length E1o DNA into pET-14b, and similarly to clone the 5' end of mature human E1o (1-153 a.a) into pET-14b, pGEX-2T, and pET-30a respectively (see chapter 3). The 5' region of human E1o (1-166 a.a), previously cloned in the laboratory into pET-14b by G. Singh (2008), was used as a PCR template to produce 5' constructs of E1o encoding 60 a.a, and 90 a.a segments into pET-14b, pGEX-2T and pET-30a (see chapter 3).

Amplification was carried out in a PTC-100$^{TM}$ programmable thermo-cycler (Genetic Research Instrumentation), and the reactions were set up using the Expand High Fidelity PCR System (Roche, USA). Typically, PCR was carried out in a 50µL reaction volume containing 0.25mM dNTP (mix of dTTP, dCTP, dGTP, and dATP), 1.5-2.0mM $MgCl_2$, 1x PCR buffer, template DNA, 2.0U *Taq* polymerase (Roche), sterile water and 0.2µM of each specific primer (forward and reverse). PCR was carried out under reaction conditions of activation, denaturation, annealing (temperature defined by the $T_m$ of the primers), and extension at 72$^oC$. The annealing temperature was calculated as 5$^oC$ lower than the lowest $T_m$ of the primers used. $T_m$ was calculated by the following; ($T_m$ = 2(A + T) + 4(C +G) $^oC$). Typical annealing reactions were performed in the range 50 °C to 59 °C. (Details of the PCR cycle times and reaction amounts are described in chapter 3). The quality and quantity of PCR product was assessed by agarose gel electrophoresis (see section 2.2.4). PCR products were subjected to direct cloning or alternatively cloned via TOPO/TA kits (Invitrogen).

## 2.2.7 TOPO TA cloning

TOPO TA cloning is an efficient one-step cloning strategy for insertion of *Taq* polymerase-amplified PCR products into a plasmid vector. The PCR products were generated with a single, 3'-A overhang to each end and ligated into a linearized cloning vector with single, 3'-T overhangs using the TOPO TA cloning kit from Invitrogen. The cloning was performed according to the manufacturer's specifications using the pCR2.1-TOPO vector (see section 2.2.2).

Briefly, a cloning reaction (6µl) was set up in an eppendorf tube containing 2µl fresh PCR product, 2µl diluted salt solution (1.2M NaCl, 0.06M $MgCl_2$), 1µl pCR2.1-TOPO vector and 1µl sterile $H_2O$ before mixing gently and incubating for 20 min at room temperature. It was then placed on ice followed by transformation into one shot chemically competent cells (TOP10) supplied in the kit (see section 2.3.4). The TOPO cloning vector system was used in the cloning of the N-terminal E1o-60 truncate (Ser11-Ala70), N-terminal E1o-90 truncate (Ser1-Val90), and N-terminal E1o-153 truncate (Ser1-Phe153) into pGEX-2T respectively (see chapter 3).

However, the N-terminal E1o-60 truncate (Ser11-Ala70), N-terminal E1o-90 truncate (Ser1-Val90), and N-terminal E1o-153 truncate (Ser1-Phe153) were cloned directly into pET-14b and pET-30a respectively. Mature human E1o cDNA (1-962 a.a) was cloned directly into pET-14b (see chapter 3).

## 2.2.8 Digestion of DNA with restriction enzymes and ligation

Restriction digests of plasmids and PCR products were performed using restriction enzymes purchased from Promega in accordance with the manufacturer's instructions. The DNA was digested with appropriate restriction enzymes either as a step prior to cloning or for diagnostic purposes. Plasmid DNA (40µl) was digested in a reaction containing 8µl of appropriate enzymes (10U/µl), and 8µl of the appropriate buffer (10x) as provided by the manufacturer. The reaction volume was made up to 80µl with sterile $dH_2O$. Digestion was performed in eppendorf tubes and carried out at 37°C for 4 h.

If a single restriction enzyme was used to digest the plasmid DNA, 2U of calf intestinal phosphatase (Promega, USA) was added to the total volume 1 h before the end of the reaction to promote dephosphorylation of 5' termini and prevent re-ligation.

PCR products (30µl) were digested in a total volume of 60µl with appropriate enzymes (10U/µl) as described above for 3 h at 37°C. Both digested plasmid and digested PCR products were run on a 1-2% (w/v) agarose gel and purified as described in section 2.2.5.

## 2.2.9 Ligation

Ligation reactions were set up using the T4 Quick Ligation Kit from New England Biolabs (UK) according to the manufacturer's instructions. T4 DNA ligase catalyses phosphodiester bond formation between the 5' phosphate and 3' hydroxyl termini of adjacent DNA molecules

(Sambrook and Russell 2001). Various ratios of linear plasmid and insert (1:1, 1:3 and 1:5) were ligated together including a sample containing the plasmid only as a negative control. The reaction was performed in a total volume of 10µl containing 1µl T4 DNA ligase, and 1µl reaction buffer (10x). The volume of the reaction was made up to 10µl with sterile $dH_2O$. The reaction was incubated overnight at room temperature before transformation into an appropriate strain of competent *E. coli*, either DH5α or TOP10 (Invitrogen, UK), and grown overnight on LB plates containing the appropriate antibiotic (Amp) at 37$^{o}$C (see section 2.3.4). Details of the restriction enzymes and ligation conditions used in this study are described in chapter 3.

### 2.2.10 Confirmation of cloning by restriction digestion and sequencing

The correct sequence and orientation of the constructs was confirmed by restriction digestion and sequencing. Diagnostic digestion was performed using restriction enzymes employed in plasmid construction (see section 2.2.8). Digests were subsequently analysed by agarose gel electrophoresis. If the inserted fragment was correct, bands would be seen at the appropriate size in the agarose gel as illustrated by the DNA ladder. Once recombinant clones were identified these were sent for DNA sequencing (University of Dundee) to confirm the exact coding sequence. The sequencing results were read and analysed with Chromas software (version; 2.01).

In order to ensure the correct sequence of the full-length E1o construct (2886bp), the following sequencing primers were sent with the samples:

1st Forward 5'-GATGCTGATCTGGACTCCTCC-3'

1st Reverse 5'- GGCTTCCCAGAGGACCAGGGC-3'

2nd Forward 5'-GGCATGTATCACCGCAGGATC-3'

2nd Reverse 5'-CTCATACTCAGGCTGGTTGAC-3'

## 2.3 Bacterial strains

***E. coli* DH5α** (Stratagene, USA) was used for propagation of plasmid vectors and also carries the *lac* I gene used when performing blue/white screening.

**TOP10 Chemically competent cells:** (Invitrogen, UK) were used for propagation of plasmid vectors and also carries the *mcr*A mutation that allows methylated DNA not to be recognized as foreign. It is a high transformation efficiency strain.

***E.coli* BL21 (DE3) pLysS** (Invitrogen, UK) was used for expression of toxic and non-toxic recombinant proteins**.** It contains the λ DE3 lysogen that encodes T7 RNA polymerase to induce high level T7 expression and also carries the pLysS plasmid that encodes T7 lysozyme.

***E.coli* BL21 Star (DE3) pLysS:** (Invitrogen, UK) was used for non-toxic recombinant protein over-expression. It carries the *rne*131 mutation resulting potentially in higher protein expression than BL21 (DE3) pLysS strains due to the increased stability of mRNA.

## 2.3.1 Bacterial media

**Luria Broth (LB):** Prepared by dissolving 10g bacto tryptone, 10g NaCl and 5g bacto yeast extract per litre of distilled $H_2O$, pH 7.0. The media were autoclaved before use.

**LB agar plates:** As LB medium with 15g/l of Bacto Agar added before adjusting the pH and sterilization.

**Super optimal broth with catabolite repression (SOC) medium** was prepared by dissolving 20g bacto-tryptone, 5g bacto yeast extract, 8.6mM NaCl, 2.5mM KCl, and 20mM glucose per litre of distilled $H_2O$, pH adjusted to 7.0. The medium was autoclaved before use.

**Modified-rich LB (Terrific broth)** was prepared by dissolving 1.2% (w/v) bacto tryptone, 2.4% (w/v) bacto yeast extract, 0.5% (w/v) NaCl, 4.0% (v/v) glycerol, 0.72M $K_2HPO_4$ and 0.17M $KH_2PO_4$ per litre of distilled $H_2O$, pH adjusted to 7.0. The medium was autoclaved before use.

**Selection media** were prepared with addition of antibiotics (50μg/ml ampicillin, 34μg/ml chloramphenicol and 25μg/ml kanamycin) wherever necessary.

## 2.3.2 Preparation of competent cells

Chemically competent cells were made using the calcium chloride protocol as described by Maniatis and colleagues (Maniatis *et al.* 1987b). A single colony of the appropriate bacterial *E. coli* strain was picked and cultured overnight in 5ml LB. This was subcultured into 100ml LB and grown at 37°C with constant shaking until the optical density ($OD_{600}$) was about 0.5. The culture was then chilled on ice for 5 min before spinning in an Allegra$^{Tm}$ 6R centrifuge at 3,000xg for 10 min at 4°C in a 50ml sterile Falcon tube. The pellet was gently suspended in 20ml ice cold sterilized filtered buffer I (10mM $CaCl_2$, 100mM RbCl, 50mM $MnCl_2$, 15% (v/v) glycerol, 30mM $CH_3COOK$, pH 5.8). The cells were re-spun as before and the supernatant discarded. By gentle pipetting the pellet was finally re-suspended in 2ml of ice cold sterile buffer II (75mM $CaCl_2$, 10mM RbCl, 15% (v/v) glycerol, 10mM MOPS buffer, pH 6.5). The solution was then chilled for 15 min on ice and separated into 50µl aliquots prior to storage at -80°C until required.

## 2.3.3 Bacterial cell storage

Bacterial strains may be stored for long term use at low temperatures (-80°C) in 30% to 40% (v/v) glycerol. Occasionally, the bacterial cells could be stored for short term storage (2-3 weeks) on LB plates at 4°C. To recover bacterial strains from -80°C glycerol stocks, a sterile toothpick was used to scrape some of the ice and the bacterial cells streaked out on the appropriate medium.

### 2.3.4 Bacterial transformation

Frozen competent *E. coli* cells (50µl) were removed from the -80°C freezer and thawed on ice at room temperature. Plasmid DNA (1-2µl) was mixed with thawed cells and incubated on ice for 15-30 min before being heat shocked at 42°C for 35s (TOPO10/BL21 star (DE3) pLysS) or 90s (DH5α/ BL21 (DE3) pLysS). The cells were then incubated on ice for a further 2 min before being mixed with 450µl of warm sterile LB medium or 900µl warm sterile SOC medium and incubated at 37°C with continuous shaking for 1 h. Aliquots (100-200µl) of the suspension were spread on LB agar plates with the appropriate antibiotics and incubated overnight at 37°C. All steps were carried out under sterile conditions.

## 2.4 Protein methods

### 2.4.1 Protein over-expression

For overnight cultures (16 h), 50ml LB medium supplemented with the appropriate antibiotic(s) (Table 2.5) was inoculated with a single bacterial colony containing the expression plasmid picked from a LB agar antibiotic plate and incubated at 37°C, with shaking at 200 rpm.

A 10ml aliquot of the overnight culture was added to 500ml of LB supplemented with the appropriate antibiotic(s) and further incubated at 37°C with constant shaking. Protein over-expression was induced by the addition of 1mM IPTG when the $OD_{600}$ reached 0.5-0.8 and grown for 3-5 h at 30$^{o}$C or overnight at 18 $^{o}$C /15$^{o}$C. For over-expression of E2o, 0.1mM lipoic acid was also added to the medium in order to maximise lipoylation. Details of various protein

induction temperatures and time intervals employed in this study are described in chapter 3. Bacterial cells were harvested in a JA14 rotor in a Beckman J2-21 by centrifugation at 4°C, 10,000xg for 15min. Pellets were stored at -20°C until further use. In order to monitor bacterial growth and protein expression, samples (1ml) were taken before induction ($t_0$) and after the induction periods $t_3$, $t_4$ and $t_{16}$ before harvesting by centrifugation in a bench top microfuge at 13,000xg for 10 min to pellet the cells. The pellet was re-suspended in Laemmli sample buffer (2% (w/v) SDS, 10% (w/v) sucrose, 62.5mM Tris-HCl, pH 6.8 and a small amount of Pyronin Y dye), adding 10µl per 0.1 $OD_{600}$ unit of the sample. Over-expression of the relevant protein was checked by SDS-PAGE (see section 2.4.3).

| Antibiotic | Plasmid | Stock solution | Selective conditions |
|---|---|---|---|
| Ampicillin (Amp) | pET-14b, pGEX-2T | 50 mg/ml in $dH_2O$ | 50 µg/ml |
| Chloramphenicol (Chl) | pLysS | 34 mg/ml in ethanol | 34 µg/ml |
| Kanamycin (Kan) | pET-28b, pET-30a | 25 mg/ml in $dH_2O$ | 25 µg/ml |

**Table 2.5: Antibiotics and selection conditions used in this study**

## 2.4.2 Protein solubility

In order to check protein solubility, bacterial cells from small (50ml) cultures were harvested in a Beckman Allegra TM 6R centrifuge at 4°C, 3,000xg for 15 min and re-suspended in 3ml binding buffer (see chapter 3 for details). The bacterial extract was passed 4 times through a French Pressure Cell (Thermo Electron Corporation, UK) at 950 psi to lyse the cells. The disrupted cells were then spun in a bench-top centrifuge at 4 °C, 13,000xg for 10 min. The protein supernatant (soluble fraction) and pellet suspension (insoluble fraction) were re-suspended in an equal volume of Laemmli sample buffer. The solubility of the recombinant protein was viewed by SDS-PAGE (see section 2.4.3).

## 2.4.3 Polyacrylamide gel electrophoresis (PAGE)

Polyacrylamide gel electrophoresis (PAGE) techniques are used to separate components of a protein mixture based on their size and net charge. It provides high resolution of proteins or protein complexes under the appropriate conditions.

### 2.4.3.1 Sodium dodecyl sulphate PAGE (SDS-PAGE)

Sodium dodecyl sulphate PAGE (SDS-PAGE) was performed as described by Laemmli (Laemmli 1970). Proteins were separated under denaturing conditions in the presence of sodium dodecyl sulphate (SDS). Using 3% stacking and 10-18% resolving gels (depending on the molecular mass of the protein of interest) gels (9 cm x 9 cm x 1.5 mm) were prepared using the solutions listed in Table 2.6.

| Gels/Buffers | Ingredients |
|---|---|
| SDS resolving gel | 10-18% (w/v) acrylamide<br>0.1% (w/v) SDS<br>0.1% (w/v) APS<br>0.1% TEMED<br>0.5 M Tris-HCl buffer, pH 8.8 |
| SDS stacking gel | 3.0% (w/v) acrylamide<br>0.06% (w/v) SDS<br>0.1% (w/v) APS<br>0.1% TEMED<br>0.5 M Tris-HCl buffer, pH 6.8 |
| 10x SDS running buffer | 0.2M glycine<br>1% (w/v) SDS<br>0.49M Tris-HCl buffer, pH 8.3 |
| 1x Laemmli sample buffer | Trace of pyronin Y<br>2% (w/v) SDS<br>10% (w/v) sucrose<br>62.5mM Tris-HCl buffer, pH 6.8 |

**Table 2.6: SDS-PAGE gel/buffers used in this study**

Protein samples were resuspended in Laemmli sample buffer, DTT (150mM) and boiled for 5 min at 100$^{o}$C prior to separation on a 10-18% SDS-PAGE gel depending on the molecular mass of the relevant protein. Typically, 5-15µl sample was loaded per well. Protein samples were run alongside molecular mass markers to allow estimation of the protein's subunit $M_r$ values. SDS-PAGE was carried out at a constant voltage (400V) and 50mA/gel in 1x SDS running buffer (Laemmli 1970). Gels were stained for protein with 0.1% (w/v) Coomassie Brilliant Blue G250, 10% (v/v) acetic acid, 50% (v/v) methanol with shaking for 20-30 min at room temperature before being de-stained with 10% (v/v) glacial acetic acid, 10% (v/v) methanol overnight.

Alternatively, and for superior resolution when necessary, samples were run on pre-cast 4-12% NUPAGE®Novex Bis-Tris gradient gels in an XCell *SureLock*™ Mini-Cell using the 2-(N-morpholino) ethane sulfonic acid (MES) buffer (0.1% SDS, 1mM EDTA, 50mM MES, 50mM Tris-base, pH 7.3) supplied by Invitrogen. Proteins were separated at 180-200V and 120mA for 1 h. The preparation of protein samples and staining/de-staining procedures were performed as described above.

### 2.4.3.2 Non-denaturing gel (native PAGE)

While in SDS-PAGE, protein separation depends mainly on molecular mass, in native PAGE the separation depends on both the protein's net charge and its size. Native PAGE was performed in a similar manner to SDS-PAGE without the presence of SDS in the gels, sample buffer or running buffer. The samples were not boiled prior to analysis.

Proteins were resolved under non-denaturing conditions using the method of Bollag and colleagues (Bollag *et al.* 1996a). Each gel comprised a 5% stacking gel and a 6-10% resolving gel depending on the protein of interest. Gels and buffers, prepared for making native PAGE gels are listed in Table 2.7.

| Gels/Buffers | Ingredients |
|---|---|
| 4x Resolving gel | 6-10% (w/v) acrylamide<br>0.1% (w/v) APS<br>0.1% TEMED<br>1.5 M Tris-HCl buffer, pH 8.8 |
| 4x Stacking gel | 5.0% (w/v) acrylamide<br>0.1% (w/v) APS<br>0.1% TEMED<br>0.5 M Tris-HCl buffer, pH 6.8 |
| 10x Running buffer | 192mM glycine<br>25mM Tris-HCl buffer, pH 8.8 |
| 5x Sample buffer | 0.05% (w/v) Bromophenol blue<br>50% (v/v) glycerol<br>312.5mM Tris-HCl buffer, pH 6.8 |

**Table 2.7: Native-PAGE gels/buffers used in this study**

Typically samples were re-suspended in 1x sample buffer with subsequent loading of samples onto the gel. Electrophoresis was carried out at constant voltage (100V) and 10mA/gel in 1x running buffer for 4-6 h. The gels were viewed after staining with Coomassie Brilliant Blue dye as described above (see section 2.4.3.1).

## 2.4.4 Protein purification

Details of all buffers used during protein purification are described in chapter 3.

### 2.4.4.1 Bacterial cell disruption

The pelleted bacteria were re-suspended in appropriate binding buffer (see chapter 3) in the presence of complete EDTA-free protease inhibitors (Roche, UK). Cells were disrupted by 4 passes through a French pressure cell at 950 psi (see section 2.4.2). The disrupted cells were then spun in a JA-17 rotor in a Beckman J2-MC centrifuge at 4$^{o}$C, 10,000xg for 15 min to remove non-soluble material.

### 2.4.4.2 Purification of His-tagged proteins

Recombinant proteins over-expressed with His-tag were purified by metal chelate affinity chromatography on a BioCAD SPRINT$^{TM}$ workstation (Applied Biosystems, USA) using a MC POROS 20 psi column (Applied Biosystems, USA; 7.8ml column volume (CV). The column was initially washed with 5 CV strip solution (50mM EDTA, 1M NaCl) to remove any remaining metal ions from a previous purification, followed by 5 CV $dH_2O$. The flow rate was kept constant at 10 ml/min. Zinc ions (100mM $ZnCl_2$) were loaded onto the column (30 CV) at pH 4.5 to minimize precipitation of metal hydroxide complexes. To remove excess zinc ions, the column was washed with 5 CV $dH_2O$ followed by 5 CV 0.5M NaCl. Prior to protein loading, the column was equilibrated with 5 CV elution buffer (100mM NaCl, 500mM imidazole, 50mM $KH_2PO_4$, pH 6.0) followed by 10 CV binding buffer (100mM NaCl, 10mM imidazole, 50mM $KH_2PO_4$, pH 8.0).

The cell lysates (20ml) (section 2.4.4.1) were then applied to the column in 5ml aliquots and the column washed thoroughly in binding buffer. After the final injection the column was washed with 8 CV of binding buffer. The bound protein was eluted from the column in a 0-100% gradient of elution buffer (8 CV). Elution fractions (2ml) were collected and analysed by SDS-PAGE. Peak fractions were then pooled and either subjected to dialysis or concentrated for further use. The column was cleaned after use with 2 CV strip buffer (50mM EDTA, 1M NaCl) followed by 0.5M NaCl and $dH_20$. The column was stored in 20% (v/v) ethanol at room temperature.

#### *2.4.4.2.1 Cleavage of His-tag*

Purified His-tagged proteins were dialysed against appropriate buffer and concentrated (see section 2.4.5). Cleavage of the His-tag was achieved by adding 10 U thrombin (GE Healthcare, UK; supplied as a powder) per mg of protein and incubated with gentle shaking either at room temperature overnight or at 37 °C for 2-16 h. The quality of cleaved protein was determined by SDS-PAGE analysis (see section 2.4.3.1).

### 2.4.4.3 Purification of GST-tagged proteins

The purification of GST fusion proteins was achieved by using a glutathione Sepharose 4B column with bed volume 5ml (GE Healthcare, UK), attached to a BioCAD 700E$^{TM}$ workstation (Applied Biosystems, USA). The column was initially washed with 5 CV $dH_2O$ and then equilibrated with PBS (140mM NaCl, 2.7mM KCl, 10mM $Na_2HPO_4$, and 1.8mM $KH_2PO_4$,

pH 7.3) at 2.5ml/min. Protein samples (20ml) (see section 2.4.4.1) were passed through the column followed by 5 CV of PBS at a rate of 1.5 ml/min. To minimise non-specific binding, the column was washed with 12 CV PBS until a zero baseline was achieved. Protein was eluted from the column using 5 CV elution buffer (20mM reduced glutathione, 50mM Tris-HCl, pH 8.0). Elution fractions (2ml) were collected, analysed by SDS-PAGE (see section 2.4.3.1) and dialysed for further experiments.

#### *2.4.4.3.1 Removal of GST*

GST was removed from GST fusion proteins by thrombin cleavage. Purified protein (see section 2.4.4.3) was buffer exchanged into PBS buffer by concentration (see section 2.4.5). Thrombin was added at 10 U per mg protein and incubated at room temperature overnight. To confirm the cleavage, a number of samples were taken at various time intervals and viewed by SDS-PAGE (see section 2.4.3.1).

### 2.4.4.4 Purification of maltose binding proteins (MBP)

Maltose binding protein (MBP) affinity chromatography used to purify recombinant proteins tagged with MBP was carried out using a BioCAD 700E$^{TM}$ Workstation (Applied Biosystems, USA). A MBP Trap HP column (GE Healthcare, UK, bed volume, 5ml) was equilibrated with 6 CV binding buffer (200mM NaCl, 1.0mM EDTA, 20mM Tris-HCl, pH 7.4) at 2.5ml/min. Samples (20ml) were loaded at a rate of 1.5ml/min. The column was then washed with 10 CV binding buffer until the baseline returned to zero. The bound protein was eluted by washing the

column with 5 CV elution buffer (15mM maltose, 200mM NaCl, 1mM EDTA, 20mM Tris-HCl, pH 7.2) and fractions (2ml) were collected. The peak fractions were concentrated and visualised by SDS-PAGE after staining with Coomassie Brilliant Blue (see section 2.4.3.1).

Column regeneration was achieved by stripping with 5 CV 0.5M NaOH followed by an extended wash with $dH_2O$. The column was stored in 20% (v/v) ethanol at 4 $^oC$ for further use.

### 2.4.4.5 Gel filtration chromatography (GFC)

Gel filtration chromatography (GFC) or size exclusion chromatography is based on the ability of the gel filtration media to separate molecules according to size. A 120ml bed volume HiPrep 16/60 Sephacryl S-300 High Resolution column (GE Healthcare, UK) attached to a BioCAD 700E$^{TM}$ workstation (Applied Biosystems, USA) was equilibrated at room temperature with 2 CV of appropriate buffer at a flow rate of 1ml/min (see chapter 3). Typically, 1ml concentrated sample (see section 2.4.5) was injected onto the column at a flow rate of 1ml/min. Peak fractions were collected as 1ml fractions in running buffer at a flow rate of 1ml/min and visualised by SDS-PAGE (see section 2.4.3.1).

The column was cleaned after use with 0.1 CV 200mM NaOH followed by 2 CV $dH_20$ and stored in 20% (v/v) ethanol at room temperature for longer periods.

### 2.4.4.6 Purification of PDC and OGDC from bovine heart

PDC and OGDC from bovine heart were available in the laboratory (see chapter 6). Both complexes were purified as described by Stanley and Perham (Stanley and Perham 1980) with some modifications (De Marcucci and Lindsay 1985a). Bovine PDC and OGDC were stored at concentration of 10mg/ml in 50% (v/v) glycerol at -20°C.

## *2.4.5 Dialysis and protein concentration*

In order to match/exchange buffers for biophysical experiments, proteins were dialysed against 4-5L of the buffer of choice overnight at 4°C with continual stirring on a magnetic stirrer and a minimum of 3 buffer changes at 2 h time intervals. Dialysis was carried out using either dialysis tubing or dialysis cassettes (Pierce, USA) with an appropriate molecular mass cut off (10,000 MWCO) for the majority of experiments. Dialysis cassettes were employed according to manufacturer's instructions. Dialysis tubing membrane (size 9, diameter 1.125") was obtained from Pierce, USA and prepared as described by Bollag and colleagues (Bollag *et al.* 1996b). Alternatively, for low molecular mass proteins e.g. truncated N-terminal E1o (60 a.a.), 1KDa cutoff (2ml) tubes (supplied by Amersham, USA) were used according to the manufacturer's instructions.

Peak fractions following protein purification (see section 2.4.4) were pooled and concentrated using Amicon ultra concentrators with appropriate molecular mass cut offs (1KDa, 10kDa and 30kDa) supplied by Fisher chemicals, UK. Samples were centrifuged at 3,000xg in a Beckman Allegra $^{Tm}$ 6R centrifuge at 4$^{o}$C for 3-6 h until the desired volume was achieved.

### 2.4.5.1 Precipitation and concentration of protein by acetone

Appropriate protein concentration is essential for obtaining good results in SDS-PAGE. Acetone precipitation was employed for rapid protein concentration on occasions. Three volumes of ice-cold acetone were added to 200µl sample protein and kept for 20 min on ice. The sample was centrifuged at 13,000xg, 4 $^{o}$C for 6 min, the supernatant was discarded and the pellet air dried. For SDS-PAGE, the pellet was suspended in 20-50µl Laemmli sample buffer.

## *2.4.6 Determination of protein concentration*

Protein concentration was measured by absorbance of the protein at 280nm and its molar extinction coefficient (ε) (see section 2.4.6.2). Alternatively, protein concentration was determined by the Bradford method (Bradford 1976) (see section 2.4.6.3).

### 2.4.6.1 Spectrophotometric equipment

Bacterial growth $OD_{600}$ was measured using an Ultrospec 4300 pro UV/visible spectrophotometer in disposable plastic cuvettes. In addition, OGDC/PDC activity, inhibition assays (see chapter 6) and protein concentration on occasions were measured using a Shimadzu UV-2101 PC scanning spectro-photometer in UV quartz cuvettes (1ml, 10mm path-length, Jencons, USA).

### 2.4.6.2 Protein absorbance

Routinely, an Ultrospec 4300 Pro UV/visible spectrophotometer was used to determine protein absorbance at 280nm. Since E3 contains FAD, its estimation was carried out using the FAD extinction coefficient at 450nm. The molar extinction coefficient (ε) of the majority of protein constructs was determined by computing the protein sequence in the EXPASY suite (http://expasy.org/tools/protparam.html).

The molar concentration of the protein was calculated by dividing the measured protein absorbance at 280nm or at 450nm (in the case of E3) by the extinction coefficient, whereas the protein concentration in (mg/ml) was calculated by multiplying the molar concentrations by the respective molecular mass of the protein. To check for DNA or RNA contamination, the $A_{280}$:$A_{260}$ ratio of the protein was monitored. The molecular masses and extinction coefficients of proteins used in this study are listed in Table 2.8.

| Protein | Plasmid vector | Extinction coefficient ($M^{-1}cm^{-1}$) | Subunit molecular mass (Da) |
|---|---|---|---|
| E3 His-tag | pET-14b | 11,300 (FAD) | 52,885 |
| E2o His-tag | pET-14b | 11,585 | 43,585 |
| E2o His-tag | pET-28b | 11,585 | 43,585 |
| E3BP-SBD GST | pGEX-2T | 43,110 | 33,428 |
| E1o-60 His-tag | pET-14b | 15,470 | 9,021 |
| E1o-60 GST | pGEX-2T | 58,580 | 32,776 |
| E1o-60 MBP | pET-30a | 81,820 | 47,305 |
| E1o-90 His-tag | pET14b | 15,470 | 11,984 |
| E1o-90 GST | pGEX-2T | 58,580 | 35,944 |
| E1o-90 MBP | pET-30a | 81,820 | 50,474 |
| E1o-153 His-tag | pET-14b | 18,450 | 18,858 |
| E1o-153 GST | pGEX-2T | 61,560 | 42,856 |
| E1o-153 MBP | pET-30a | 84,800 | 57,372 |
| E1o His-tag | pET-14b | 122,825 | 111,175 |
| wt GST | pGEX-2T | 43,110 | 26,311 |
| wt MBP | pET-30a | 66,350 | 40,838 |
| Cleaved E1o-60 | -- | 15,470 | 6,485 |
| Synthetic Pep.: 1 | -- | 8,480 | 2,847 |
| Synthetic Pep.: 2 | -- | 6,990 | 2,721 |
| Synthetic Pep.: 3 | -- | 15,470 | 7,041 |

**Table 2.8: Molecular mass and extinction coefficients of proteins used in this study**
wt, wild-type.

### 2.4.6.3 Bradford method

The Bradford method (Bradford 1976) was also performed to determine protein concentration. Standard curves were plotted by using increasing concentrations of BSA (Sigma, UK). Unknown protein samples and standards were diluted in $dH_2O$ followed by adding 1ml Bradford reagent (BioRad, UK) (0.01% (w/v) Coomassie Blue G250, 5% (v/v) $H_3PO_4$ and 5% (v/v) ethanol) that complexes with the protein of interest. Samples were incubated at room temperature for 10 min prior to detection at 595 nm using a Shimadzu UV-2101 PC scanning spectrophotometer.

### 2.4.6.4 OGDC/PDC assays

Assay of overall OGDC and PDC activity was performed according to the method of Brown and Perham (Brown and Perham 1976). Assays were carried out at 30 $^{o}$C in plastic cuvettes. Typically, 10µg complex (OGDC or PDC) was added to the mixture containing 670µl solution A (3mM $NAD^+$, 2mM $MgCl_2$ , 0.2mM ThDP and 50mM potassium phosphate buffer, pH 7.6) and 14µl solution B (130mM cysteine-HCl and 6.8mM CoASH). The assay was initiated by addition of 14µl solution C (100mM 2-oxoglutarate for OGDC assays or 100mM pyruvate for PDC assays) and mixed rapidly. The OGDC and PDC activities were measured by monitoring NADH formation at 340nm using a Shimadzu UV-2101 PC scanning spectrophotometer. Activities were expressed as U/ml, where one unit (U) of activity is defined as the amount of enzyme required to convert 1µmol of substrate to product per minute under the conditions of the assay. Details of all buffers used for inhibition of OGDC and PDC activities using N-terminal E1o and E3BP-SBD constructs are described in chapter 6.

## 2.4.7 Western blotting

Proteins to be immunoblotted were resolved by SDS-PAGE and transferred electrophoretically onto nitrocellulose membrane (ECL Hybond, Amersham) in the presence of transfer buffer (192mM glycine, 20% (v/v) methanol, 25mM Tris-HCl, pH 7.3) at 30 V, 200mA for 2 h using Cell II™ blotting system supplied by Invitrogen. After transfer the nitrocellulose membrane was stained with Ponceau S dye (Sigma, UK) to allow the visualization of the transferred proteins. The nitrocellulose membrane was then washed with $dH_2O$ to remove stain prior to immunoblotting. At this step, the immunoblotting methodology differs slightly depending on the primary antibody as described below.

### 2.4.7.1 Anti-His-tag antibody

The nitrocellulose membrane was blocked overnight with Qiagen blocking buffer (0.1g blocking powder, 1ml blocking reagent buffer, 1% (v/v) Tween-20) at 4 °C with continuous shaking in order to prevent non-specific binding. The membrane was then washed 3 x 10 min in TBST buffer (150mM NaCl, 0.1% (v/v) Tween-20, 50mM Tris-HCl, pH 7.4). The wash buffer was discarded and the membrane incubated with a 1:2000 dilution of the QIAexpress Penta-His HRP conjugate antibody (Qiagen, UK) for 2 h with shaking at room temperature. QIAexpress Penta-His antibody was already conjugated with horseradish peroxidase; therefore no secondary antibody was required. At this point, extensive washes with TBST were performed to remove any unbound antibody.

Detection was carried out using enhanced chemiluminescence (ECL western blotting detection kit) (GE Healthcare, UK) as per the manufacturer's instructions. Chemiluminescence was then visualised using X-ray film (Kodak, UK). Exposure times were typically 1min.

### 2.4.7.2 Anti-GST antibody

Following protein transfer, membranes were blocked overnight with Qiagen blocking buffer at 4 °C with continuous shaking. The membrane was then incubated with a 1:5000 dilution of the anti-GST HRP conjugate antibody (GE Healthcare, UK) for 1 h with shaking at room temperature. After that the membrane was washed three times in TBST buffer for 10 min each time to remove excess antibody. As anti-GST antibody has the secondary horseradish peroxidase (HRP) antibody attached to it, no secondary antibody is required. Protein blots were developed using the ECL western blotting detection kit (GE Healthcare, UK) according to the manufacturer's instructions and exposed on X-ray film (Kodak, UK).

### 2.4.7.3 Other antibodies

After transferring protein onto the nitrocellulose membrane, the membrane was incubated overnight with blocking buffer (15mM NaCl, 5% (w/v) non-fat dried milk, 0.25% (v/v) Tween-20, 20mM Tris-HCl buffer, pH 7.2) at 4°C with continuous shaking. The nitrocellulose membrane was then washed 3 x 5 min in TBST buffer. Primary antibody (polyclonal anti-bovine E3 or E1o rabbit anti-bodies) and secondary antibody (anti-rabbit IgG) incubation was carried out in TBST buffer containing 5% (w/v) non-fat dried milk. Membrane was incubated with the

primary antibody for 1 h on a shaker at room temperature at a 1:1000-3000 dilution. The nitrocellulose membrane was then washed 3 x 5 min in TBST buffer in order to remove unbound primary antibody. The anti-rabbit IgG secondary antibody (Sigma, UK) was applied (1:20,000 dilution) for 1 h at room temperature with continuous shaking. This was followed by 4 wash cycles of TBST buffer, each for 10 min time intervals. Protein blots were developed using the ECL western blotting detection kit (GE Healthcare, UK) according to the manufacturer's instructions and exposed on the X-ray film (Kodak, UK).

#### 2.4.7.4 Stripping the nitrocellulose membrane

Following detection of proteins by ECL, nitrocellulose membranes can be stripped of bound antibody and re-probed with a different antibody. The membrane was washed 3 x 10 min in TBST buffer at room temperature. The wash buffer was discarded and the membrane was incubated with the stripping buffer (0.1% (w/v) SDS, 1% (v/v) Tween-20, 200mM glycine, pH 2.2) at room temperature with continuous shaking. At this stage the membrane was incubated with PBS (130mM NaCl, 27mM KCl, 4.3mM $Na_2HPO_4$, 1.4mM $KH_2$ $PO_4$ , pH 7.4) at room temperature with continuous shaking. The nitrocellulose membrane was then washed 3 x 5 min in TBST buffer in order to prepare the membrane for the next immunoblot.

### 2.4.8 Peptide Arrays

Peptide libraries were produced by automatic SPOT synthesis and synthesised on continuous cellulose membrane supports on Whatman 50 cellulose membranes using Fmoc-chemistry with the AutoSpot-Robot ASS 222 (University of Glasgow). Nitrocellulose membrane was equilibrated in absolute ethanol followed by shaking for 10 min and washing with TBST buffer (150mM NaCl, 0.1% (v/v) Tween-20, 50mM Tris-HCl, pH 7.4) at room temperature. Excess binding sites were blocked by immersing the nitrocellulose membrane in Qiagen blocking buffer (0.1g blocking powder, 1ml blocking reagent buffer, 1% (v/v) Tween-20) for 2 h at room temperature.

Protein was added (10-15μg/ml) with shaking overnight in the cold room. The membrane was washed three times with TBST buffer, each for 15 min. After these washes, the membrane was incubated with a 1:2000 dilution of the QIAexpress Penta-His HRP conjugate antibody (Qiagen, UK) at room temperature for 2 h (in the case of anti-His tag antibody which is already conjugated with horseradish peroxidase, no secondary antibody is required). Excess antibody was removed by several changes of TBST buffer after incubation for 10 min at room temperature with shaking.

Detection of immune complex was carried out according to the manufacturer's instructions employing the ECL western blotting reagents kit (GE Healthcare, UK).

## 2.4.9 Synthetic Peptides

Synthetic peptides used in this study corresponding to segments of the N-terminal region of E1o were obtained from Genscript, UK. Synthetic peptides were synthesized by GenScript's FlexPeptide™ technology. In addition, a 65-meric peptide corresponding to amino acids Ser11 to Glu75 of the E1o N-terminal region was purchased from LifeTein LLC., USA. Synthetic peptide purity (>90%) was confirmed by mass spectrometry and analytical HPLC. Stock concentrations (>10 mg/ml) of the peptides were prepared in the buffer of choice by vigorous pipetting, and the working concentrations prepared by further dilution. The synthetic peptides used in this study are listed in Table 2.9.

| Synthetic peptides | Sequence | Number of amino acids | Molecular mass (Da) | Purity |
|---|---|---|---|---|
| Synthetic Pep. 1 | SGTSSNYVEEMYCAWLENPKSVHKS | 25 | 2,847 | 95 % |
| Synthetic Pep. 2 | WDIFFRNTNAGAPPGTAYQSPLPLS | 25 | 2,721 | 98% |
| Synthetic Pep. 3 | SGTSSNYVEEMYCAWLENPKSVHKSWDIFFRNTNAGAPPGTAYQSPLPLSRGSLAAVAHAQSLVE | 65 | 7,041 | 91% |

**Table 2.9: Synthetic peptides used in this study**

# 2.5 Biophysical methods

## 2.5.1 Circular dichroism (CD)

Circular dichroism was used to perform secondary structural characterisation of peptides covering the N-terminal region of E1o. CD measures differences in the absorption of left-handed polarized light versus right-handed polarized light which arise due to structural asymmetry. Proteins were dialysed against 20mM $KH_2PO_4$ buffer, pH 7.5 overnight at 4 °C and protein concentrations adjusted as required. CD experiments were performed at room temperature on a Jasco J-810 spectro-polarimeter scanning the spectra in the far and near UV regions at a scan speed of 50nm/min and a bandwidth of 1nm. All CD experiments were performed and analysed in collaboration with Dr. S. Kelly, University of Glasgow.

## 2.5.2 Isothermal titration calorimetry (ITC)

Isothermal titration calorimetry (ITC) is a quantitative method for analyzing molecular interactions (affinity, thermodynamics and stoichiometry). ITC measures the heat absorbed or heat released due to the binding reaction between the molecules under investigation. This straightforward technique allows for direct determination of a complete thermodynamic profile comprising changes in enthalpy ($\Delta H^o$), entropy ($\Delta S^o$), and in Gibbs free energy ($\Delta G^o$), stoichiometry of binding ($N$) and association constant ($K_a$). The $\Delta G^o$ is calculated from the Gibbs equation $\Delta Go = -RT\ln Ka$ or $\Delta Go = \Delta H^o - T\Delta S^o$.

Briefly, ITC experiments are performed using a method of titration where the ITC instrument consists of two cells (reference cell and sample cell) are contained within an adiabatic jacket and a syringe containing a ligand that is injected into a sample cell. A series of injections (approx. 28 injections), 10µl each are performed at 3 min time-intervals. Protein concentration in the syringe was 15-20 fold more concentrated than the cell sample protein. During the injection of the protein into the sample cell, heat is released or absorbed depending on whether the reaction is exothermic or endothermic and the heat signal will approach zero when the saturation is achieved. Titrations of protein into buffer as a control reaction were performed and subtracted from the integrated binding data. The peak of each injection is related to the heat change associated with the reaction. Fitting of the isotherm gives the complete thermodynamic profile parameters.

ITC was used to determine the affinity and ratio of binding between E2o, E3 and/or N-terminal E1o constructs as described by Jung and colleagues (Jung *et al.* 2002). ITC experiments were carried out in a VP-ITC microcalorimeter (MicroCal Inc., USA).

All proteins were dialysed overnight against the buffer of choice. Data were analysed using non-linear regression in the MicroCal ORIGIN software package, assuming a simple binding model. ITC experiments and analyses were performed in collaboration with Mrs. Margaret Nutley, University of Glasgow.

### 2.5.3 Mass spectrometry

Mass spectrometry is a useful tool for biochemical research. It is an analytical technique used to measure the mass-to-charge ratio of proteins. It gives accurate molecular mass measurements that help to confirm the purity of the samples. Mass spectroscopy analysis was carried out by the Astbury centre, University of Leeds, UK. Samples were prepared by dissolving protein (50-100μM) in 20mM ammonium acetate, pH 7.5.

## 2.6 Bioinformatic methods

### 2.6.1 Database screens

NCBI (http://www.ncbi.nlm.nih.gov/sites/entrez?db=protein), Prosite (http://prosite.expasy.org), Pfam (http://www.sanger.ac.uk) and SSDB (http://www.kegg.jp/kegg/ssdb/) databases were used for screening human proteins, isoforms and motifs and were sorted according to their species of origin.

### 2.6.2 Blast searches

In order to search for protein homology and sequence similarity, BLASTP online software with parameters (Human, database: non-Ref seq. protein, expect=0.001, filter: default, compare protein sequence) of the NCBI-BLAST suite (http://blast.ncbi.nlm.nih.gov/Blast.cgi) was used.

### 2.6.3 Sequence alignments

Sequence comparison and alignments between two sequences were computed using LALIGN (http://www.ch.embnet.org/software/LALIGN_form.html) with settings (Alignment method: local, number of reported sub-alignments:3, matrix: default, opening gap penalty: -14, extending gap penalty:-4). Alignment of multiple sequences was carried out using the ClustalW2 program (http://www.ebi.ac.uk/Tools/msa/clustalw2/) with default settings and sequences submitted in FASTA format.

### 2.6.4 Protein structure predictions

To predict the possible 3D structure of the E1o N-terminal region that has no apparent sequence similarity to the SBDs of E2p, E2b and E3BP-PDC, on-line platforms for protein structure predictions I-TASSER (http://zhanglab.ccmb.med.umich.edu/I-TASSER/) and SWISS-MODEL (http://swissmodel.expasy.org) were employed.

A 3D model structure was also built based on multiple-threading alignments by LOMETS (http://zhanglab.ccmb.med.umich.edu/LOMETS/). Amino acid sequences were supplied in FASTA format. Alignment of structures was carried out using the TM-align program (http://zhanglab.ccmb.med.umich.edu/TM-align/) and structures submitted in pdb format.

## 2.7 Data analysis

Statistical analysis of the data and graph production in chapter 6 were performed on a personal computer using the stat-graphics computer software EXCEL (ver. 2007 for Windows, Microsoft Office) to obtain the standard deviation (SD), standard error (SE), standard error of the mean (SEM) and student t-test. Assays were carried out in triplicate. Student t-test values were represented as the significance of the difference between two groups of samples.

# Chapter 3

# Cloning, protein over-expression and purification

## 3.1 Introduction

Recombinant DNA technology is a powerful approach in the study of molecular biology. It has proved to be an ideal biological tool for the production and investigation of specific proteins in biology or biomedical science and has many practical applications in medicine, industry and agriculture. For example, a large number of medically- important proteins are now produced in this way and have replaced their animal equivalents in the treatment of human diseases e.g. human follicle-stimulating hormone (Loumaye *et al.* 1995), human growth hormone (Goeddel *et al.* 1979a), insulin (Goeddel *et al.* 1979b) and somatostatin (Itakura *et al.* 1977).

To achieve stabilisation and/or facilitate purification of recombinant proteins in *E. coli*, several affinity tags have been produced including his-tags (His), glutathione S-transferase (GST), maltose binding protein (MBP) and calmodulin binding protein (CBP). Use of MBP is based on its affinity for amylose on chromatography resins. The pGEX-2T vector contains a GST tag (26 kDa polypeptide) attached to the N- or C-terminus of the target protein and binds glutathione on affinity columns. MBP and GST tags have been employed routinely to increase the solubility of small proteins or individual domains expressed in *E. coli*. His tags are sequences of 6-10 histidine residues attached to the N- or C-terminus that can bind metal ions ($Ni^{2+}$, $Zn^{2+}$ or $Co^{2+}$) exploiting the high affinity of imidazole for these ions (Lindner *et al.* 1992). His tags have also been known to increase the overall solubility of the protein and improve protein folding. The pET-14b plasmid is a powerful system developed for expression of recombinant proteins in

*E. coli*. It has a T7 promoter and encodes a six histidine (His) sequence at its 5' terminus followed by a thrombin cleavage site, three cloning sites and a T7 terminator. Recombinant protein expression is dependent on the cell strain and several conditions e.g. composition of the medium, temperature and the sequence of the protein under investigation. Bacterial strains demonstrate a higher degree of recombinant protein tolerance than mammalian cells. Expression at 30-37 $^{o}$C often produces maximum yields of protein, although there is a greater tendency to form inclusion bodies caused by aggregation and improper protein folding.

Human OGDC and PDC are major multi-enzyme assemblies that control vital committed steps in carbohydrate metabolism. The subunit organization of OGDC is the least studied and most poorly understood compared to PDC and BCOADC. Most previous studies have employed native complex purified from various organisms; however, the separation of individual components has proved difficult owing to the tight association of E1o with the E2o core. Moreover, the components of 2-oxoacid dehydrogenase complexes (OGDC, PDC, and BCOADC) are all encoded by the nuclear genome and transported post-translationally to mitochondria prior to assembly (Thekkumkara *et al.* 1988; Maas and Bisswanger 1990; Wang *et al.* 2002). To resolve difficulties in simulating and studying assembly using the native complex, access to recombinant proteins is increasingly able to resolve many of these challenges.

For example, individual recombinant PDC enzymes have been successfully over-expressed in *E. coli* and subsequently purified and reconstituted to yield fully-active complex (unpublished data, G. Singh, 2008) with a similar specific activity to native human heart PDC (Palmer *et al.* 1993). Previously, constituent components of PDC had been successfully produced by

recombinant DNA technology on several occasions (Leung *et al.* 1990; Quinn *et al.* 1993; Ciszak *et al.* 2001; Ciszak *et al.* 2003; Hiromasa *et al.* 2004; Smolle *et al.* 2006). However, a mammalian OGDC recombinant model has not yet been established owing to difficulties in producing active full-length E1o, although recombinant E2o from various organisms have been successfully over-expressed (Berg *et al.* 1995; Ricaud *et al.* 1996; Knapp *et al.* 1998; Jones *et al.* 2000; Koike *et al.* 2000; Suzuki *et al.* 2002; Nakai *et al.* 2008).

Human OGDC is built around a 24-meric E2o 'core' enzyme, to which multiple copies of E1o and E3 bind tightly but non-covalently. It differs significantly from PDC/BCOADC, as it does not contain any SBD for E1o or E3 and there is no equivalent to E3BP in this complex. Hence, human E2o has a unique structure comprising only two domains (LD and CTD), unlike E2p and E2b (Reed and Hackert 1990; Perham 1991; Wallis *et al.* 1996; Sanderson *et al.* 1996a; Knapp *et al.* 1998; Frank *et al.* 2005). Previous selective proteolysis and immunological analysis in our laboratory has suggested that the N-terminal region of mammalian E1o may be important for maintaining the structural integrity of the OGDC by interacting with both E2o and E3 (Rice *et al.* 1992; McCartney *et al.* 1998). Therefore, the major objective of this thesis is to investigate the role of E1o N-terminal region in maintaining the structural integrity of the OGDC and to map/identify the precise region thought to be involved in maintaining critical contacts with E3 and possibly also E2o.

The main purpose of this chapter is to describe the cloning, expression and purification of 9 short E1o N-terminal constructs based on peptide array data (chapter 4). Three are in His-tag form (60, 90 and 153 a.a.s), three produced as GST-fusion proteins (60, 90 and 153 a.a.s)

and three as MBP-fusion proteins (60, 90 and 153 a.a.s) corresponding to the putative binding regions for E2o/E3 interaction in order to obtain a better understanding of the subunit organisation of this complex. Subsequently, the recombinant proteins purified in this chapter were tested for their ability to bind to E2o and E3 both *in vitro* and *in vivo* (chapter 4 & chapter 5).

Initial attempts were also made in this chapter to produce a recombinant active human OGDC by cloning and expression of mature human E1o and by expression and purification of human E2o and E3.

# 3.2 Materials and Methods

## 3.2.1 Cloning

### 3.2.1.1 Cloning of N-terminal E1o constructs (E1o-60, E1o- 90 and E1o-153) in pET-14b (His-tag form)

N-terminal E1o-60 truncate (11-70 a.a), N-terminal E1o-90 truncate (1-90 a.a), and N-terminal E1o-153 truncate (1-153 a.a) were cloned directly into the pET-14b vector. Primers were designed to the relevant 5' and 3' regions of human mitochondrial E1o cDNA (heart isoform; OGDH-H). All oligonucleotides were ordered from Sigma, UK on the 25 mmol scale. While the E1o-60 fragment was cloned into the *BamHI* restriction site for insertion into pET-14b, the E1o-90 and E1o-153 fragments were engineered with *NdeI* and *BamHI* restriction sites at the 5' and 3' termini to permit directional cloning. To clone E1o-60 into pET-14b, an

extra base was incorporated before the start codon to confer the correct reading frame. The forward and reverse primers and restriction sites are shown in Figure 3.1.

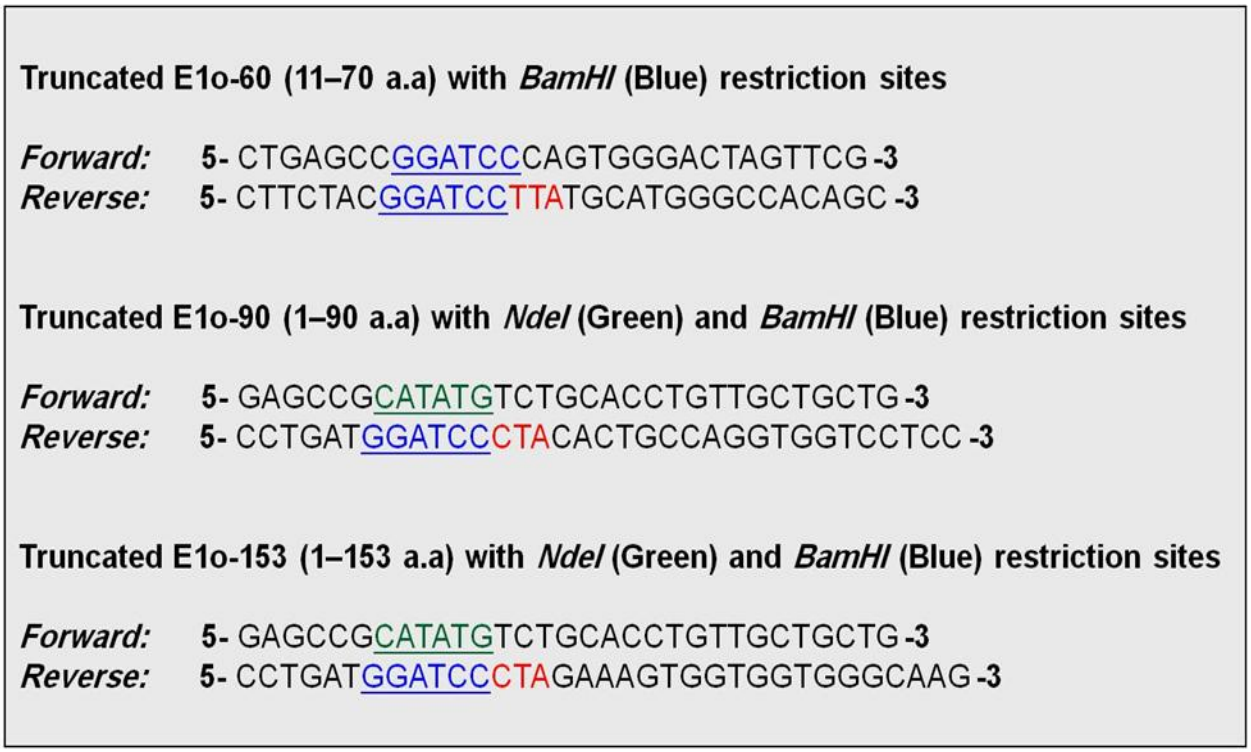


**Figure 3.1: Primer sequences for the truncated N-terminal E1o constructs: E1o-60, E1o-90 and E1o-153 (His-tag form)**
Restriction endo-nuclease recognition sites are underlined and coloured. Stop codons are indicated in red.

The 5' region of human E1o (1-166 a.a), previously cloned in the laboratory into pET-14b by G. Singh (2008), was used as a PCR template to produce 5' constructs of E1o encoding the fragments 60 a.a and 90 a.a into pET-14b. A putative E1o human cDNA clone obtained from Source Bioscience Ltd, UK was used as the PCR template to amplify and clone the 5' end of mature human E1o (1-153 a.a) into pET-14b. To minimise errors in base incorporation, the

reactions were set up using the Expand High Fidelity PCR System (Roche, USA). PCR was carried out in a 50µl reaction volume containing 200µM of each dNTP, 1.5 mM $MgCl_2$, 1x PCR buffer, 80ng template DNA, 2.0U *Taq* polymerase (Roche), sterile water and 0.2µM of each primer. Negative control reactions without DNA template were also set up and PCR was carried out as shown in Table 3.1.

| | Step | Temperature ($^oC$) | Time |
|---|---|---|---|
| **1** | Initial denaturation | 94 | 1 min |
| **2** | Denaturation | 94 | 18 s |
| **3** | Annealing | 50 | 30 s |
| **4** | Extension | 72 | 50 s |
| **5** | Repeat steps 2-4 for 25 cycles | | |
| **6** | Extension | 72 | 5 min |
| **7** | Cooling | 4 | 1-24 h |

**Table 3.1: PCR cycle reactions: E1o-60, E1o-90 and E1o-153 (His-tag form)**
PCR programme using Expand High Fidelity DNA Polymerase.

The quality and quantity of PCR products was assessed on a 1.5-2% (w/v) agarose gel alongside a 1kb DNA Step Ladder. The PCR product was excised from an agarose gel under UV light, using a sterile scalpel and purified using Qiagen gel extraction kit (see section 2.2.5).

The E1o-60 PCR product and pET-14b vector were digested with *BamHI* to generate cohesive ends. To prevent pET-14b self-ligation, 5'-phosphates were removed by adding 1 unit of calf intestinal alkaline phosphatase for 30 min subsequent to digestion. The E1o-90 and E1o-153 PCR products were digested with *Nde*I and *BamHI* for directional insertion into the vector as described in section 2.2.8. Both digested plasmid and digested PCR products were run on a 1.5-2% (w/v) agarose gel and purified as described in section 2.2.5.

Ligation reactions were set up using the T4 Quick Ligation Kit from New England Biolabs (UK). Different ratios (1:1, 1:3 and 1:5) of linear plasmid and insert were ligated including a mixture containing the plasmid only as a negative control. The reaction was performed using 1µl T4 DNA ligase, and 1µl reaction buffer (10x). The reaction was incubated overnight at room temperature before transformation into *E. coli* DH5α.

The correct sequence and orientation of the constructs was confirmed by restriction digestion and sequencing. Diagnostic digestion was performed using *BamHI* (for the E1o-60 clone) or *Nde*I and *BamHI* (for the E1o-90 & E1o-153 clones) as described in section 2.2.8. Digests were subsequently analysed by agarose gel electrophoresis. The recombinant plasmids were sent for DNA sequencing (University of Dundee) to confirm the exact coding sequence.

### 3.2.1.2 Cloning of N-terminal E1o constructs (E1o-60, E1o-90 and E1o-153) in pGEX-2T (GST-fusion proteins)

Recombinant plasmid (pET-14b) encoding the human N-terminal E1o (1-166 a.a) (G. Singh, 2008) and a putative E1o human cDNA clone (Source Bioscience Ltd, UK) served as templates to amplify the N-terminal E1o-60 truncate (11-70 a.a), N-terminal E1o-90 truncate (1-90 a.a), and the N-terminal E1o-153 truncate (1-153 a.a) respectively. Subsequently, PCR products were cloned into pGEX-2T via the TOPO TA cloning kit (Invitrogen). Primers (Sigma, UK) with appropriate restriction sites employed in the PCR reaction are shown in Figure 3.2.

**Truncated E1o-60 (11–70 a.a) with *BamHI* (Blue) restriction sites**

***Forward:*** **5-** GAGCCCGGATCCAGTGGGACTAGTTCG **-3**
***Reverse:*** **5-** CTTCTACGGATCCTTATGCATGGGCCACAGC **-3**

**Truncated E1o-90 (1–90 a.a) with *BamHI* (Blue) and *EcoRI* (Green) restriction sites**

***Forward:*** **5-** GAGCCGGGATCCTCTGCACCTGTTGCTGCTG **-3**
***Reverse:*** **5-** CCTGATGAATTCCTACACTGCCAGGTGGTCCTCC **-3**

**Truncated E1o-153 (1–153 a.a) with *BamHI* (Blue) restriction sites**

***Forward:*** **5-** GAGCCGGGATCCTCTGCACCTGTTGCTGCTG **-3**
***Reverse:*** **5-** CCTGATGGATCCCTAGAAAGTGGTGGTGGGCAAG **-3**

**Figure 3.2: Primer sequences for the truncated N-terminal E1o constructs: E1o-60, E1o-90 and E1o-153 (GST-fusion proteins)**
Restriction endo-nuclease recognition sites are underlined and coloured. Stop codons are indicated in red.

Amplification was carried out using the Expand High Fidelity PCR System (Roche, USA). Typically, PCR was carried out in a 50µl reaction volume containing 0.25mM dNTP, 2.0mM $MgCl_2$, 1x PCR buffer, 100ng template DNA, 2.0U *Taq* polymerase (Roche), sterile water and 0.2µM of each specific primer (forward and reverse) which were pre-heated to 95 $^{o}$C for 5 min. Negative control reactions were also performed. Details of the PCR cycle times and reaction temperatures are listed in Table 3.2.

| | Step | Temperature ($^{o}$C) | Time |
|---|---|---|---|
| **1** | Initial denaturation | 95 | 2 min |
| **2** | Denaturation | 95 | 15 s |
| **3** | Annealing | 50 | 30 s |
| **4** | Extension | 72 | 45 s |
| **5** | Repeat steps 2-4 for 24 cycles | | |
| **6** | Extension | 72 | 7 min |
| **7** | Cooling | 4 | 1-24 h |

**Table 3.2: PCR cycle reactions: E1o-60, E1o-90 and E1o-153 (GST-fusion proteins)**
PCR programme using Expand High Fidelity DNA Polymerase.

PCR samples were analysed by agarose gel electrophoresis on a 1.5-2% (w/v) agarose gel and the DNA extracted from the gel as described in section 2.2.5. The TOPO TA cloning vector system was used as described in section 2.2.7 to facilitate cloning of PCR products of N-terminal E1o-60 truncates (11-70 a.a), E1o-90 (1-90 a.a) and E1o-153 (1-153 a.a) into the pGEX-2T vector. The cloning was performed according to the manufacturer's specifications via the

pCR2.1-TOPO vector (see section 2.2.2). TOPO cloning and pGEX-2T vectors were subjected to restriction digestion according to the clone of interest. The E1o-60 and E1o-153 PCR products from the TOPO cloning vector were digested with *BamHI* to generate cohesive ends. For the single restriction digests, the digested pGEX-2T vector was treated with calf intestinal phosphatase for 1 h at 37 $^{o}$C to remove phosphate groups in order to prevent self-ligation. The E1o-90 PCR product from the TOPO cloning vector was digested with *BamHI* and *EcoRI* for cloning into the vector as described in sections 2.2.7 and 2.2.8. After digestion, PCR products from the TOPO cloning vector and pGEX-2T vector were run on a 1.5-2% (w/v) agarose gel and purified using the gel extraction kit. DNA was eluted in 30µl elution buffer as described in section 2.2.5.

A series of ligation reactions were set up using the T4 Quick Ligation Kit with varying ratios of insert:vector (1:1, 1:3 and 1:5) plus a control reaction without insert as described in section 3.2.1.1. The ligation mixes were incubated overnight at room temperature and transformed into TOP10 chemically competent cells (Invitrogen, UK) the following day. The transformations were placed on LB-agar plates supplemented with 50µg/ml ampicillin and incubated overnight at 37°C. To confirm the presence of an insert of the correct size, diagnostic digests were performed on the purified recombinant plasmids using *BamHI* - *EcoRI* (for the E1o-90 clone) or *BamHI* (for the E1o-60 and E1o-153 clones) as described in section 2.2.8. DNA was gel-purified and analysed on 1.5-2% (w/v) agarose gels alongside a 1kb DNA ladder. The recombinant plasmids were sent for DNA sequencing (University of Dundee) to confirm the exact coding sequence.

### 3.2.1.3 Cloning of N-terminal E1o constructs (E1o-60, E1o-90 and E1o-153) in pET-30a (MBP-fusion proteins)

A putative clone of E1o human cDNA (Source Bioscience Ltd, UK) was used as the PCR template to amplify and clone the 5' end of mature human E1o-60 (11-70 a.a), E1o-90 (1-90 a.a) and E1o-153 (1-153 a.a) into pET-30a. The maltose binding protein (MBP) cloned into the pET-30a vector was kindly gifted by Dr. Brian Smith, Glasgow University.

Oligonucleotides (Sigma, UK) were designed to the 5' and 3' regions included *BamHI* and *HindIII* sites that were used for cloning all 3 constructs. The forward and reverse primers and restriction sites are shown in Figure 3.3.

**Truncated E1o-60 (11–70 a.a) with *BamHI* (Blue) and *HindIII* (Green) restriction sites**

***Forward:*** **5-** GAGCCGGGATCCAGTGGGACTAGTTCGAAC **-3**
***Reverse:*** **5-** CTTGTACAAGCTTCTATGCATGGGCCACAGC **-3**

**Truncated E1o-90 (1–90 a.a) with *BamHI* (Blue) and *HindIII* (Green) restriction sites**

***Forward:*** **5-** GAGCCGGGATCCTCTGCACCTGTTGCTGCTG **-3**
***Reverse:*** **5-** CCTGATAAGCTTCTACACTGCCAGGTGGTCCTC **-3**

**Truncated E1o-153 (1–153 a.a) *BamHI* (Blue) and *HindIII* (Green) restriction sites**

***Forward:*** **5-** GAGCCGGGATCCTCTGCACCTGTTGCTGCTG **-3**
***Reverse:*** **5-** CCTGATAAGCTTCTAGAAAGTGGTGGTGGGCAAG **-3**

**Figure 3.3: Primer sequences for the truncated N-terminal E1o constructs: E1o-60, E1o-90 and E1o-153 (MBP-fusion proteins)**
Restriction endo-nuclease recognition sites are underlined and coloured. Stop codons are indicated in red.

PCR was performed using the Expand High Fidelity PCR System (Roche, USA) in the same manner as the PCR amplification for production of GST-fusion proteins as described above (section 3.2.1.2) with some modifications in conditions of activation, denaturation and annealing. The reaction cycles comprising 7 steps are shown in Table 3.3.

| | Step | Temperature ($^{o}$C) | Time |
|---|---|---|---|
| **1** | Initial denaturation | 94 | 2 min |
| **2** | Denaturation | 94 | 45 s |
| **3** | Annealing | 55 | 45 s |
| **4** | Extension | 72 | 1 min |
| **5** | Repeat steps 2-4 for 26 cycles | | |
| **6** | Extension | 72 | 10 min |
| **7** | Cooling | 4 | 1-24 h |

**Table 3.3: PCR cycle reactions: E1o-60, E1o-90 and E1o-153 (MBP-fusion proteins)**
PCR programme using Expand High Fidelity DNA Polymerase.

Following PCR, samples were subjected to agarose gel electrophoresis on a 1.8% (w/v) gel and the DNA purified from the gel. The PCR product and pET-30a vector were digested with *BamHI* and *HindIII* for directional insertion into the vector as described in section 2.2.8. Purified digested PCR products for ligation into pET-30a was also performed by the same routine ligation protocol using the T4 Quick Ligation Kit with various ratios of insert:vector (1:1, 1:3 and 1:5) as described in section 3.2.1.1. Plasmids were then digested with *BamHI* and *HindIII* to confirm the presence of an insert of the correct size as described in section 2.2.8. DNA was sent for sequence confirmation as previously described.

### 3.2.1.4 Cloning of human full-length E1o in pET-14b (His-tag form)

A putative E1o human cDNA clone (IMAGE ID 100004510-OCAA-22-D1) obtained from Source Bioscience Ltd, UK was used as the PCR template to amplify and clone mature human E1o (2886bp) into pET-14b. Primers (Sigma, UK) were designed to the 5' and 3' regions of mature human E1o cDNA with the introduction of *NdeI* and *XhoI* restriction sites. Both ends (5' and 3' termini) of the primer were typically designed with a CG clamp to increase binding efficiency. Primers with appropriate restriction sites employed in the PCR reaction are shown in Figure 3.4.

**Full-length E1o with *NdeI* (Blue) and *XhoI* (Green) restriction sites**

***Forward:*** **5-** GTTTCTTCATATGTCTGCACCTGTTGCTGCTGAGCCC**-3**
***Reverse:*** **5-** GTTTCTTCTCGAGCTAGTGGGTCTTCTTGTTGCCGGTGGC **-3**

**Figure 3.4: Primer sequences for the full-length E1o construct (His-tag form)**
Restriction endo-nuclease recognition sites are underlined and coloured. Stop codons are indicated in red.

PCR reactions were set up using the Expand High Fidelity PCR System (Roche, USA). A typical reaction mixture in a total volume of 50µl included 2mM $MgCl_2$, 1µl dNTP mix (0.25mM each of dATP, dCTP, dGTP, and dTTP), 1µl pre-heated (95 °C) specific forward and reverse primers, 50ng of DNA template, 5µl reaction buffer (10x) and 2.6 U of Expand polymerase prepared in a

total volume of 50µl with sterile $dH_2O$. Negative control reactions without DNA template were also set up. PCR cycles are shown in Table 3.4.

| | Step | Temperature ($^oC$) | Time |
|---|---|---|---|
| **1** | Initial denaturation | 95 | 2 min |
| **2** | Denaturation | 95 | 15 s |
| **3** | Annealing | 50 | 30 s |
| **4** | Extension | 72 | 3.3 min |
| **5** | Repeat steps 2-4 for 26 cycles | | |
| **6** | Extension | 72 | 7 min |
| **7** | Cooling | 4 | 1-24 h |

**Table 3.4: PCR cycle reactions: human full-length E1o (His-tag form)**
PCR programme using Expand High Fidelity DNA Polymerase.

PCR samples were analysed by gel electrophoresis on a 1% (w/v) agarose gel and the DNA extracted as described in section 2.2.5. The PCR product and plasmid were digested with *NdeI* and *XhoI* for directional insertion into the vector. Typically, digests were performed at 37°C in a total volume of 60µl containing 30µl DNA, *NdeI* (5U/µl) and *XhoI* (5U/µl) in appropriate reaction buffer for 3 h. Both digested plasmid and PCR products were run on a 1% (w/v) agarose gel and purified as described in section 2.2.5.

PCR fragments containing the desired sticky ends were ligated directly into appropriately digested pET-14b. Ligation reactions were performed by the same routine ligation protocol described in section 2.2.9. However, the ligation was conducted at various ratios of vector to insert (1:1, 1:3 and 1:5) in a total volume of 20µl. The resultant recombinant DNA was transformed into *E. coli* DH5α cells which were grown overnight at 37$^{o}$C on LB plates containing 50µg/ml ampicillin (see section 2.3.4). Individual colonies were then grown overnight at 37$^{o}$C in 5ml aliquots of ampicillin-supplemented LB. Plasmid purification was carried out as described in section 2.2.3. Diagnostic digestion was performed using *NdeI* and *XhoI* as described in section 2.2.8. Recombinant plasmids with appropriate sequencing primers were sent for DNA sequencing (University of Dundee) to confirm the exact coding sequence (see section 2.2.10).

## 3.2.2 Protein over-expression

All His-tagged constructs encoding E1o, E2o and E3 were expressed in *E. coli* BL21 (DE3) pLysS whereas E1o-60, E1o-90 and E1o-153 were expressed in the *E.* coli BL21 Star (DE3) pLysS strain. GST and MBP constructs were also transformed into *E. coli* BL21 (DE3) pLysS. Protein over-expression of His-tag, MBP and GST fusion proteins was performed using a standard protocol as described in section 2.4.1. Induction of protein expression was initiated by addition of 1mM IPTG. In the case of E2o, the culture was supplemented with lipoic acid prior to induction. His-tagged constructs (E1o-60, E1o-90, E1o-153 and full-length E1o) over-expression was attempted at 18°C for overnight. Protein over-expression and solubility was checked by SDS-PAGE and western blotting as described in sections 2.4.3 and 2.4.7. The over-expression plasmids used in this study are listed in Table 3.5.

| Protein | Plasmid vector | *E.coli* strain | Antibiotic$^R$ | Temp ($^o$C) | Time (h) |
|---|---|---|---|---|---|
| E3 His-tag | pET-14b | BL21 (DE3) pLysS | Amp, Chl | 30 | 4 |
| E2o His-tag | pET-14b | BL21 (DE3) pLysS | Amp, Chl | 30 | 4 |
| E1o-60 His-tag | pET-14b | BL21 Star (DE3) pLysS | Amp, Chl | 18 | 18 |
| E1o-90 His-tag | pET-14b | BL21 Star (DE3) pLysS | Amp, Chl | 18 | 18 |
| E1o-153 His-tag | pET-14b | BL21 Star (DE3) pLysS | Amp, Chl | 18 | 18 |
| E1o-60 GST | pGEX-2T | BL21 (DE3) pLysS | Amp | 30 | 4 |
| E1o-90 GST | pGEX-2T | BL21 (DE3) pLysS | Amp | 30 | 4 |
| E1o-153 GST | pGEX-2T | BL21 (DE3) pLysS | Amp | 30 | 4 |
| E1o-60 MBP | pET-30a | BL21 (DE3) pLysS | Kan | 30 | 4 |
| E1o-90 MBP | pET-30a | BL21 (DE3) pLysS | Kan | 30 | 4 |
| E1o-153 MBP | pET-30a | BL21 (DE3) pLysS | Kan | 30 | 4 |
| Full-length E1o | pET-14b | BL21 (DE3) pLysS | Amp, Chl | 18 | 18 |
| wt GST | pGEX-2T | BL21 (DE3) pLysS | Amp | 30 | 4 |
| wt MBP | pET-30a | BL21 (DE3) pLysS | Kan | 30 | 4 |

**Table 3.5: Over-expression plasmids and selection conditions used in this study**
The various antibiotics used namely, chloramphenicol (Chl), ampicillin (Amp) and kanamycin (Kan) are denoted. wt, wild-type.

## 3.2.3 Protein purification

Metal chelate chromatography was used to purify His-tagged proteins while GST fusion proteins were isolated by use of a glutathione Sepharose 4B column. His-tagged proteins (E2o and E3) and GST fusion proteins (E1o-60, E1o-90 and E1o-153) were enriched using two rounds of chromatographic purification to achieve high yields and purity. An MBP Trap HP column was used to purify MBP-fusion proteins. Technical details of the protein purification are described in section 2.4.4. Details of the purification buffers used during this project are listed in Table 3.6.

| Fusion form | Protein | Purification | Binding buffer | Elution buffer | Elution gradient |
|---|---|---|---|---|---|
| His-tag | Full-length E1o | MC | 50mM $KH_2PO_4$, pH 8.0 100mM NaCl, 10mM imidazole | 50mM $KH_2PO_4$, pH 6.0 100mM NaCl, 500mM imidazole | 0-100% |
| | E2o | MC | 50mM $KH_2PO_4$, pH 8.0 100mM NaCl, 10mM imidazole | 50mM $KH_2PO_4$, pH 6.0 100mM NaCl, 500mM imidazole | 0-100% |
| | | GFC | 50mM $KH_2PO_4$, pH 7.4 20mM NaCl, 2mM EDTA | None | None |
| | E3 | MC | 50mM $KH_2PO_4$, pH 8.0 100mM NaCl, 10mM imidazole | 50mM $KH_2PO_4$, pH 6.0 100mM NaCl, 500mM imidazole | 0-100% |
| | | GFC | 50mM $KH_2PO_4$, pH 7.4 20mM NaCl, 2mM EDTA | None | None |
| | E1o-60 | MC | 50mM $KH_2PO_4$, pH 8.0 100mM NaCl, 10mM imidazole | 50mM $KH_2PO_4$, pH 6.0 100mM NaCl, 500mM imidazole | 0-100% |
| | E1o-90 | | | | |
| | E1o-153 | | | | |
| MBP | E1o-60 | MBP affinity | 20mM Tris-HCl, pH 7.4 200mM NaCl, 1mM EDTA | 20mM Tris-HCl, pH 7.2 15mM maltose, 200mM NaCl, 1mM EDTA | 5 CV |
| | E1o-90 | | | | |
| | E1o-153 | | | | |
| GST | E1o-60 | GST affinity | PBS (140mM NaCl, 2.7mM KCl, 10mM $Na_2HPO_4$, and 1.8mM $KH_2PO_4$, pH 7.3) | 20mM reduced glutathione, 50mM Tris-HCl, pH 8.0 | 5 CV |
| | E1o-90 | | | | |
| | E1o-153 | GFC | 50mM $KH_2PO_4$, pH 7.4 20mM NaCl, 2mM EDTA | None | None |

**Table 3.6: Purification buffers used in this study**

CV is column volume while MC, GFC GST and MBP denote metal chelate, gel filtration chromatography, GST affinity chromatography, and MBP affinity chromatography, respectively.

# 3.3 Results and discussion

## 3.3.1 Cloning

### 3.3.1.1 Cloning of N-terminal E1o constructs (E1o-60, E1o 90 and E1o-153) in pET-14b (His-tag forms)

Three mature N-terminal E1o fragments were successfully cloned encoding 60 a.a. (11-70), 90 a.a. (1-90) and 153 a.a. (1-153) as His-tag fusion proteins. Amplification of the DNA sequences corresponding to residues 11-70, 1-90 and 1-153 was successful and yielded the expected 180bp, 270bp and 459bp PCR products respectively as shown in Figure 3.5.

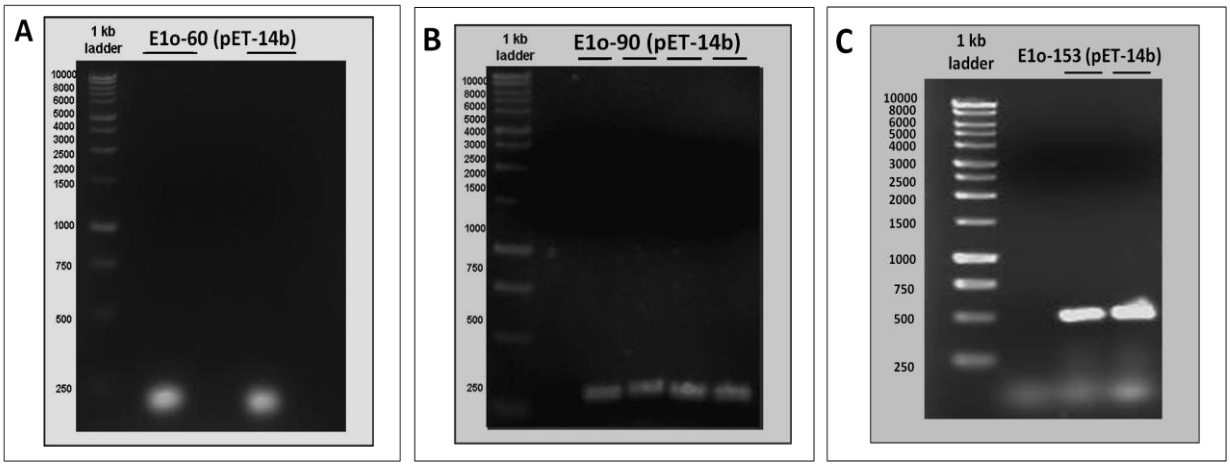


**Figure 3.5: PCR amplification of N-terminal E1o segments (pET-14b)**
PCR mixtures (5µl) were resolved on 2% agarose gels and the DNA viewed under UV light after staining with ethidium bromide. Band sizes are indicated in bp. (A) PCR amplification of E1o-60 (11-70). A positive result was seen by the presence of a single band of expected size ~180 bp. (B) PCR amplification of E1o-90 (1-90). A positive result was seen by the presence of a single band of expected size ~270 bp. (C) PCR amplification of E1o-153 (1-153). A positive result was seen by the presence of a single band of expected size ~460 bp.
Lanes contain replicate samples from the PCR reactions.

Digested PCR products were then successfully cloned into the pET-14b vector. Ligation of digested inserts (E1o-60, E1o-90 and E1o-153) into pET-14b resulted in formation of recombinant plasmids E1o-60-pET14b, E1o-90-pET14b and E1o-153-pET14b.

E1o-60-pET14b plasmid was then digested successfully with *BamHI*. Analysis of the digests on a 2% (w/v) agarose gel confirmed the presence of an insert of the correct size (approx. 180bp) as shown in Figure 3.6A. Similarly, digestion of E1o-90-pET14b and E1o-153-pET14b plasmids with *NdeI* and *BamHI* indicated successful cloning, resulting in single bands of 270bp and 459bp respectively (Fig. 3.6B & 3.6C). The correct recombinant plasmid sequences were confirmed by DNA sequencing (see section 2.2.10).

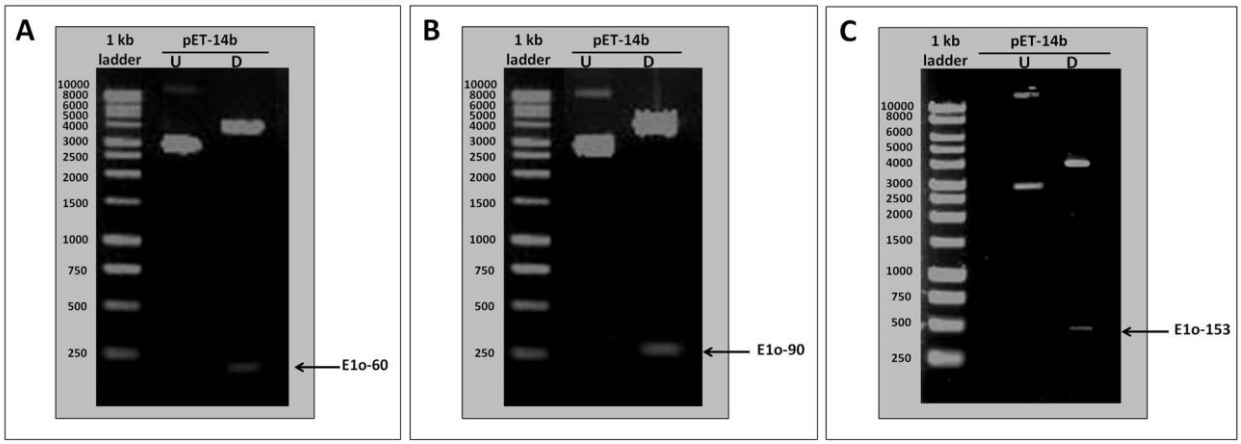


**Figure 3.6: Restriction digestion of N-terminal E1o constructs (pET-14b)**
DNA samples were resolved on 2% agarose gels and then stained with ethidium bromide. Stained agarose gels were viewed under UV light. U & D denote undigested and digested pET-14b. Band sizes are indicated in bp. Restriction digestion of recombinant plasmids showing the presence of inserts of the expected sizes. (A) Diagnostic digest of cloned product E1o-60-pET14b showing ~ 180bp insert. (B) Diagnostic digest of cloned product E1o-90-pET14b showing ~ 270bp insert. (C) Diagnostic digest of cloned product E1o-153-pET14b showing ~ 460bp insert.

### 3.3.1.2 Cloning of N-terminal E1o constructs (E1o-60, E1o-90 and E1o-153) in pGEX-2T (GST fusion proteins)

Mature N-terminal E1o fragments encoding 60 a.a. (11-70), 90 a.a. (1-90) and 153 a.a. (1-153) were also successfully cloned into pGEX-2T. Amplification of these DNA sequences was successful and yielded the expected 180bp, 270bp and 459bp PCR products respectively as shown in Figure 3.7.

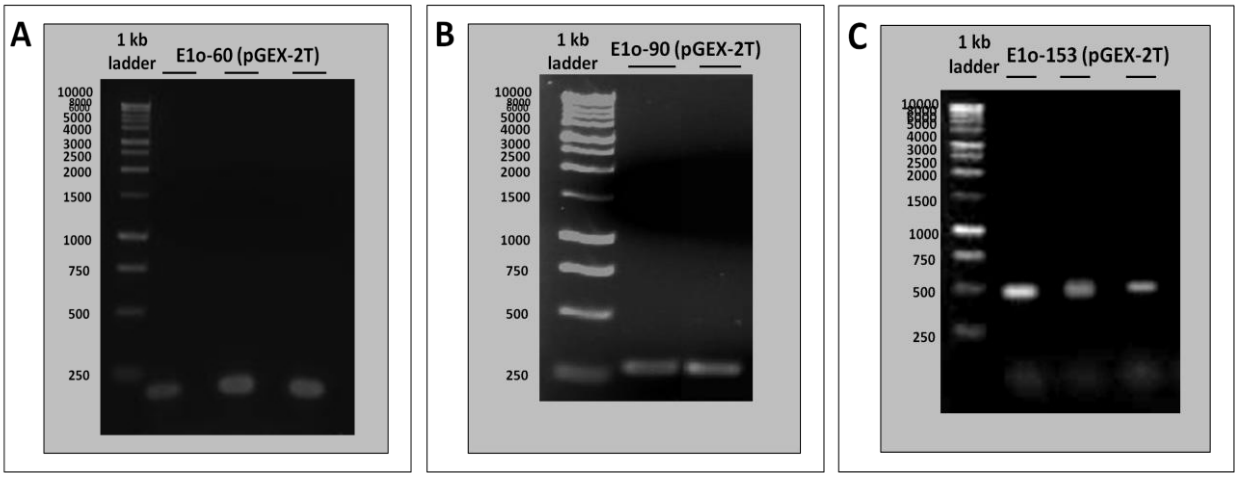


**Figure 3.7: PCR amplification of N-terminal E1o constructs (pGEX-2T)**
PCR mixtures (5µl) were resolved on 2% agarose gels and the DNA viewed under UV light after staining with ethidium bromide. Band sizes are indicated in bp. (A) PCR amplification of E1o-60 (11-70). A positive result was seen by the presence of a single band of expected size ~180 bp. (B) PCR amplification of E1o-90 (1-90). A positive result was seen by the presence of a single band of expected size ~270 bp. (C) PCR amplification of E1o-153 (1-153). A positive result was seen by the presence of a single band of expected size ~460 bp.

The PCR products were successfully cloned into the pCR2.1-TOPO vector (see section 2.2.7). Purified inserts E1o-60, E1o-90 and E1o-153 from the TOPO ligations were then digested along with wild-type pGEX-2T plasmid using *BamHI* and *EcoRI*.

Following ligation of digested inserts (E1o-60, E1o-90 and E1o-153) into the pGEX-2T vector, recombinant plasmids E1o-60-pGEX-2T, E1o-90-pGEX-2T and E1o-153-pGEX-2T were produced.

E1o-60-pGEX-2T and E1o-153-pGEX-2T plasmids were digested successfully with *BamHI*. Analysis of the digests on a 2% (w/v) agarose gel confirmed the presence of inserts of the correct sizes, 180bp and 459bp, respectively as shown in Figure 3.6A & 3.6C.

Similarly, digestion of E1o-90-pET14b recombinant plasmid with *BamHI* and *EcoRI* indicated successful cloning, resulting in single band of approx. 270bp (Fig. 3.6B). The correct recombinant plasmid sequences were confirmed by DNA sequencing (see section 2.2.10).

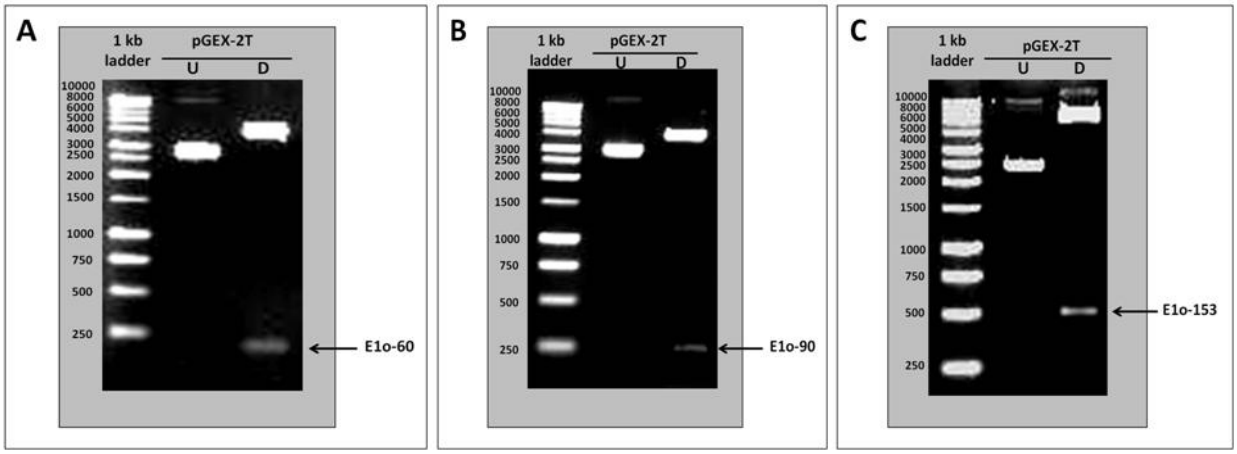


**Figure 3.8: Restriction digestion of N-terminal E1o constructs (pGEX-2T)**
DNA samples were resolved on 2% agarose gels and then stained with ethidium bromide. Stained agarose gels were viewed under UV light. U & D denote undigested and digested pGEX-2T. Band sizes are indicated in bp. Restriction digestion of recombinant plasmids showing the presence of inserts of the expected sizes. (A) Diagnostic digest of cloned product E1o-60-pGEX-2T showing ~ 180bp insert. (B) Diagnostic digest of cloned product E1o-90-pGEX-2T showing ~270bp insert. (C) Diagnostic digest of cloned product E1o-153-pGEX-2T showing ~ 460bp insert.

### 3.3.1.3 Cloning of N-terminal E1o constructs (E1o-60, E1o-90 and E1o-153) in pET-30a (MBP fusion proteins)

Short mature N-terminal E1o fragments encoding to the predicted binding region for E2o/E3 (60 a.a, 90 a.a and 153 a.a) were successfully cloned into pET-30a. The E1o-60, E1o-90 and E1o-153 sequences corresponding to 11-70, 1-90 and 1-153 a.a., respectively were successfully amplified by PCR using Expand High Fidelity PCR System (Fig. 3.9). *BamHI* and *HindIII* restriction sites were used for cloning all 3 constructs via the classical cloning approach.

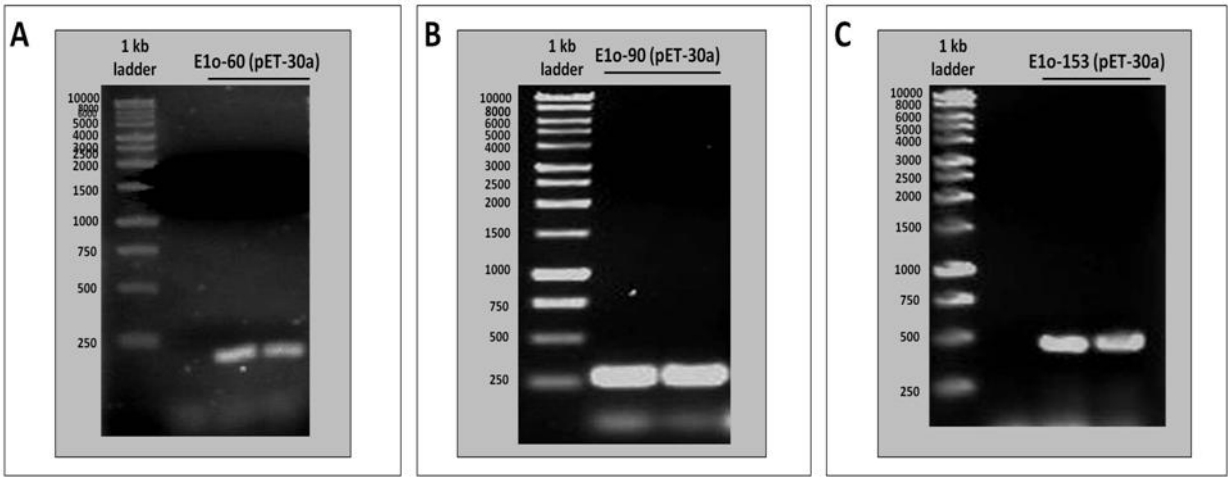


**Figure 3.9: PCR amplification of N-terminal E1o constructs (pET-30a)**
PCR mixtures (5µl) were resolved on 2% agarose gels and the DNA viewed under UV light after staining with ethidium bromide. Band sizes are indicated in bp. (A) PCR amplification of the E1o-60 (11-70). A positive result was seen by the presence of a single band of expected size ~180 bp. (B) PCR amplification of the E1o-90 (1-90). A positive result was seen by the presence of a single band of expected size ~270 bp. (C) PCR amplification of the E1o-153 (1-153). A positive result was seen by the presence of a single band of expected size ~460 bp.

The PCR amplified inserts (E1o-60, E1o-90 and E1o-153) were digested with *BamHI* and *HindIII* and subsequently ligated into digested pET-30a resulting in the ligated products E1o-60-pET30a, E1o-90-pET30a and E1o-153-pET30a, respectively.

Successful cloning of E1o-60, E1o-90 and E1o-153 was confirmed via diagnostic digests with *BamHI* and *HindIII* that yielded the expected 180bp, 270bp and 459bp products respectively (Fig. 3.10). This was further confirmed by DNA sequencing (see section 2.2.10).

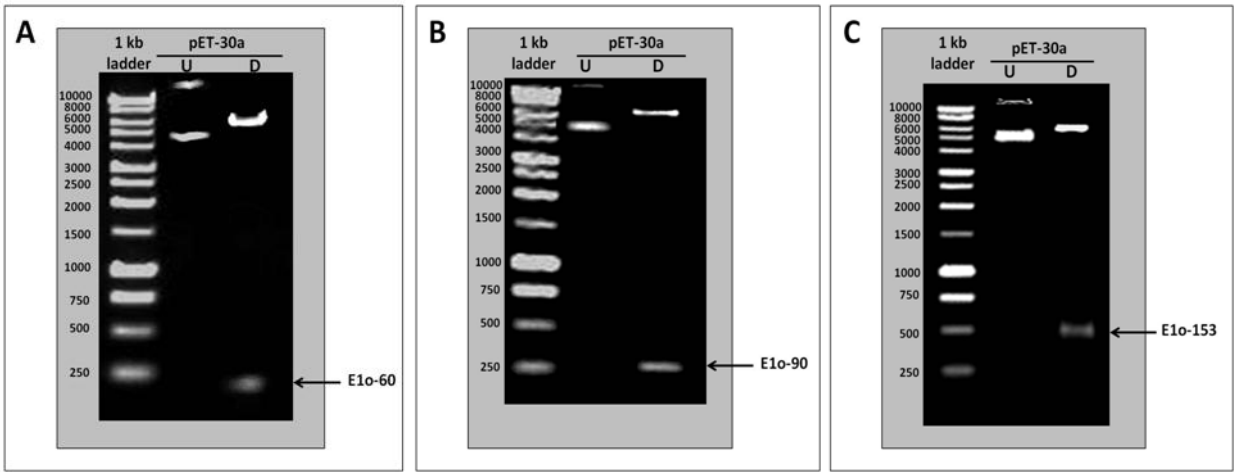


**Figure 3.10: Restriction digestion of N-terminal E1o constructs (pET-30a)**
DNA samples were resolved on 2% agarose gels and then stained with ethidium bromide. Stained agarose gels were viewed under UV light. U & D denote undigested and digested pET-30a. Band sizes are indicated in bp. Restriction digestion of recombinant plasmids showing the presence of inserts of the expected sizes. (A) Diagnostic digest of cloned product E1o-60-pET30a showing ~ 180bp insert. (B) Diagnostic digest of cloned product E1o-90-pET30a showing ~ 270bp insert. (C) Diagnostic digest of cloned product E1o-153-pET30a showing ~ 460bp insert.

### 3.3.1.4 Cloning of human full-length E1o in pET-14b (His-tag form)

The mature, full-length, human E1o construct was successfully cloned with an N-terminal His-tag sequence. Amplification of the DNA sequence corresponding to residues 1-962 was successful and yielded a major band of 2886bp consistent with the predicted size for E1o cDNA as shown in Figure 3.11.

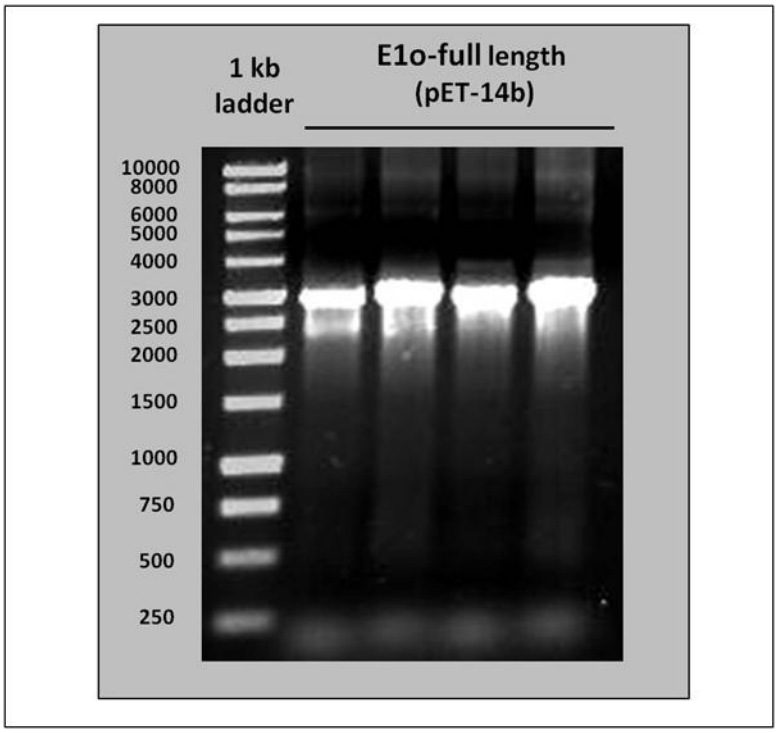


**Figure 3.11: PCR amplification of human full-length E1o (pET-14b)**
PCR mixtures (5µl) were resolved on 1% agarose gels and the DNA viewed under UV light after staining with ethidium bromide. Band sizes are indicated in bp. PCR amplification of full-length E1o (1-962). A positive result was seen by the presence of a single band of expected size ~2900 bp.
Lanes contain replicate samples from the PCR reactions.

Using T4 DNA ligase with restriction enzymes *NdeI* and *XhoI*, the PCR product was successfully incorporated into pET-14b yielding a full-length, His-tagged copy of the mature human E1o cDNA sequence.

The E1o-pET14b plasmid was then digested successfully with *NdeI* and *XhoI*. Analysis of the digests on a 1% (w/v) agarose gel confirmed the presence of an insert of the correct size (approx. 2886bp) as shown in Figure 3.12. The correct sequence and reading frame were confirmed by DNA sequencing (see section 2.2.10).

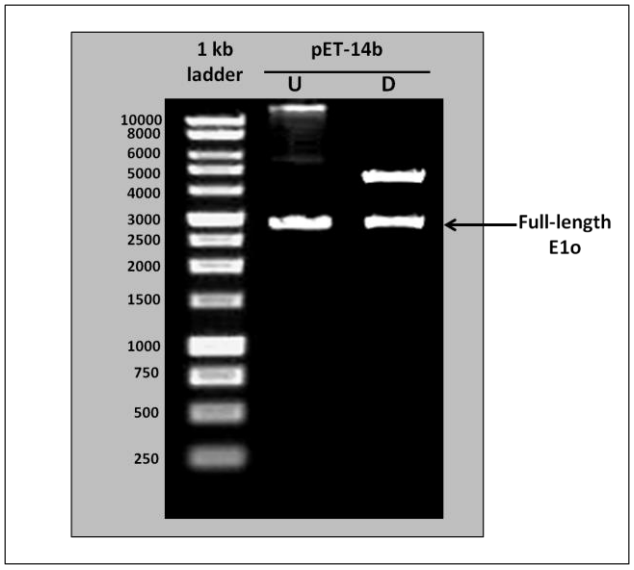


**Figure 3.12: Restriction digestion of human full-length E1o construct (pET-14b)**
DNA samples were resolved on 1% agarose gels and then stained with ethidium bromide. Stained agarose gels were viewed under UV light. U & D denote undigested and digested pET-14b. Band sizes are indicated in bp. Restriction digestion of recombinant plasmids showing the presence of inserts of the expected sizes. Diagnostic digest of cloned E1o-pET14b showing ~ 2900bp insert.

## 3.3.2 Protein over-expression

### *3.3.2.1 Over-expression of E1o-60, E1o-90 and E1o-153 (His-tag forms)*

To produce His-tagged N-terminal E1o polypeptides, human N-terminal E1o constructs (E1o-60, E1o-90 and E1o-153) in pET-14b were transformed individually into *E. coli* BL21 (DE3) pLysS cells. Over-expression in LB media was induced at 30$^{o}$C with 1mM IPTG for 4 h as described in Materials and Methods, section 2.4.1. On SDS-PAGE analysis, it was found that the N-terminal fragments failed to over-express under these conditions (data not shown). Possibly owing to the small size of mRNA, the *E. coli* BL21 (DE3) pLysS cells did not prove a suitable vehicle for over-expression under these conditions. However, by adjusting various parameters, suitable conditions for His-tagged N-terminal E1o fragment expression were established to be low temperature and growth in a modified rich LB media (Terrific broth) after transforming into *E. coli* BL21 Star (DE3) pLysS. This strain carries the *rne*131 mutation resulting in potentially higher protein expression as a result of increased mRNA stability.

However, even under optimal conditions, expression of human His-tagged, N-terminal E1o constructs (E1o-60, E1o-90 and E1o-153) at low temperature (18$^{o}$C), 1mM IPTG for 18 h still produced low yields of protein (Fig. 3.13). The induced proteins were of the correct expected sizes, approx. 8, 10 and 18 kDa respectively. The presence of small amounts of His-tagged, N-terminal E1o fragments (E1o-60, E1o-90 and E1o-153) in these cell extracts was subsequently confirmed after purification by probing with an anti-His tag antibody (Fig. 3.20B, 3.21B & 3.22B).

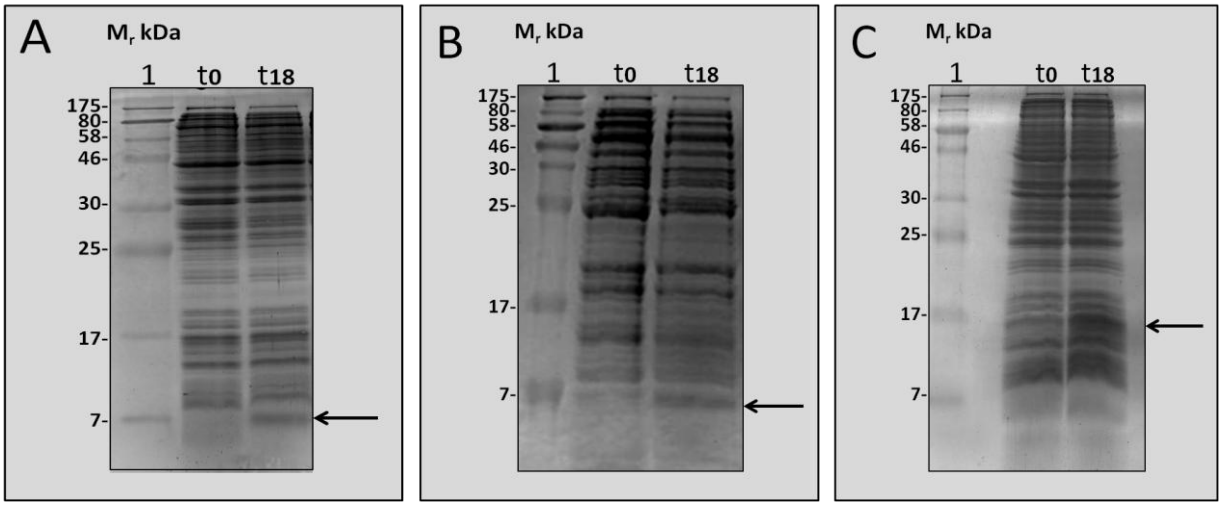


**Figure 3.13: Expression of N-terminal E1o constructs: E1o-60, E1o-90 and E1o-153 (His-tag forms)**

N-terminal E1o constructs were expressed over 18 h at 18°C in *E. coli* BL21 Star (DE3) pLysS. Cells were grown in Terrific broth. Samples were taken at the time of induction (t0) and after 18 h (t18). Samples were denatured in the presence of 150mM DTT at 100°C for 5 min and resolved on an 18% SDS/polyacrylamide gel. Protein bands were visualised using Coomassie Brilliant Blue. Lane 1, molecular mass markers. The arrow on the right of the gel indicates over-expressed protein. (A) SDS-PAGE analysis of E1o-60 showing poor expression at the expected size, ~ 8 kDa. (B) SDS-PAGE analysis of E1o-90 showing poor expression at the expected size, ~ 10 kDa. (C) SDS-PAGE analysis of E1o-153 showing poor expression at the expected size, ~ 18 kDa.

### *3.3.2.2 Over-expression of E1o-60, E1o-90 and E1o-153 (GST fusion proteins)*

Human N-terminal E1o fragments (E1o-60, E1o-90 and E1o-153) were cloned individually into pGEX-2T to form the plasmids E1o-60-pGEX-2T, E1o-90-pGEX-2T and E1o-153 pGEX-2T. The plasmids were then transformed into the *E. coli* expression strain BL21 (DE3) pLysS. Recombinant protein over-expression was successfully carried out at 30°C for 4 h and induced by the addition of 1mM IPTG as described in Materials and Methods, section 2.4.1.

SDS-PAGE analysis of samples taken at the time of induction and after 4 h demonstrated the presence of over-expressed E1o-60, E1o-90 and E1o-153. Bands at 32, 36 and 43kDa were observed corresponding to the predicted subunit $M_r$ values of the E1o-60, E1o-90 and E1o-153 GST fusion proteins (Fig. 3.14). SDS-PAGE analysis revealed that the majority of the protein was soluble and reactive with anti-GST antibody as assessed by Western blotting (data not shown).

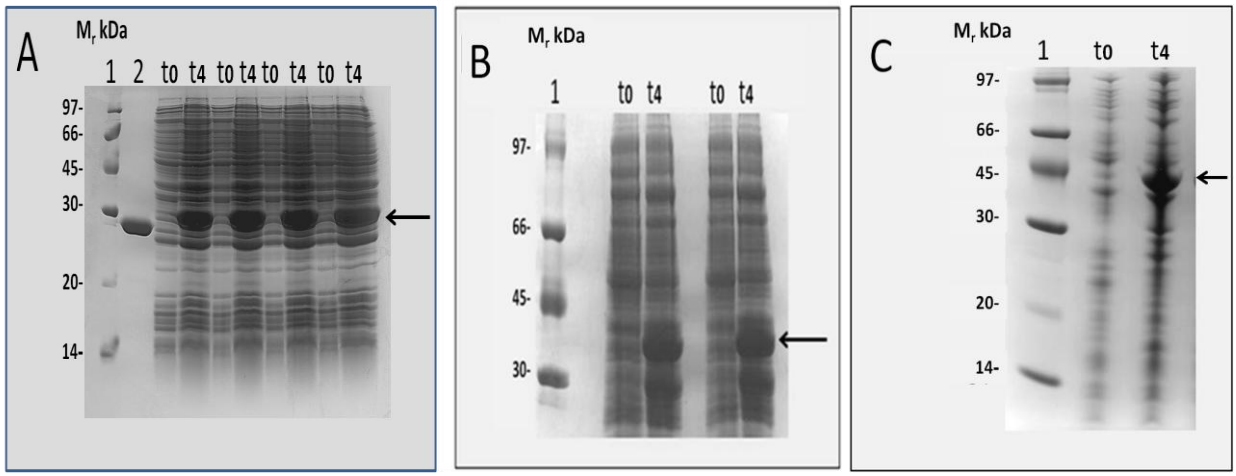


**Figure 3.14: Over-expression of N-terminal E1o constructs: E1o-60, E1o-90 and E1o-153 (GST fusion proteins)**

N-terminal E1o constructs were expressed for 4 h at 30°C in *E. coli* BL21 (DE3) pLysS. Cells were grown in LB media. Samples were taken at the time of induction (t0) and after 4 h (t4). Samples were denatured in the presence of 150mM DTT at 100°C for 5 min and resolved on a 10% SDS/polyacrylamide gel. Protein bands were visualised using Coomassie Brilliant Blue. Lane 1, molecular mass markers; lane 2, purified GST as control (~ 26 kDa). The arrow on the right of the gel indicates over-expressed protein. (A) SDS-PAGE analysis of E1o-60 over-expression showing large yields of E1o-60 at the expected size (~ 32 kDa). (B) SDS-PAGE analysis of E1o-90 over-expression showing large yields of E1o-90 at the expected size (~36 kDa). (C) SDS-PAGE analysis of E1o-153 over-expression showing good yields of E1o-153 at the expected size (~ 43 kDa).

### 3.3.2.3 Over-expression of E1o-60, E1o-90 and E1o-153 (MBP fusion proteins)

Each of the N-terminal E1o constructs, E1o-60, E1o-90 and E1o-153 (pET-30a vector), were transformed individually into competent *E. coli* BL21 (DE3) pLysS cells for over-expression. The over-expression of all constructs was carried out successfully at 30°C for a 4 h induction period. Figure 3.15 shows the level of expression of E1o-60, E1-90 and E1o-153, respectively.

The solubility of the over-expressed proteins was analysed by the standard protocol (see section 2.4.2) and resolved by SDS-PAGE. All of the over-expressed protein was found in the soluble fraction (data not shown).

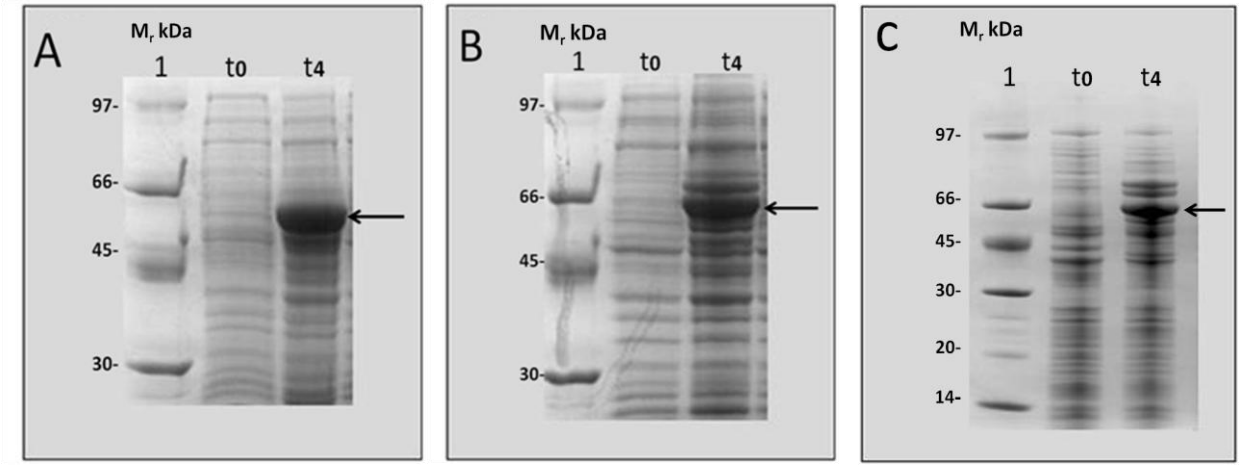


**Figure 3.15: Over-expression of N-terminal E1o constructs: E1o-60, E1o-90 and E1o-153 (MBP fusion proteins)**

N-terminal E1o constructs were expressed for 4 h at 30°C in *E. coli* BL21 (DE3) pLysS. Cells were grown in LB media. Samples were taken at the time of induction (t0) and after 4 h (t4). Samples were denatured in the presence of 150mM DTT at 100°C for 5 min and resolved on a 10% SDS/polyacrylamide gel. Protein bands were visualised using Coomassie Brilliant Blue. Lane 1, molecular mass markers. The arrow on the right of the gel indicates over-expressed protein. (A) SDS-PAGE analysis of E1o-60 over-expression showing large yields (~ 48 kDa). (B) SDS-PAGE analysis of E1o-90 over-expression showing large yields (~ 50 kDa). (C) SDS-PAGE analysis of E1o-153 over-expression showing good yields (~58 kDa).

### 3.3.2.4 Over-expression of human full-length E1o (His-tag form)

Human full-length E1o construct was cloned into pET-14b and transformed into competent *E. coli* BL21 (DE3) pLysS cells for over-expression. Over-expression was attempted at 30 °C (data not shown) and 18 °C with 1mM IPTG. Conclusively, for the first time, human E1o (subunit $M_r$ ~ 110 kDa) was successfully over-expressed in an *E. coli* cell system. Moreover, over-expression of human full-length E1o at a low temperature (18$^{o}$C) for 18 h provided good yields of protein (Fig. 3.16A). The protein was of the correct size (~ 110 kDa). The identity of full-length E1o was also confirmed by Western blotting with anti-His tag antibody (Fig. 3.16B).

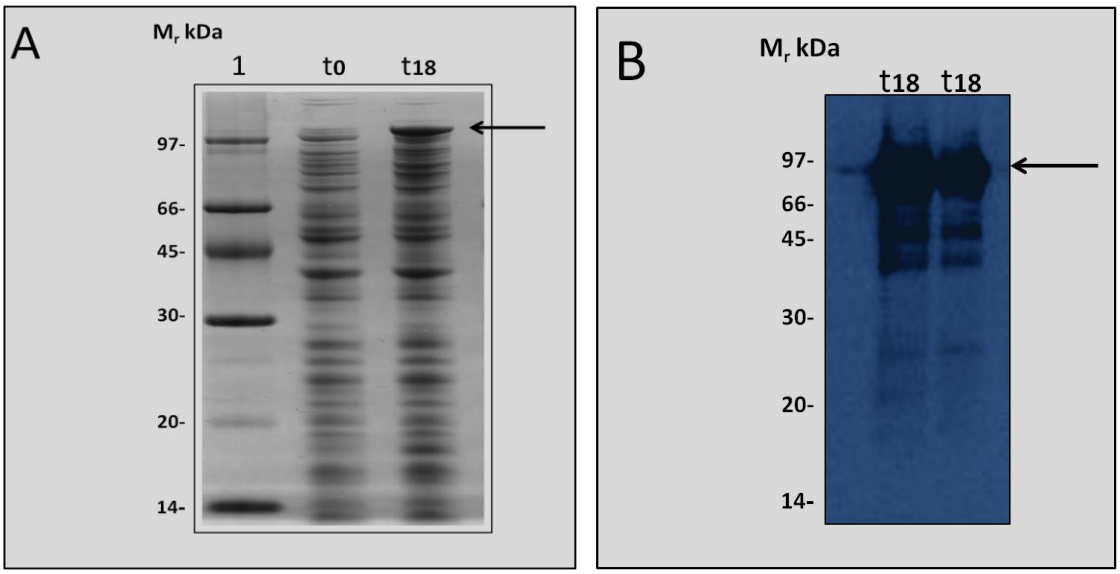


**Figure 3.16: Over-expression of human E1o (His-tag form)**
E1o was expressed over 18 h at 18°C in *E. coli* BL21 (DE3) pLysS. Cells were grown in LB media. Samples were taken at the time of induction (t0) and after 18 h (t18). Samples were denatured in the presence of 150mM DTT at 100°C for 5 min and resolved on a 10% SDS/polyacrylamide gel. Protein bands were visualised using Coomassie Brilliant Blue. Lane 1, molecular mass markers. The arrow on the right of the gel indicates over-expressed protein. (A) SDS-PAGE analysis of full-length E1o over-expression showing good yields at the expected size (~ 110 kDa). (B) Western blot analysis of full-length E1o. The presence of His-tagged full-length E1o was confirmed by Western blotting with anti-His tag antibody.

Solubility analysis of the over-expressed human full-length E1o at a low temperature (18$^{o}$C) was performed as described in the Materials and Methods (see section 2.4.2). The vast majority of the protein was found to be insoluble (Fig. 3.17).

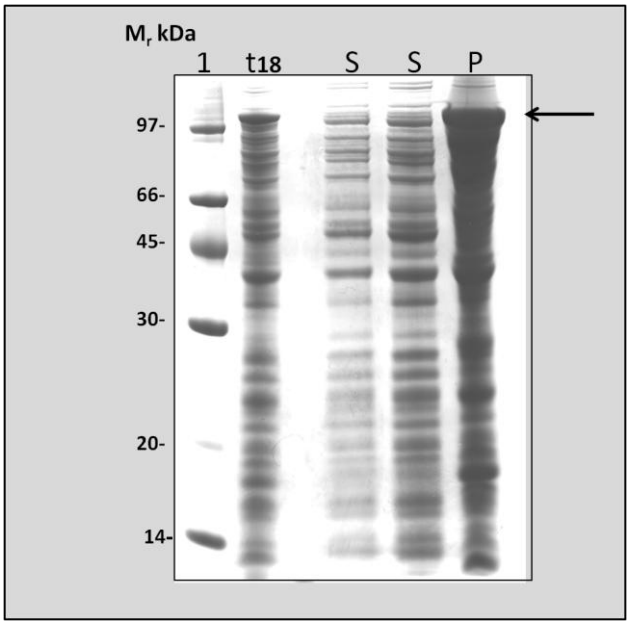


**Figure 3.17: Solubility analysis of human E1o (His-tag form)**
E1o was expressed over 18 h at 18°C in the *E. coli* BL21 (DE3) pLysS. Cells were grown in LB media. Samples were taken after 18 h (t18). Samples were denatured in the presence of 150mM DTT at 100°C for 5 min and resolved on a 10% SDS/polyacrylamide gel. Protein bands were visualised using Coomassie Brilliant Blue. Lane 1, molecular mass markers. The arrow on the right of the gel indicates fusion protein. Following over-expression of full-length E1o, the bacterial cells were centrifuged at 4°C, 3,000xg for 15 min and re-suspended in 3ml binding buffer. The bacterial extract was passed 4 times through a French Pressure Cell at 950 psi. Disrupted cells (100µl) were then centrifuged at 4°C, 13,000xg for 10 min and the supernatant (90µl) resuspended in an equal volume of Laemmli sample buffer while the pellet was re-suspended and washed 3 times with PBS buffer. Finally, the washed pellet was resuspended in an equal volume of Laemmli sample buffer (100µl). An equal volume (10µl) of the protein supernatant (S) and pellet suspension (P) was loaded on SDS-PAGE to view the solubility. SDS-PAGE analysis shows full-length E1o was largely insoluble and present in the pellet fraction (P).

E1o is a homodimer of two 110 kDa subunits ($\alpha_2$). Typically, *E. coli* has not proved an effective host for expressing or promoting the correct folding of large proteins (> 70 kDa). In such cases the expressed protein is usually insoluble and accumulates as inclusion bodies.

Failure to produce soluble recombinant protein is often the result of improper protein folding during the protein expression. Misfolding of expressed recombinant proteins in prokaryotic hosts often occurs as a result of rapid protein expression, high expression temperature, use of a stronger promoter such as T7 and lack of suitable chaperones. However, a number of approaches are available to improve expressed protein solubility including co-transformation of plasmids encoding the main *E. coli* chaperones (GroEL and GroES) (Zeilstra-Ryalls *et al.* 1991), decreasing the rate of protein synthesis by lowering the growth temperature (Zhang *et al.* 2003), choice of a suitable *E. coli* strain and use of a weaker promoter (e.g. T5).

Previously, over-expression of soluble recombinant E1p proved difficult in our laboratory; however, cloning into the pQE-9 vector and transforming into *E. coli* M15 cells allowed successful low-level production of active, soluble E1p (Korotchkina *et al.* 1995; Singh 2008). The pQE-9 vector contains the T5 promoter, while, *E. coli* M15 cells contains the pREP4 plasmid that encodes the *lac* repressor (Korotchkina *et al.* 1995).

No successful cloning, expression and purification of active, recombinant mammalian E1o has been reported in the literature to date. Unfortunately, further attempts to obtain active, soluble E1o in this study were limited by time constraints.

### 3.3.2.5 Over-expression of human E2o (His-tag form)

An E2o construct in pET-14b was already available in the laboratory. The E2o construct was transformed into *E. coli* BL21 (DE3) pLysS. Over-expression was successfully carried out at 30°C for 4 h after induction with 1mM IPTG and supplementation with lipoic acid (see section 2.4.1). SDS-PAGE analysis revealed large yields of over-expressed protein of the expected size (~ 48 kDa) (Fig. 3.18). The solubility of the expressed E2o was analysed by the standard protocol (see section 2.4.2) and found by SDS-PAGE to be present in the soluble fraction (data not shown).

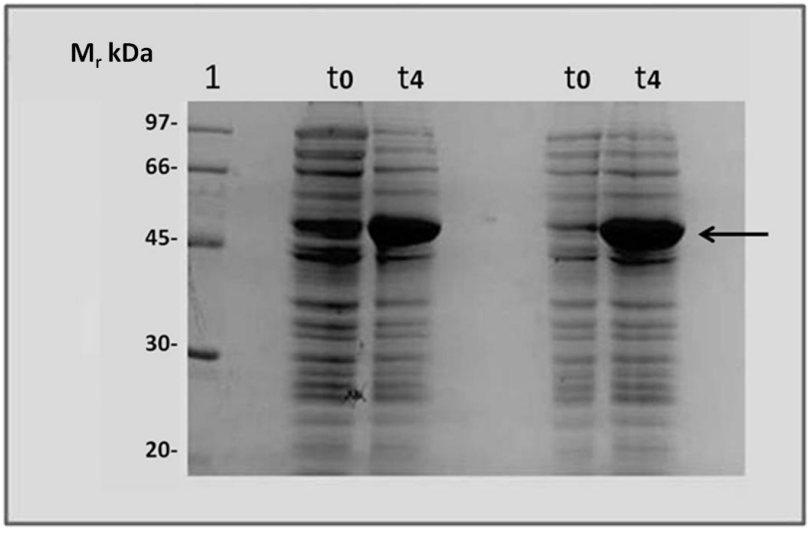


**Figure 3.18: Over-expression of human E2o (His-tag form)**
E2o was expressed for 4 h at 30°C in *E. coli* BL21 (DE3) pLysS. Cells were grown in LB media. Samples were taken at the time of induction (t0) and after 4 h (t4). Samples were denatured in the presence of 150mM DTT at 100°C for 5 min and resolved on a 10% SDS/polyacrylamide gel. Protein bands were visualised using Coomassie Brilliant Blue. Lane 1, molecular mass markers. The arrow on the right of the gel indicates over-expressed protein. SDS-PAGE analysis of E2o over-expression showing large yields at the expected size (~ 48 kDa).

### 3.3.2.6 Over-expression of human E3 (His-tag form)

His-tagged E3 cloned into pET-14b (already available in the laboratory) was expressed at 30°C, 1mM IPTG for 4 h. Levels of over-expression were analysed by SDS-PAGE, indicating high yields of protein at the expected size (~ 52 kDa) (Fig. 3.19). The solubility of the E3 was also confirmed (data not shown).

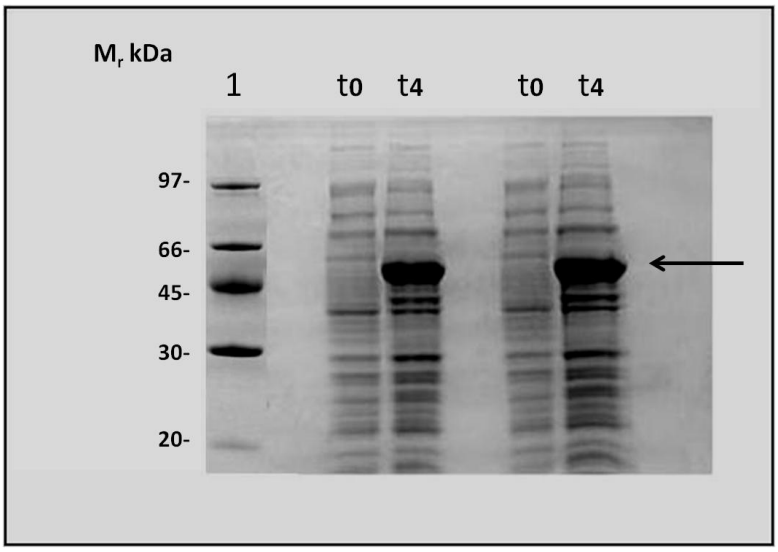


**Figure 3.19: Over-expression of human E3 (His-tag form)**
E3 was expressed over 4 h at 30°C in *E. coli* BL21 (DE3) pLysS. Cells were grown in LB media. Samples were taken at the time of induction (t0) and after 4 h (t4). Samples were denatured in the presence of 150mM DTT at 100°C for 5 min and resolved on a 10% SDS/polyacrylamide gel. Protein bands were visualised using Coomassie Brilliant Blue. Lane 1, molecular mass markers. The arrow on the right of the gel indicates over-expressed protein. SDS-PAGE analysis of E3 over-expression showing large yields at the expected size (~ 52 kDa).

## 3.3.3 Protein purification

### *3.3.3.1 Purification of E1o-60, E1o-90 and E1o-153 (His-tag form)*

Over-expression of human His-tagged N-terminal E1o constructs (E1o-60, E1o-90 and E1o-153) at low temperature (18$^{o}$C), 1 mM IPTG for 18 h indicated poor yields of protein. However, E1o-60, E1o-90 and E1o-153 were purified by metal chelate affinity chromatography (Fig. 3.20A, 3.21A & 3.22A). Since the levels of protein were low, the identities of purified His-tagged N-terminal E1o fragments were confirmed by Western blotting using anti-His tag antibody (Fig. 3.20B, 3.21B & 3.22B).

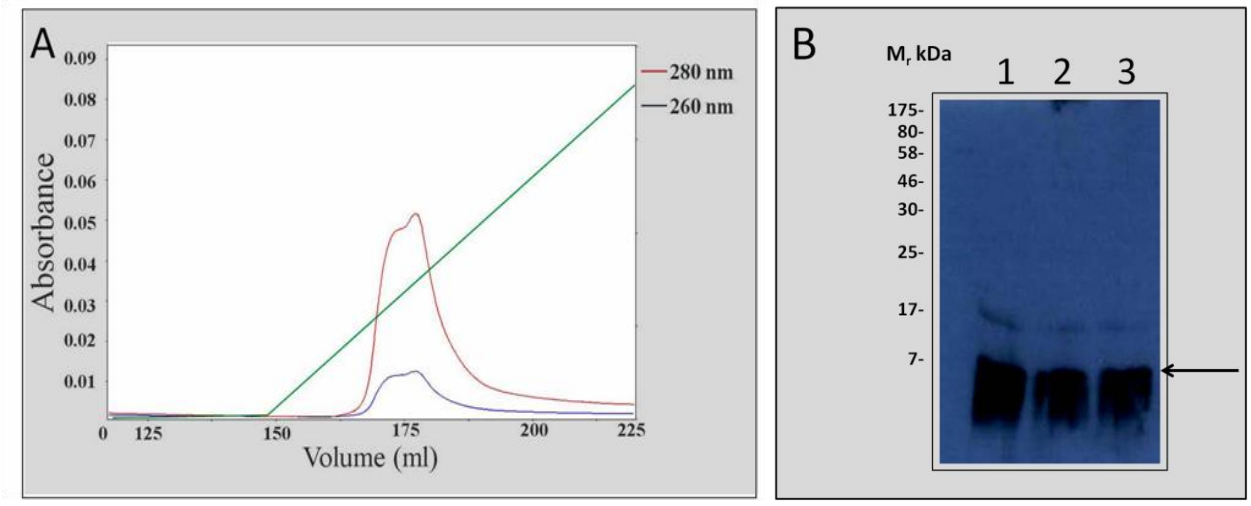


**Figure 3.20: Purification of E1o-60 (His-tag form)**
(A) Metal chelate affinity chromatography of E1o-60 (pET-14b). Cell lysates (20ml) were applied to the column in 5ml aliquots (see section 2.4.4). Bound protein was eluted from the column in a 0-100% gradient of elution buffer (8 CV) over the vol. 160-230 ml. The imidazole gradient (0-500 mM) used for elution is shown in green. Absorbance of eluted protein was measured at 280 nm (red line) and possible DNA/RNA contamination was monitored at 260 nm (blue line). Peak fractions were collected and analysed by Western blotting. (B) Western blot analysis of purified E1o-60 His-tag form. The presence of purified His-tagged E1o-60 was confirmed (lanes 1, 2 & 3) by anti-His tag antibody (1 in 2000 dilution) (see section 2.4.7.1). Molecular mass markers in kDa are shown. The arrow on the right of the blot indicates purified protein.

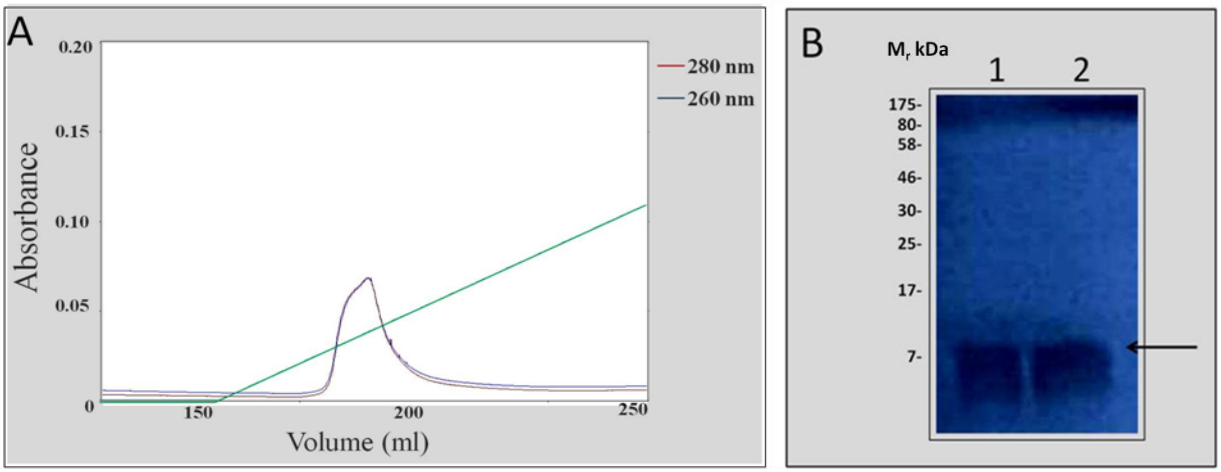


**Figure 3.21: Purification of E1o-90 (His-tag form)**
(A) Metal chelate affinity chromatography of E1o-90 (pET-14b). Cell lysates (20ml) were applied to the column in 5ml aliquots (see section 2.4.4). Bound protein was eluted from the column in a 0-100% gradient of elution buffer (8 CV) over the vol. 160-250 ml. The imidazole gradient (0-500mM) used for elution is shown in green. Absorbance of eluted protein was measured at 280 nm (red line) and possible DNA/RNA contamination was monitored at 260 nm (blue line). Peak fractions were collected and analysed by Western blotting. (B) Western blot analysis of purified E1o-90 His-tag form. The presence of purified His-tagged E1o-90 was confirmed (lanes 1 & 2) by anti-His tag antibody (1 in 2000 dilution) (see section 2.4.7.1). Molecular mass markers in kDa are shown. The arrow on the right of the blot indicates purified protein.

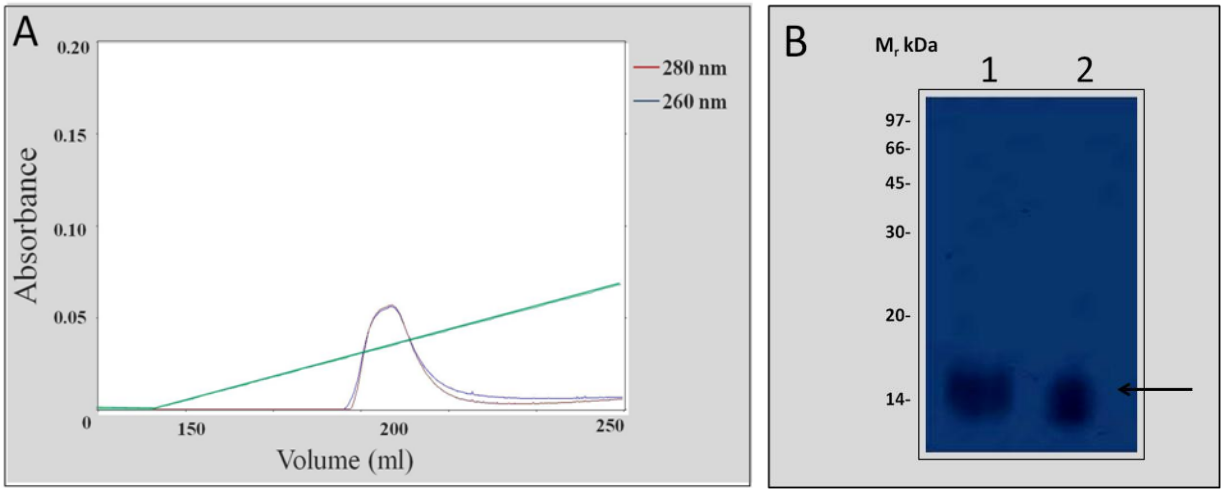


**Figure 3.22: Purification of E1o-153 (His-tag form)**
(A) Metal chelate affinity chromatography of E1o-153 (pET-14b). Cell lysates (20ml) were applied to the column in 5ml aliquots (see section 2.4.4). Bound protein was eluted from the column in a 0-100% gradient of elution buffer (8 CV) over the vol. 140-250 ml. The imidazole gradient (0-500mM) used for elution is shown in green. Absorbance of eluted protein was measured at 280 nm (red line) and possible DNA/RNA contamination was monitored at 260 nm (blue line). Peak fractions were collected and analysed by Western blotting. (B) Western blot analysis of purified E1o-153 His-tag form. The presence of purified His-tagged E1o-153 was confirmed (lanes 1 & 2) by anti-His tag antibody (1 in 2000 dilution) (see section 2.4.7.1). Molecular mass markers in kDa are shown. The arrow on the right of the blot indicates purified protein.

A number of expression strategies and conditions were attempted including alterations in growth media, expression temperature (Zhang *et al.* 2003) and bacterial strain which all failed to produce high yields of recombinant protein. Owing to insufficient protein over-expression and unsatisfactory protein purification these constructs were not employed further in this project.

### 3.3.3.2 Purification of E1o-60, E1o-90 and E1o-153 (GST fusion proteins)

Purification of GST-tagged E1o-60, E1o-90 and E1o-153 required only a single purification step using a glutathione Sepharose 4B column (bed volume, 5ml). However, in order to obtain high purity samples for ITC experiments, gel filtration chromatography was also employed. Figures 3.23 & 3.24 clearly show successful purification of E1o-60 and E1o-90 GST fusion proteins in high yield.

GST-tagged E1o-153 was purified in the same manner as the E1o-60 and E1o-90 GST. On SDS-PAGE analysis, this recombinant protein was found to be extremely susceptible to degradation (Fig. 3.25). The initial purification was successful; however, rapid proteolysis occurred at 4$^{o}$C over 24-48 h during which time significant amounts (>50%) of the intact fusion protein degraded and multiple bands were observed including free GST (~26 kDa). A variety of different approaches were tried in attempts to decrease protein degradation. These included various types of inhibitor cocktails, treating samples with bovine serum albumin (BSA) prior to French press treatment and growing the cells at low temperature, all without success.

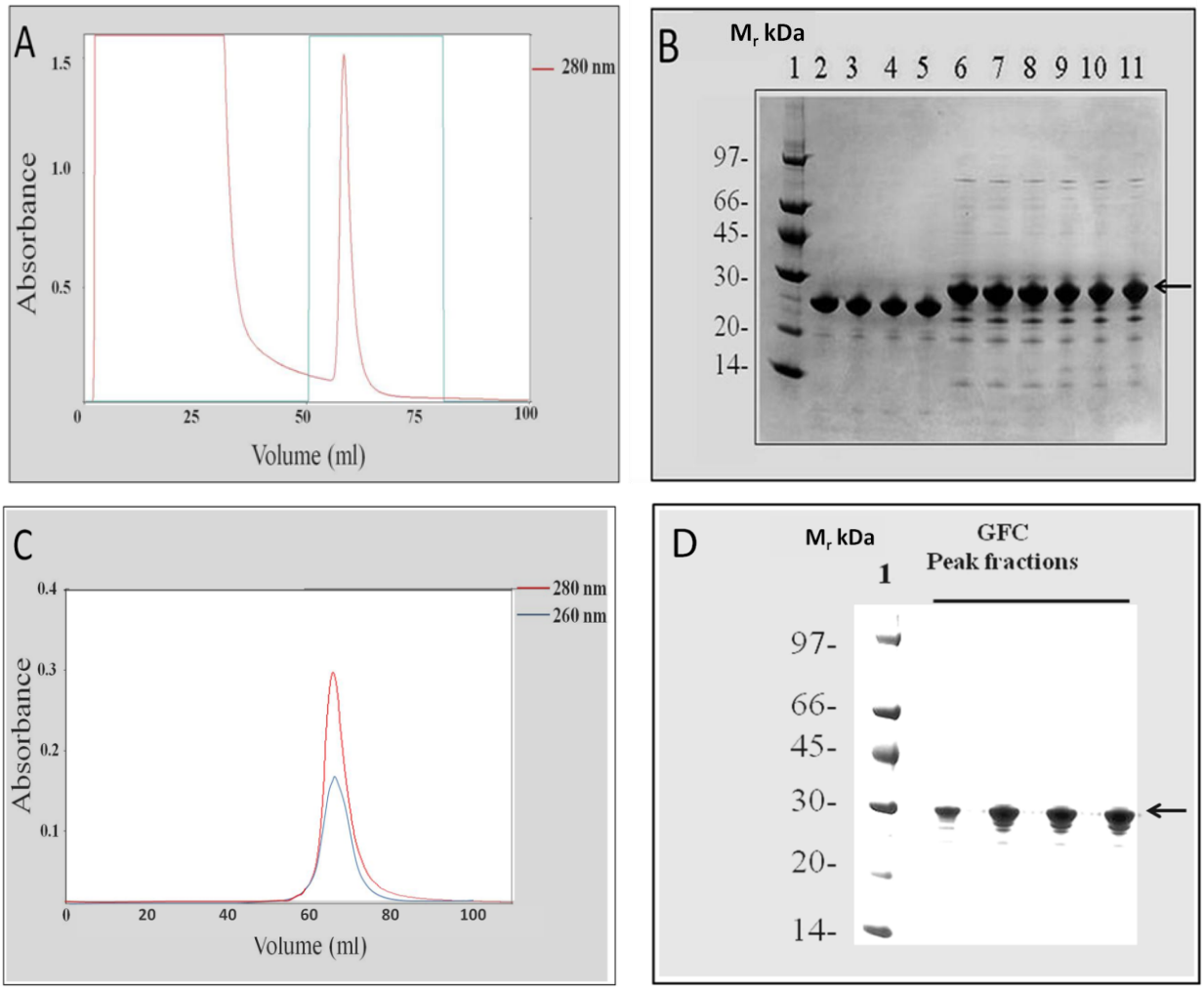


**Figure 3.23: Purification of E1o-60 (GST fusion protein)**
(A) Glutathione affinity chromatography of E1o-60 (pGEX-2T). Cell lysates (20ml) were applied to the column in 5ml aliquots (see section 2.4.4). Bound protein was eluted from the column using 5 CV elution buffer (20mM reduced glutathione, 50mM Tris-HCl, pH 8.0). The reduced glutathione buffer step used for elution is shown in green. Absorbance of eluted protein was measured at 280 nm (red line). Peak fractions were collected and analysed by SDS-PAGE. (B) SDS-PAGE analysis of eluted protein peak. Lane 1, molecular mass markers; lanes 2-5, purified wt GST-protein as control; lanes 6-11, purified E1o-60 stained with Coomassie Brilliant Blue. The arrow on the right of the blot indicates purified protein. (C+D) Gel filtration profile of E1o-60 with eluted peak at ~ 69 ml. The purity of the final E1o-60 preparation was assessed by SDS-PAGE analysis and showed large yields of pure E1o-60 corresponding to the main GFC peak. Lane 1, molecular mass markers.

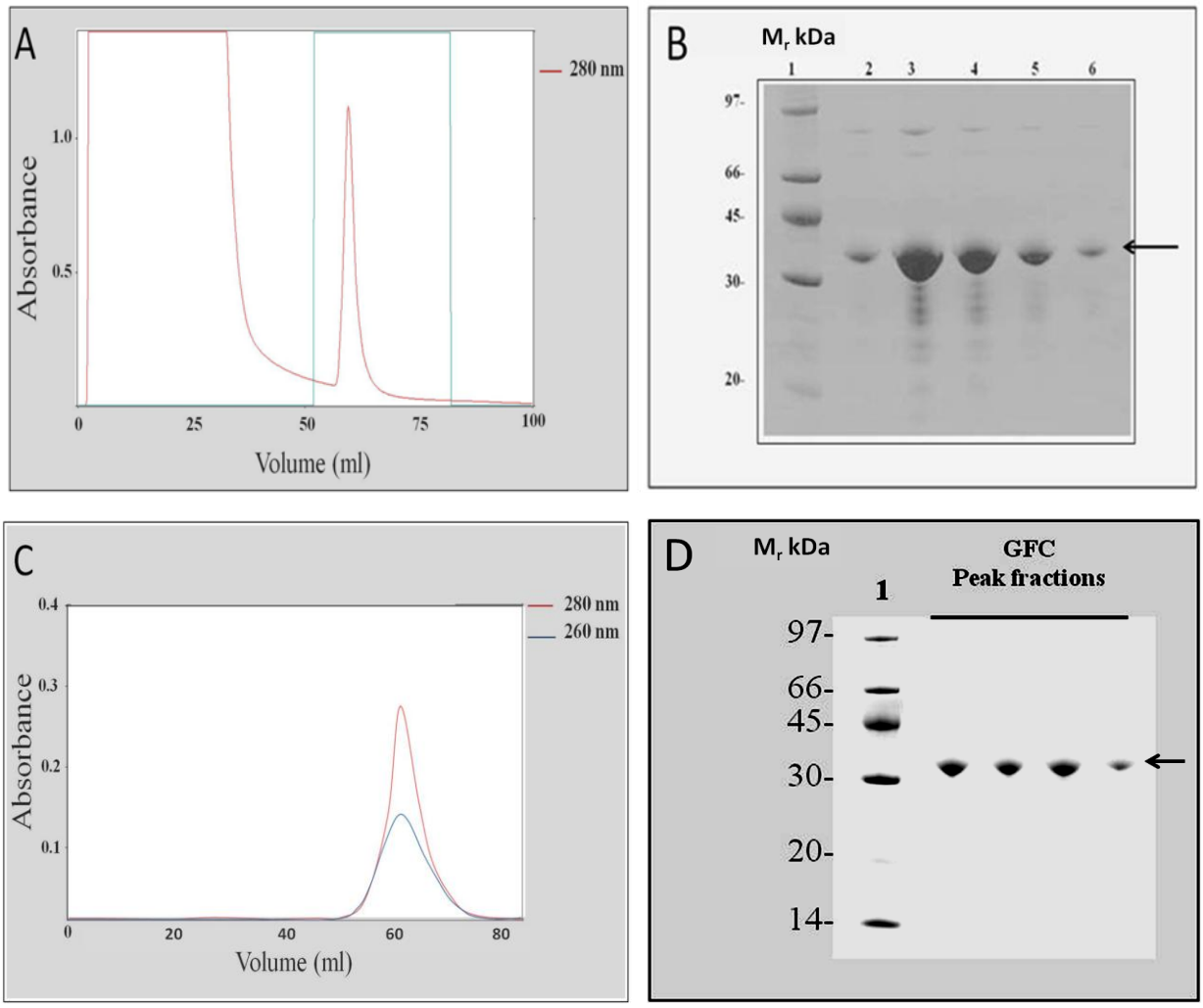


**Figure 3.24: Purification of E1o-90 (GST fusion protein)**

(A) Glutathione affinity chromatography of E1o-90 (pGEX-2T). Cell lysates (20ml) were applied to the column in 5ml aliquots (see section 2.4.4). Bound protein was eluted from the column using 5 CV elution buffer (20mM reduced glutathione, 50mM Tris-HCl, pH 8.0). The reduced glutathione buffer step used for elution is shown in green. Absorbance of eluted protein was measured at 280 nm (red line). Peak fractions were collected and analysed by SDS-PAGE. (B) SDS-PAGE analysis of eluted protein peak. Lane 1, molecular mass markers; lanes 2-6, purified E1o-90 stained with Coomassie Brilliant Blue. The arrow on the right of the blot indicates purified protein. (C+D) Gel filtration profile of E1o-90 with eluted peak at ~ 63 ml. The purity of the final E1o-90 preparation was assessed by SDS-PAGE analysis and showed large yields of pure E1o-90 corresponding to the main GFC peak. Lane 1, molecular mass markers.

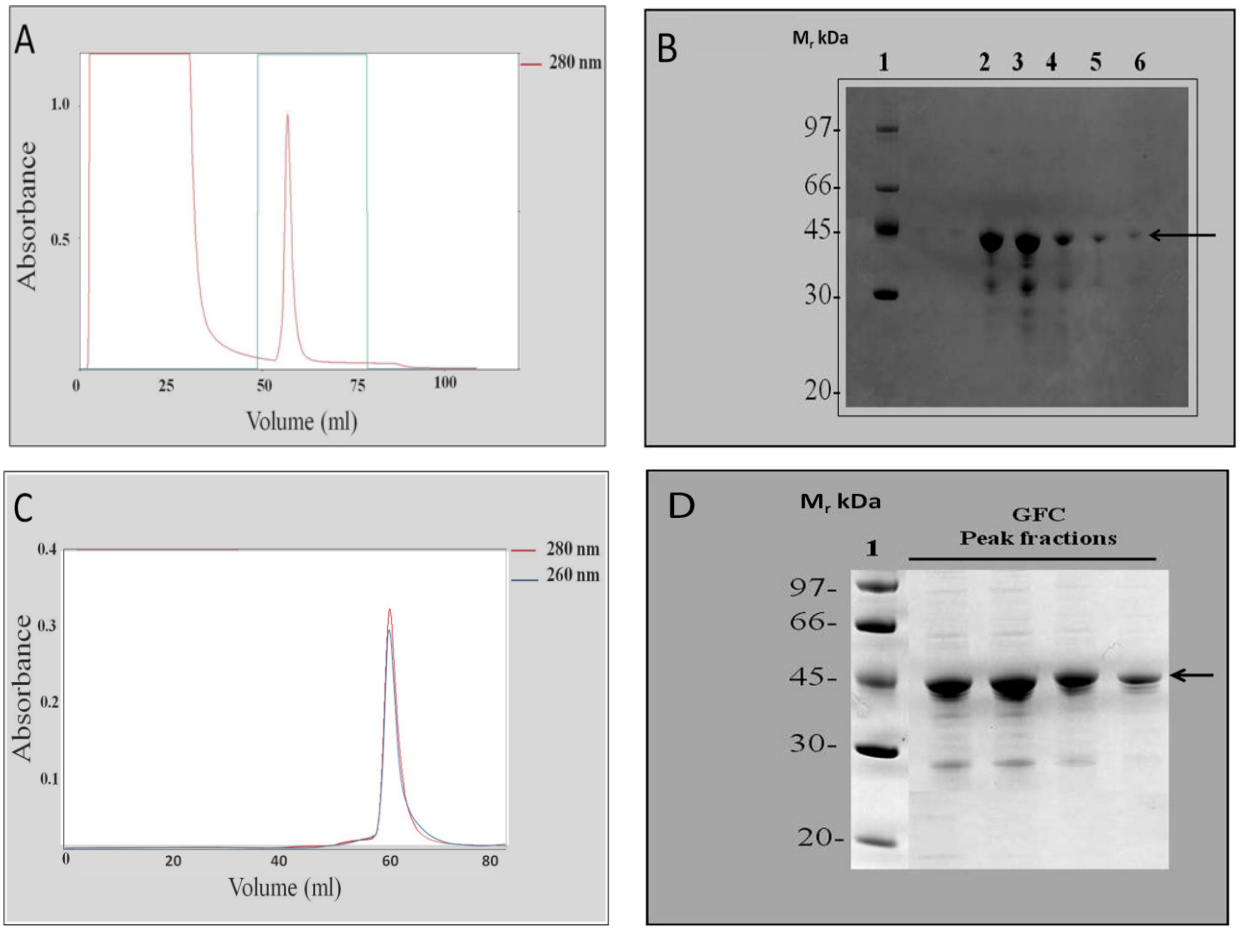


**Figure 3.25: Purification of E1o-153 (GST fusion protein)**
(A) Glutathione affinity chromatography of E1o-153 (pGEX-2T). Cell lysates (20ml) were applied to the column in 5ml aliquots (see section 2.4.4). Bound protein was eluted from the column using 5 CV elution buffer (20mM reduced glutathione, 50mM Tris-HCl, pH 8.0). The reduced glutathione buffer step used for elution is shown in green. Absorbance of eluted protein was measured at 280 nm (red line). Peak fractions were collected and analysed by SDS-PAGE. (B) SDS-PAGE analysis of eluted protein peak. Lane 1, molecular mass markers; lanes 2-6, purified E1o-153 stained with Coomassie Brilliant Blue. The arrow on the right of the blot indicates purified protein. (C+D) Gel filtration profile of E1o-153 with eluted peak at ~ 60 ml. The purity of the final E1o-153 preparation was assessed by SDS-PAGE analysis and shows limited degradation of E1o-153 corresponding to the main GFC peak. Lane 1, molecular mass markers.

### 3.3.3.3 Purification of E1o-60, E1o-90 and E1o-153 (MBP fusion proteins)

MBP fusion proteins (E1o-60, E1o-90 and E1o-153) were purified using an MBP Trap HP column. Figures 3.26 & 3.27 show purification steps for E1o-60 and E1o-90 indicating significant degradation of both proteins. It is possible that extensive proteolytic degradation occurs during protein expression or during the purification process itself. Many attempts were made to decrease the extent of protein degradation without success. Addition of BSA and more protease inhibitors prior to French press treatment, growth of cells at low temperatures and use of a rapid purification process did not improve protein stability. Owing to this problem neither of these constructs was employed for subsequent experiments in this study. SDS-PAGE analysis of purified E1o-153 was also found to be sensitive to degradation although this was less problematic than the E1o-60 and E1o-90 MBP fusion proteins (Fig. 3.28).

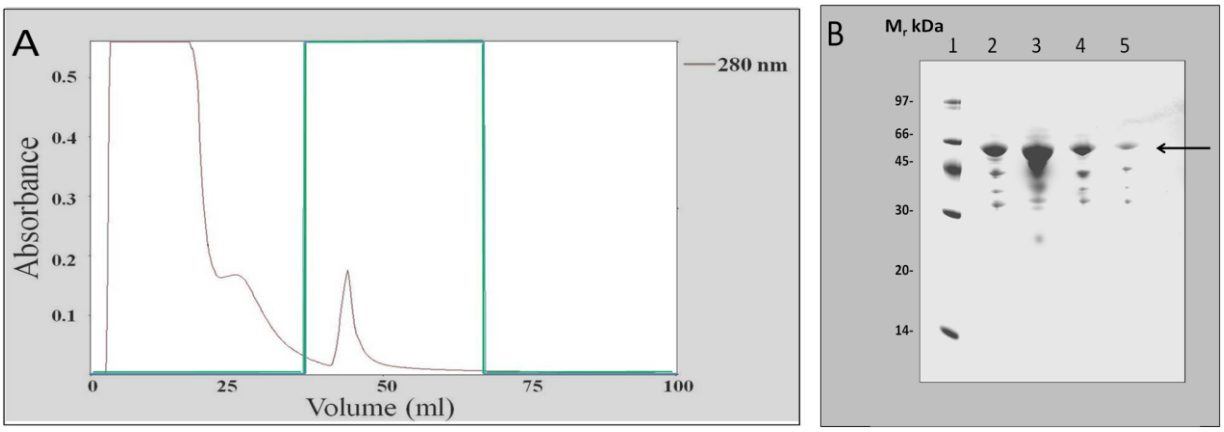


**Figure 3.26: Purification of E1o-60 (MBP fusion protein)**
(A) Maltose binding protein (MBP) affinity chromatography of E1o-60. Cell lysates (20ml) were applied to the column in 5ml aliquots (see section 2.4.4). Bound protein was eluted from the column using 5 CV elution buffer step (15mM maltose, 200mM NaCl, 1mM EDTA, 20mM Tris-HCl, pH 7.2). The maltose buffer step used for elution is shown in green. Absorbance of eluted protein was measured at 280 nm (grey line). Peak fractions were collected and analysed by SDS-PAGE. (B) SDS-PAGE analysis of eluted protein peak. Lane 1, molecular mass markers; lanes 2-5, purified E1o-60 stained with Coomassie Brilliant Blue showing significant degradation. The arrow on the right of the blot indicates purified full-length protein.

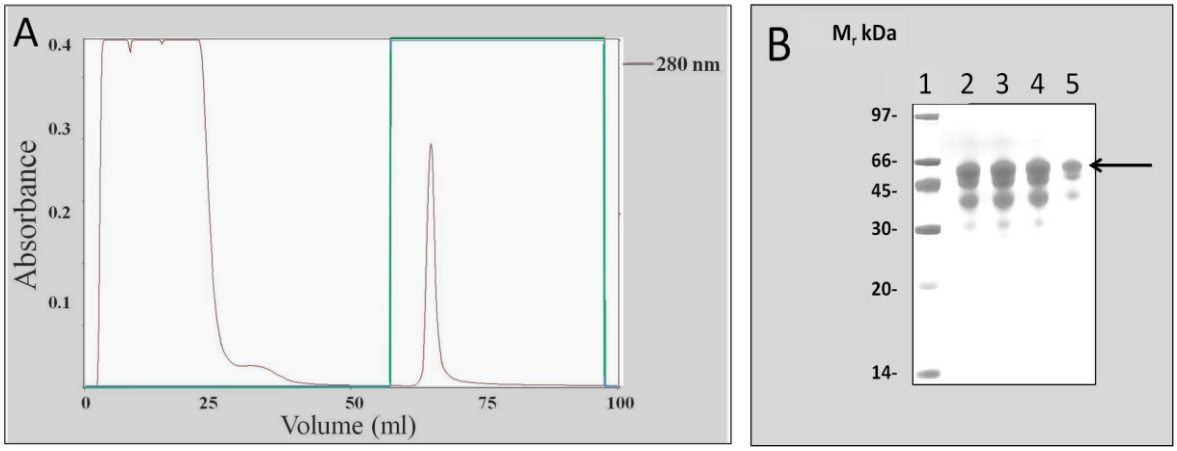


**Figure 3.27: Purification of E1o-90 (MBP fusion protein)**
(A) Maltose binding protein (MBP) affinity chromatography of E1o-90. Cell lysates (20ml) were applied to the column in 5ml aliquots (see section 2.4.4). Bound protein was eluted from the column using 5 CV elution buffer (15mM maltose, 200mM NaCl, 1mM EDTA, 20mM Tris-HCl, pH 7.2). The maltose buffer step used for elution is shown in green. Absorbance of eluted protein was measured at 280 nm (grey line). Peak fractions were collected and analysed by SDS-PAGE. (B) SDS-PAGE analysis of eluted protein peak. Lane 1, molecular mass markers; lanes 2-5, purified E1o-90 stained with Coomassie Brilliant Blue showing significant degradation. The arrow on the right of the blot indicates purified full-length protein.

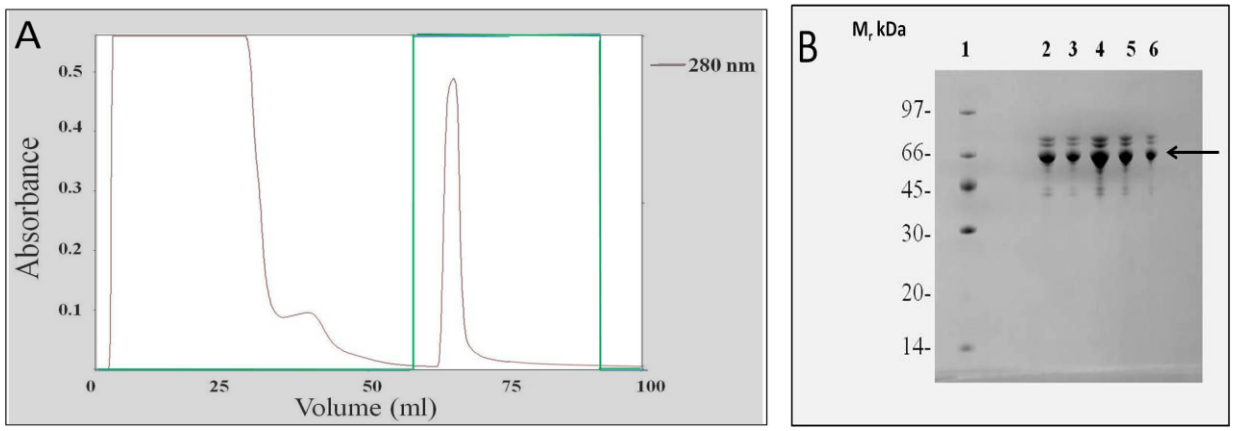


**Figure 3.28: Purification of E1o-153 (MBP fusion protein)**
(A) Maltose binding protein (MBP) affinity chromatography of E1o-153. Cell lysates (20ml) were applied to the column in 5ml aliquots (see section 2.4.4). Bound protein was eluted from the column using 5 CV elution buffer (15mM maltose, 200mM NaCl, 1mM EDTA, 20mM Tris-HCl, pH 7.2). The maltose buffer step used for elution is shown in green. Absorbance of eluted protein was measured at 280 nm (grey line). Peak fractions were collected and analysed by SDS-PAGE. (B) SDS-PAGE analysis of eluted protein peak. Lane 1, molecular mass markers; lanes 2-6, purified E1o-153 stained with Coomassie Brilliant Blue. The arrow on the right of the blot indicates purified full-length protein.

### 3.3.3.4 Purification of human E2o (His-tag form)

His-tagged E2o was purified by metal chelate chromatography (Fig. 3.29A). Purified fractions were then gel filtered using GFC buffer (20mM NaCl, 2mM EDTA, 50 mM $KH_2PO_4$, pH 7.4) in order to remove all residual protein contaminants (Fig. 3.29C). SDS-PAGE revealed a high yield of pure protein (Fig. 3.29B & 3.29D).

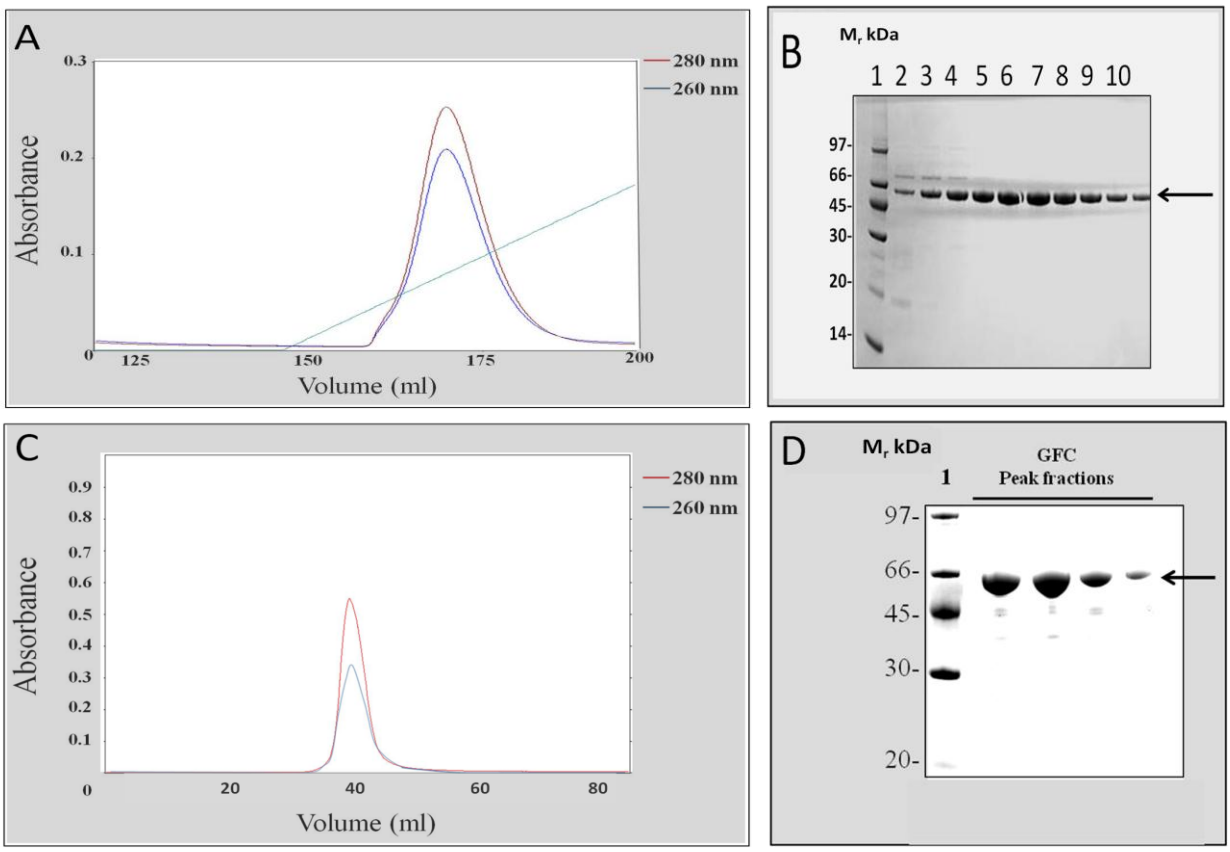


**Figure 3.29: Purification of human E2o (His-tag form)**
(A) Metal chelate affinity chromatography of E2o. Cell lysates (20ml) were applied to the column in 5ml aliquots (see section 2.4.4). Bound protein was eluted from the column in a 0-100% gradient of elution buffer (8 CV) over the vol. 145-200 ml. The imidazole gradient (0-500mM) used for elution is shown in green. Absorbance of eluted protein was measured at 280 nm (red line) and possible DNA/RNA contamination was monitored at 260 nm (blue line). Peak fractions were collected and analysed by SDS-PAGE. (B) SDS-PAGE analysis of eluted protein peak. Lane 1, molecular mass markers; lanes 2-10, purified E2o stained with Coomassie Brilliant Blue. The arrow on the right of the blot indicates purified protein. (C+D) Gel filtration profile of E2o being eluted at or near the void volume (~ 40ml). The purity of the final E2o preparation was assessed by SDS-PAGE analysis and showed large yields of pure E2o corresponding to the main GFC peak. Lane 1, molecular mass markers.

### 3.3.3.5 Purification of human E3 (His-tag form)

Purification of E3 was very similar to the E2o purification, being achieved by a two step process involving an initial metal chelate chromatography step (Fig. 3.30A) followed by gel filtration (Fig. 3.30C). The purified E3 was yellow in colour indicating the incorporation of the FAD cofactor. SDS-PAGE confirmed the high purity of the E3 preparation (Fig. 3.30B & 3.30D).

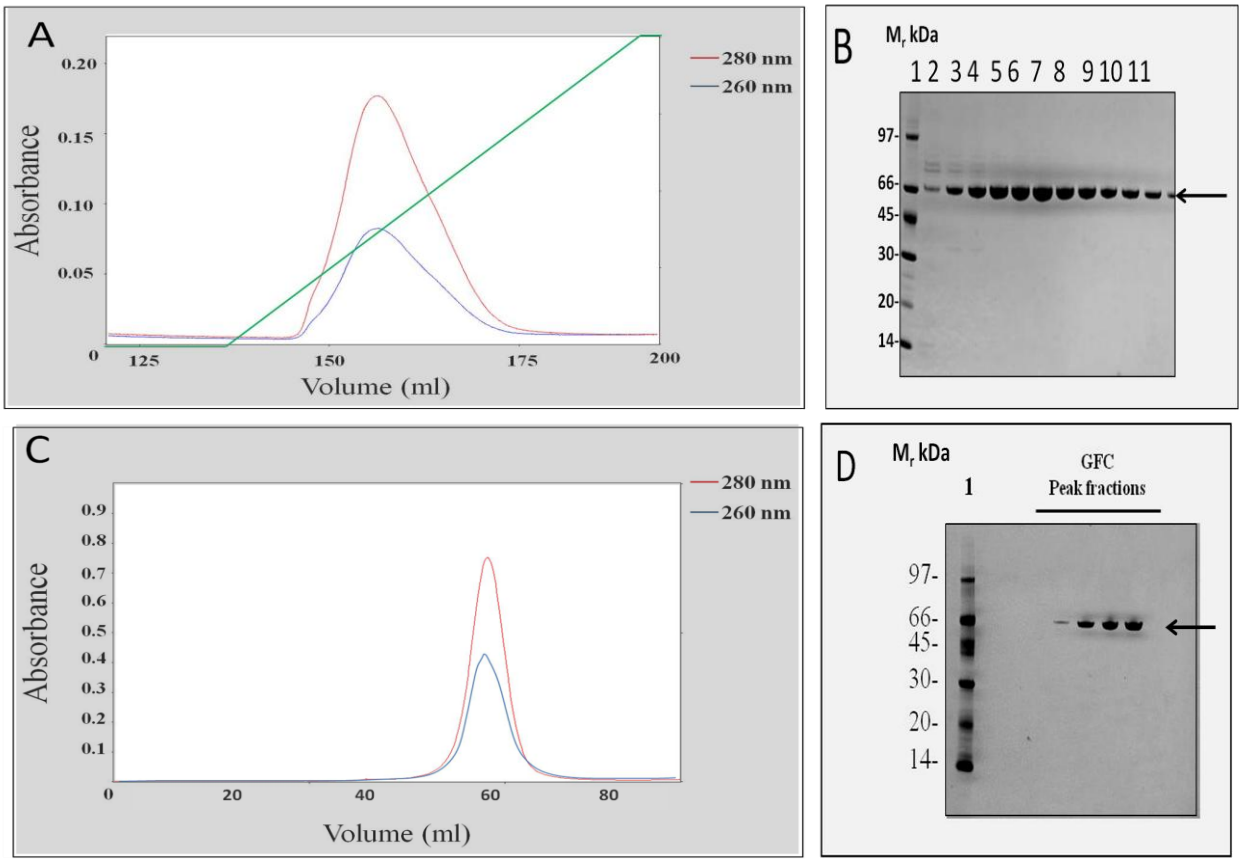


**Figure 3.30: Purification of human E3 (His-tag form)**
(A) Metal chelate affinity chromatography of E3. Cell lysates (20ml) were applied to the column in 5ml aliquots (see section 2.4.4). Bound protein was eluted from the column in a 0-100% gradient of elution buffer (8 CV) over the vol. 145-200 ml. The imidazole gradient (0-500mM) used for elution is shown in green. Absorbance of eluted protein was measured at 280 nm (red line) and possible DNA/RNA contamination was monitored at 260 nm (blue line). Peak fractions were collected and analysed by SDS-PAGE. (B) SDS-PAGE analysis of eluted protein peaks. Lane 1, molecular mass markers; lanes 2-11, purified E3 stained with Coomassie Brilliant Blue. The arrow on the right of the blot indicates purified protein. (C+D) Gel filtration profile of E3 being eluted at ~ 60 ml. The purity of the final E3 preparation was assessed by SDS-PAGE analysis and showed large yields of pure E3 corresponding to the main GFC peak. Lane 1, molecular mass markers.

## 3.4 Summary

The main purpose of this chapter was to clone, express and purify a series of short human E1o N-terminal constructs and the constituent mature E1o, E2o and E3 enzymes of the human OGDC. The solubility and yields achieved for all purified proteins are summarised in Table 3.7. The successfully purified proteins and N-terminal fragments were then used for a variety of experiments as described in subsequent chapters.

| Protein | Plasmid vector | Cloning and Expression | Solubility | Yields (mg/l) | Degradation |
|---|---|---|---|---|---|
| E3 | pET-14b | Successful | Soluble | 30-40 | None |
| E2o | pET-14b | Successful | Soluble | 40-50 | None |
| E1o-60 | pET-14b | Successful | Soluble | Poor | N/A |
| E1o-90 | pET-14b | Successful | Soluble | Poor | N/A |
| E1o-153 | pET-14b | Successful | Soluble | Poor | N/A |
| E1o-60 | pGEX-2T | Successful | Soluble | 30-40 | None |
| E1o-90 | pGEX-2T | Successful | Soluble | 25-35 | None |
| E1o-153 | pGEX-2T | Successful | Soluble | 25-35 | Significant degradation |
| E1o-60 | pET-30a | Successful | Soluble | 5-10 | Significant degradation |
| E1o-90 | pET-30a | Successful | Soluble | 10-15 | Significant degradation |
| E1o-153 | pET-30a | Successful | Soluble | 15-20 | Minor degradation |
| Full-length E1o | pET-14b | Successful | In-soluble | N/A | N/A |
| wt GST | pGEX-2T | N/A | Soluble | 30-40 | None |
| wt MBP | pET-30a | N/A | Soluble | 20-30 | None |

**Table 3.7: Summary of cloning and protein purification yields**
N/A, Not applicable; wt, wild-type.

# Chapter 4

# Preliminary structural characterization of the N-terminal region of E1o and investigation of its interaction with E3

## *4.1 Introduction*

2-oxoacid dehydrogenase complexes are large multimeric assemblies located in the mitochondrial matrix. These macromolecular structures serve as paradigms for understanding protein structure-function relationships, the biological significance of protein assemblies and protein-protein interactions in general.

The PDC, OGDC and BCOADC are highly-ordered assemblies of 3 distinct enzymes, designated E1, E2 and E3, that jointly regulate critical steps in glucose metabolism and the degradation of the branched-chain amino acids. The catalytic reaction requires significant coupling between these three enzymes (Reed 1974; Yeaman 1986; Lindsay 1989; Perham 1991). OGDC catalyses the rate-limiting step in the TCA cycle in many species. The importance of this complex is highlighted by its selective inactivation in the pathology of several neurodegenerative conditions, particularly those associated with oxidative stress disorders such as Alzheimer's disease.

In mammalian PDC, E2p and an E2p-related subunit (E3BP) form the structural core to which E1p and E3 enzymes are bound via a specific E1p-SBD on E2p and an E3-SBD located on E3BP (Neagle and Lindsay 1991; Izard *et al.* 1999; Hiromasa *et al.* 2004). In BCOADC, a single SBD

located on E2b binds both E1b and E3 (Clarkson and Lindsay 1991; Kalia *et al.* 1993; Nakano *et al.* 1994). In contrast, E2o does not contain any obvious SBD for E1o or E3 and there is no equivalent to E3BP in this complex. Hence, human E2o has a unique structure comprising only two domains (LD and CTD) (Bradford *et al.* 1987; Wagenknecht *et al.* 1990; Nakano *et al.* 1994; Koike *et al.* 2000). In mammalian cells, E3 is an FAD containing flavoprotein that is common to all 3 multienzyme complexes (PDC, OGDC and BCOADC).

E1o exists as a homodimer ($\alpha_2$) whereas E1p and E1b exist as heterotetramers ($\alpha_2\beta_2$). It is a ThDP-dependent enzyme that catalyses the oxidative decarboxylation step with transfer of a succinyl group to an E2o-linked lipoic acid moiety. A number of mammalian E1o isoforms have been identified. The major human E1o isoform is encoded by the *OGDH* gene (heart isoform, OGDH-H). Additionally there are two further isoforms; OGDH-L (brain isoform) and DHTKD1 mitochondrial hypothetical protein (Szabo *et al.* 1994; Koike 1998; Bunik and Degtyarev 2008a; Bunik and Fernie 2009).

Previous research has established that the N-terminal region of E1o is involved in the overall maintenance of OGDC integrity and assembly. Selective proteolysis of E1o with trypsin at a single site located near its N-terminus results in dissociation of E3 and a large, active E1' species from the core assembly with simultaneous loss of overall complex activity (Kresze *et al.* 1981; Rice *et al.* 1992; McCartney *et al.* 1998). Moreover, N-terminal sequence analysis of mammalian E1o indicates that sequences located in this region display limited similarity to corresponding sequences in E3BP suggesting that the N-terminal region of E1o may be involved in interacting with E3 (Rice and Lindsay 1991; Rice *et al.* 1992). In addition, a previous

crystallography study of a bacterial E1o has indicated that it cannot be crystallized unless its N-terminal region (77 a.a. in length) is removed (Frank *et al.* 2007). These studies suggest that the N-terminal region of E1o may be natively-disordered and possibly involved in interacting with both E2o and E3.

Initially, this chapter presents preliminary data for the structural characterization of the N-terminal region of E1o using synthetic peptides and circular dichroism (CD). In parallel with these experiments, a basic bio-informatics approach was employed to determine if this N-terminal region was predicted to form a stable 3-D structure similar to the SBDs of E2p, E2b and E3BP. In addition, sequence comparison and alignment of the main E1o isoforms was investigated.

The main thrust of this chapter concerns an investigation into the ability of the E1o N-terminal region to associate with E3 and mapping of the E1o segment involved in subunit binding in order to understand more fully its role in maintaining OGDC integrity.

To achieve these goals, a range of biochemical and biophysical approaches was applied including: (a) peptide array analysis to test the ability of N-terminal E1o segments to bind E3; (b) ala-scanning to identify key docking sites; (c) use of synthetic peptides to N-terminal E1o segments; (d) native polyacrylamide gel electrophoresis; (e) isothermal titration calorimetry; (f) gel filtration and (g) GST affinity chromatography.

# 4.2 Results and analysis

## 4.2.1 Structural characterization of the N-terminal region of E1o

To investigate the N-terminal region of E1o in more detail and to test the potential of this region to fold into an ordered 3-D conformation, two synthetic peptides N-terminal E1o 25 meric (Ser11 - Ser35) (SGTSSNYVEEMYCAWLENPKSVHKS, peptide 1) and E1o (Trp36 - Ser60) (WDIFFRNTNAGAPPGTAYQSPLPLS, peptide 2) were purchased from Genscript, UK (see Materials and Methods, section 2.4.9). These peptides were designed based on peptide array data showing strong association with E3 (see section 4.2.3.1) and checked by SDS-PAGE (Fig. 4.1).

Moreover, a 65-meric peptide corresponding to amino acids Ser11 to Glu75 of the N-terminal region of E1o (peptide 3) was also purchased from LifeTein LLC., USA. Owing to the hydrophobicity of peptide 3, it was necessary to dissolve it in organic solvents e.g. dimethyl sulfoxide (DMSO) or employ acidic conditions e.g. 0.1M acetic acid.

A number of experiments were performed using peptide 3 including ITC and native-PAGE without success (data not shown). Moreover, it became apparent that extensive aggregation of peptide 3 and its limited solubility in physiological buffers made these experiments unfeasible.

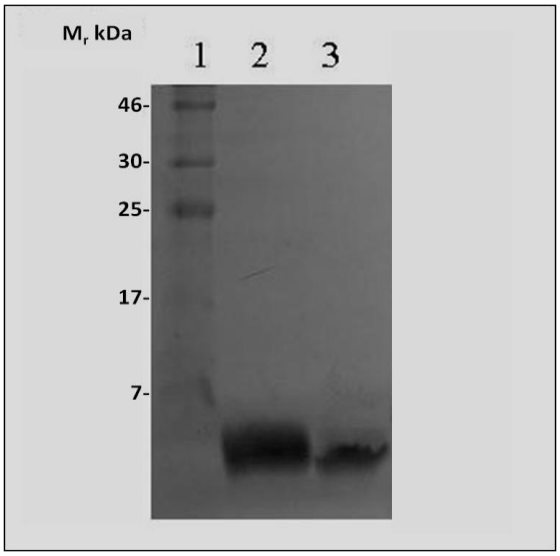


**Figure 4.1: SDS-PAGE analysis of synthetic peptides**
Samples were denatured in the presence of 150mM DTT at 100°C for 5min and resolved on an 18% SDS/polyacrylamide gel. Protein bands were visualised by Coomassie Brilliant Blue staining. Lane 1, molecular mass markers. SDS-PAGE analysis of synthetic peptides showing peptide 1 (~ 3 kDa, lane 2) and peptide 2 ( ~ 2.8 kDa, lane 3).

Peptides 1 and 2 both dissolved readily in aqueous solutions at neutral pH. The molecular masses and molar extinction coefficient (ε) of these peptides were determined by computing the protein sequences in the EXPASY suite (see section 2.4.6). Moreover, mass spectrophotometry was employed for confirmation of the exact molecular mass of both peptides. Analysis was carried out by the Astbury centre, University of Leeds. Samples were prepared by dissolving 100μM peptide in 20mM ammonium acetate at pH 7.5 (see section 2.5.3).

It was found that the molecular mass of the peptides 1 and 2 were 2,847 Da and 2,721 Da, respectively (Fig. 4.2 & 4.3) within one Dalton of the predicted molecular masses as calculated from their amino acid sequences.

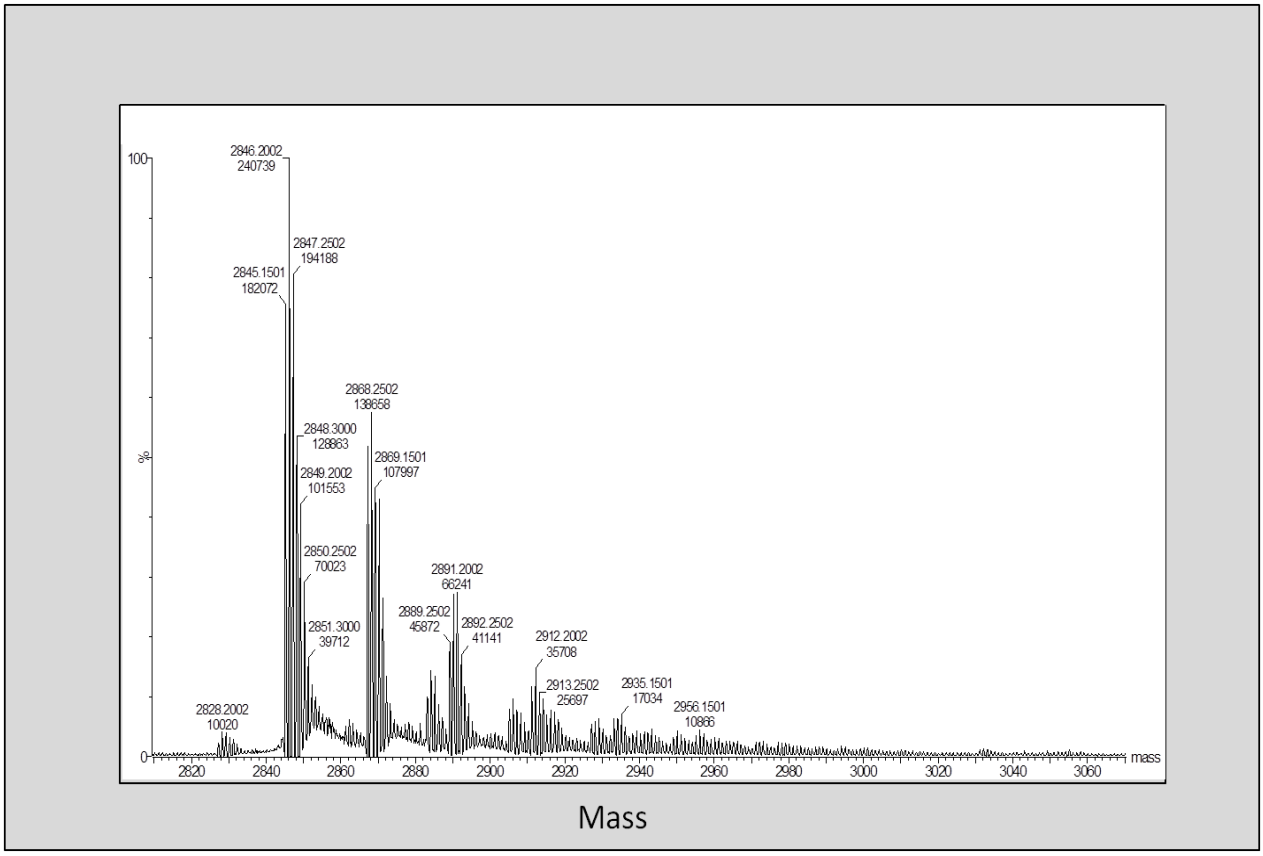


**Figure 4.2: Molecular mass spectrum of synthetic peptide 1**
MS analysis of synthetic 25-meric peptide (Ser11 to Ser35). The peptide is measured at 2846.2 Da which is within one Da of the expected calculated mass of 2847.1 Da.

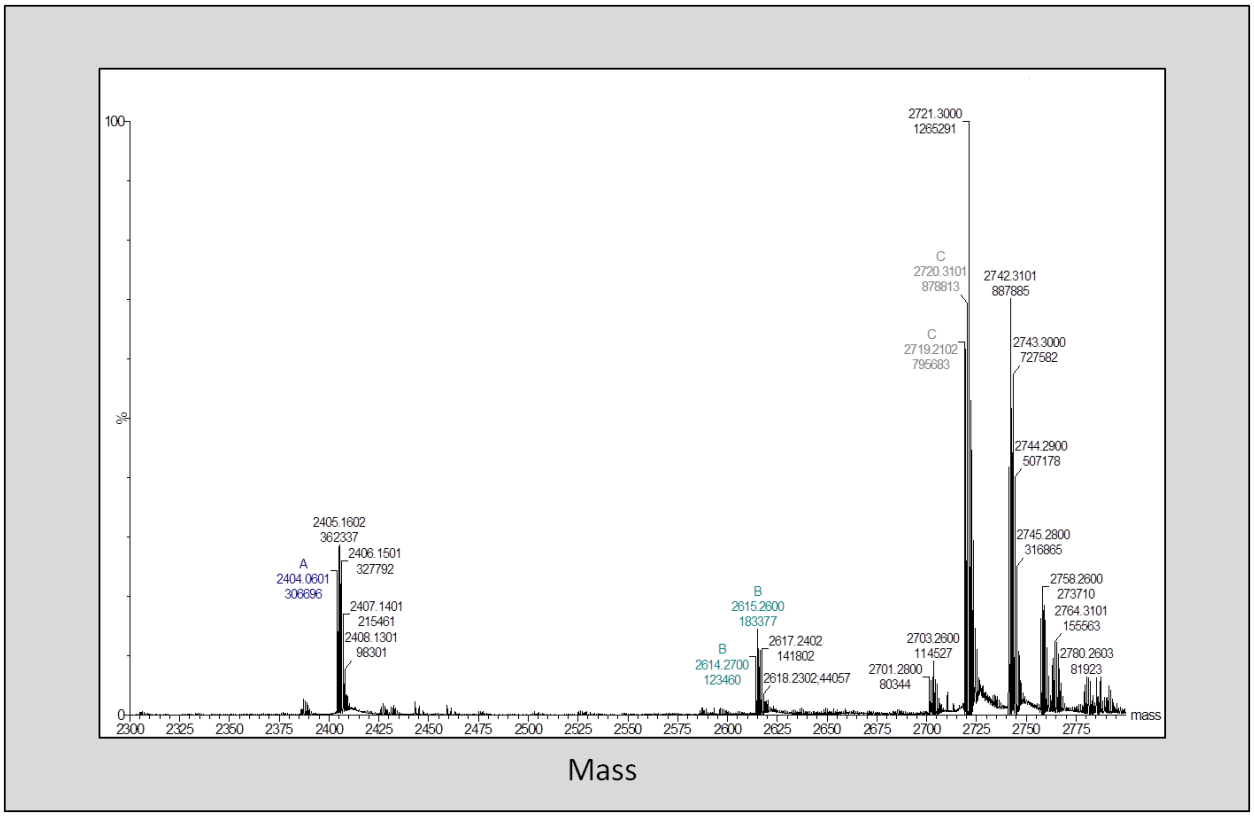


**Figure 4.3: Molecular mass spectrum of synthetic peptide 2**
MS analysis of synthetic 25-meric peptide (Trp36 to Ser60). The peptide is measured at 2721.3 Da which is within one Da of the expected calculated mass of 2721.0 Da.

Structural characterization of the E1o N-terminal peptides was initially performed using circular dichroism to determine their tendency to form characteristic secondary structures. CD measures differences in the absorption of left-handed polarized light versus right-handed polarized light that arise due to structural asymmetry, in particular α-helix and β-sheet formation.

For CD studies, peptides 1 and 2 were dialysed against 20mM $KH_2$ $PO_4$ buffer at pH 7.5. Experiments were performed at room temperature on a Jasco J-810 spectro-polarimeter scanning the spectra in the far and near UV regions (see section 2.5.1).

Peptides 1 and 2 were titrated with increasing concentrations of 2,2,2, trifluoroethanol (TFE). Analysis of the data revealed that peptide 1 (25-meric, Ser11 to Ser35) comprised 47% α-helix, 8% β-strand, 14% turns and 31% random coil at 50% TFE (Fig. 4.4). Peptide 2 (25-meric, Trp36 to Ser60) comprised 27% α-helix, 11% β-strands, 25% turns and 37% random coil at 50% TFE (Fig. 4.5). Both peptides demonstrated an ability to form α-helix in TFE as evidenced by the presence of double minima at approx. 208 and 220 nm. Peptide 2 showed less ability to adopt an α-helical conformation than peptide 1 which starts to fold at approx. 10% TFE. All CD experiments were carried out and analysed in collaboration with Dr. S. Kelly, University of Glasgow.

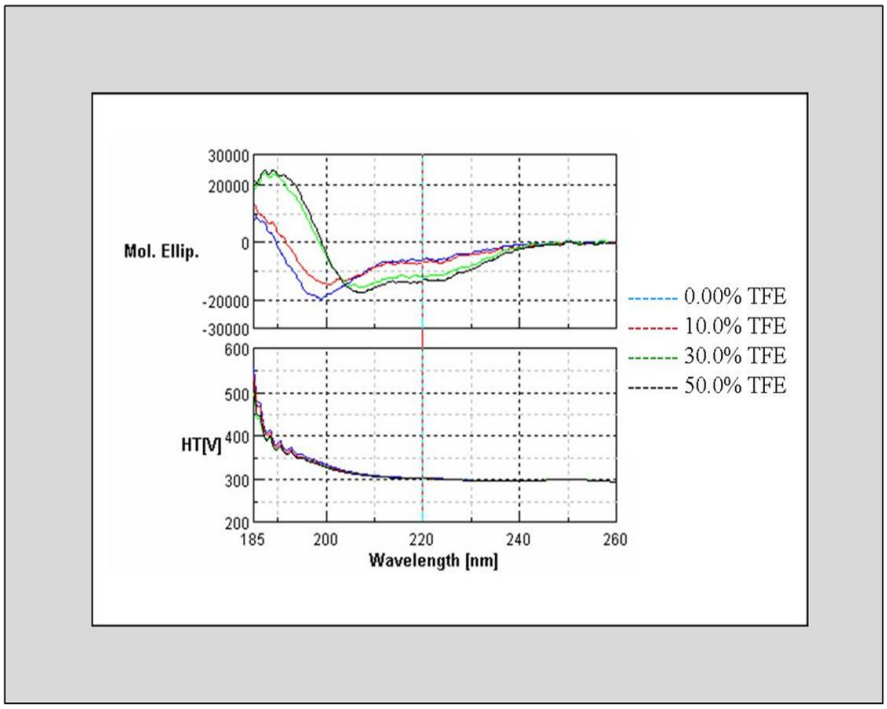


**Figure 4.4: Circular dichroism spectra of synthetic peptide 1**
Far UV CD spectra (185-260nm) of peptide 1 (25-meric, Ser11 to Ser35) in the absence of 2,2,2, trifluoro-ethanol (TFE) (blue) and increasing concentrations of TFE. Peptide 1 starts folding at ~ 10% TFE.

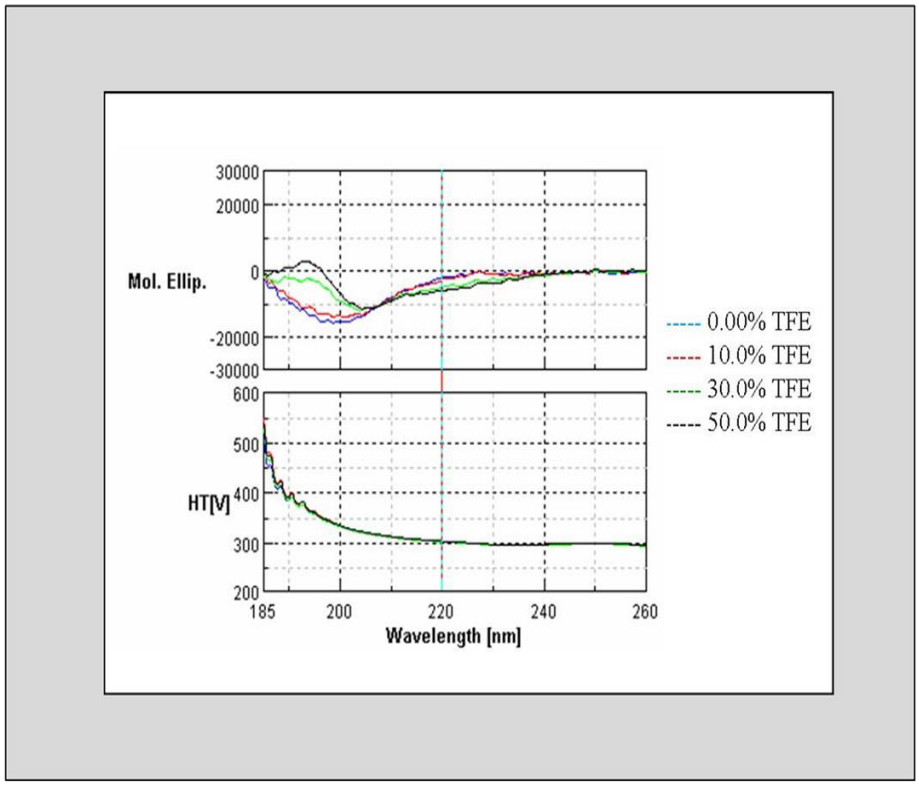


**Figure 4.5: Circular dichroism spectra of synthetic peptide 2**
Far UV CD spectra of peptide 2 (25-meric, Trp36 to Ser60) in the absence of TFE (blue) and increasing concentrations of TFE. Peptide 2 showed less ability to fold into an α-helical conformation starting to fold at ~ 30% TFE.

Secondary structure analysis of these 2 N-terminal E1o peptides covering the putative E3 binding domain revealed that they can adopt an α-helical conformation under appropriate conditions. To extend these analyses, structure prediction was carried out on the E1o N-terminal region. In general, the aim of protein structure prediction is to compute the likely 3-D conformation of the protein or polypeptide of interest based on their primary amino acid sequence. Both, I-TASSER and Swiss-model servers were employed to predict the 3-D structure of the E1o N-terminal region (see Materials and Methods, section 2.6.4).

I-TASSER (Zhang 2008) and Swiss-model (Guex and Peitsch 1997; Schwede *et al.* 2003; Arnold *et al.* 2006) online systems depend on searching for sequences of similar overall character by protein threading (I-TASSER) or significant sequence homology (Swiss-model) to polypeptides of known 3-D structure in the Protein Data Bank (PDB). Once one or more of these polypeptide sequences are selected, they are then used as templates to predict the 3-D structure of the target protein. I-TASSER predicts the 3-D structure of the E1o N-terminal region generating 5 possible models. These models are selected based on the best C-score that represents the degree of similarity to the templates. Typically, C-scores are scaled in the range (-5 to 2) where positive values reflect a high quality model.

Figures 4.6 shows the 3-D structure prediction for the human N-terminal region of E1o (1-77 a.a.) that has been generated by I-TASSER. The N-terminal E1o-77 (Ser1-Gln77) sequence was provided in FASTA format to http://zhanglab.ccmb.med.umich.edu/I-TASSER/, generating 5 models with C-scores; -1.43, -2.91, -3.47, -3.57 and -3.89 respectively. Interestingly, a 3-D structure prediction of E1o-77 (1-77 a.a.) using Swiss-model failed to generate any models suggesting that no homologous sequences exist in the database.

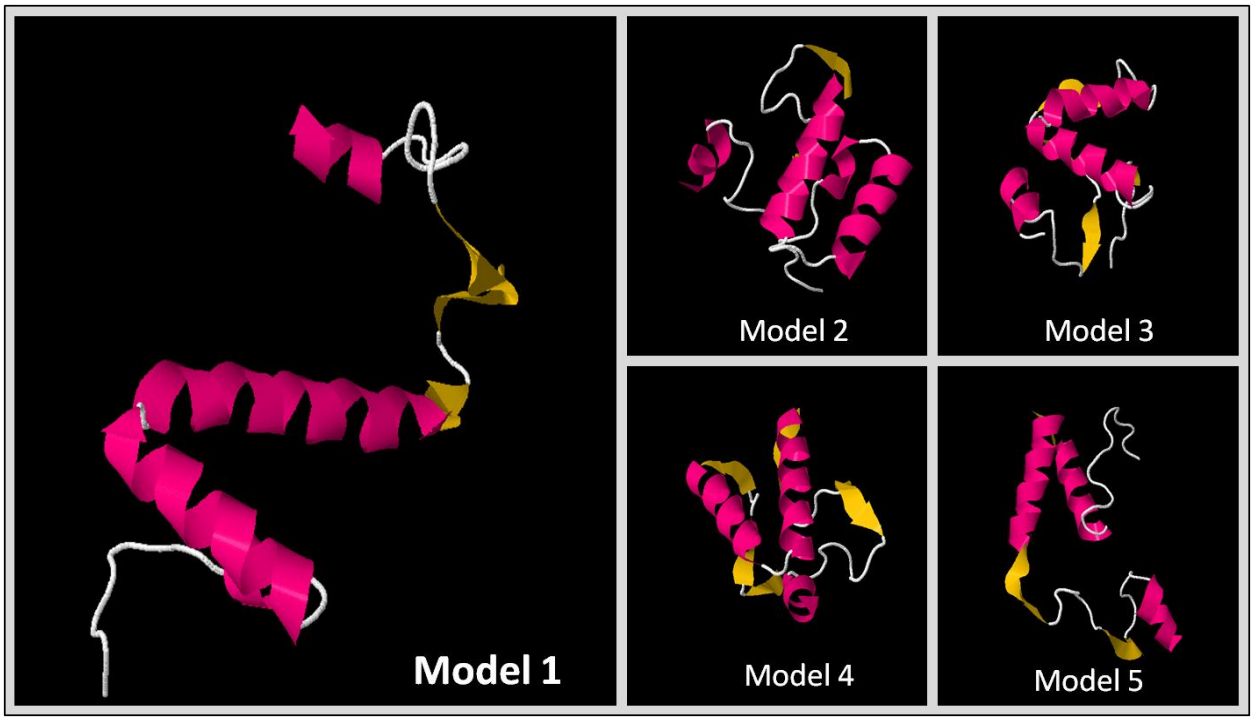


**Figure 4.6: 3-D structure predication of human N-terminal E1o-77**
Prediction of 3-D structure for human N-terminal E1o-77 (Ser1-Gln77). The 3-D structure was predicted by I-TASSER (Zhang 2008) and generated 5 models based on C-score. Model 1 has highest C-score (-1.43). Human N-terminal E1o-77 is coloured according to secondary structure as follows: α-helix (pink) and β-sheet (yellow).

## 4.2.2 Structural prediction for human E1o and sequence alignment of main E1o isoforms

In order to obtain a structural model for full-length human E1o (OGDH-H), the crystal structure obtained for the *E. coli* E1o was used as a template by I-TASSER (Frank *et al.* 2007). The two sequences display 38.8% identity in a 957 a.a. overlap (Fig. 4.7). Structural predictions for human E1o are shown in Figure 4.8. The 5 models generated had C-scores of 0.69, -1.89, -2.04, -2.12 and -2.12, respectively.

In addition, Figure 4.9 shows a ThDP binding site prediction for human E1o (OGDH-H) generated by I-TASSER using the crystal structure of the *SucA* domain of *Mycobacterium smegmatis* alpha-ketoglutarate decarboxylase complexed with ThDP as a template (Wagner *et al.* 2011). The predicted binding site residues in the human E1o model are Glu378, Ala379, Ala380, Asp381, Gly407, Gly410, Asp411, Ala412, Ala413, Glu422, Val442, Asn443, Asn444 and His473. Interestingly, the human E1o model clearly indicates that the E1o N-terminal region is exposed on the surface of the homodimer (Fig. 4.8). As both subunits in the E1o homodimer associate in a 'head-to-head' fashion, it is apparent that both exposed E1o N-terminal domains are likely to be located in close proximity at one end of the molecule (Frank *et al.* 2007).


**Figure 4.7: Sequence alignment of human E1o and *E. coli* E1o**

The amino acid sequence of human E1o (OGDH-H) and *E. coli* E1o (Frank *et al.* 2007) were aligned. An asterisk (*) indicates positions that have a fully conserved residue. A colon (:) indicates conservation between residues with strongly similar properties. A period (.) indicates conservation between residues with weakly similar properties. Hydrophobic residues are shown in red. Acidic and basic residues are shown in blue and magenta respectively. Residues with hydroxyl, sulfhydryl or amine groups are depicted in green.

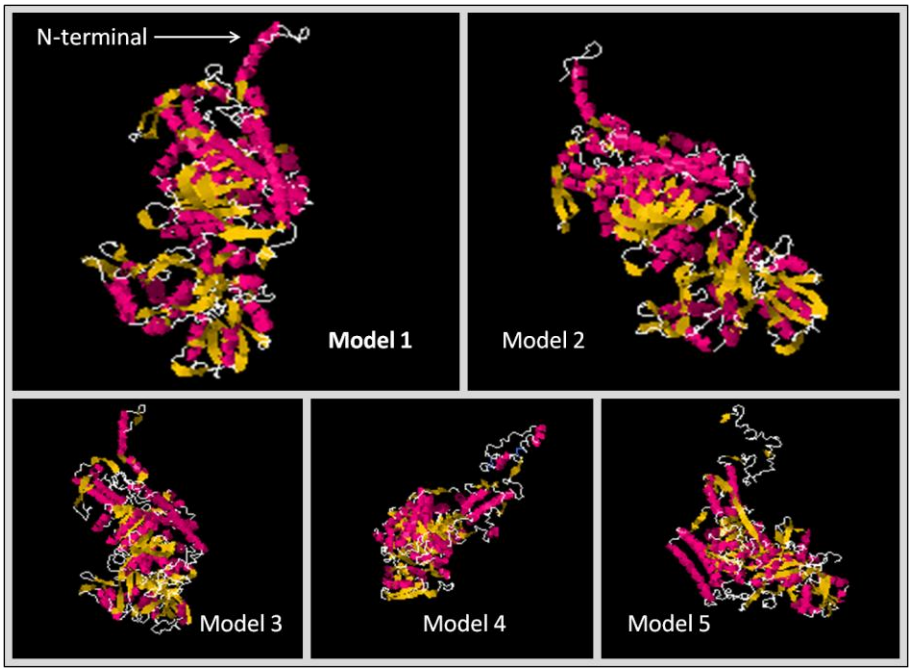


**Figure 4.8: 3-D structure predication of human E1o**
Prediction of 3-D structures for human E1o (OGDH-H, 1-962 a.a.) (monomer). The 3-D structure was predicted by I-TASSER (Zhang 2008) and generated 5 models based on C-score. Model 1 had the highest C-score (0.69). Human E1o is coloured according to secondary structure in pink (α-helix) and yellow (β-sheet). The N-terminal region of human E1o is indicated.

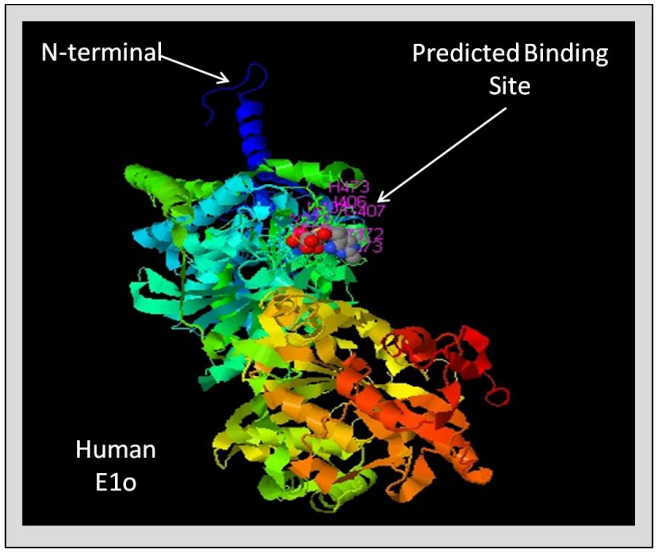


**Figure 4.9: ThDP binding site prediction for human E1o**
ThDP binding site prediction of human E1o (OGDH-H, 1-962 a.a.) (monomer) was generated by I-TASSER (Zhang 2008). N-terminal sequence of the predicted 3-D model is indicated. The predicted binding site residues are Glu378, Ala379, Ala380, Asp381, Gly407, Gly410, Asp411, Ala412, Ala413, Glu422, Val442, Asn443, Asn444 and His473.

Different isoforms of human E1o have been reported and these may have different modes of regulation. These isoforms appear to be produced in a tissue-specific manner and a number of transcript variants have been detected originating from different human chromosomes (Szabo *et al.* 1994; Koike 1995; Koike 1998; Bunik and Degtyarev 2008a; Bunik and Fernie 2009).

Three main human E1o and/or E1o-like isoforms (isoforms 1, 2 and 3) have been identified and characterised in the NCBI database. Sequence alignment of the human E1o isoforms was performed using ClustalW2 (see section 2.6.3) under default parameters (Fig. 4.10). Isoform 1 (GenBank Reference Sequence: BAA06836.1) represents the main so-called heart isoform (OGDH-H, 962 a.a.). It is encoded by the *OGDH* gene that is localised on chromosome 7 p14-p13. Multiple sequence alignment (Fig. 4.10) shows that this isoform contains all the essential residues and domains including a ThDP binding domain, catalytic domain and three putative $Ca^{2+}$-binding sites.

Isoform 2 or the so-called brain E1o isoform (OGDH-L) (NCBI Reference Sequence: NP-060715.2) was isolated from human brain tissue (Bunik and Fernie 2009). The *OGDH-L* gene is located on the chromosome 10 q11.23. Figure 4.10 shows that isoform 2 (OGDH-L) conserves all the main structural features and domain organization of human E1o (OGDH-H). It has a high degree of the sequence similarity (81.3% identity in an 898 a.a. overlap), although the highest similarity is observed within their catalytic domains. Moreover, sequence alignment of the N-terminal region (1-167 a.a.) of E1o isoform 2 shows 75.2% identity in a 149 a.a. overlap with E1o (OGDH-H).

Human E1o isoform 3 (NCBI Reference Sequence: NP-061176.3), also referred to as mitochondrial hypothetical protein (DHTKD1), is encoded by the *DHTKD1* gene that is also located on chromosome 10 (Nagase *et al.* 2001; Collins *et al* 2002).

Isoform 3 (919 a.a.) represents an additional putative 2-oxoglutarate dehydrogenase-like protein. Its cDNA has been isolated from human uterus, kidney, and brain. Multiple sequence alignment (Fig. 4.10) shows that the N-terminal region of E1o isoform 3 (DHTKD1), is poorly conserved and is about 60 amino acid shorter than the corresponding N-terminal region of E1o (OGDH-H). Sequence comparison of isoform 3 with E1o (OGDH-H) predicts only 40.1% identity in an 836 a.a. overlap. Despite the lower identity of isoform 3, it still retains a putative ThDP binding domain and catalytic domain.

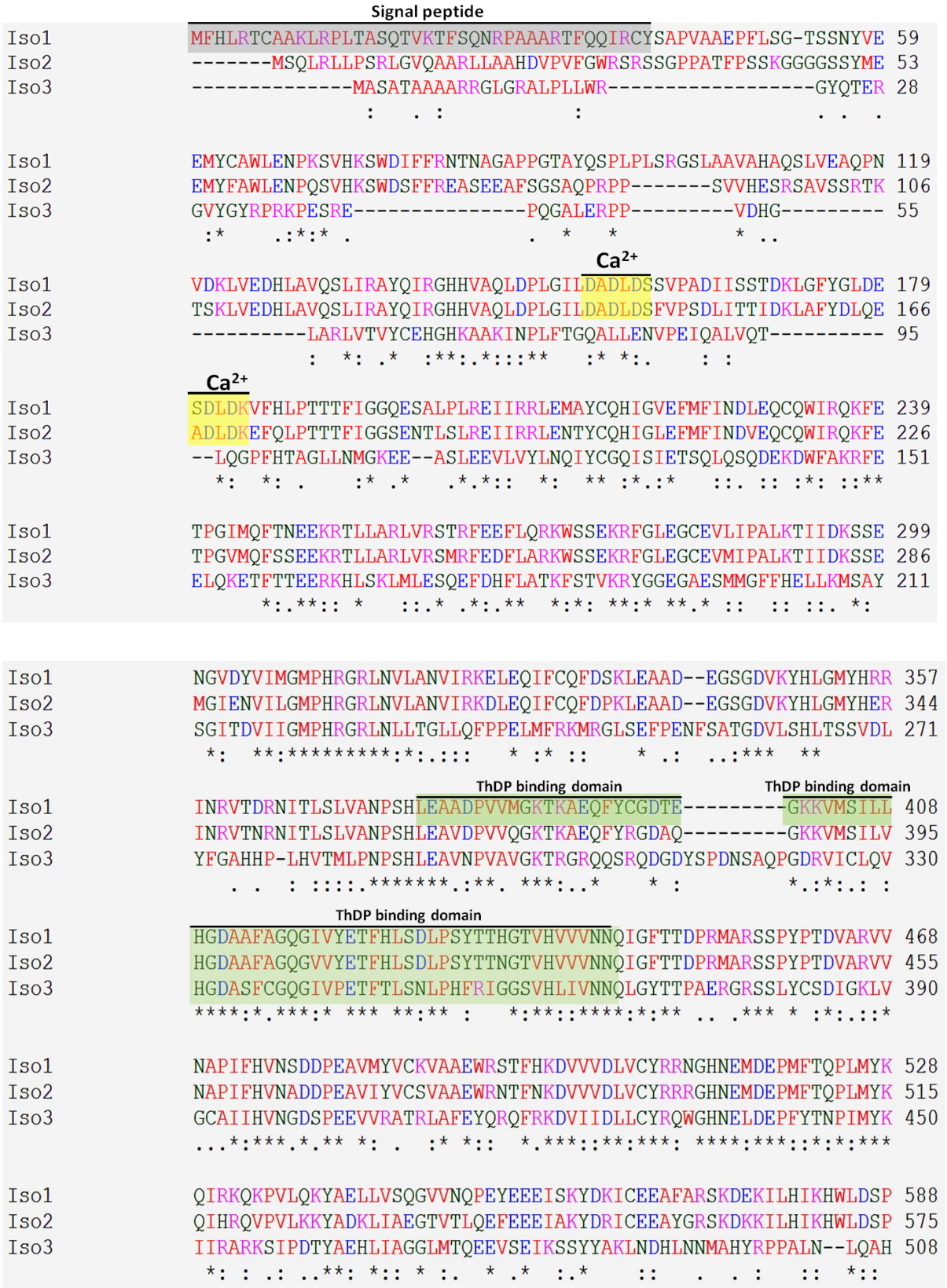
Signal peptide
Ca2+
Ca2+
ThDP binding domain
ThDP binding domain
ThDP binding domain


**Figure 4.10: Multiple sequence alignment of the human E1o isoforms**
The amino acid sequence of human E1o (isoform 1, OGDH-H, 1-962 a.a.), human E1o isoform 2 (OGDH-L, NCBI Ref. Seq.: NP-060715.2) and human E1o isoform 3 (DHTKD1, NCBI Ref. Seq.: NP-061176.3) were aligned. An asterisk (*) indicates positions that have a fully conserved residue. A colon (:) indicates conservation between residues with strongly similar properties. A period (.) indicates conservation between residues with weakly similar properties. Hydrophobic residues are shown in red. Acidic and basic residues are shown in blue and magenta respectively. Residues with hydroxyl, sulfhydryl or amine groups are depicted in green. The signal peptide sequences are marked in gray. The putative $Ca^{2+}$-binding sites (boxed in yellow) and ThDP binding domains (boxed in light green) are shown.

## 4.2.3 Investigation of the interaction between the N-terminal region of E1o and E3

The main purpose of this section was to test the ability of the E1o N-terminal region to interact with E3 as a first step to explain the role of this segment in maintaining the integrity of the OGDC.

### *4.2.3.1 Peptide array analysis*

Peptide array analysis was employed to define the key N-terminal regions of E1o involved in E3 binding. N-terminal E1o segments were analysed by peptide array technology as shown in Figure 4.11.

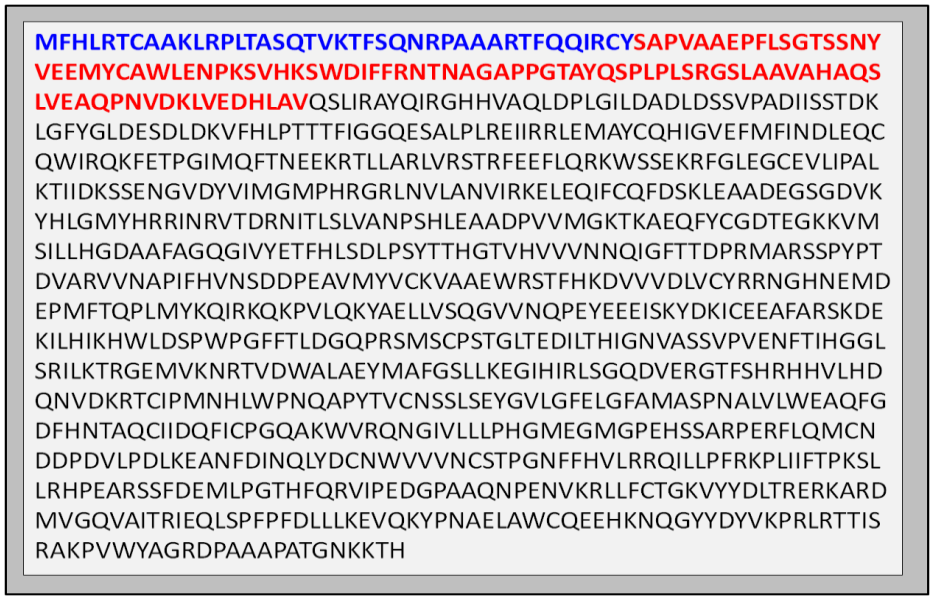


**Figure 4.11: Amino acid sequence of the human E1o precursor**
The N-terminal region of mature E1o (OGDH-H) thought to be involved in E3 binding is shown in red. Its 40 a.a. mitochondrial targeting sequence is shown in blue. The human E1o isoform (OGDH-H) sequence was taken from the GenBank database (GenBank Ref. Seq.: BAA06836.1).

Recombinant pET-14b plasmid housing the coding sequence of mature human E3 was transformed into *E. coli* DH5α, and then successfully over-expressed in *E. coli* BL21 (DE3) pLysS as a His-tagged fusion protein at 30°C after induction with IPTG (see section 3.3.2.6). E3 was purified by zinc chelate chromatography as described in Materials and Methods, section 2.4.4.2. After the initial isolation, E3 was further purified by gel filtration in GFC buffer (150mM NaCl, 50mM $KH_2PO_4$, pH 7.5) using a Sephacryl HiPrep S-300 High Resolution column attached to a BioCAD 700E workstation (see section 3.3.3.5).

To define a possible interaction between the E1o N-terminal region (Fig. 4.11) and E3, immobilised peptide spots of overlapping 25-meric peptides, each shifted by five amino acids (Fig. 4.12C) covering the entire N-terminal region of mature E1o were probed for interaction with E3 (Fig. 4.12B) or HRP-Ab alone as control (Fig. 4.12A) as described in Materials and Methods, section 2.4.8. Peptide array analysis shows a strong reaction with peptides 3, 5, 6, 7, 8, 9 and 10 incorporating amino acids extending from Ser11 to Ala70 suggesting this E1o segment is pivotal in promoting E3 binding. In addition, peptides 2, 4 and 12 showed a weak interaction with E3. The experiment was performed in triplicate using fresh peptide arrays and E3. Equivalent results were obtained on each occasion.

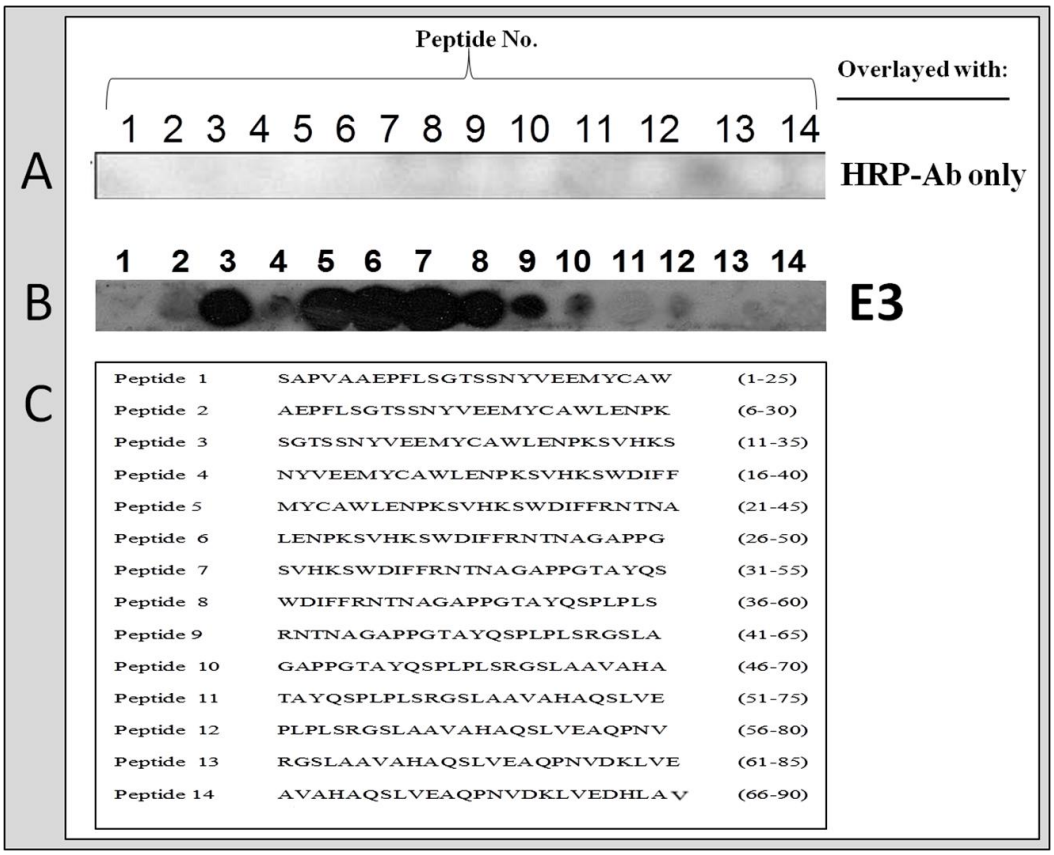


**Figure 4.12: Probing an E1o N-terminal peptide library with E3**
Immobilised peptide spots of overlapping 25-meric peptides, each shifted by five amino acids covering the entire N-terminal region of E1o were probed for interaction with either E3, or HRP-Ab alone as control. Samples were probed with His-tag Ab (HRP-Ab) and detected by ECL. (A) E1o N-terminal peptide array overlayed with HRP-Ab alone as control shows no reactive binding with all peptides (1-14). (B) Peptide array analysis of E3 binding with N-terminal E1o segments in TBST buffer (150mM NaCl, 0.1% (v/v) Tween-20, 50mM Tris-HCl, pH 7.4) shows reactive binding with peptides 3, 5, 6,7,8,9 and 10. Weak reactive binding with peptides 2, 4 and 12 was also evident. (C) E1o N-terminal overlapping peptide array (peptides 1-14).

In order to define key amino acids that are implicated in E3 binding within this suite of 25-meric peptides, alanine scanning was carried out on peptides 3-10 in which each amino acid within individual peptides was substituted in turn by alanine (or aspartic acid) as shown in Table 4.1.

| POS. | PEPTIDE NO. 3 | POS. | PEPTIDE NO. 4 |
|---|---|---|---|
| **A23** | **SGTSSNYVEEMYCAWLENPKSVHKS** | **B20** | **NYVEEMYCAWLENPKSVHKSWDIFF** |
| A24 | **A**GTSSNYVEEMYCAWLENPKSVHKS | B21 | **A**YVEEMYCAWLENPKSVHKSWDIFF |
| A25 | S**A**TSSNYVEEMYCAWLENPKSVHKS | B22 | N**A**VEEMYCAWLENPKSVHKSWDIFF |
| A26 | SG**A**SSNYVEEMYCAWLENPKSVHKS | B23 | NY**A**EEMYCAWLENPKSVHKSWDIFF |
| A27 | SGT**A**SNYVEEMYCAWLENPKSVHKS | B24 | NYV**A**EMYCAWLENPKSVHKSWDIFF |
| A28 | SGTS**A**NYVEEMYCAWLENPKSVHKS | B25 | NYVE**A**MYCAWLENPKSVHKSWDIFF |
| A29 | SGTSS**A**YVEEMYCAWLENPKSVHKS | B26 | NYVEE**A**YCAWLENPKSVHKSWDIFF |
| A30 | SGTSSN**A**VEEMYCAWLENPKSVHKS | B27 | NYVEEM**A**CAWLENPKSVHKSWDIFF |
| B01 | SGTSSNY**A**EEMYCAWLENPKSVHKS | B28 | NYVEEMY**A**AWLENPKSVHKSWDIFF |
| B02 | SGTSSNYV**A**EMYCAWLENPKSVHKS | B29 | NYVEEMYC**D**WLENPKSVHKSWDIFF |
| B03 | SGTSSNYVE**A**MYCAWLENPKSVHKS | B30 | NYVEEMYCA**A**LENPKSVHKSWDIFF |
| B04 | SGTSSNYVEE**A**YCAWLENPKSVHKS | C01 | NYVEEMYCAW**A**ENPKSVHKSWDIFF |
| B05 | SGTSSNYVEEM**A**CAWLENPKSVHKS | C02 | NYVEEMYCAWL**A**NPKSVHKSWDIFF |
| B06 | SGTSSNYVEEMY**A**AWLENPKSVHKS | C03 | NYVEEMYCAWLE**A**PKSVHKSWDIFF |
| B07 | SGTSSNYVEEMYC**D**WLENPKSVHKS | C04 | NYVEEMYCAWLEN**A**KSVHKSWDIFF |
| B08 | SGTSSNYVEEMYCA**A**LENPKSVHKS | C05 | NYVEEMYCAWLENP**A**SVHKSWDIFF |
| B09 | SGTSSNYVEEMYCAW**A**ENPKSVHKS | C06 | NYVEEMYCAWLENPK**A**VHKSWDIFF |
| B10 | SGTSSNYVEEMYCAWL**A**NPKSVHKS | C07 | NYVEEMYCAWLENPKS**A**HKSWDIFF |
| B11 | SGTSSNYVEEMYCAWLE**A**PKSVHKS | C08 | NYVEEMYCAWLENPKSV**A**KSWDIFF |
| B12 | SGTSSNYVEEMYCAWLEN**A**KSVHKS | C09 | NYVEEMYCAWLENPKSVH**A**SWDIFF |
| B13 | SGTSSNYVEEMYCAWLENP**A**SVHKS | C10 | NYVEEMYCAWLENPKSVHK**A**WDIFF |
| B14 | SGTSSNYVEEMYCAWLENPK**A**VHKS | C11 | NYVEEMYCAWLENPKSVHKS**A**DIFF |
| B15 | SGTSSNYVEEMYCAWLENPKS**A**HKS | C12 | NYVEEMYCAWLENPKSVHKSW**A**IFF |
| B16 | SGTSSNYVEEMYCAWLENPKSV**A**KS | C13 | NYVEEMYCAWLENPKSVHKSWD**A**FF |
| B17 | SGTSSNYVEEMYCAWLENPKSVH**A**S | C14 | NYVEEMYCAWLENPKSVHKSWDI**A**F |
| B18 | SGTSSNYVEEMYCAWLENPKSVHK**A** | C15 | NYVEEMYCAWLENPKSVHKSWDIF**A** |

| POS. | PEPTIDE NO. 5 | POS. | PEPTIDE NO. 6 |
|---|---|---|---|
| **C17** | **MYCAWLENPKSVHKSWDIFFRNTNA** | **D14** | **LENPKSVHKSWDIFFRNTNAGAPPG** |
| C18 | **A**YCAWLENPKSVHKSWDIFFRNTNA | D15 | **A**ENPKSVHKSWDIFFRNTNAGAPPG |
| C19 | M**A**CAWLENPKSVHKSWDIFFRNTNA | D16 | L**A**NPKSVHKSWDIFFRNTNAGAPPG |
| C20 | MY**A**AWLENPKSVHKSWDIFFRNTNA | D17 | LE**A**PKSVHKSWDIFFRNTNAGAPPG |
| C21 | MYC**D**WLENPKSVHKSWDIFFRNTNA | D18 | LEN**A**KSVHKSWDIFFRNTNAGAPPG |
| C22 | MYCA**A**LENPKSVHKSWDIFFRNTNA | D19 | LENP**A**SVHKSWDIFFRNTNAGAPPG |
| C23 | MYCAW**A**ENPKSVHKSWDIFFRNTNA | D20 | LENPK**A**VHKSWDIFFRNTNAGAPPG |
| C24 | MYCAWL**A**NPKSVHKSWDIFFRNTNA | D21 | LENPKS**A**HKSWDIFFRNTNAGAPPG |
| C25 | MYCAWLE**A**PKSVHKSWDIFFRNTNA | D22 | LENPKSV**A**KSWDIFFRNTNAGAPPG |
| C26 | MYCAWLEN**A**KSVHKSWDIFFRNTNA | D23 | LENPKSVH**A**SWDIFFRNTNAGAPPG |
| C27 | MYCAWLENP**A**SVHKSWDIFFRNTNA | D24 | LENPKSVHK**A**WDIFFRNTNAGAPPG |
| C28 | MYCAWLENPK**A**VHKSWDIFFRNTNA | D25 | LENPKSVHKS**A**DIFFRNTNAGAPPG |
| C29 | MYCAWLENPKS**A**HKSWDIFFRNTNA | D26 | LENPKSVHKSW**A**IFFRNTNAGAPPG |
| C30 | MYCAWLENPKSV**A**KSWDIFFRNTNA | D27 | LENPKSVHKSWD**A**FFRNTNAGAPPG |
| D01 | MYCAWLENPKSVH**A**SWDIFFRNTNA | D28 | LENPKSVHKSWDI**A**FRNTNAGAPPG |
| D02 | MYCAWLENPKSVHK**A**WDIFFRNTNA | D29 | LENPKSVHKSWDIF**A**RNTNAGAPPG |
| D03 | MYCAWLENPKSVHKS**A**DIFFRNTNA | D30 | LENPKSVHKSWDIFF**A**NTNAGAPPG |
| D04 | MYCAWLENPKSVHKSW**A**IFFRNTNA | E01 | LENPKSVHKSWDIFFR**A**TNAGAPPG |
| D05 | MYCAWLENPKSVHKSWD**A**FFRNTNA | E02 | LENPKSVHKSWDIFFRN**A**NAGAPPG |
| D06 | MYCAWLENPKSVHKSWDI**A**FRNTNA | E03 | LENPKSVHKSWDIFFRNT**A**AGAPPG |
| D07 | MYCAWLENPKSVHKSWDIF**A**RNTNA | E04 | LENPKSVHKSWDIFFRNTN**D**GAPPG |
| D08 | MYCAWLENPKSVHKSWDIFF**A**NTNA | E05 | LENPKSVHKSWDIFFRNTNA**A**APPG |
| D09 | MYCAWLENPKSVHKSWDIFFR**A**TNA | E06 | LENPKSVHKSWDIFFRNTNAG**D**PPG |
| D10 | MYCAWLENPKSVHKSWDIFFRN**A**NA | E07 | LENPKSVHKSWDIFFRNTNAGA**A**PG |
| D11 | MYCAWLENPKSVHKSWDIFFRNT**A**A | E08 | LENPKSVHKSWDIFFRNTNAGAP**A**G |
| D12 | MYCAWLENPKSVHKSWDIFFRNTN**D** | E09 | LENPKSVHKSWDIFFRNTNAGAPP**A** |

| POS. | PEPTIDE NO. 7 | POS. | PEPTIDE NO. 8 |
|---|---|---|---|
| **E12** | **SVHKSWDIFFRNTNAGAPPGTAYQS** | **F09** | **WDIFFRNTNAGAPPGTAYQSPLPLS** |
| E13 | **A**VHKSWDIFFRNTNAGAPPGTAYQS | F10 | **A**DIFFRNTNAGAPPGTAYQSPLPLS |
| E14 | S**A**HKSWDIFFRNTNAGAPPGTAYQS | F11 | W**A**IFFRNTNAGAPPGTAYQSPLPLS |
| E15 | SV**A**KSWDIFFRNTNAGAPPGTAYQS | F12 | WD**A**FFRNTNAGAPPGTAYQSPLPLS |
| E16 | SVH**A**SWDIFFRNTNAGAPPGTAYQS | F13 | WDI**A**FRNTNAGAPPGTAYQSPLPLS |
| E17 | SVHK**A**WDIFFRNTNAGAPPGTAYQS | F14 | WDIF**A**RNTNAGAPPGTAYQSPLPLS |
| E18 | SVHKS**A**DIFFRNTNAGAPPGTAYQS | F15 | WDIFF**A**NTNAGAPPGTAYQSPLPLS |
| E19 | SVHKSW**A**IFFRNTNAGAPPGTAYQS | F16 | WDIFFR**A**TNAGAPPGTAYQSPLPLS |
| E20 | SVHKSWD**A**FFRNTNAGAPPGTAYQS | F17 | WDIFFRN**A**NAGAPPGTAYQSPLPLS |
| E21 | SVHKSWDI**A**FRNTNAGAPPGTAYQS | F18 | WDIFFRNT**A**AGAPPGTAYQSPLPLS |
| E22 | SVHKSWDIF**A**RNTNAGAPPGTAYQS | F19 | WDIFFRNTN**D**GAPPGTAYQSPLPLS |
| E23 | SVHKSWDIFF**A**NTNAGAPPGTAYQS | F20 | WDIFFRNTNA**A**APPGTAYQSPLPLS |
| E24 | SVHKSWDIFFR**A**TNAGAPPGTAYQS | F21 | WDIFFRNTNAG**D**PPGTAYQSPLPLS |
| E25 | SVHKSWDIFFRN**A**NAGAPPGTAYQS | F22 | WDIFFRNTNAGA**A**PGTAYQSPLPLS |
| E26 | SVHKSWDIFFRNT**A**AGAPPGTAYQS | F23 | WDIFFRNTNAGAP**A**GTAYQSPLPLS |
| E27 | SVHKSWDIFFRNTN**D**GAPPGTAYQS | F24 | WDIFFRNTNAGAPP**A**TAYQSPLPLS |
| E28 | SVHKSWDIFFRNTNA**A**APPGTAYQS | F25 | WDIFFRNTNAGAPPG**A**AYQSPLPLS |
| E29 | SVHKSWDIFFRNTNAG**D**PPGTAYQS | F26 | WDIFFRNTNAGAPPGT**D**YQSPLPLS |
| E30 | SVHKSWDIFFRNTNAGA**A**PGTAYQS | F27 | WDIFFRNTNAGAPPGTA**A**QSPLPLS |
| F01 | SVHKSWDIFFRNTNAGAP**A**GTAYQS | F28 | WDIFFRNTNAGAPPGTAY**A**SPLPLS |
| F02 | SVHKSWDIFFRNTNAGAPP**A**TAYQS | F29 | WDIFFRNTNAGAPPGTAYQ**A**PLPLS |
| F03 | SVHKSWDIFFRNTNAGAPPG**A**AYQS | F30 | WDIFFRNTNAGAPPGTAYQS**A**LPLS |
| F04 | SVHKSWDIFFRNTNAGAPPGT**D**YQS | G01 | WDIFFRNTNAGAPPGTAYQSP**A**PLS |
| F05 | SVHKSWDIFFRNTNAGAPPGTA**A**QS | G02 | WDIFFRNTNAGAPPGTAYQSPL**A**LS |
| F06 | SVHKSWDIFFRNTNAGAPPGTAY**A**S | G03 | WDIFFRNTNAGAPPGTAYQSPLP**A**S |
| F07 | SVHKSWDIFFRNTNAGAPPGTAYQ**A** | G04 | WDIFFRNTNAGAPPGTAYQSPLPL**A** |

| POS. | PEPTIDE NO. 9 | POS. | PEPTIDE NO. 10 |
|---|---|---|---|
| **G06** | **RNTNAGAPPGTAYQSPLPLSRGSLA** | **H03** | **GAPPGTAYQSPLPLSRGSLAAVAHA** |
| G07 | **A**NTNAGAPPGTAYQSPLPLSRGSLA | H04 | **AD**PPGTAYQSPLPLSRGSLAAVAHA |
| G08 | R**A**TNAGAPPGTAYQSPLPLSRGSLA | H05 | GA**A**PGTAYQSPLPLSRGSLAAVAHA |
| G09 | RN**A**NAGAPPGTAYQSPLPLSRGSLA | H06 | GAP**A**GTAYQSPLPLSRGSLAAVAHA |
| G10 | RNT**A**AGAPPGTAYQSPLPLSRGSLA | H07 | GAPP**A**TAYQSPLPLSRGSLAAVAHA |
| G11 | RNTN**D**GAPPGTAYQSPLPLSRGSLA | H08 | GAPPG**A**AYQSPLPLSRGSLAAVAHA |
| G12 | RNTNA**A**APPGTAYQSPLPLSRGSLA | H09 | GAPPGT**D**YQSPLPLSRGSLAAVAHA |
| G13 | RNTNAG**D**PPGTAYQSPLPLSRGSLA | H10 | GAPPGTA**A**QSPLPLSRGSLAAVAHA |
| G14 | RNTNAGA**A**PGTAYQSPLPLSRGSLA | H11 | GAPPGTAY**A**SPLPLSRGSLAAVAHA |
| G15 | RNTNAGAP**A**GTAYQSPLPLSRGSLA | H12 | GAPPGTAYQ**A**PLPLSRGSLAAVAHA |
| G16 | RNTNAGAPP**A**TAYQSPLPLSRGSLA | H13 | GAPPGTAYQS**A**LPLSRGSLAAVAHA |
| G17 | RNTNAGAPPG**A**AYQSPLPLSRGSLA | H14 | GAPPGTAYQSP**A**PLSRGSLAAVAHA |
| G18 | RNTNAGAPPGT**D**YQSPLPLSRGSLA | H15 | GAPPGTAYQSPL**A**LSRGSLAAVAHA |
| G19 | RNTNAGAPPGTA**A**QSPLPLSRGSLA | H16 | GAPPGTAYQSPLP**A**SRGSLAAVAHA |
| G20 | RNTNAGAPPGTAY**A**SPLPLSRGSLA | H17 | GAPPGTAYQSPLPL**A**RGSLAAVAHA |
| G21 | RNTNAGAPPGTAYQ**A**PLPLSRGSLA | H18 | GAPPGTAYQSPLPLS**A**GSLAAVAHA |
| G22 | RNTNAGAPPGTAYQS**A**LPLSRGSLA | H19 | GAPPGTAYQSPLPLSR**A**SLAAVAHA |
| G23 | RNTNAGAPPGTAYQSP**A**PLSRGSLA | H20 | GAPPGTAYQSPLPLSRG**A**LAAVAHA |
| G24 | RNTNAGAPPGTAYQSPL**A**LSRGSLA | H21 | GAPPGTAYQSPLPLSRGS**A**AAVAHA |
| G25 | RNTNAGAPPGTAYQSPLP**A**SRGSLA | H22 | GAPPGTAYQSPLPLSRGSL**D**AVAHA |
| G26 | RNTNAGAPPGTAYQSPLPL**A**RGSLA | H23 | GAPPGTAYQSPLPLSRGSLA**D**VAHA |
| G27 | RNTNAGAPPGTAYQSPLPLS**A**GSLA | H24 | GAPPGTAYQSPLPLSRGSLAA**A**AHA |
| G28 | RNTNAGAPPGTAYQSPLPLSR**A**SLA | H25 | GAPPGTAYQSPLPLSRGSLAAV**D**HA |
| G29 | RNTNAGAPPGTAYQSPLPLSRG**A**LA | H26 | GAPPGTAYQSPLPLSRGSLAAVA**A**A |
| G30 | RNTNAGAPPGTAYQSPLPLSRGS**A**A | H27 | GAPPGTAYQSPLPLSRGSLAAVAH**D** |
| H01 | RNTNAGAPPGTAYQSPLPLSRGSL**D** | | |

## Table 4.1: Alanine substitution array for peptides 3-10

Individual amino acids within each 25-meric peptide (peptides 3-10) were substituted by alanine (**A**) as shown above. Alanine residues present originally were substituted by aspartic acid (**D**). The position (Pos.) of the corresponding peptide within the original nitrocellulose membrane peptide array is shown by letter and number (e.g. A23). The first row of each table (shown in bold) represents wild-type (wt) peptide.

The alanine substitution array was probed with E3 in TBST buffer (150mM NaCl, 0.1% (v/v) Tween-20, 50mM Tris-HCl, pH 7.4) as described previously. N-terminal E1o amino acid substitutions that resulted in a marked loss of binding capacity were considered to be important for E3 interaction. It was found that amino acid substitutions at positions A29, A30, B01, B02, B05, B08, D08, F15, F16, G23, G25, G27, H04, H09, H18, H22, H23, H25 and H27 markedly reduce the ability of the relevant peptides to bind E3. These correspond to Asn16, Tyr17, Val18, Glu19, Tyr22, Trp25, Arg41, Asn42, Gly46, Ala47, Ala52, Leu57, Leu59, Arg61, Leu64, Ala65, Ala66, Ala68 and Ala70 (Figure 4.13).

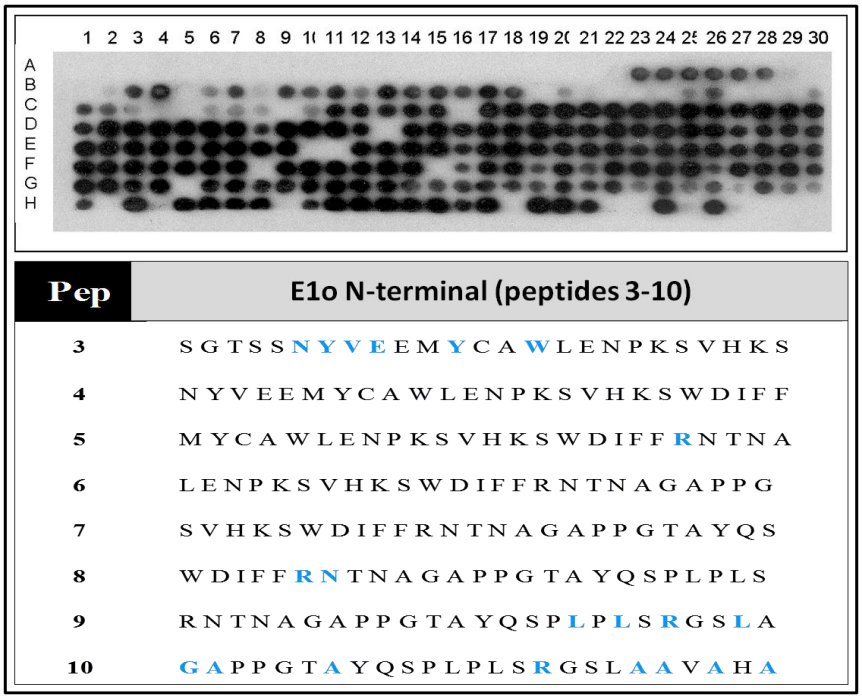


**Figure 4.13: Alanine substitution array for peptides 3-10 from the E1o N-terminal region probed with E3**

Immobilised peptide spots were probed for their interaction with E3. Samples were treated with His-tag Ab (HRP-Ab) and detected by ECL. Dark spots signify positive binding. The amino acid residues of human E1o (N-terminal) thought to be important in binding between the E1o N-terminus and E3 by using alanine substitution are shown in blue.

Peptide array data on the interaction of N-terminal E1o with E3 described above (Fig. 4.12 & 4.13) were obtained in the presence of 150mM NaCl to minimize non-specific binding. In view of the well-established salt sensitivity of the E3 interaction with intact OGDC, the N-terminal E1o peptides were probed with E3 in the presence of increasing NaCl concentrations (up to 500mM) (Fig. 4.14). E3 binding was markedly reduced at higher NaCl concentrations confirming the salt sensitivity of these interactions. The effect of NaCl concentration in this range on overall bovine OGDC activity was also investigated in chapter 6.

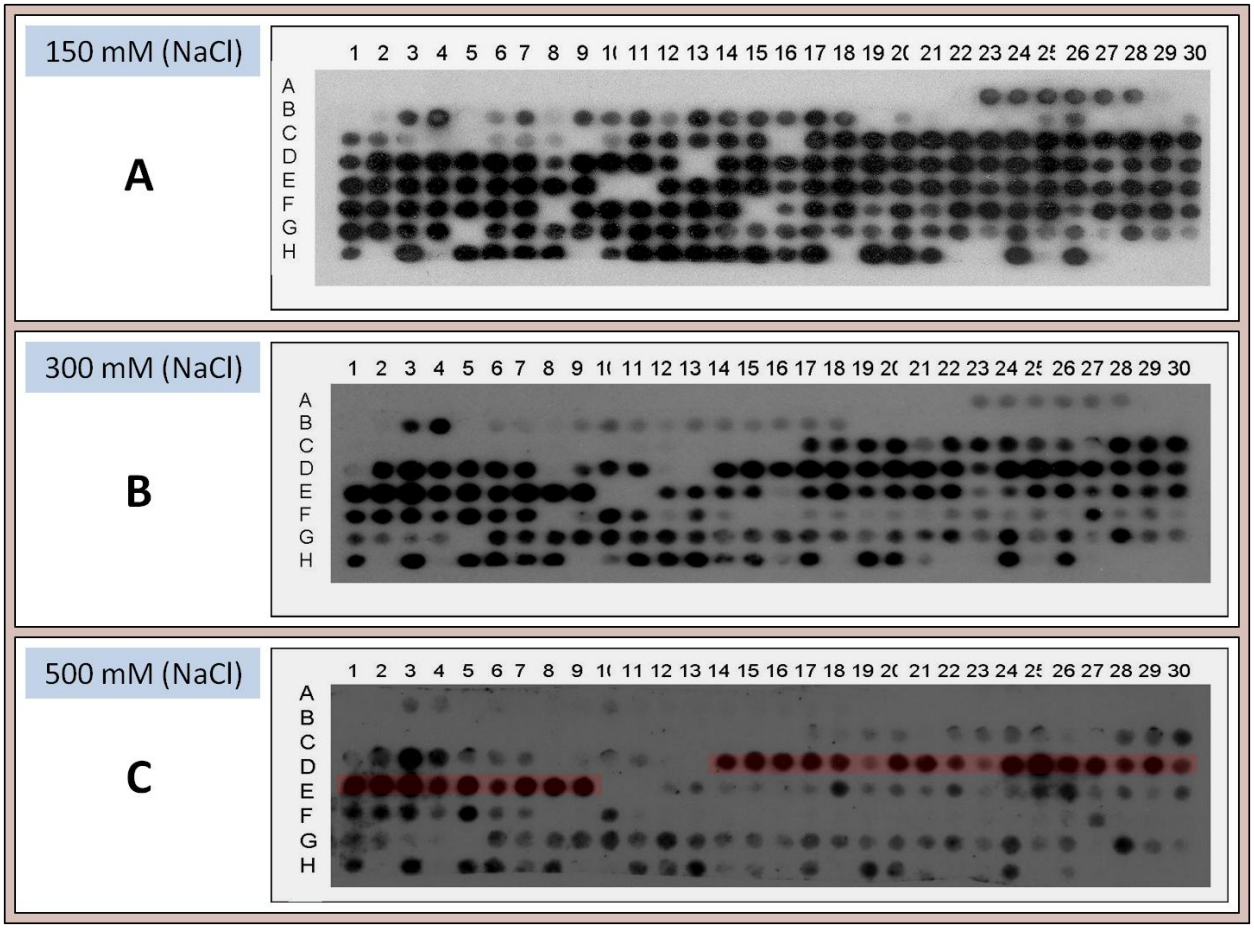


**Figure 4.14**: **Peptide array analysis: effect of increasing salt**
Immobilised peptide spots were probed for their interaction with E3. Samples were treated with His-tag Ab (HRP-Ab) and detected by ECL. (A), (B), and (C) alanine substitution array of E3 binding with N-terminal E1o peptides at different salt concentrations (150mM NaCl, 300mM NaCl, and 500mM NaCl respectively). Dark spots signify positive binds. A general reduction in E3 binding to all peptides was observed with elevated salt treatment. Peptide 6 (highlighted in red) showing the most resistance to increasing ionic strength.

### 4.2.3.2 Investigation of the interaction between N-terminal E1o peptides and E3 by isothermal titration calorimetry (ITC)

Based on peptide array analysis, two synthetic E1o peptides (Ser11 to Ser35) and E1o (Trp36 to Ser60) were purchased from Genscript, UK (see section 2.4.9). ITC is one of the most quantitative methods for analyzing molecular interactions. The N-terminal E1o peptide (Trp36 to Ser60) and E3 were dialysed overnight against 150mM NaCl, 50mM $KH_2$ $PO_4$, pH 7.4 (see section 2.4.5). The E1o peptide (710µM) was injected in 10µl aliquots into the reaction cell containing 16.5µM E3 at 25°C.

By measuring the heats of interaction of E1o with E3, complex formation was found to be exothermic as evidenced by negative peaks in the ITC output. The data confirmed binding of E1o to E3 ($K_d$ = 35.7µM; $K_a$ = 2.79 x $10^4$ $M^{-1}$). Binding was also characterised by a favourable enthalpy change ($\Delta H$ = -7309 kcal/mol) and entropy change ($\Delta S$ = -4.170 kcal/mol). The stoichiometry of binding suggests that two molecules of E1o can bind to one E3 homodimer (Fig. 4.15). Examination of a possible interaction between the E1o N-terminal peptide (Ser11 to Ser35) and E3 was also performed in same manner. However, no significant binding was observed with this peptide (data not shown).

The data indicated that the 25-meric peptide covering Trp36 to Ser60 interacted more strongly with E3 than an equivalent peptide covering the segment Ser11 to Ser35. Interestingly, Trp36 to Ser60 also represented the region that displayed the strongest interaction with E3 and was also most resistant to high salt treatment in peptide array studies (Fig. 4.14) confirming its central importance of this sequence in E3 binding.

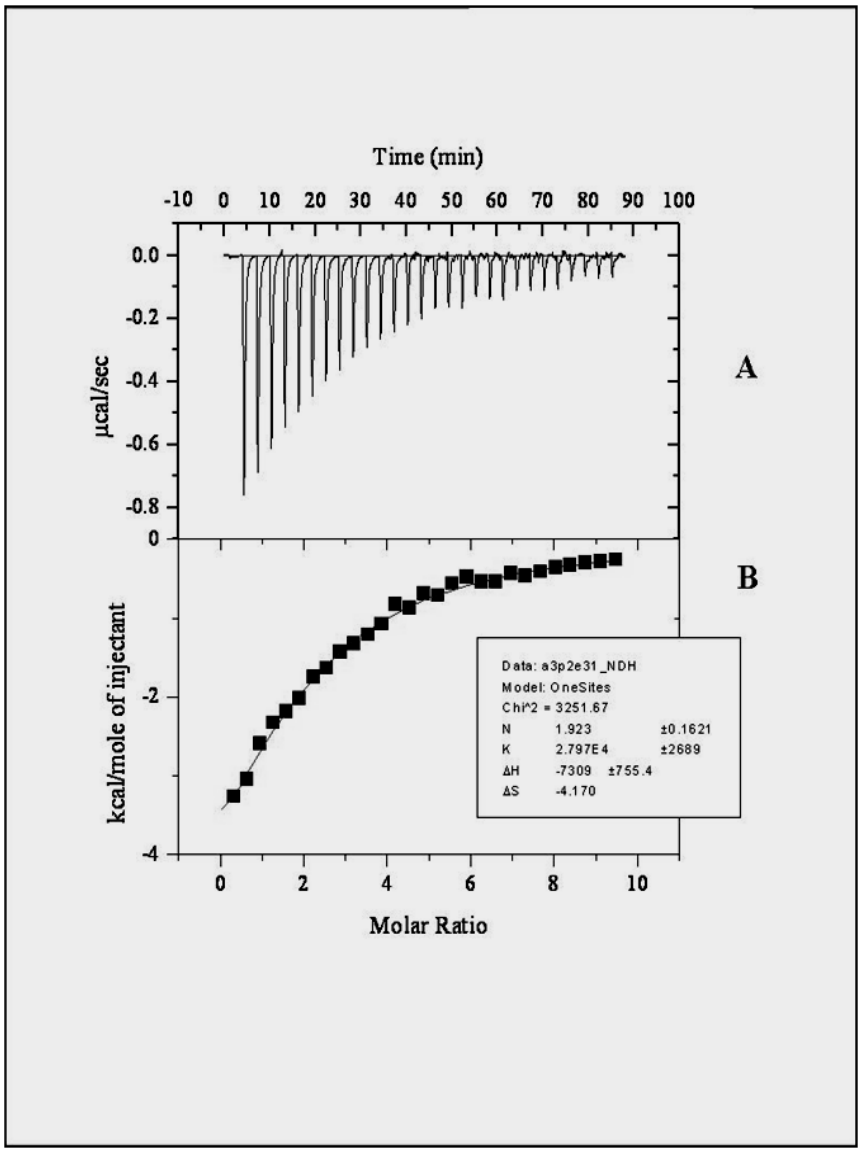


**Figure 4.15: ITC of N-terminal E1o 25-meric peptide (Trp36 to Ser60) and E3**
(A) Raw data obtained from a series of 10 µl injections of E1 into E3 at 25°C and plotted as heat change versus time. (B) Plotting the areas under the peaks in (A) against the molar ratio of E1 injected as calculated by the ORIGIN software package. The best fit shown was obtained by least-squares fitting using a simple binding model (see section 2.5.2). The stoichiometry of binding (*N*) suggests that two molecules of E1o are bound per molecule of E3. The calculated values for stoichiometry, affinity constant (*K*), enthalpy change ($\Delta H$) and entropy change ($\Delta S$) are shown in the insert. ITC experiments and analyses were performed in collaboration with Mrs. Margaret Nutley, University of Glasgow.

### 4.2.3.3 Investigation of the interaction between the N-terminal E1o-60 (Ser11-Ala70) and E3

In order to investigate the interaction of an extended E1o N-terminal segment with E3, the human E1o N-terminal 60-meric truncate (Ser11-Ala70) was successfully cloned into the pGEX-2T vector via the TOPO TA cloning Kit (see section 3.3.1.2). E1o-60 was subsequently over-expressed and purified as a GST fusion protein (see section 3.3.2.2 & 3.3.3.2). Moreover, two alternative E1o-60 (Ser11-Ala70) constructs were also successfully cloned into pET-14b (His-tagged E1o-60) and pET-30a (MBP E1o-60), respectively (see sections 3.3.11 & 3.3.1.3). Owing to poor yields of E1o-60 His-tag fusion protein (see section 3.3.3.1) and extensive degradation of E1o-60 MBP (see section 3.3.3.3), neither construct was employed for E3 binding studies.

#### 4.2.3.3.1 Investigation of the interaction between the E1o-60 GST fusion protein and E3 using glutathione Sepharose 4B chromatography

To establish more clearly evidence for a direct interaction between E1o and E3 in native OGDC, an E1o-60 GST fusion protein (Ser11-Ala70) and E3 were over-expressed individually at 30 ºC for 4-5 h. E3 contained an N-terminal His-tag (see section 3.3.2.6), whereas E1o-60 was produced as a C-terminal GST fusion protein. Purified samples were dialysed against PBS (see section 2.4.5), the two proteins were incubated in a 1:1 molar ratio for 5 min at room temperature and applied to a glutathione Sepharose 4B column attached to a BioCAD 700E workstation. Two separate peaks of eluted protein were observed (Fig. 4.16A). On SDS-PAGE analysis of the individual peaks, it was found that the first peak (flow through) contained E3 and

traces of unbound E1o-60 GST, whereas the second peak (eluted with glutathione) contained only E1o-60 GST (Fig. 4.16B). This result was also verified by Western blotting using anti-GST-Ab (data not shown). Thus no stable association between E3 and the E1o N-terminal fragment (60 a.a.) could be detected under these conditions. However, it was possible that steric hindrance effects owing to the presence of the large GST fusion protein could prevent access of the small E1o peptide to its E3 partner.

In the same manner, E1o-60 GST and E3 were also pre-incubated with a molar excess of E1o-60 GST (1:2) and similar results were obtained (data not shown).

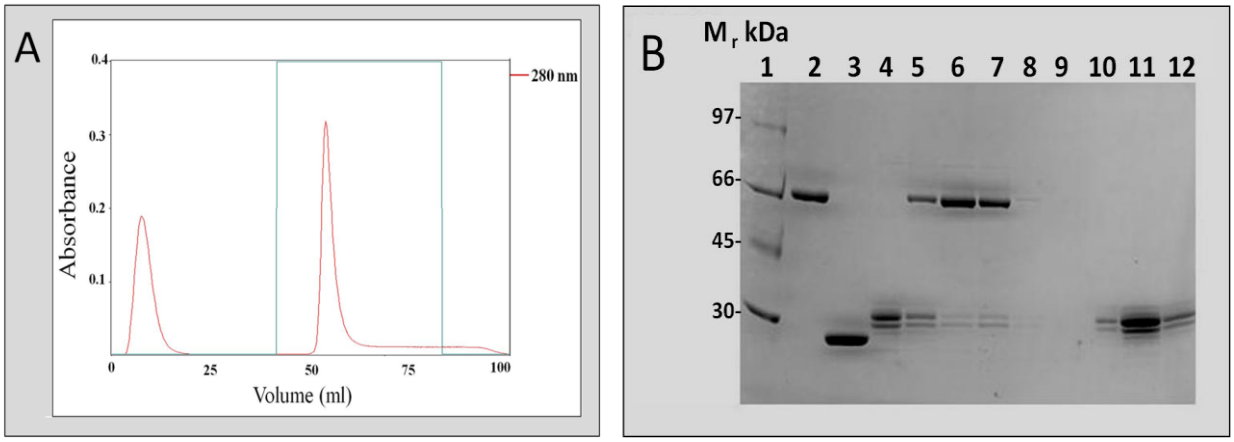


**Figure 4.16: Lack of interaction between E1o-60 GST and E3**
(A) E1o-60 GST and E3 were pre-incubated for 5 min at room temperature followed by separation on a glutathione Sepharose column. E1o-60 GST and E3 were physically mixed in a 1:1 molar ratio. The purified proteins (2ml) were applied to a glutathione Sepharose 4B column in a 2ml aliquot. Bound protein was eluted from the column using 5 CV elution buffer (20mM reduced glutathione, 50mM Tris-HCl, pH 8.0). The reduced glutathione buffer step used for elution is shown in green. Absorbance of eluted protein was measured at 280 nm (red line). Peak fractions (2ml) were collected and analysed by SDS-PAGE. (B) SDS-PAGE (10%) analysis of eluted protein peaks stained with Coomassie Brilliant Blue. Lane 1, molecular mass markers; lane 2, purified E3 as control; lane 3, GST as control; lane 4, purified E1o-60 GST as control; lane 5, mixture of E1o-60 GST/E3; lanes 6-8, flow through and lanes 10-12, elution fractions. No E3 band was detected in the elution fractions.

#### 4.2.3.3.2 Investigation of a potential interaction between E1o-60 GST and E3 using ITC

E1o-60 GST and E3 were dialysed overnight against 50mM NaCl, 50mM $KH_2$ $PO_4$, pH 7.4 and concentrated (see section 2.4.5). E1o-60 GST at a concentration of 680μM was injected in 10μl aliquots into the reaction cell containing 45μM E3 at 25°C (Fig. 4.17) and at 15°C (data not shown). Data were analysed using non-linear regression with the MicroCal ORIGIN software package, assuming a simple binding model. Titrations of E1o-60 GST into E3 were identical to the titrations of E1o-60 GST into buffer indicating that the small changes observed are caused by heats of dilution. As stated previously, GST is a dimeric protein of 50 kDa and its presence might prevent binding to its small E1o partner owing to steric hindrance effects.

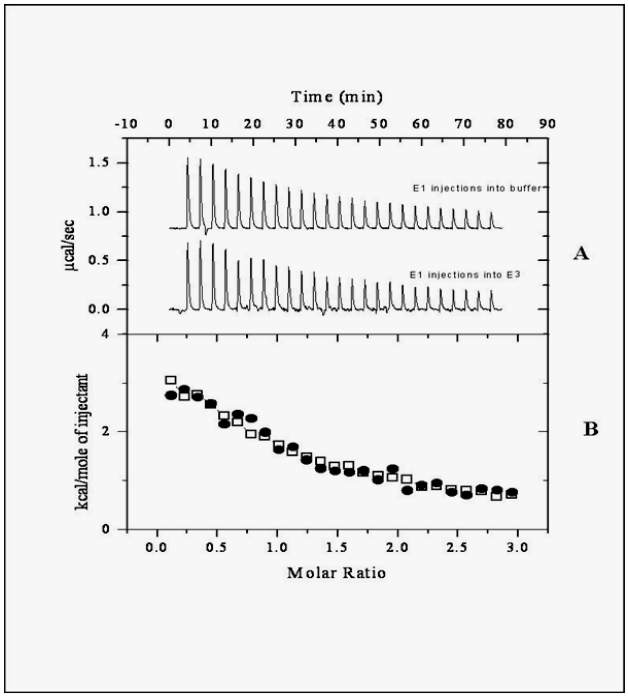


**Figure 4.17: ITC of N-terminal E1o-60 GST and E3**
(A) Raw data obtained from a series of 10μl injections of E1o-60 GST into E3 at 25°C and plotted as heat change versus time. (B) Plotting the areas under the peaks in (A) against the molar ratio of E1o-60 GST injected as calculated by the ORIGIN software package. The best fit shown was obtained by least-squares fitting using a simple binding model (see section 2.5.2). ITC experiments and analyses were performed in collaboration with Mrs. Margaret Nutley, University of Glasgow.

#### 4.2.3.3.3 Investigation of a possible interaction between the E1o-60 GST and E3 using native PAGE

E1o-60 GST and E3 were over-expressed and purified individually as described previously (see sections 3.3.2 & 3.3.3). Subsequently, both proteins were dialysed simultaneously against PBS buffer, pH 7.5 (see section 2.4.5). Samples were concentrated and their concentration measured as described in section 2.4.6. Native PAGE was performed under standard conditions (for more details, refer to section 2.4.3.2).

E1o-60 GST and E3 were physically mixed in various molar ratios, keeping the amount of E3 constant at 5µg. Samples were incubated at 25 $^{o}$C for 15 min in PBS buffer, pH 7.5. Protein samples were loaded onto Tris-glycine gels (5% stacking, 8% resolving gel) and subjected to native PAGE (Fig. 4.18).

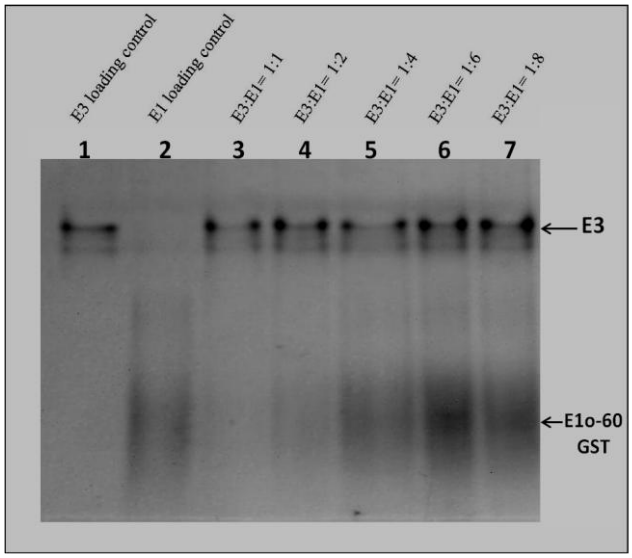


**Figure 4.18: Native PAGE of E1o-60 GST and E3 at various stoichiometries**
Native PAGE (8%) analysis of stoichiometric mixtures of E1o-60 GST and E3. Samples were pre-incubated at 25°C for 15 min prior to suspending in sample buffer. Electrophoresis was carried out at constant voltage (100V) and 10mA/gel in 1x running buffer for 6 h. Samples were viewed after staining with Coomassie Brilliant Blue. The arrows on the right of the blot indicate E3 and E1o-60 GST proteins respectively. Lane 1, E3 (5µg) as control; lane 2, E1o-60 GST (30µg) as control. As the amount of E1o-60 GST was increased (5-40µg), no E3 bandshift corresponding to formation of an E1o-60 GST/E3 sub-complex could be detected (lanes 3,4,5,6 and 7).

E1o-60 GST was seen to migrate as a diffuse band on native gels. Moreover, no E3 bandshift was observed even on addition of a large molar excess of E1o-60 GST, again indicating that there was no stable association between these two species.

To rule out possible steric hindrance effects, the GST-tag was removed from the E1o-60 fusion protein by thrombin cleavage. Purified GST-tagged E1o-60 was dialysed against PBS, pH 7.5. Approximately 10 U of thrombin were added per mg of protein and incubated at room temperature overnight. Cleavage of the GST-tag was viewed by SDS-PAGE (Fig. 4.19).

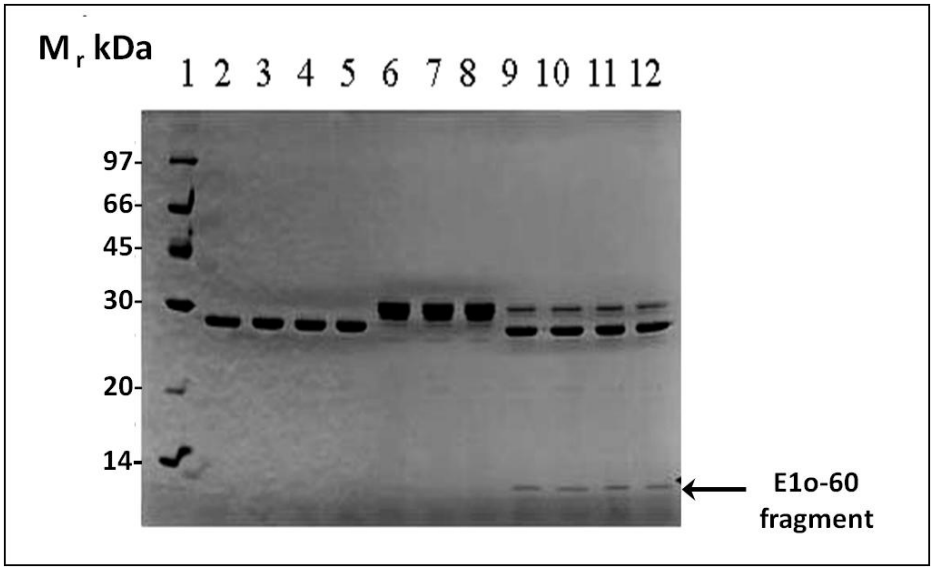


**Figure 4.19: Cleavage of the E1o-60 GST fusion protein**
SDS-PAGE (16%) analysis of cleavage of E1o-60 GST by thrombin visualised by staining with Coomassie Brilliant Blue. Lane 1, molecular mass markers; lanes 2-5, GST controls; lanes 6-8, E1o-60 GST fusion protein; lanes 9-12, E1o-60 GST digested with thrombin. Samples were digested with 10 U of thrombin per mg of protein overnight at 25°C. The arrow on the right of the blot indicates the E1o-60 fragment at the expected size (~ 7 kDa).

Figure 4.19 shows that 80-90% of E1o-60 GST was cleaved in this case. Temperature, incubation time and amount of thrombin added were optimized by monitoring digestion at various times (30 min, 1h, 2h, 4h and overnight) prior analyses by SDS-PAGE (data not shown). To avoid proteolysis caused by excess thrombin, minimal amounts of thrombin were used in this study.

Unexpectedly, following cleavage of E1o-60 GST and glutathione Sepharose 4B chromatography to remove free GST, it was found that the vast majority of cleaved E1o-60 remained associated with its GST fusion partner indicating tight non-specific binding (data not shown). This unanticipated observation provided additional evidence to account for the lack of success in detecting a direct association between this E1o-GST construct and native E3.

### *4.2.3.4 Investigation of the interaction between the N-terminal E1o-90 (Ser1-Val90) and E3*

The cDNA sequence encoding E1o-90 (Ser1-Val90) was successfully cloned into the pGEX-2T vector via the TOPO TA cloning Kit (see section 3.3.1.2) and the corresponding peptide subsequently over-expressed and purified (see section 3.3.2.2 & 3.3.3.2). In addition, the same construct was also successfully sub-cloned into pET-14b and pET-30a (see sections 3.3.11 & 3.3.1.3). However, owing to the poor yields of the E1o-90 His-tag protein (pET-14b, see section 3.3.3.1) and extensive degradation of the E1o-90 MBP fusion protein (pET-30a, see section 3.3.3.3), neither construct was employed in ITC binding experiments as these require 5-30mg of pure intact protein in most cases.

#### 4.2.3.4.1 Investigation of a possible interaction between the E1o-90 GST fusion protein and E3 using glutathione Sepharose 4B chromatography

E1o-90 GST and E3 were expressed separately in *E. coli* (DE3) pLysS cells at 30 ºC for 3-5 h. After individual expression, bacterial pellets were disrupted by French press treatment and purified using GST affinity and zinc chelate chromatography, respectively. Purified samples were dialysed simultaneously against PBS, pH 7.4. The two proteins were incubated in a 1:1 molar ratio for 5 min at room temperature and passed through a glutathione Sepharose 4B column attached to a BioCAD 700E workstation. Two separate peaks of eluted protein were observed (Fig. 4.20A). On SDS-PAGE analysis of the individual peaks, it was found that the first peak (flow through) contained E3 and traces of unbound E1o-90 GST, while, the second eluted peak contained bound E1o-90 GST and E3 (Fig. 4.20B). The presence of a band of the predicted size for E3 in the E1o-90 GST elution peak confirmed a possible association of E3 with this E1o-90 GST construct.

To minimise the possibility of non-specific binding, the column was extensively washed with 12 CV PBS (150mM NaCl, 2.7mM KCl, 10mM $Na_2HPO_4$ and 1.8mM $KH_2PO_4$, pH 7.4) until a zero baseline was achieved. In addition, the last two tubes at zero baseline prior to elution were collected and analysed by SDS-PAGE (Fig. 4.20C) and Western blotting (data not shown). Specific binding between E1o-90 GST and E3 was again observed on elution with glutathione whereas no E3 band was evident in the last two tubes of the washing stage (Fig. 4.20B & 4.20C).

These results were also verified by Western blotting using an anti-His tag antibody (penta-His HRP conjugate antibody) and anti-GST HRP conjugate antibody (Fig. 4.20D). Western blotting revealed conclusively that E1o-90 GST (Ser1-Val90) was able to associate with E3, supporting the peptide array results (Fig. 4.12 & 4.13). In contrast, no stable association between E3 and E1o-60 (Ser11-Ala70) could be detected under similar conditions.

In an analogous manner, N-terminal E1o-153 GST (Ser1-Phe153) was also examined for its ability to interact with E3 using glutathione Sepharose 4B chromatography to detect complex formation. Similar to E1o-90 GST, it was found that E1o-153 GST was able to promote E3 binding in a post-translational fashion (data not shown). Moreover, the presence of E3 in the E1o-153 GST/E3 elution peak was further confirmed using Western blotting despite extensive degradation of the purified E1o-153 GST.

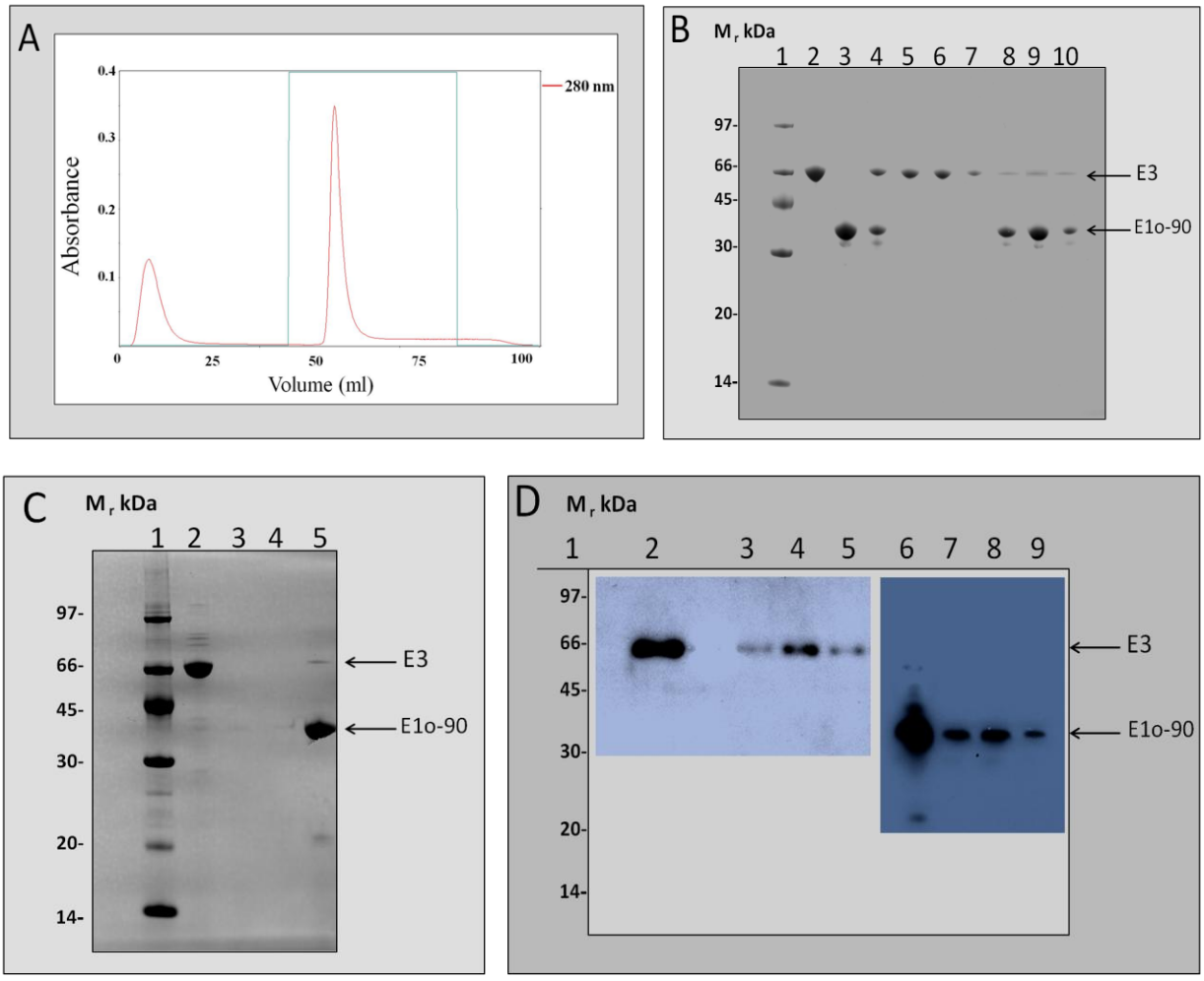


**Figure 4.20: Association of E1o-90 GST and E3**

(A) E1o-90 GST and E3 were pre-incubated in a 1:1 molar ratio for 5 min at room temperature. The purified proteins (2ml) were applied to a glutathione Sepharose 4B column in a 2ml aliquot. The bound protein was eluted from the column using 5 CV elution buffer (20mM reduced glutathione, 50mM Tris-HCl, pH 8.0). The reduced glutathione buffer step used for elution is shown in green. Absorbance of eluted protein was measured at 280 nm (red line). Peak fractions (2ml) were collected and analysed by either SDS-PAGE or Western blotting. (B) SDS-PAGE (10%) analysis of eluted protein peaks stained with Coomassie Brilliant Blue. Lane 1, molecular mass markers; lane 2, purified E3 as control; lane 3, purified E1o-90 GST as control; lane 4, mixture of E1o-90 GST/E3 prior to column addition; lanes 5-7, flow through and lanes 8-10, elution peak. E3 was detected in the elution peak. The arrows on the right of the blot indicate E3 and E1o-90 GST proteins, respectively. (C) SDS-PAGE (10%) analysis of the last two tubes at zero baseline of the extended wash stage prior to elution. Lane 1, molecular mass markers; lane 2, purified E3 as control; lanes 3-4, last two tubes at zero baseline of wash stage prior to elution; lane 5 (elution peak), confirming the presence of E3. (D) Western blot analysis of elution peak. Lane 2, purified E3 as control; lane 6, purified E1o-90 GST as control. The presence of E3 in the elution peak was confirmed (lanes 3, 4 & 5) with anti-His tag antibody (1 in 2000 dilution) (see section 2.4.7.1), while, the presence of E1o-90 GST was also confirmed (lanes 7, 8 & 9) with anti-GST HRP conjugate antibody (1 in 5000 dilution) (see section 2.4.7.2).

#### 4.2.3.4.2 Investigation of the interaction between the E1o-90 GST and E3 using ITC

The N-terminal construct (E1o-90 GST) (Ser1-Val90) and E3 were purified, dialysed overnight against 50mM NaCl, 50mM $KH_2PO_4$, pH 7.4 and concentrated (see section 2.4.5). E1o-90 GST at a concentration of 410μM was injected in 10μl aliquots into the reaction cell containing 20μM E3 at 25°C (Fig. 4.21). Data were analysed using non-linear regression in the MicroCal ORIGIN software package, assuming a simple binding model.

Measuring the heats of interaction of E1o-90 GST with E3, complex formation was found to be endothermic (positive peaks in the ITC input). The data confirmed the binding of E1o-90 GST to E3 ($K_d$ = 15.3μM; $K_a$ = 6.46 x $10^4$ $M^{-1}$). Binding was characterised by a favourable enthalpy change ($\Delta H$ = -8587 kcal/mol) and entropy change ($\Delta S$= -6.793 kcal/mol). The stoichiometry of binding was estimated to be one mole of E1o-90 GST per mole of E3. The altered 1:1 stoichiometry was anticipated as both E1o-90 GST and E3 are homodimers. In contrast, the observed binding stoichiometry of the Trp36-Ser60 peptide monomer with E3 was 2:1 suggesting the presence of 2 accessible binding sites on dimeric E3 (Fig. 4.15). Positive evidence for an interaction between E1o-90 GST and E3 as opposed to the negative results obtained for the shorter E1o-60 GST construct are consistent with the idea that steric hindrance by the GST fusion partner may be an important contributory factor in the latter case.

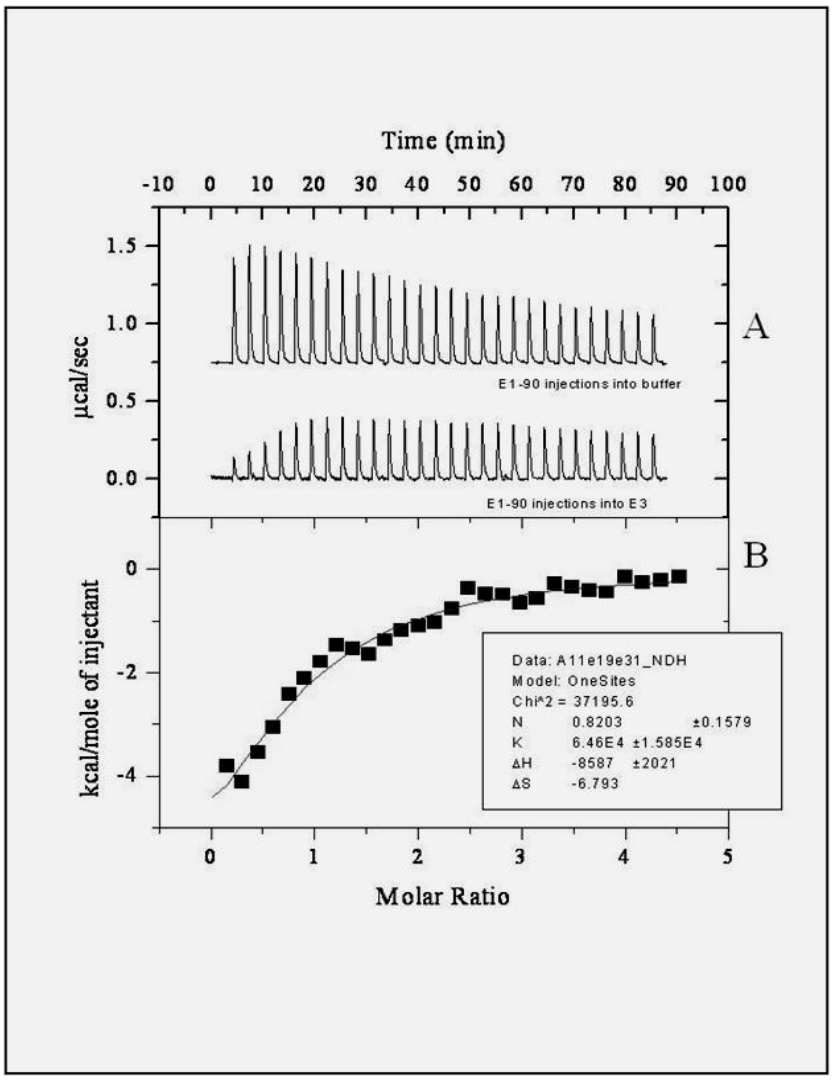


**Figure 4.21: ITC analysis of N-terminal E1o-90 GST (Ser1-Val90) interaction with E3**
(A) Raw data obtained from a series of 10µl injections of E1o-90 GST into E3 at 25°C and plotted as heat changes versus time. (B) Plotting the areas under the peaks in (A) (E1o-90 GST injections into E3) against the molar ratio of E1o-90 GST injected as calculated by the ORIGIN software package. The best fit shown was obtained by least-squares fitting using a simple binding model (see section 2.5.2). The stoichiometry of binding (*N*) is one E1o-90 GST homodimer per E3 homodimer. The calculated values for stoichiometry, affinity constant (*K*), enthalpy change (Δ*H*) and entropy change (Δ*S*) are shown in the insert. ITC experiments and analyses were performed in collaboration with Mrs. Margaret Nutley, University of Glasgow.

### 4.2.3.5 Investigation of the interaction between E1o-153 MBP (Ser1-Phe153) and E3 by ITC

The cDNA sequence encoding the human N-terminal E1o truncate (Ser1-Phe153) was successfully cloned into pET-30a (see section 3.3.1.3) and subsequently over-expressed and purified (see section 3.3.2.3 & 3.3.3.3). Preliminary studies suggested that E1o-153 MBP construct was less susceptible to rapid proteolysis than the corresponding GST fusion protein.

E1o-153 MBP and E3 were dialysed overnight against PBS (50mM NaCl, 2.7mM KCl, 10mM $Na_2HPO_4$ and 1.8mM $KH_2PO_4$, pH 7.4) and concentrated (see section 2.4.5). E3 (400μM) was injected in 10μl aliquots into the reaction cell containing 60μM E1o-153 MBP at 30°C (Fig. 4.22). Data were analysed using non-linear regression in the MicroCal ORIGIN software package, assuming a simple binding model.

On measuring heats of interaction of E1o-153 MBP with E3, complex formation was found to be endothermic (positive peaks in the ITC input). The data showed evidence of strong binding between E1o-153 MBP and E3 ($K_d$ = 1.1μM; $K_a$ = 8.64 x $10^5$ $M^{-1}$). Binding was characterised by a favourable enthalpy change ($\Delta H$ = -348.8 kcal/mol) and entropy change ($\Delta S$= 26.01 kcal/mol). However, a low $N$ value of 0.171 was recorded. The experiment was repeated 3 times at various protein concentrations and temperatures (10°C and 25°C) with similar results (data not shown). The reduction in $N$ value and small $\Delta H$ changes observed probably reflected aggregation and/or degradation of E1o-153 MBP in the reaction cell or lack of correct folding. In addition, partial precipitation of E1o-153 MBP was apparent at

the end of the ITC experiments. Thus, while a positive interaction was observed between this extended E1o-153 MBP construct and E3, any quantitative evaluation of the affinity, thermodynamics and stoichiometry of this interaction must be treated with considerable caution.

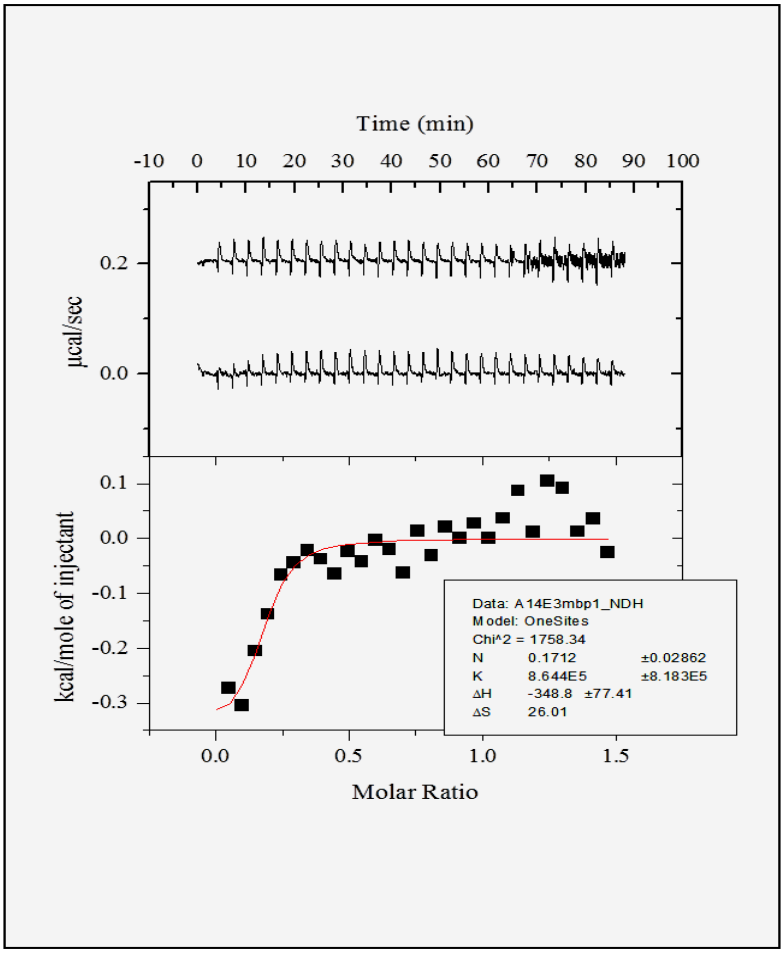


**Figure 4.22: ITC analysis of E1o-153 MBP (Ser1-Phe153) interaction with E3**
(A) Raw data obtained from a series of 10µl injections of E3 into E1o-153 MBP at 30°C were plotted as heat versus time. (B) Plotting the areas under the peaks in (A) (E3 injections into E1o-153 MBP) against the molar ratio of E3 injected as calculated by the ORIGIN software package. The best fit shown was obtained by least-squares fitting using a simple binding model (see section 2.5.3). The best values for stoichiometry (*N*), affinity constant (*K*), enthalpy change ($\Delta H$) and entropy change ($\Delta S$) are shown in the insert. ITC experiments and analyses were performed in collaboration with Mrs. Margaret Nutley, University of Glasgow.

## 4.3 Discussion

Human E2o lacks an equivalent SBD for E1o and E3 to those identified in bacterial E2o and in the E2s or E3BPs of its companion mammalian complexes, PDC and BCOADC (Bradford *et al.* 1987; Packman and Perham 1987; Wagenknecht *et al.* 1990; Nakano *et al.* 1994). Thus the overall organisation and modes of interaction of the three constituent enzymes (E1o, E2o and E3) in native, mammalian OGDC have not yet been elucidated partly owing to its large molecular mass and distinctive domain structure of its E2o core. In addition, separation of active E1o from the intact E2o assembly under non-denaturing conditions has proved difficult as has the ability to produce soluble recombinant native E1o. Thus to date, most OGDC dissociation/association studies have been limited to analysis of native complexes purified from various sources.

The data presented in this chapter demonstrate that the N-terminal region of human E1o interacts directly with E3 highlighting its key role in maintaining the structural integrity of the complex. Direct evidence confirming this novel function for the E1o N-terminal region, in particular a.a 10-90, was obtained using peptide array technology (Fig. 4.12 & 4.13), isothermal titration calorimetry (Fig. 4.15, 4.21 & 4.22) and direct biochemical binding studies using affinity chromatography (Fig. 4.20).

In this chapter, the first aim was to perform a preliminary structural characterization of the E1o N-terminal region in order to test its tendency to attain an ordered 3-D structure or remain in a dynamic (natively-disordered) state. In general, protein-protein interactions mediated by specific non-covalent interactions depend on the presence of highly organised, well-structured binding

sites. Secondary or tertiary structural elements contribute to formation of complementary hydrophilic/hydrophobic surfaces that promote specific interactions with its cognate partner protein. The tendency of the E1o N-terminal region to form α-helix or β-pleated sheet was determined by CD. Short segments of this region did have the ability to adopt an α-helical structure that was evident at increasing TFE concentrations (Fig. 4.4 & 4.5). Moreover, the 3-D structure prediction of human E1o N-terminal region (Fig. 4.6) and full-length E1o (Fig. 4.8 & 4.9) highlighted the potential presence of 2 short α-helical segments while the remainder of the domain was largely 'random coil'. Structure prediction of full-length human E1o also indicated that the two N-terminal regions were highly accessible on the surface of the protein and may be in close proximity at one end of the homodimer. In summary, all these findings suggest that the E1o N-terminal domain is highly dynamic although perhaps containing 2 short stretches of α-helix. Interestingly, supporting the role of this region in promoting E3 binding, the overall structural characteristics of the human E1o N-terminus appear similar in character to the E3BP-SBD, a topic that is investigated in more detail in chapter 7.

As stated above, our data confirm a role for the E1o N-terminal region in E3 binding. These findings are in agreement with previous biochemical and immunological studies on mammalian OGDC. Rice and colleagues (1992) showed that specific proteolysis of bovine E1o with trypsin at a single site (Arg77) located near the E1o N-terminus resulted in loss of overall complex activity. Loss of activity was caused by dissociation of a large catalytically-active E1' fragment and E3 from the E2o core assembly highlighting the critical role of this region in ensuring overall complex stability. This enhanced susceptibility to proteolysis suggested that the E1o N-terminus is highly accessible and dynamic, an observation also suggested by its highly

immunogenic character (McCartney *et al.* 1998). Interestingly, immunological analysis has shown that the N-terminal sequence of E1o has limited structural/sequence similarity with human E3BP as E1o-antiserum cross-reacts weakly with E3BP while anti-E3BP-specific serum was also able to recognize E1o (Rice *et al.* 1992; McCartney *et al.* 1998). The data presented in this chapter are also consistent with a recent crystallographic study of a bacterial E1o as described by Frank and colleagues (2007). These authors found that *E. coli* E1o proved intractable to crystallisation prior to removal of a 77 a.a. N-terminal fragment. Difficulties in protein crystallisation are often limited by the presence of flexible, dynamic and native disordered regions.

Amino acid sequence comparison of E1o from different sources including yeast, gram negative bacteria (*E. coli*.), porcine and human tissue employed by Koike and colleagues (Koike *et al.* 1992; Koike 1998) have indicated that human E1o has 37% and 40% sequence identity with the *E. coli* E1o and yeast E1o respectively. Furthermore, this study revealed that human E1o has high sequence identity (93%) with porcine E1o.

Importantly, distinct isoforms of mammalian E1o have been identified recently. The human *OGDH* gene located on chromosome 7 encoding E1o is known as the heart isoform (OGDH-H) (Szabo *et al.* 1994; Koike 1995; Koike 1998). There are two additional, well-characterised isoforms; human brain E1o isoform (OGDH-L) (Bunik and Fernie 2009) and a mitochondrial hypothetical protein (DHTKD1) (Bunik and Degtyarev 2008a). Sequence comparison of the 3 main human E1o or E1o-like isoforms; OGDH-H, OGDH-L and DHTKD1 termed isoforms 1, 2 and 3, respectively reveals that the N-terminal region of OGDH-H (1-167 a.a.) is highly conserved in OGDH-L (Fig. 4.10). Moreover, OGDH-L (1-1010 a.a.) shows 81.3%

identity in a 898 a.a. overlap with OGDH-H. In contrast, the N-terminal region of human E1o isoform 3 (DHTKD1) is about 60 amino acid shorter than the corresponding N-terminal region of OGDH-H. Sequence comparison of isoform 3 with E1o OGDH-H reveals only a 40.1% identity in a 836 a.a. overlap. Despite the distinctive nature of isoform 3, it still retains a putative ThDP binding domain and catalytic domain.

A recent report has established that the disease 2-oxoadipic aciduria occurs as a result of a defect in the DHTKD1 gene that is characterised by elevated levels of 2-oxoaminoadipate and 2-oxoadipate leading to ataxia, muscular hypotonia and epilepsy (Danhauser *et al.* 2012). This recent study has established that the DHTKD1 isoform is a *bona fide* gene product involved in lysine and tryptophan catabolism; however, it is unclear at this stage whether it functions as an individual enzyme or as a component of a multimeric complex.

## 4.3 Summary

This chapter has described the structural and binding characteristics of the N-terminal region of E1o, in particular its ability to interact with E3. The data presented in this chapter can be summarized as follows:

- Two short segments of N-terminal region of human E1o have the potential ability to adopt an α-helical conformation.

- The majority of the N-terminal region is predicted to be highly dynamic and accessible on the surface of the E1o homodimer.

- The N-terminal region of human E1o has similar overall 3-D structural characteristics to E3BP-SBD.

- Direct evidence has been obtained by a variety of techniques highlighting the key importance of the N-terminal region of human E1o in mediating E3 binding in mammalian OGDC.

# Chapter 5

# Investigation of a possible interaction between the N-terminal region of E1o and E2o

## 5.1 Introduction

The basic organisation of the OGDC is defined by the self-assembly of its central E2o enzyme to form a 24-meric cube to which multiple copies of E1o and E3 are attached non-covalently. In PDC and BCOADC, E2 also forms the structural cores of these complexes. They are assembled from multiple identical subunits to form a 24-meric cube or 60-meric pentagonal dodecahedron to which E1 and E3 enzymes are bound via a specific SBD located on E2b in BCOADC or E2p and E3BP (an E2-related subunit) in PDC. Previous studies have shown that the sequence of human E2o is unusual in lacking an obvious E3 binding or E1o binding domain (Spencer *et al.* 1984; Bradford *et al.* 1987; Packman and Perham 1987; Wagenknecht *et al.* 1990; Westphal and de Kok 1990; Nakano *et al.* 1994).

As discussed previously, the N-terminal region of E1o has been identified as a key region involved in maintenance of overall complex integrity, specifically via its interaction with E3 (Kresze *et al.* 1981; Rice *et al.* 1992; McCartney *et al.* 1998).

Interestingly, however, cleavage of E1o in this N-terminal region (a.a. 77 in bovine OGDC) also leads to dissociation of a large active E1' homodimeric species from the central core implicating this region in mediating E1o-E2o interactions. Full-length E1o is highly unstable as a free enzyme and can only be removed from the native E2o core by stringent treatments e.g. 3M $MgCl_2$ that cause partial core disassembly (Rice *et al.* 1992). These observations raise the possibility that E1o is tightly integrated into the E2o core in a manner similar to E3BP in the E2p core. Importantly, E3BP has been shown recently (a) to be incorporated into the E2p core in a co-translational fashion and (b) partly replace E2p within the E2p:E3BP assembly (Vijayakrishnan *et al.* 2010).

The main purpose of this chapter was to investigate the ability of the N-terminal region of E1o to interact with the E2o either post-translationally *in vitro* or co-translationally *in vivo*. Initially, the hypothesis that E2o and E3 were incapable of interacting directly as anticipated from the apparent absence of an E3-SBD on E2o was tested by gel filtration chromatography and ITC.

As a corollary, this chapter also provides new insights into the steps required for generating a recombinant model of OGDC for future genetic and biomedical studies on naturally-occurring and mutant forms of the complex.

# 5.2 Results and analysis

## *5.2.1 Investigation of a possible interaction between E2o and E3*

A possible direct interaction between E2o and E3 was investigated using GFC and ITC. Both enzymes (E2o and E3) were individually over-expressed and purified as described previously (see section 3.3.2 & 3.3.3).

### 5.2.1.1 Investigation of a possible E2o:E3 interaction using gel filtration chromatography

In this study, E2o and E3 were expressed separately in *E. coli* (DE3) pLysS cells at 30 ºC for 5 h. After individual expression, bacterial pellets were disrupted by French press treatment and purified using zinc chelate chromatography. Purified enzymes were dialysed simultaneously against 20mM NaCl and 20mM potassium phosphate, pH 7.5. The two enzymes were mixed in a 1:1 molar ratio and passed through a HiPrep 16/60 Sephacryl S-300 high resolution column attached to a BioCAD 700E workstation. Two separate peaks of eluted protein were observed (Fig. 5.1A). On SDS-PAGE analysis of the individual peaks (Fig. 5.1B), it was found that the first peak eluting at or near the void volume (~ 40ml) contained only E2o whereas the second peak contained E3 indicating that on mixing the two subunits did not associate post-translationally. These results were also confirmed by Western blotting using anti-E3 polyclonal antibody (Fig. 5.1C).

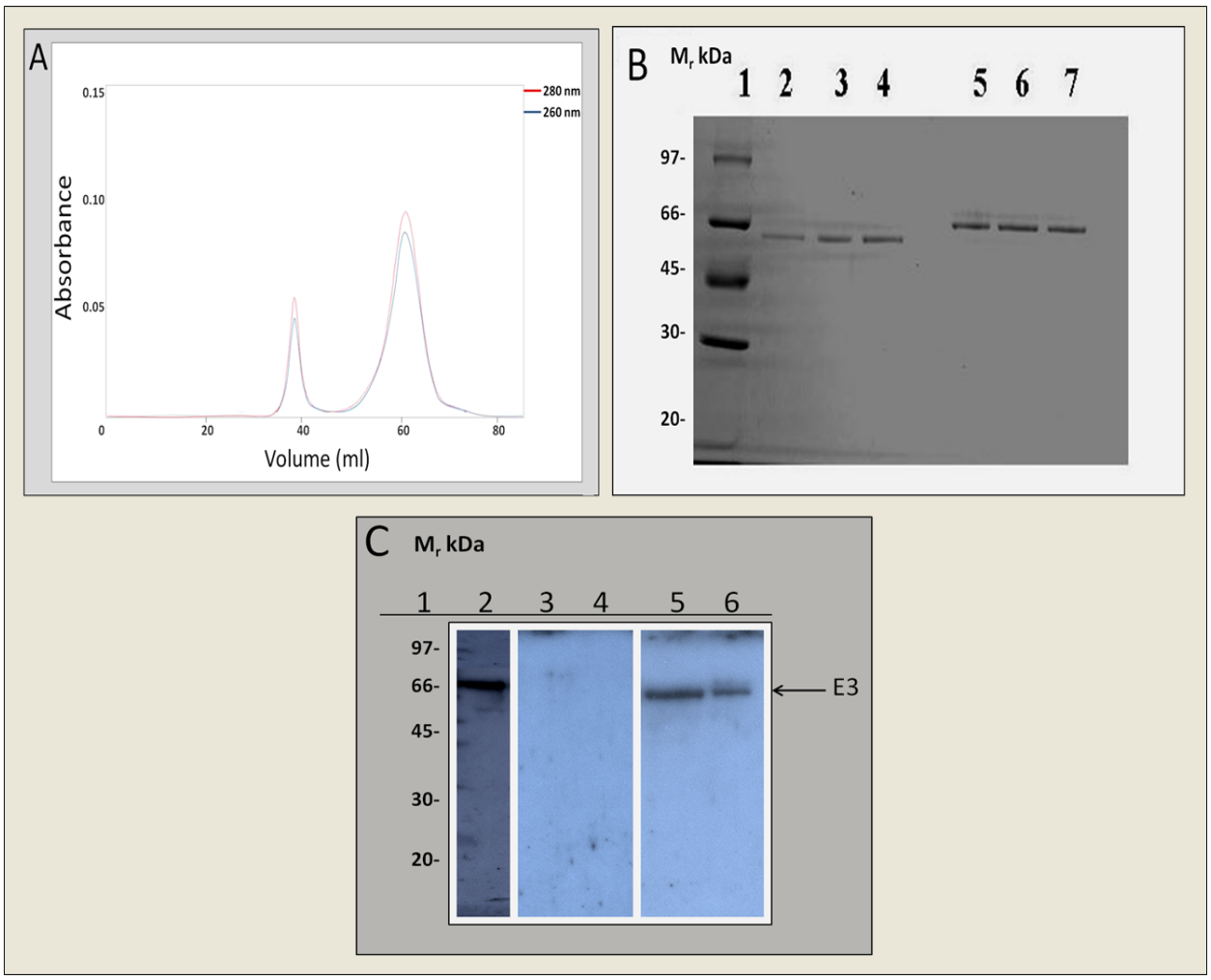


**Figure 5.1: Investigation of a possible interaction between E2o and E3 using GFC**

(A) Post-translational mixing of E2o and E3 followed by gel filtration on a HiPrep 16/60 Sephacryl S-300 high resolution column. E2o and E3 were mixed in a 1:1 molar ratio. The purified proteins were applied to the column in a 1ml aliquot and eluted using 1 CV GFC buffer (20mM NaCl, 2mM EDTA, 20mM $KH_2PO_4$, pH 7.4,). Two eluted peaks were observed, E2o being eluted at ~40 ml, while, E3 eluted at ~ 60 ml. Absorbance of eluted proteins was measured at 280 nm (red line) and possible DNA/RNA contamination was monitored at 260 nm (blue line). Peak fractions were collected and analysed by SDS-PAGE. (B) SDS-PAGE (16%) analysis of protein peaks stained with Coomassie Brilliant Blue. Lane 1, molecular mass markers; lane 2, purified E2o as control; lanes 3 & 4, first peak (E2o) elution fractions at expected size; lane 5, purified E3 as control and lanes 6-7, second peak (E3) elution fractions at expected size. (C) Western blot analysis of eluted peaks. Lane 1, molecular mass markers; lane 2, purified E3 as control; lanes 3 & 4, first elution peak; lanes 5 & 6, second elution peak. The presence of E3 in second elution peak was confirmed with anti-E3 antibody (1 in 1000 dilution) (see section 2.4.7.3). No E3 band was detected in the first elution peak (E2o). Thus, no stable association between E2o and E3 was observed under these conditions.

### 5.2.1.2 Investigation of a possible E2o:E3 interaction using ITC

E2o and E3 were dialysed overnight against 30mM $KH_2$ $PO_4$, pH 7.4, 30mM NaCl and concentrated (see section 2.4.5). E3 (198μM) was injected in 10μl aliquots into the reaction cell containing 35μM E2o at 25 ºC (Fig. 5.2). Data were analysed using non-linear regression in the MicroCal ORIGIN software package, assuming a simple binding model. Titrations of E3 with E2o were similar to the dilution of the E3 into the buffer.

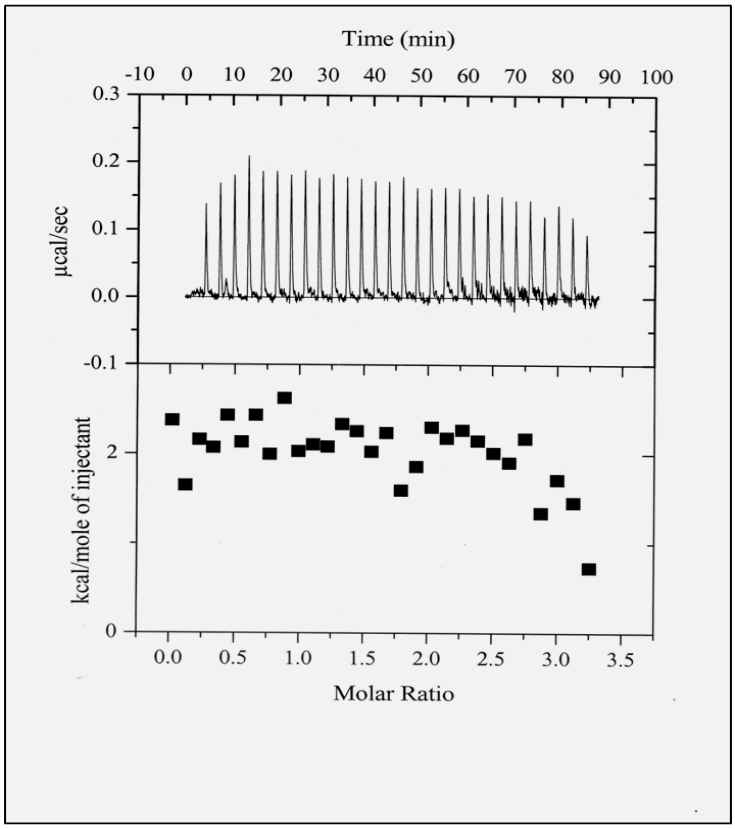


**Figure 5.2: ITC analysis of a possible E2o and E3 interaction**
(A) Raw data obtained from a series of 10μl injections of E3 into E2o at 25°C and plotted as heat versus time. (B) Plotting the areas under the peaks in (A) against the molar ratio of E3 injected as calculated by the ORIGIN software package. The best fit shown was obtained by least-squares fitting using a simple binding model (see section 2.5.3). No binding was detected as no heat exchange was observed. ITC experiments and analyses were performed in collaboration with Mrs. Margaret Nutley, University of Glasgow.

## 5.2.2 Investigation of a possible post-translational interaction between N-terminal E1o constructs and E2o

A possible post-translational interaction between human N-terminal E1o GST fusion proteins (E1o-60, E1o-90 and E1o-153) and E2o was investigated using affinity chromatography and GFC. Owing to the high molecular mass of human E2o ($M_r$ ~ 1.0 million), native-PAGE was not employed in this case. In addition, investigation of a potential, post-translational interaction between N-terminal E1o constructs (E1o-60, E1o-90 and E1o-153 GST fusion proteins) and E2o using ITC was not performed as a result of time constraints.

In this section, the N-terminal E1o GST truncates (E1o-60, E1o-90 & E1o-153) and E2o were individually over-expressed and purified as described previously (see section 3.3.2 & 3.3.3).

### 5.2.2.1 Investigation of a possible interaction between E1o-90 GST and E2o using glutathione Sepharose 4B chromatography

In this experiment, E1o-90 GST and E2o were expressed individually in *E. coli* (DE3) pLysS cells at 30 ºC for 3-5 h. After individual expression, bacterial pellets were disrupted by French press treatment and purified using GST affinity chromatography and zinc chelate chromatography respectively. Purified enzymes were dialysed simultaneously against PBS, pH 7.4. The two enzymes were mixed post-translationally (1:1 molar ratio) and passed through a glutathione Sepharose 4B column attached to a BioCAD 700E workstation. Two separate peaks of eluted protein were observed (Fig. 5.3A). On SDS-PAGE analysis of the individual peaks, it was found that the first peak (flow through) contained E2o and traces of unbound E1o-90 GST,

while, the second eluted peak contained only E1o-90 GST (Fig. 5.3B) and no clear band of E2o was observed. Thus no stable association between E2o and N-terminal E1o-90 could be detected under these conditions. This result was verified by Western blotting using an anti-His tag antibody (penta-His HRP conjugate antibody) and anti-GST HRP conjugate antibody (data not shown).

N-terminal GST fusion constructs; E1o-60 and E1o-153 were also examined for their ability to interact with E2o using glutathione affinity chromatography and showed similar results (data not shown).

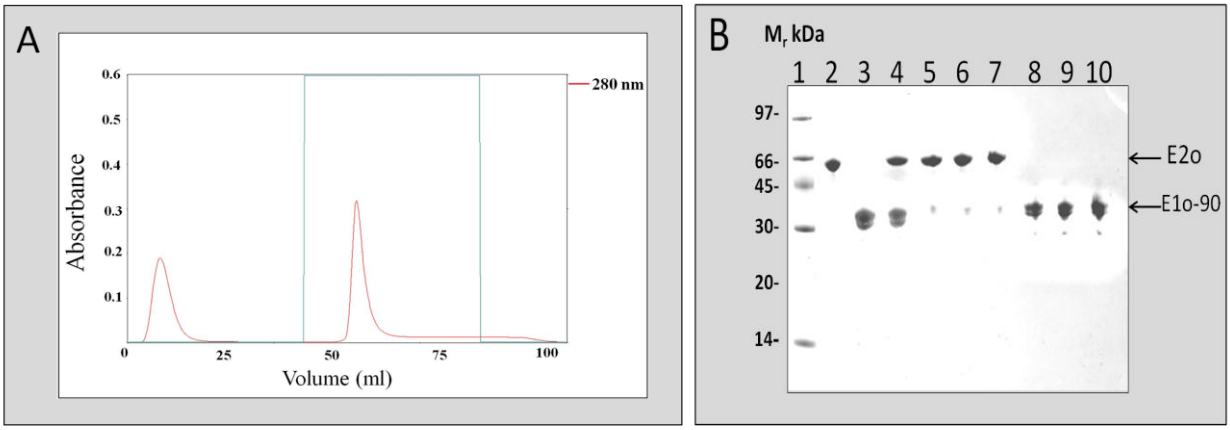


**Figure 5.3: Investigation of a possible interaction between E1o-90 GST and E2o using glutathione affinity chromatography**

(A) Post-translational mixing of E1o-90 GST and E2o followed by glutathione Sepharose chromatography. E1o-90 GST and E2o were mixed in a 1:1 molar ratio. Purified proteins were applied to the column in a 2ml aliquot. Bound protein was eluted from the column using 5 CV elution buffer (20mM reduced glutathione, 50mM Tris-HCl, pH 8.0). The reduced glutathione buffer step used for elution is shown in green. Absorbance of eluted protein was measured at 280 nm (red line). Peak fractions were collected and analysed by SDS-PAGE. (B) SDS-PAGE (10%) analysis of eluted protein peaks stained with Coomassie Brilliant Blue. Lane 1, molecular mass markers; lane 2, purified E2o as control; lane 3, purified E1o-90 GST as control; lane 4, mixture of E1o-90 GST/E2o prior to chromatography; lanes 5-7, flow through and lanes 8-10, elution fraction. No E2o band was detected in elution fractions (lanes 8, 9 and 10). The arrows on the right of the blot indicate E2o and E1o-90 GST proteins respectively.

### 5.2.2.2 Investigation of a possible interaction between E1o-90 GST and E2o using GFC

In this experiment, E2o and E1o-90 GST were expressed separately in *E. coli* (DE3) pLysS cells at 30 ºC for 4-5 h. After individual expression, bacterial pellets were disrupted by French press treatment and purified using zinc chelate chromatography (in case of E2o) and glutathione affinity chromatography (in case of E1o-90 GST). Purified enzymes were dialysed simultaneously against 20mM NaCl, 20mM potassium phosphate, pH 7.5. The two enzymes were mixed in a 1:1 (molar ratio) and passed through a HiPrep 16/60 Sephacryl S-300 high resolution column attached to a BioCAD 700E workstation. Two separate peaks of eluted protein were observed (Fig. 5.4A). On SDS-PAGE analysis of the individual peaks (Fig. 5.4B), it was found that the first peak eluting at or near the void volume (~ 40ml) contained only E2o whereas the second peak contained E1o-90 GST confirming that on mixing the two purified proteins did not associate post-translationally.

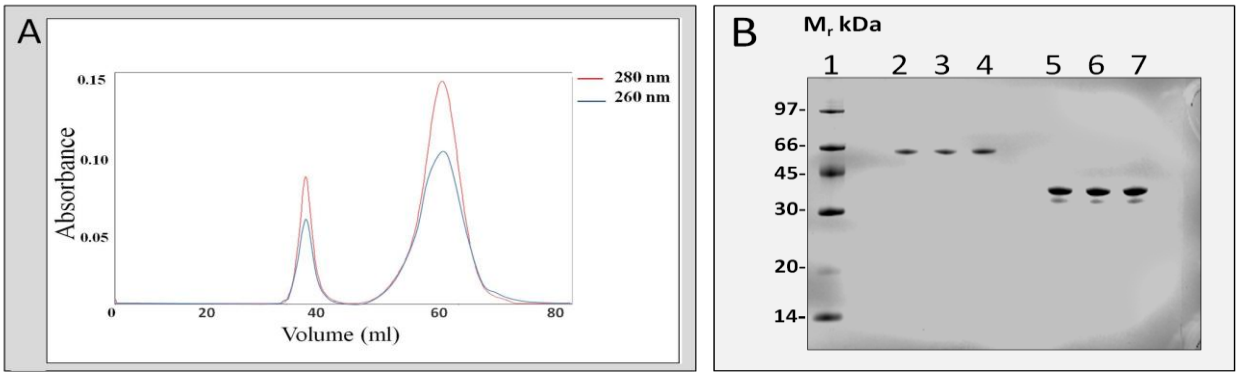


**Figure 5.4: Investigation of a possible interaction between E2o and E1o-90 GST by GFC**
(A) Post-translational mixing of E2o and E1o-90 GST followed by gel filtration chromatography on a HiPrep 16/60 Sephacryl S-300 high resolution column. E2o and E1o-90 GST were mixed in a 1:1 (molar ratio). Purified proteins were applied to the column in a 1ml aliquot. Proteins were eluted from the column using 1 CV GFC buffer (20mM NaCl, 2mM EDTA, 20mM $KH_2PO_4$, pH 7.4). Two eluted peaks were observed, E2o being eluted at ~ 40 ml, while, E1o-90 GST eluted at ~ 63 ml. Absorbance of eluted proteins was measured at 280 nm (red line) and possible DNA/RNA contamination was monitored at 260 nm (blue line). Peak fractions were collected and analysed by SDS-PAGE. (B) SDS-PAGE (10%) analysis of eluted protein peaks stained with Coomassie Brilliant Blue. Lane 1, molecular mass markers; lane 2, purified E2o as control; lanes 3 & 4, first peak (E2o) elution fractions at correct expected size; lane 5, purified E1o-90 GST as control and lanes 6 & 7, second peak (E1o-90 GST) elution fractions at correct expected size. No stable association between E2o and E1o-90 GST was observed under these conditions.

The purified N-terminal E1o-60 and E1o-153 GST fusion proteins were also examined for their ability to interact with E2o using GFC and showed similar results (data not shown).

## 5.2.3 Investigation of a potential co-translational interaction between N-terminal E1o and E2o

Previous experiments (section 5.2.2) demonstrated conclusively that the N-terminal region of E1o was unable to form a stable complex with E2o as judged by either glutathione affinity chromatography or GFC. In this section, a role for the E1o N-terminus in mediating a possible interaction with E2o in a co-translation fashion was investigated.

### 5.2.3.1 Investigation of a potential co-translational interaction between E1o-60 and E2o

Initially, the cDNA encoding His-tagged E2o was housed in pET-28b (kanamycin resistant) whereas the N-terminal E1o-60 (Ser11-Ala70) was housed in pGEX-2T (ampicillin resistant). These two plasmids were successfully co-transformed into *E. coli* BL21 (DE3) pLysS cells by dual antibiotic selection and over-expressed at 30 °C for 4 h (Fig. 5.5). The pellet (500 ml culture) was divided into two and separately disrupted by French press treatment. Two tablets of protease inhibitors (EDTA free) were added prior to disruption. The soluble supernatant fractions were purified by zinc chelate chromatography and glutathione Sepharose 4B affinity chromatography, respectively (Fig. 5.6A & 5.6C).

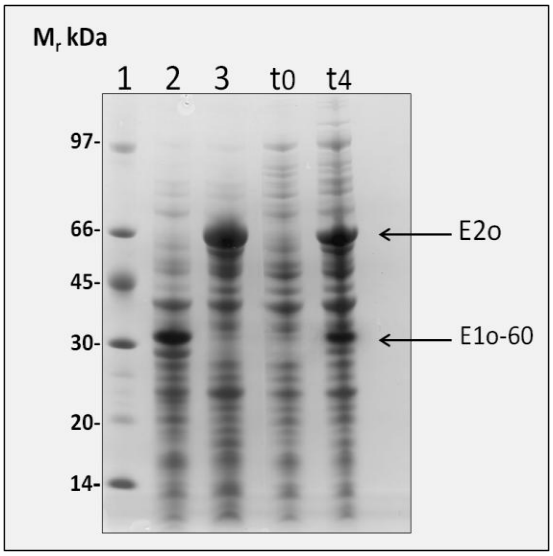


**Figure 5.5: Co-expression of the N-terminal E1o-60 GST fusion protein and His-tagged E2o**
Human N-terminal E1o-60 GST and E2o were co-transformed into *E. coli* BL21 (DE3) pLysS cells and over-expressed at 30 °C for 4 h. Cells were grown in LB media. Samples were taken at the time of induction (t0) and after 4 h (t4). Samples were denatured in the presence of 150mM DTT at 100°C for 5min and resolved on a 10% SDS/polyacrylamide gel. Protein bands were visualised using Coomassie Brilliant Blue. Lane 1, molecular mass markers; lane 2, E1o-60 GST over-expression as control; lane 3, E2o over-expression as control; co-expression of E2o and E1o-60 GST fusion protein at (t0) and (t4). The arrows on the right of the gel indicate over-expressed protein at correct expected sizes.

SDS-PAGE analysis of the purified fractions by zinc chelate chromatography or glutathione affinity chromatography (Fig. 5.6B & 5.6D) showed no evidence for the formation of an E1o-60:E2o sub-complex. No band of E1o-60 GST was apparent in the His-tagged E2o peak purified by zinc chelate chromatography (Fig. 5.6B). Conversely, no E2o could be detected in the E1o-60 GST peak purified by glutathione affinity chromatography (Fig. 5.6D). This result was also confirmed by Western blotting using anti-GST tag antibody and anti-His tag antibody (data not shown).

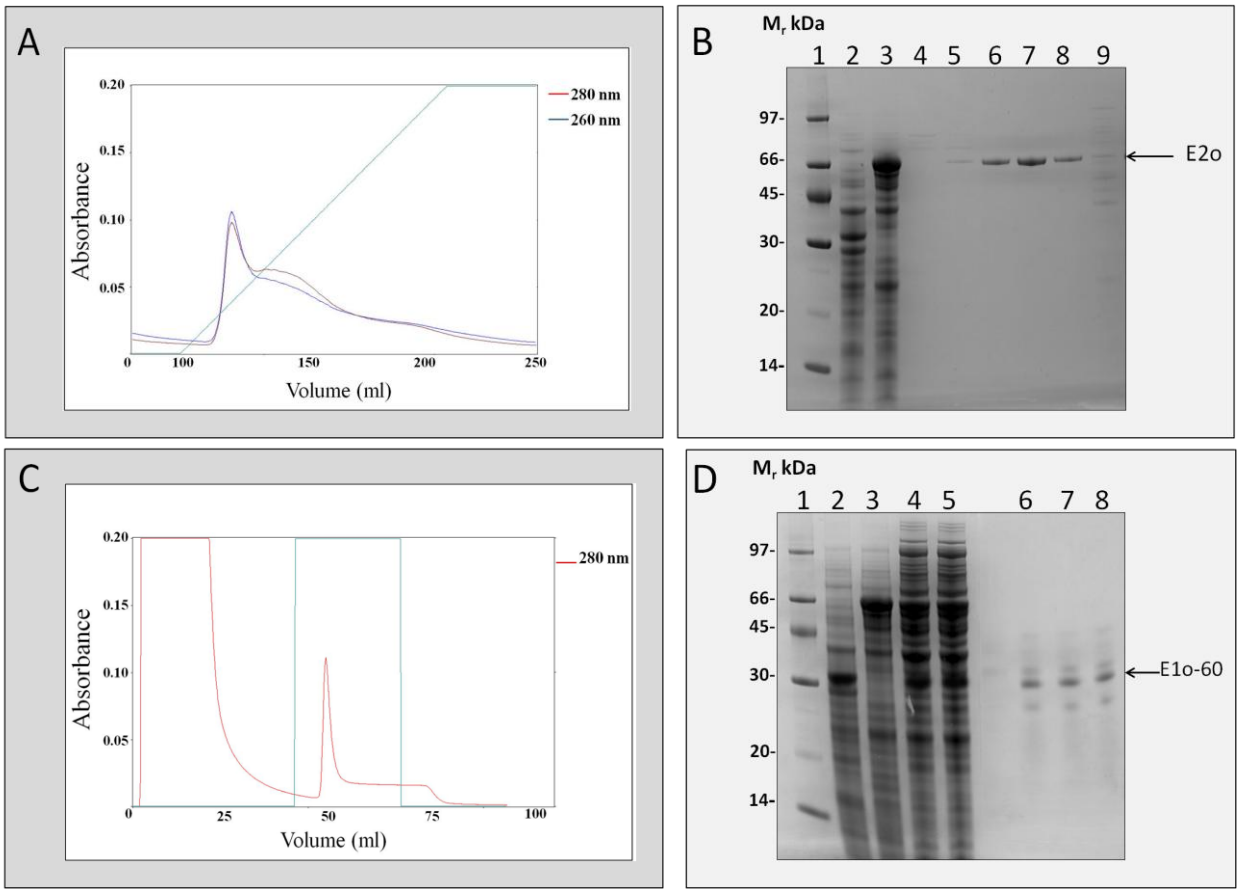


**Figure 5.6: Purification of co-expressed E1o-60 GST and E2o**

Human N-terminal E1o-60 GST and E2o were co-transformed into *E. coli* BL21 (DE3) pLysS cells and over-expressed at 30 °C for 4 h. Cells were grown in LB media. (A) Metal chelate affinity chromatography of co-expressed E1o-60 GST and E2o. The cell lysates were applied to the column in 5ml aliquots (see section 2.4.4). Bound protein was eluted from the column in a 0-100% gradient of elution buffer (8 CV). The imidazole gradient (0-500mM) used for elution is shown in green. Absorbance of eluted protein was measured at 280 nm (red line) and possible DNA/RNA contamination was monitored at 260 nm (blue line). Peak fractions (2ml) were collected and analysed by SDS-PAGE. (B) SDS-PAGE (10%) analysis of eluted protein peak stained with Coomassie Brilliant Blue. Lane 1, molecular mass markers; lane 2, over-expression of E1o-60 GST as control; lane 3, over-expression of E2o as control; lanes 4-8, purified co-expressed E1o-60 GST and E2o; lane 9, unbound protein. The arrow on the right of the blot indicates purified protein. No E1o-60 GST band was observed in elution fractions. (C) Glutathione affinity chromatography of co-expressed E1o-60 GST and E2o. The cell lysates were applied to the column in 5ml aliquots (see section 2.4.4). Bound protein was eluted from the column using 5 CV elution buffer (20mM reduced glutathione, 50mM Tris-HCl, pH 8.0). The reduced glutathione buffer step used for elution is shown in green. Absorbance of eluted protein was measured at 280 nm (red line). Peak fractions (2ml) were collected and analysed by SDS-PAGE. (D) SDS-PAGE (10%) analysis of eluted protein peak stained with Coomassie Brilliant Blue. Lane 1, molecular mass markers; lane 2, over-expression of E1o-60 GST as control; lane 3, over-expression of E2o as control; lanes 4 & 5, co-expression of E1o-60 GST and E2o (t4) as control; lanes 6-8, purified co-expressed E1o-60 GST and E2o. The arrow on the right of the blot indicates purified protein. No E2o band was observed in elution fractions.

### 5.2.3.2 Investigation of a potential co-translational interaction between E1o-90 and E2o

A kanamycin resistant plasmid encoding His-tagged E2o (pET-28b) and an ampicillin resistant plasmid encoding E1o-90 GST (Ser1-Val90) were successfully co-transformed into *E. coli* BL21 (DE3) pLysS cells and over-expressed at 30 °C for 4 h (Fig. 5.7). The pellet (500 ml culture) was divided in two and disrupted separately using French press treatment. Two tablets of protease inhibitors (EDTA free) were added prior to disruption. The soluble supernatant fractions were purified by zinc chelate chromatography and glutathione Sepharose 4B affinity chromatography, respectively (Fig. 5.8A & 5.9A).

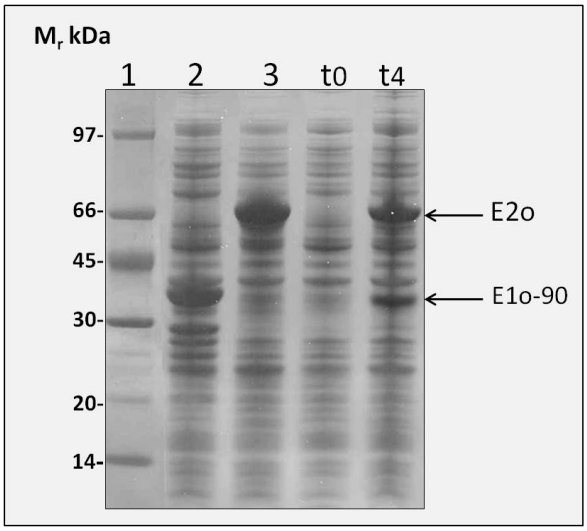


**Figure 5.7: Co-expression of the N-terminal E1-90 GST fusion protein and His-tagged E2o**
Human N-terminal E1o-90 GST and E2o were co-transformed into *E. coli* BL21 (DE3) pLysS cells and over-expressed at 30 °C for 4 h. Samples were taken at the time of induction (t0) and after 4 h (t4). Samples were denatured in the presence of 150mM DTT at 100°C for 5min and resolved on a 10% SDS/polyacrylamide gel. Protein bands were visualised using Coomassie Brilliant Blue. Lane 1, molecular mass markers; lane 2, E1o-90 GST over-expression as control; lane 3, E2o over-expression as control; co-expression of E2o and E1o-90 GST fusion protein at (t0) and (t4). The arrows on the right of the gel indicate over-expressed proteins at correct expected sizes.

SDS-PAGE analysis of the His-tagged E2o fractions purified by zinc chelate chromatography showed the presence of an additional band of the predicted size for E1o-90 GST suggesting a possible integration of E2o with the E1o fragment (Fig. 5.8B). The identity of N-terminal E1o-90 GST present in the purified His-tagged E2o peak was confirmed by Western blotting using anti-GST tag antibody (Fig. 5.8C).

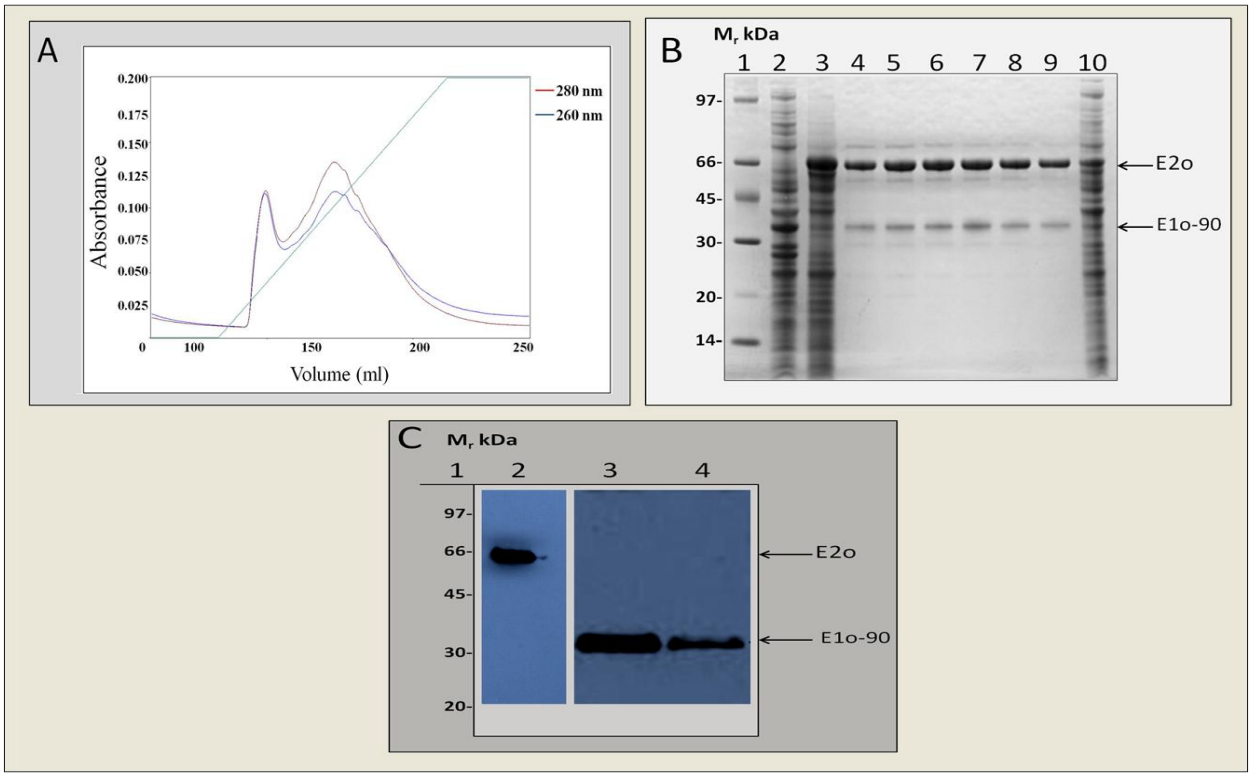


**Figure 5.8: Purification of co-expressed E1o-90 GST and E2o by metal chelate chromatography**

Human N-terminal E1o-90 GST and E2o plasmids were co-transformed into *E. coli* BL21 (DE3) pLysS cells and over-expressed at 30 °C for 4 h. (A) Metal chelate affinity chromatography of co-expressed E1o-90 GST and E2o. The cell lysate was applied to the column in 5ml aliquots (see section 2.4.4). Bound protein was eluted from the column in a 0-100% gradient of elution buffer (8 CV). The imidazole gradient (0-500 mM) used for elution is shown in green. Absorbance of eluted protein was measured at 280 nm (red line) and possible DNA/RNA contamination was monitored at 260 nm (blue line). Peak fractions (2ml) were collected and analysed by SDS-PAGE and Western blotting. (B) SDS-PAGE (12%) analysis of eluted protein peak stained with Coomassie Brilliant Blue. Lane 1, molecular mass markers; lane 2, over-expression of E1o-90 GST as control; lane 3, over-expression of E2o as control; lanes 4-9, purified co-expressed E1o-90 GST and E2o; lane 10, unbound protein. The arrows on the right of the blot indicate purified proteins. The E1o-90 GST band was observed in elution fractions indicating that the E1o-90 GST integrated specifically with E2o. (C) Western blot analysis of elution peak. Lane 1, molecular mass markers; lane 2, purified E2o as control; lane 3, purified E1o-90 GST as control. The presence of E1o-90 GST in the combined elution peak was confirmed (lane 4) with anti-GST HRP conjugate antibody (1 in 5000 dilution) (see section 2.4.7.2).

Conversely, when co-expressed E1o-90 GST and E2o were purified by glutathione Sepharose 4B chromatography (Fig. 5.9A), SDS-PAGE analysis of the peak fractions showed the presence of a band of the predicted size for E2o again indicating integration of E2o with the E1o fragment (Fig. 5.9B). The identity of His-tagged E2o present in the purified E1o-90 GST peak was confirmed by Western blotting using anti-His tag antibody (Fig. 5.9C).

Human N-terminal E1o-153 GST (Ser1-Phe153) was also successfully co-expressed with E2o in the same manner as E1o-90 GST/E2o co-expression. The soluble supernatants derived from *E. coli* pLysS cells co-expressing E1o-153 GST and E2o were purified using zinc chelate chromatography and glutathione Sepharose 4B affinity chromatography as described previously (data not shown). The purified proteins on elution were resolved by SDS-PAGE (Fig. 5.10A) and their identities confirmed by Western blotting (Fig. 5.10B), although extensive degradation of E1o-153 was again evident. These results provide further support for the hypothesis that the N-terminal region of E1o co-integrates with E2o as nascent polypeptides during folding and assembly.

Importantly, the E1o-60 GST construct (Fig. 5.5 & 5.6) and free wild-type GST run as a further control (data not shown) showed no evidence for stable complex formation with E2o, while the longer E1o-90 and E1o-153 constructs (Fig. 5.8, 5.9 & 5.10) were able to integrate with E2o during their simultaneous expression.

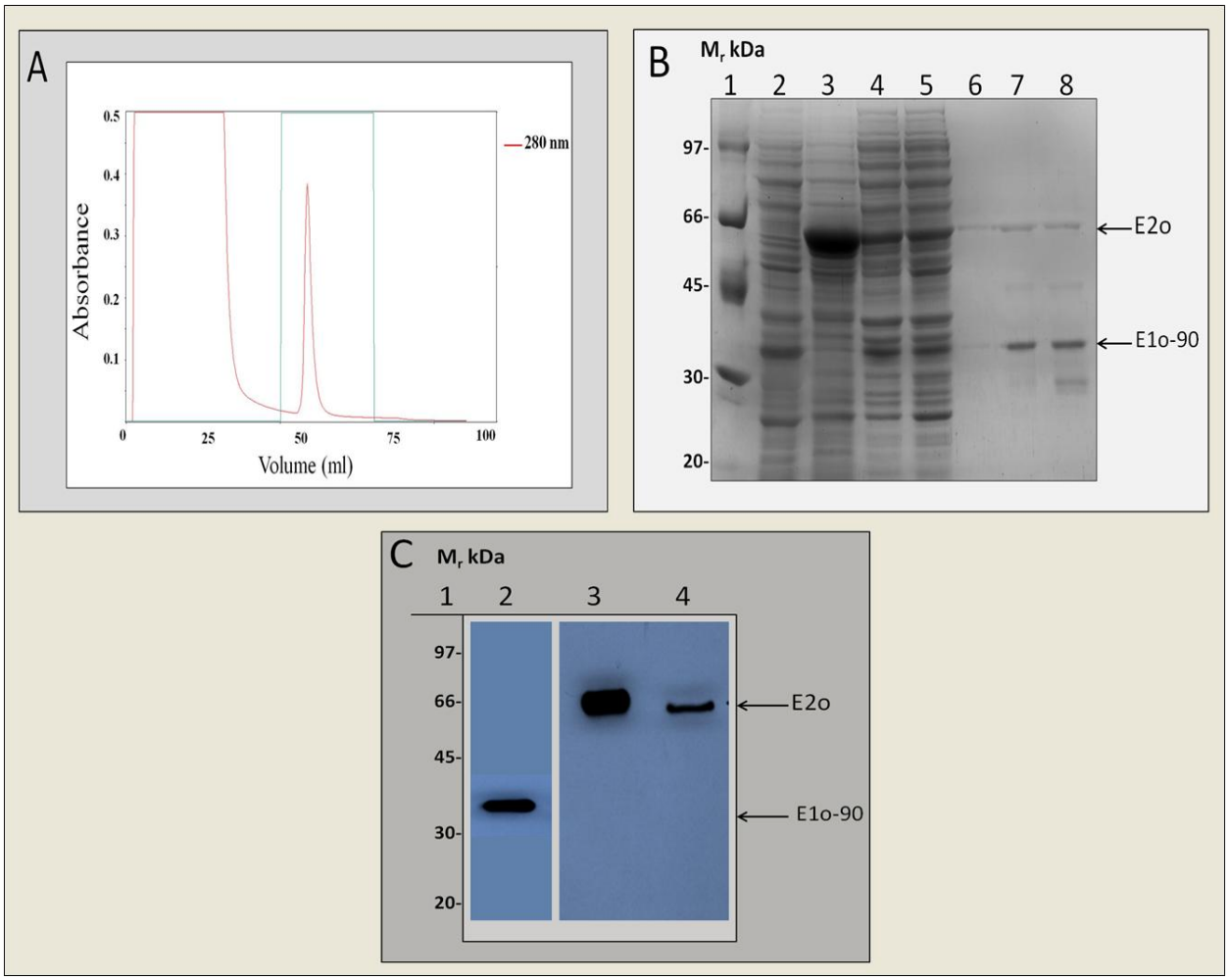


**Figure 5.9: Purification of co-expressed E1o-90 GST and E2o by glutathione affinity chromatography**

Human N-terminal E1o-90 GST and E2o plasmids were co-transformed into *E. coli* BL21 (DE3) pLysS cells and over-expressed at 30 °C for 4 h. (A) Glutathione affinity chromatography of co-expressed E1o-90 GST and E2o. The cell lysate was applied to the column in 5ml aliquots (see section 2.4.4). Bound protein was eluted using 5 CV elution buffer (20mM reduced glutathione, 50mM Tris-HCl, pH 8.0). The reduced glutathione buffer step used for elution is shown in green. Absorbance of eluted protein was measured at 280 nm (red line). Peak fractions (2ml) were collected and analysed by SDS-PAGE and Western blotting. (B) SDS-PAGE (10%) analysis of eluted protein peak stained with Coomassie Brilliant Blue. Lane 1, molecular mass markers; lane 2, over-expression of E1o-90 GST as control; lane 3, over-expression of E2o as control; lanes 4 & 5, co-expression of E1o-90 GST and E2o (t4) as control; lanes 6-8, purified co-expressed E1o-90 GST and E2o. The arrows on the right of the blot indicate purified proteins. The E2o band was observed in elution fractions indicating that the E1o-90 GST integrated specifically with E2o. (C) Western blot analysis of elution peak. Lane 1, molecular mass markers; lane 2, purified E1o-90 GST as control; lane 3, purified E2o as control. The presence of E2o in the combined elution peak was confirmed (lane 4) with anti-His tag antibody (1 in 2000 dilution) (see section 2.4.7.1).

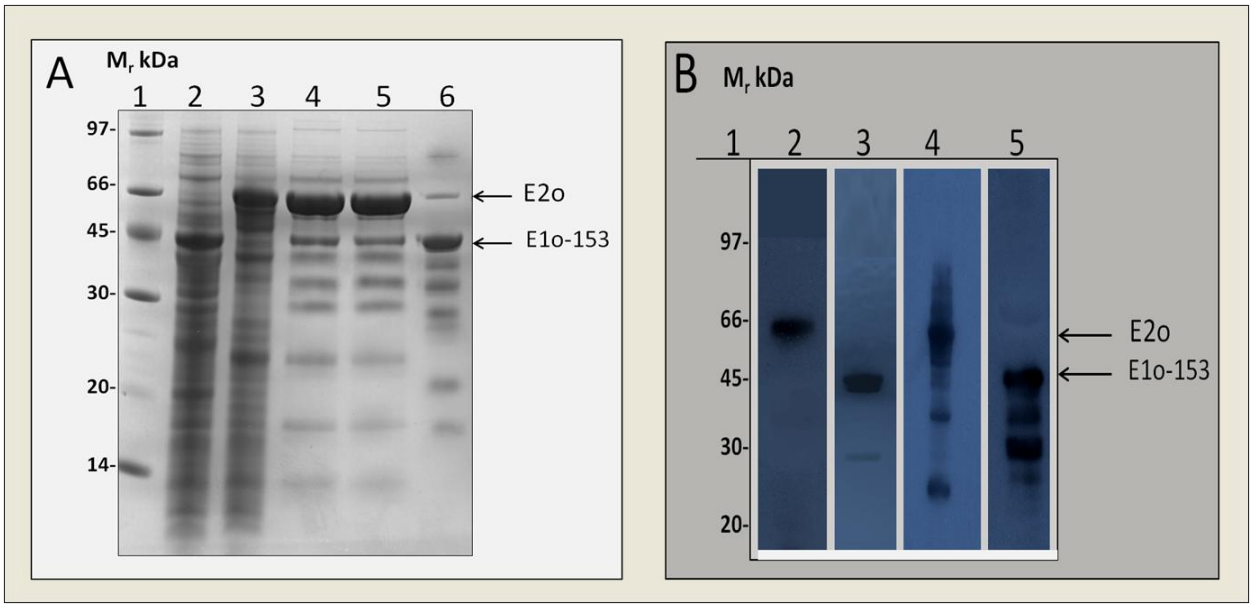


**Figure 5.10: Purification of co-expressed E1o-153 GST and E2o**
Human N-terminal E1o-153 GST and E2o plasmids were co-transformed into *E. coli* BL21 (DE3) pLysS cells and over-expressed at 30 °C for 4 h. (A) SDS-PAGE (10%) analysis of eluted protein peaks stained with Coomassie Brilliant Blue. Lane 1, molecular mass markers; lane 2, over-expression of E1o-153 GST as control; lane 3, over-expression of E2o as control; lanes 4 & 5, elution peak of co-expressed E1o-153 GST and E2o using metal chelate affinity chromatography; lane 6, elution peak of co-expressed E1o-153 GST and E2o using glutathione affinity chromatography. The arrows on the right of the blot indicate purified proteins. E2o was observed in elution peak after glutathione affinity chromatography indicating that the E1o-153 GST integrated specifically with E2o. SDS-PAGE analysis also shows extensive degradation. (C) Western blot analysis of elution peaks. Lane 1, molecular mass markers; lane 2, purified E2o as control; lane 3, purified E1o-153 GST as control. The presence of E2o in glutathione elution peak was confirmed (lane 4) with anti-His tag antibody (1 in 2000 dilution) (see section 2.4.7.1). The presence of E1o-153 GST in metal chelate elution peak was confirmed (lane 5) with anti-GST HRP conjugate antibody (1 in 5000 dilution) (see section 2.4.7.2). SDS-PAGE and Western blot analysis also shows extensive degradation of co-expressed E1o-153GST/E2o.

To check E1o-90GST/E2o sub-complex stability in high salt, a feature of the intact E1o-E2o core in the native OGDC, co-expressed E1o-90 GST and E2o were purified by zinc chelate affinity chromatography and dialysed overnight against high salt GFC buffer (500mM NaCl, 2mM EDTA, 50mM $KH_2PO_4$, pH 7.4) prior to gel filtration column in high salt (500mM NaCl) GFC buffer. A single peak at or near the void volume (~ 40ml) was observed (Fig. 5.11A). SDS-PAGE analysis of the eluted peak showed the presence of two bands corresponding to

E1o-90 GST and E2o confirming the stability of the E1o/E2o sub-complex to high salt treatment (Fig. 5.11B). The E1o/E2o sub-complex eluted at or near the void volume (~ 40ml) whereas the E1o-90 GST homodimer ($M_r$ 72,000 Da) eluted at a much later stage (~ 63ml) in the elution profile (Fig. 3.24C).

In combination, these experiments provide strong support for the existence of a stable E1o/E2o sub-complex that is resistance to high salt treatment and is exclusively assembled from nascent chains during synthesis.

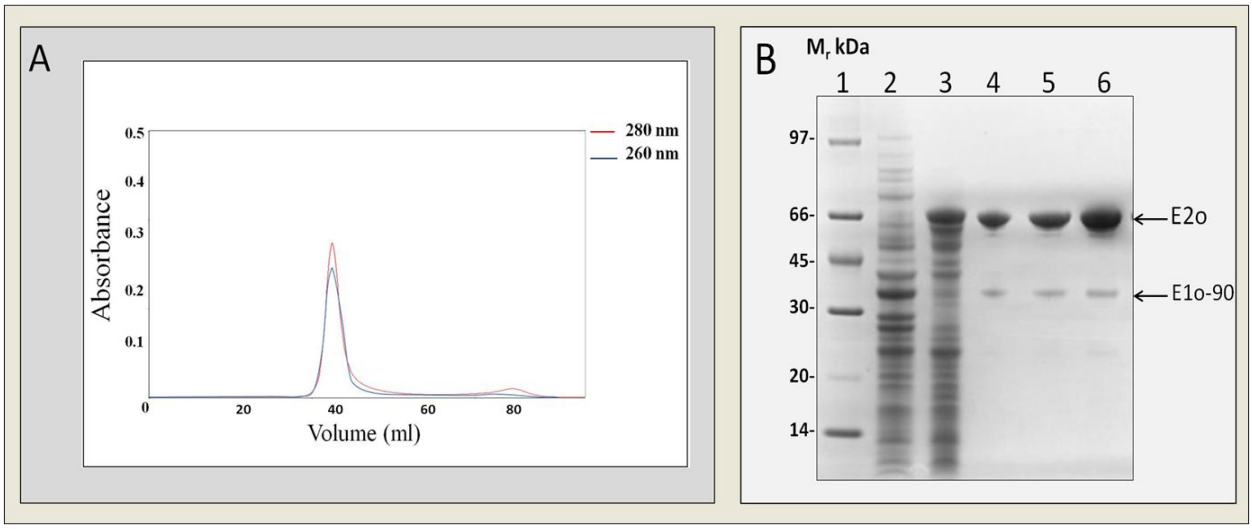


**Figure 5.11: Gel filtration of co-expressed E1o-90 GST and E2o in high salt**

Human N-terminal E1o-90 GST and E2o were co-expressed at 30 °C for 4 h. The soluble supernatant was purified by metal chelate chromatography. The purified protein peak was pooled and dialysed overnight against high salt GFC buffer (500mM NaCl, 2mM EDTA, 50mM $KH_2PO_4$, pH 7.4,). The purified protein (1ml) was gel filtered through a Sephacryl HiPrep 16/60 Sephacryl S-300 High Resolution column (GE Healthcare, UK) attached to a BioCAD 700E workstation (see section 2.4.4.5). The protein was eluted from the column using 1 CV GFC buffer (500mM NaCl, 2mM EDTA, 20mM $KH_2PO_4$, pH 7.4). (A) Gel filtration profile of co-expressed E1o-90 GST and E2o. A single elution peak was observed. E1o-90GST/E2o sub-complex being eluted at or near the void volume (~ 40ml). Absorbance of eluted proteins was measured at 280 nm (red line) and possible DNA/RNA contamination was monitored at 260 nm (blue line). (B) SDS-PAGE (10%) analysis of eluted protein peak stained with Coomassie Brilliant Blue. Lane 1, molecular mass markers; lane 2, over-expression of E1o-90 GST as control; lane 3, over-expression of E2o as control; lanes 4-6, E1o/E2o sub-complex corresponding to the single GFC peak. The presence of E1o-90 GST and E2o at high salt concentration (500mM NaCl) indicates formation of a stable and high $M_r$ E1o/E2o sub-complex.

### 5.2.4 Investigation of a direct interaction between the E1o-90 GST/E2o sub-complex and E3

This section provides a plausible approach to generating a recombinant model of OGDC highlighting the central role of the E1o N-terminal region in the integration process. However, active, recombinant, full-length mammalian E1o has not been produced to date. In this section, the co-integrated E1o-90 GST/E2o sub-complex was tested for its ability to form a stable high $M_r$ complex with E3 as judged by GFC.

Co-integrated E1o-90 GST/E2o sub-complex was assembled in *E. coli* (DE3) pLysS cells at 30 ºC for 5 h. Simultaneously, E3 was expressed in *E. coli* (DE3) pLysS cells at 30 ºC for 3 h. After expression, bacterial pellets were disrupted by French press treatment and individual E1o-90 GST/E2o sub-complex and E3 components purified using zinc chelate chromatography. Purified proteins were dialysed overnight at 4 $^{o}$C against 20mM NaCl, 20mM potassium phosphate, pH 7.5. E1o-90 GST/E2o sub-complex and E3 were mixed in a 1:2 (molar ratio) and passed through a HiPrep 16/60 Sephacryl S-300 high resolution column attached to a BioCAD 700E workstation. Two separate peaks of eluted protein were observed. The E1o-90 GST/E2o sub-complex was eluted at or near the void volume (~ 38 ml), while, free E3 homodimer was eluted at ~ 60 ml (Fig. 5.12A) consistent with its $M_r$ of 105,000 Da. On SDS-PAGE analysis of the individual peaks (Fig. 5.12B), it was found that the first peak eluting at or near the void volume contained primarily E1o-90 GST/E2o sub-complex whereas the second peak contained E3. It was difficult to detect the presence of E3 in the E1o-90 GST/E2o sub-complex by Coomassie Brilliant Blue staining as the recombinant version has a similar subunit $M_r$ to E2o. However, the presence of E3 in the first peak was confirmed by Western blotting using

anti-E3 antibody (1 in 1000 dilution) (see section 2.4.7.3). The presence of a band of the predicted size for E3 in the first elution peak confirmed a post-translational interaction of E3 with the E1o/E2o sub-complex (Fig. 5.12C) in contrast to the previous lack of evidence for a direct E2o:E3 interaction (Fig. 5.1).

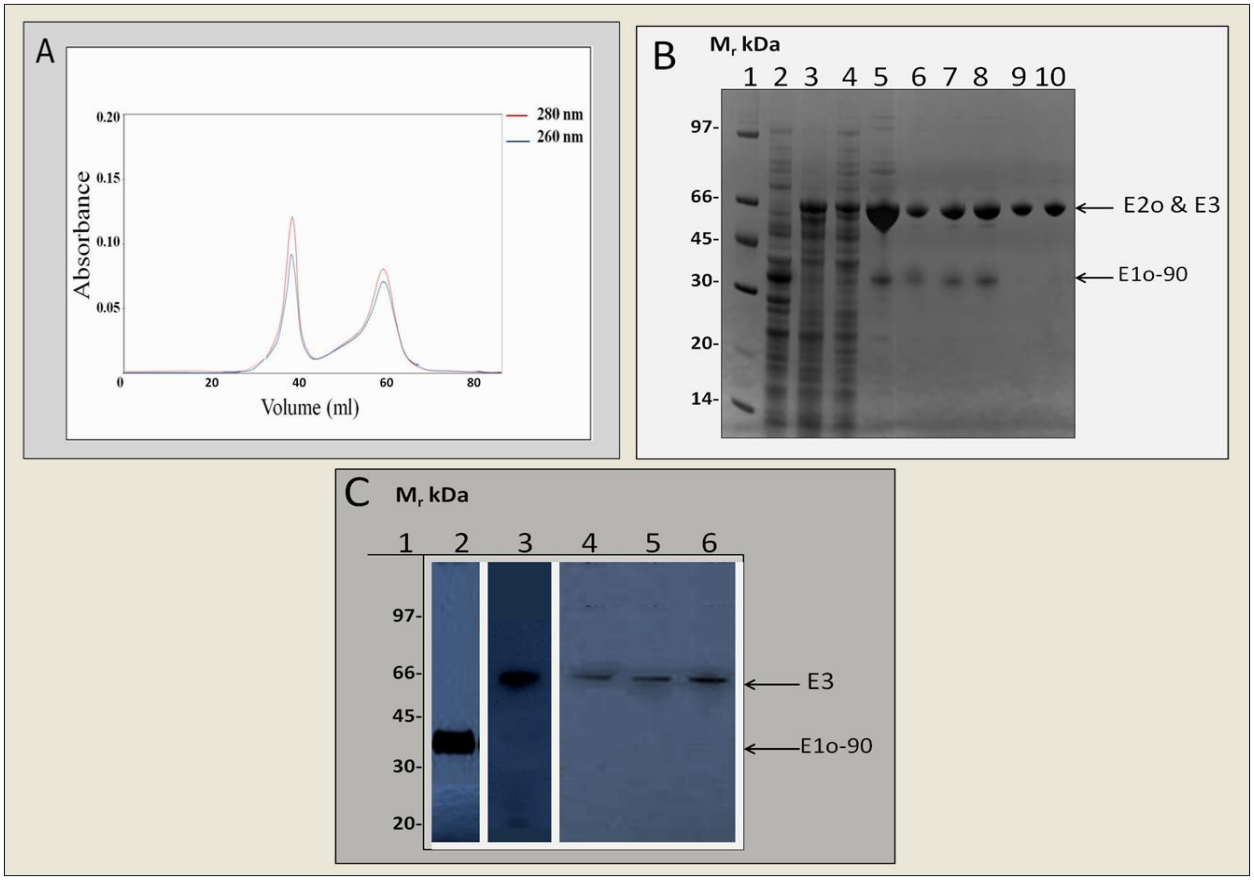


**Figure 5.12: Post-translational association of E3 with the E1o-90 GST/E2o sub-complex**
(A) Post-translational mixing of E1o-90 GST/E2o sub-complex and E3 followed by gel filtration on a HiPrep 16/60 Sephacryl S-300 high resolution column. E1o-90 GST: E2o sub-complex and E3 were mixed in a 1:2 molar ratio. Purified proteins were applied to the column in a 1ml aliquot. Proteins were eluted using 1 CV GFC buffer (20mM NaCl, 2mM EDTA, 20mM $KH_2PO_4$, pH 7.4). Two eluted peaks were observed, E1o-90 GST:E2o sub-complex being eluted at ~38 ml, while unbound E3 eluted at ~ 60 ml. Absorbance of eluted proteins was measured at 280 nm (red line) and possible DNA/RNA contamination was monitored at 260 nm (blue line). Peak fractions (1ml) were collected and analysed by SDS-PAGE and Western blotting. (B) SDS-PAGE (10%) analysis of eluted peaks stained with Coomassie Brilliant Blue. Lane 1, molecular mass markers; lane 2, over-expression of E1o-90 GST as control; lane 3, over-expression of E2o as control; lane 4; over-expression of E3 as control; lane 5, purified co-integrated E1o-90 GST/E2o sub-complex as control; lanes 6-8, first peak fractions showing E1o-90 GST/E2o sub-complex and lanes 9 & 10, second peak fractions showing E3. Owing to band E2o /E3 overlap when resolved by 10% SDS-PAGE, the presence of E3 in the first peak was confirmed by Western blotting. (C) Western blot analysis of eluted peaks. Lane 1, molecular mass markers; lane 2, purified E1o-90 GST as control; lane 3, purified E3 as control. The presence of E3 in first elution peak (E1o-90 GST/E2o sub-complex peak) was confirmed (lanes 4, 5 & 6) with anti-E3 antibody (1 in 1000 dilution) (see section 2.4.7.3).

## 5.3 Discussion

The general organisation of OGDC resembles that of its companion complexes PDC, and BCOADC, with 24 E2o subunits forming a central cubic core displaying octahedral symmetry in this instance. Mammalian E2o differs significantly from E2s of other complexes as it does not contain an analogous E3-binding and/or E1-binding domain as judged by cDNA sequence comparison. Hence, human E2o has a unique structure comprising only two domains, a single N-terminal lipoyl domain and a large C-terminal catalytic domain (CTD) that also mediates core self-assembly (Lawlis and Roche 1981).

The 60-meric mammalian E2-PDC central core houses an additional component termed E3-binding protein (E3BP), also referred to as protein X, that is responsible for high affinity E3 binding. A small discrete E1-SBD on E2p similarly directs the integration of the E1p heterotetramer. In prokaryotic OGDC, 12 copies of the E1o homodimer are reported to bind non-covalently to the E2o core while 6 copies of E3 interact with its six faces at maximal occupancy (Perham 2000). In mammalian PDC, the E2p/E3BP core binds 20-30 copies of E1p and 6-12 copies of E3 (Oliver and Reed 1982; Wagenknecht *et al.* 1990; Perham 2000; Vijayakrishnan *et al.* 2010).

The aim of this chapter was to investigate the ability of N-terminal region of human E1o to interact with E2o post-translationally or co-translationally. The evidence presented in this section strongly supports the idea that the human E1o N-terminal region is capable of co-integrating with E2o in a similar fashion to E3BP integration with E2p in PDC. In the case of E3BP, an E2-related polypeptide, is tightly integrated into the E2p core during assembly via its C-terminal

region where it supports the overall reaction of the complex by promoting the high affinity E3 binding (Hiromasa *et al.* 2004; Smolle *et al.* 2006).

In chapter 4 the role of the E1o N-terminal region in promoting E3 binding in a post-translation manner was confirmed by peptide array technology (Fig. 4.12 & 4.13), isothermal titration calorimetry (Fig. 4.15, 4.21 & 4.22) and direct biochemical binding studies using affinity chromatography (Fig. 4.20). In contrast, as shown in this chapter, the N-terminal region of E1o is incapable of interacting with E2o post-translationally (Fig. 5.3 & 5.4). In addition, binding studies between the recombinant E2o core and E3 using gel filtration and ITC showed that these two enzymes did not associate post-translationally (Fig. 5.1 & 5.2).

The mode of organisation and integration of the constituent enzymes of mammalian OGDC has been a matter of debate and speculation since sequence analyses of human E2o cDNA indicated the absence of any obvious E3 and/or E1o binding domain (Lawlis and Roche 1981; Bradford *et al.* 1987; Koike *et al.* 2000). Initially, selective proteolysis studies identified the N-terminal region of E1o to be important for maintaining the structural integrity of the complex. Immunological analysis has shown also that E1o has limited sequence and/or structural similarity with human E3BP as anti-E1o serum recognized antigenic epitopes on E3BP while anti-E3BP-specific serum was also able to recognize E1o (Rice *et al.* 1992; McCartney *et al.* 1998).

These observations and recent reports, demonstrating that E3BP forms integral part of the E2p core that can only be incorporated during its assembly suggest that E1o and its N-terminal region in particular, may play a similar pivotal role.

In this context, it has been established in this chapter that the N-terminal regions of human E1o (Ser1-Val90) and (Ser1-Phe153) can co-integrate with E2o and consequently form a stable sub-complex as shown in Figures 5.8, 5.9 and 5.10. These results were validated by Western blotting and gel filtration (Fig. 5.8C, 5.9C, 5.10B and 5.11). Moreover, co-integrated E1o/E2o complex was found to be stable at elevated salt concentrations as would be the case for the intact E1o/E2o core structure (Fig. 5.11). Importantly, the N-terminal E1o-60 (Ser11-Ala70) GST fusion failed to interact with E2o either post-translationally (see section 5.2.2.1) or co-translationally (Fig. 5.6) suggesting, either that the first 10 a.a. of the E1o N-terminus plays a central role in protein folding and integration or that steric hindrance prevents this short peptide from forming a complex with either E2o or E3. However, the N-terminal E1o-60 GST fragment can be considered as a reliable and effective negative control ruling out the possibility of non-specific binding. Additionally, free GST as further negative control also failed to interact with E2o supporting and confirming previous data.

In summary, our current findings provide the first direct evidence that the N-terminal region of human E1o has a dual role in coordinating OGDC assembly and organisation, namely mediating the co-translationally directed integration of E1o and E2o while also being responsible for the post-translational tethering of E3. These data are also consistent with earlier studies in mammalian OGDC suggesting that E1o binds more tightly to the E2o core than its E3 counterpart and can only be released under denaturing conditions (Reed and Hackert 1990). Additionally, and in agreement with our data, previous cryo-electron microscopy of *E. coli* OGDC has demonstrated that the linker gap in E2o-E3 sub-complexes was more apparent than

in E2o-E1o sub-complexes suggesting that the bridge between the E2o-E1o sub-complexes contains more mass than the E2o-E3 bridges (Wagenknecht *et al.* 1990).

A functional recombinant version of human OGDC has not yet been produced, largely owing to difficulties in generating active, recombinant full-length E1o. In this study, mature human E1o was successfully cloned and over-expressed in *E. coli* although it failed to produce soluble recombinant protein (see sections 3.3.1.4 & 3.3.2.4). As an alternative, in this chapter, the potential for post-translation interaction between an N-terminal E1o/E2o sub-complex and E3 was assessed using gel filtration. The E1o-90 GST/E2o sub-complex purified either by metal chelate or glutathione affinity chromatography (Fig. 5.8 & 5.9) was mixed in a 1:2 stoichiometry with E3. On gel filtration it was possible to detect complex formation between E1o-90 GST/E2o and E3 (Fig. 5.12). Unfortunately, only a small amount (1-2mg) of E1o-90 GST/E2 sub-complex could be generated by this approach, making it difficult to conduct ITC analysis of this interaction.

Further experiments will be necessary to substantiate these results. In particular, it will be of great interest to produce soluble, recombinant full-length E1o. One possibility would be to use a low level *E. coli* expression system such as the pQE-9 vector and *E. coli* M15 strain that has proved successful in the production of $\alpha_2$ $\beta_2$ heterotetrameric E1p (Korotchkina *et al.* 1995; Singh 2008). Moreover, further experiments using biophysical techniques including AUC, SAXS, and SANS are required to obtain more conclusive structural data on the morphology, organisation and stoichiometry of the E1o/E2o sub-complex including the possibility that it could partially replace E2o within the native core assembly.

## 5.4 Summary

This chapter has focused on investigating potential interactions between the N-terminal region of human E1o and E2, both post-translationally and co-translationally. The data presented in this chapter can be summarized as follows:

- The N-terminal region of human E1o failed to interact with the E2o post-translationally as monitored by gel filtration or affinity chromatography.

- E2o and E3 do not associate post-translationally.

- The N-terminal region of human E1o has the ability to co-integrate with E2o forming a stable complex.

- The E1o N-terminus is pivotal for mediating formation of a stable OGDC multienzyme assembly by directing self-integration with the E2o core and subsequently promoting high affinity E3 binding.

# Chapter 6

# Inhibition of OGDC and PDC activity using N-terminal E1o constructs

## 6.1 Introduction

Most pioneering studies of the 2-oxoacid dehydrogenase complexes have relied on native complexes derived from natural sources to investigate their structure, organisation and intrinsic properties. For example, OGDC has been purified to homogeneity from *E. coli* (Pettit *et al.* 1973), bovine heart (Stanley and Perham 1980), bovine kidney (Reed and Oliver 1968) and pig heart (Koike and Koike 1976) while PDC has also been isolated from many sources e.g. *E. coli* (Danson *et al.* 1979), *B. stearothermophilus* (Henderson and Perham 1980), pig liver (Roche and Cate 1977), bovine kidney (Linn *et al.* 1972) and bovine heart (Stanley and Perham 1980).

The complex-specific E2 components of 2-oxoacid dehydrogenase complexes form a large oligomeric core comprising 60 or 24 E2 copies assembled via their C-terminal domains and arranged with icosahedral or octahedral symmetry to which the E1 and E3 components are bound tightly but non-covalently. The N-terminus of E2 consists of one to three homologous lipoyl domains (each of about 80 a.a.s) according to the type of the complex and source of the organism. These are joined in tandem array by extended linker sequences (~ 20-30 a.a.s) rich in alanine and proline.

These domains are followed by a SBD about 50 amino acids in length (mammalian OGDC has no obvious SBD). The primary purpose of the SBD is to tether E1 or E3 to the E2 core and is linked in turn to a large C-terminal catalytic domain (Bradford *et al.* 1987; Packman and Perham 1987; Wagenknecht *et al.* 1990; Nakano *et al.* 1994). Mammalian PDC requires a fourth protein, dihydrolipoamide dehydrogenase-binding protein (E3BP), which is tightly associated with the E2p core. The E2p core binds 12 copies of E3BP (Sanderson *et al.* 1996a; Vijayakrishnan *et al.* 2010). Extensive characterization of E3BP has revealed close structural, functional and organizational similarities to E2p. It is composed of three domains (LD, SBD and CTD). However, E3BP contains a single lipoyl domain and is exclusively involved in mediating the stable integration of the E3 enzyme. Its C-terminal region promotes binding to the oligomeric E2p core and has no obvious enzymatic activity (Rahmatullah *et al.* 1989).

To confirm the functional importance of the N-terminal region of E1o of OGDC in securing E3 in particular, a series of E1o N-terminal constructs were tested for their ability to inhibit OGDC/PDC activity as it was predicted that they should selectively displace complex-bound E3. Initially, the effect of NaCl concentration on overall complex activity was also monitored as increasing ionic strength is well established to promote E3 dissociation in the range 0-0.5 M. These salt concentrations have only minimal effects on the individual constituent enzymes (J G. Lindsay, personal communication).

# 6.2 Results and analysis

## *6.2.1 Purification of OGDC and PDC from bovine heart*

OGDC and PDC were purified from bovine heart tissue by selective polyethylene glycol (PEG-6000) precipitation essentially as described by Stanley and Perham (Stanley and Perham 1980) with some modifications (De Marcucci and Lindsay 1985a). The final Sepharose CL-2B gel filtration step was omitted so OGDC and PDC preparations were 80-90% pure at this stage with a small amount of cross-contamination.

OGDC and PDC activity assays were conducted by monitoring NADH production at 340 nm as described in section 2.4.6.4. The subunit profiles of OGDC and PDC can be visualised using SDS-PAGE as shown in Figure 6.1. OGDC displays the expected subunit profile with $M_r$ values 110 kDa, 54 kDa and 49 kDa corresponding to E1o, E2o and E3 respectively. In addition, faint bands corresponding to PDC E1α and E1β subunits are apparent confirming minor contamination with PDC. Purified PDC also had the anticipated five subunit profile as follows: E2p, 74 kDa; E3, 54 kDa; E1α, 42 kDa; and E1β, 38 kDa plus E3BP at ~ 52 kDa.

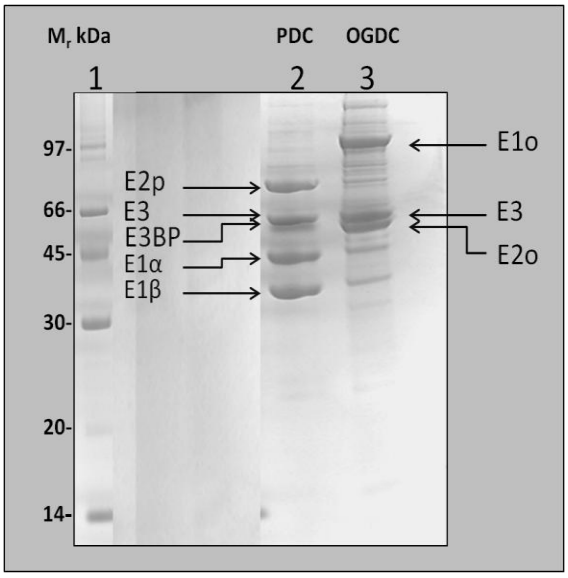


**Figure 6.1: SDS-PAGE of purified bovine OGDC and PDC**
SDS-PAGE (10%) analysis of purified OGDC and PDC. Samples were stained with Coomassie Brilliant Blue. Lane 1, molecular mass markers; lane 2, purified bovine PDC, five major bands are visible which correspond to subunits E2p, E3, E3BP, E1α and E1β; lane 3, purified bovine OGDC. E1o, E2o and E3 are visualised.

## *6.2.2 Effect of NaCl on OGDC/PDC activity*

In both OGDC and PDC, E1 binds tightly to the core primarily via hydrophobic forces whereas E3 is more loosely-associated via hydrophilic interactions. The aim of this section was to investigate the effect of high ionic strength on OGDC/PDC activity using increasing NaCl concentrations to determine the ease of E3 displacement from the core assemblies.

Purified bovine OGDC (see section 6.2.1) was added to incubations that contained solutions A and B, pH 7.8 (see Materials and Methods, section 2.4.6.4) and NaCl at concentrations from 0-1M. Incubations were maintained at 30 $^{o}$C for 3 min. At the end of 3 min, substrate (solution C) was added to the assay cuvette and NADH production measured at 340 nm. Enzyme

activity was measured over the linear part of each curve (Fig. 6.2). In the same manner, bovine PDC (see section 6.2.1) was incubated at 30°C in solutions A and B containing NaCl in the concentration range from 0 - 1.0 M for 3 min prior to initiation of the assay with substrate (solution C). PDC activity was measured at 340nm (Fig. 6.2). Assays were carried out in triplicate. Increasing NaCl levels resulted in a parallel decline in OGDC and PDC activity with 0.5M NaCl causing 85-95% inhibition in both cases (Fig. 6.2).

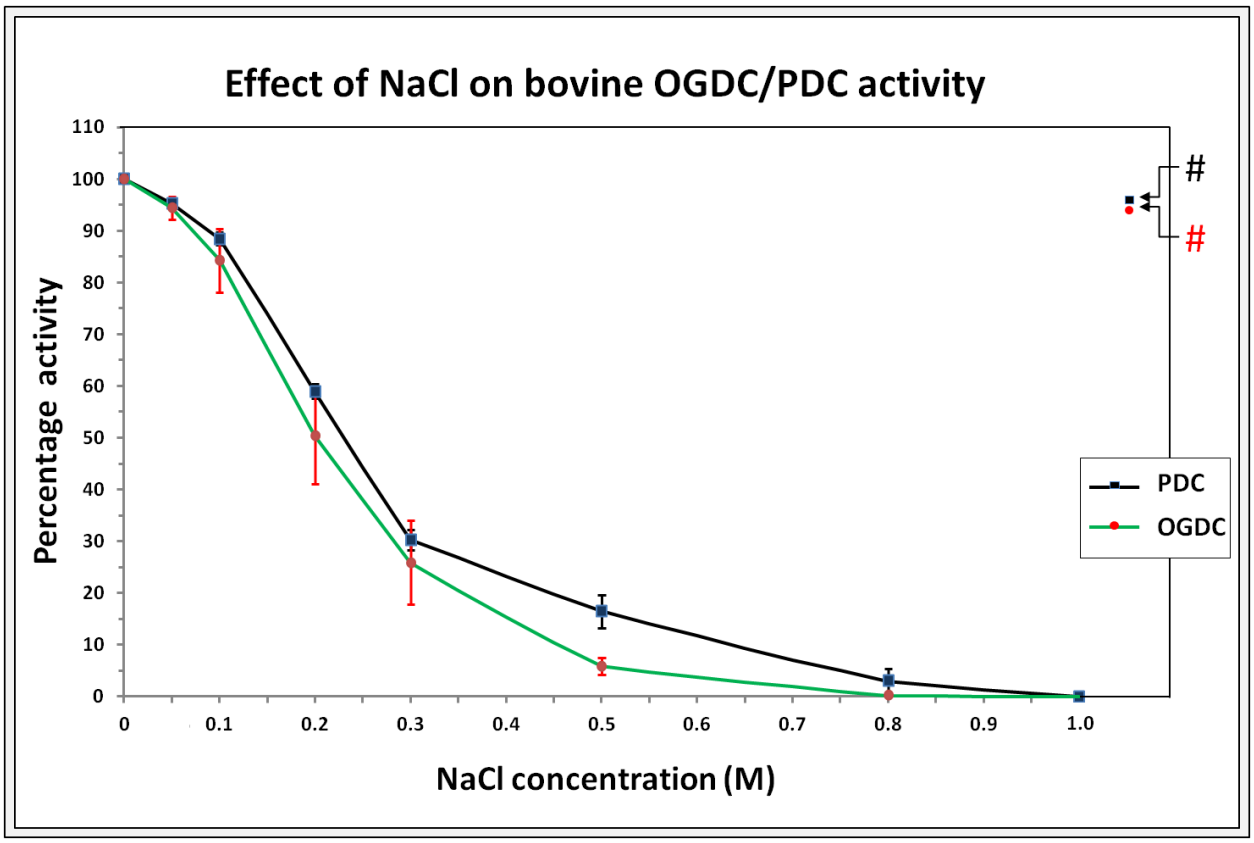


**Figure 6.2: Effect of NaCl on bovine OGDC/PDC activity**
Bovine OGDC and PDC were diluted in potassium phosphate buffer (KPi buffer) containing solution A & B, pH 7.8 (see Materials and Methods section 2.4.6.4) and varying concentrations of NaCl at 30 °C for 3 min prior to initiation of the assays with substrate (solution C). Samples at each NaCl concentration were assayed for OGDC/PDC activity. All values shown represent the mean of triplicate assays. The loss of activity with increasing NaCl concentration was plotted as the % OGDC activity (dark green line) or % PDC activity (black line) in the absence of NaCl. Single samples of OGDC (#) and PDC (#), pre-treated with 1.0 M NaCl were also diluted to reduce the NaCl concentration to ≤ 30mM prior to assay to check for reversibility.

The decline in OGDC and PDC activity at increasing NaCl concentrations is the result of E3 dissociation from the native OGDC and PDC assemblies. In agreement with this idea, loss of OGDC and PDC activity after incubation in 1.0 M NaCl was completely reversible. Ionic strength is known to have minimal effects on the activities of the individual constituent enzymes in the range 0 - 0.5 M NaCl.

### 6.2.3 Inhibition study of OGDC/PDC activity using N-terminal E1o fragments

To investigate the effect of adding increasing amounts of N-terminal E1o GST constructs as potential inhibitors of OGDC and PDC activity, both complexes and N-terminal E1o (E1o-60, E1o-90 and E1o-153) GST fusion proteins were dialysed overnight against 50mM KPi buffer ($KH_2PO_4/K_2HPO_4$), pH 7.4 (see section 2.4.5).

E1o-60 (Ser11-Ala70), E1o-90 (Ser1-Val90) and E1o-153 (Ser1-Phe153) GST fusion proteins at concentrations of 91μM and 182μM, 84μM and 167μM and 89μM and 178μM, respectively, were incubated with 10μg OGDC or 10μg PDC at 30°C for 5 min. The activities of OGDC and PDC were determined as described in Materials and Methods, section 2.4.6.4.

Addition of the E1o-60 GST constructs produced negligible inhibitory effects (5-10%) on OGDC activity. In contrast, significant inhibition (50-70%) was observed with the E1o-90 GST constructs while wild-type GST had little or no effect (Fig. 6.3).

Surprisingly, addition of the E1o-153 GST constructs induced only minor inhibition (~20-30%) compared to the wild-type GST control. The low levels of inhibition observed with E1o-153 GST (Ser1-Phe153) may relate to its ease of degradation or state of aggregation as discussed previously (see section 3.3.3.2).

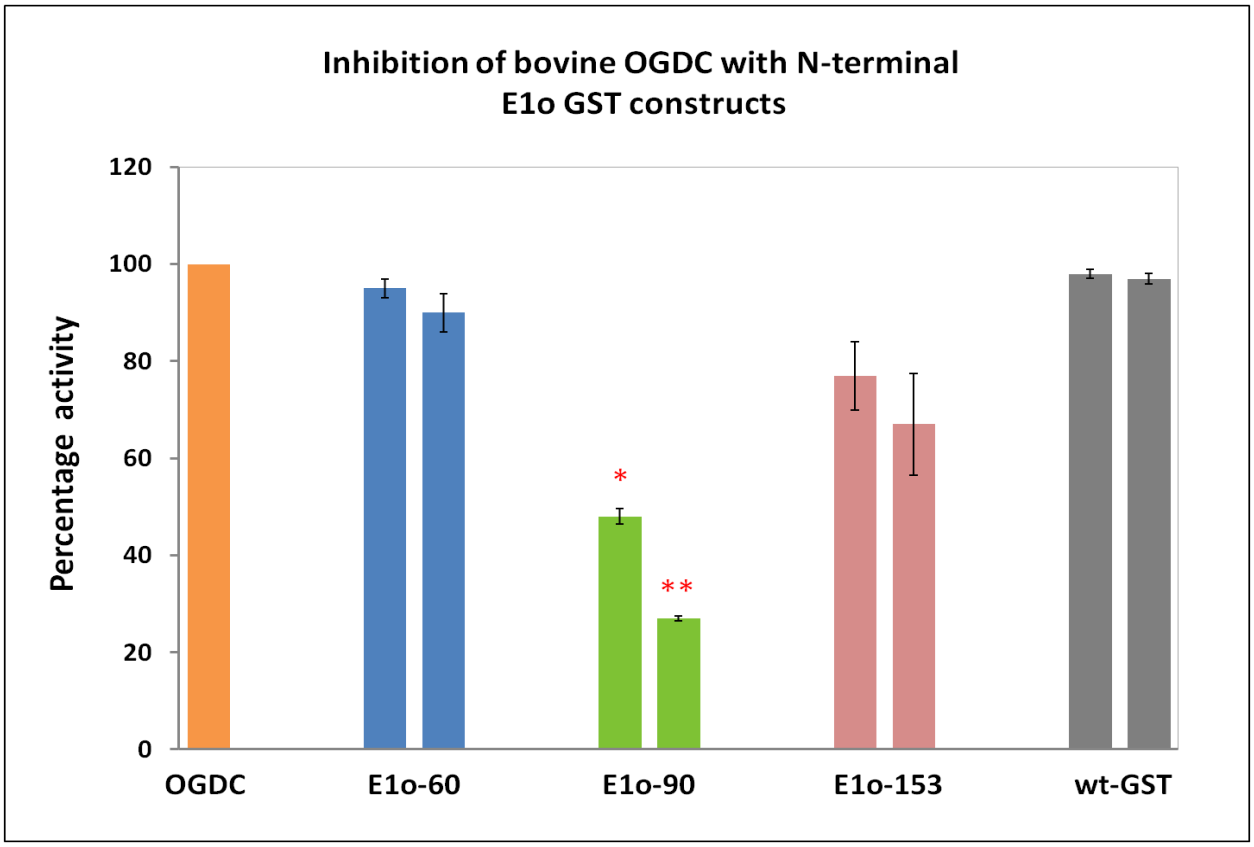


**Figure 6.3: Inhibition of bovine OGDC activity using N-terminal E1o constructs**
Histogram shows activity of bovine OGDC with the following: E1o-60 GST, 91µM and182µM, (blue bars). E1o-90 GST, 84µM and 167µM, (green bars). E1o-153 GST, 89µM and 178µM, (pink bars). The gray bars represent wild-type GST as control (110µM and 222µM). The orange bar represents OGDC as 100% activity (control). Samples were assayed in triplicate and error bars indicate extent of variation between triplicates. * $P < 0.05$ versus wt-GST (110 µM). ** $P < 0.001$ versus wt-GST (222 µM).

In the same manner, bovine PDC treated with N-terminal E1o GST constructs (E1o-60 and E1o-153) retained 80-95% of wild-type GST control activity (Fig. 6.4). Significant inhibition (20-35%) was observed with the E1o-90 GST constructs compared to the wild-type GST control.

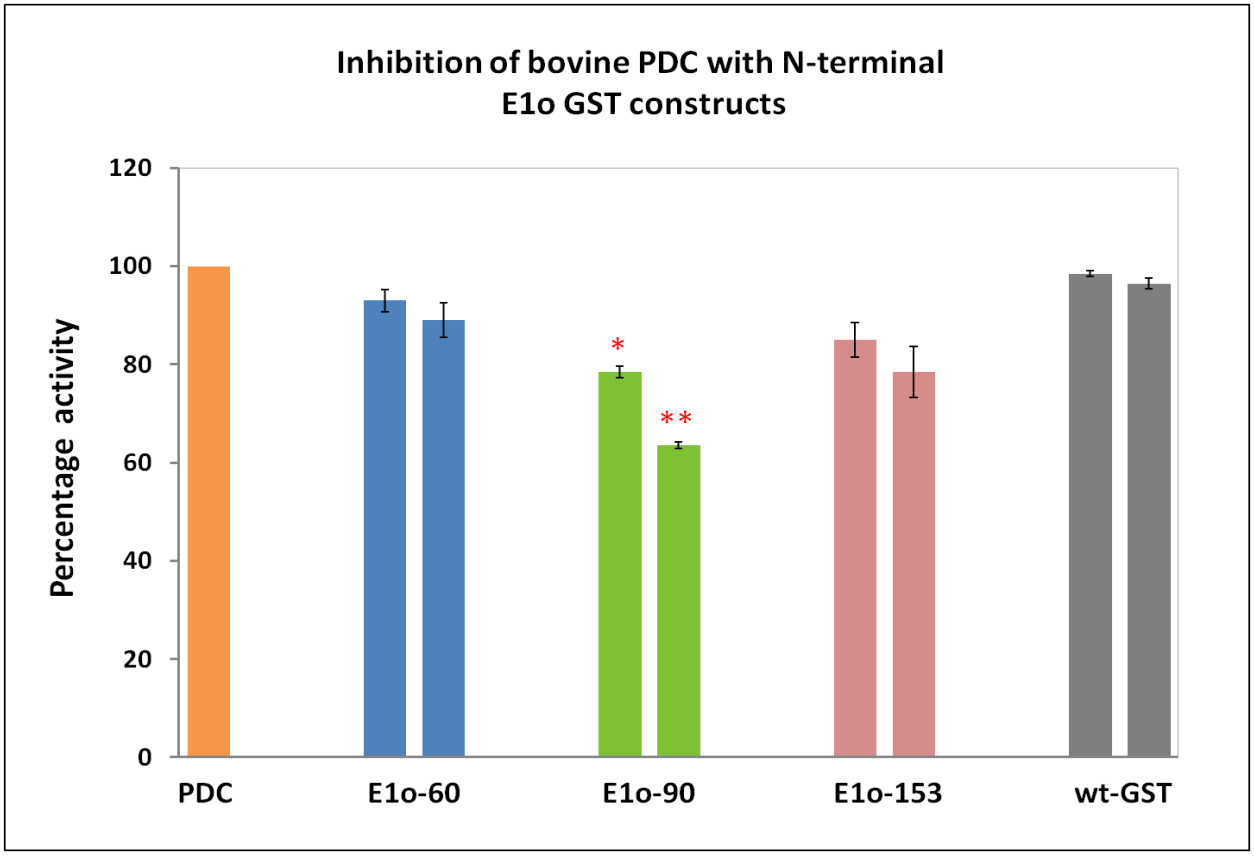


**Figure 6.4: Inhibition of bovine PDC activity using N-terminal E1o constructs**
Histogram shows activity of bovine PDC with the following: E1o- 60 GST, 91µM and 182µM, (blue bars). E1o-90 GST, 84µM and 167µM, (green bars). E1o-153 GST, 89µM and 178µM, (pink bars). The gray bars represent wild-type GST as control (110µM and 222µM). The orange bar represents PDC as 100% activity (control). Samples were assayed in triplicate and error bars indicate extent of variation between triplicates. * $P < 0.05$ versus wt-GST (110 µM). ** $P < 0.005$ versus wt-GST (222 µM).

Previous chapters (chapter 4 & 5) have shown that the E1o N-terminal region is important for maintaining the structural integrity of the OGDC. An interaction study on intact OGDC/PDC using N-terminal E1o fragments (60, 90 & 153 a.a.s.) as potential inhibitors has shown that overall OGDC activity significantly decreased by adding N-terminal E1o-90 (Ser1-Val90), presumably due to displacement of the E3 enzyme as consequence of binding between N-terminal E1o-90 and E3. Interestingly, the N-terminal E1o-90 fragment induced less inhibition of PDC activity suggesting that either the mode of E3 interaction with OGDC is distinct from its mechanism of binding to PDC or that E3 is more tightly associated with PDC.

### *6.2.4 Inhibition study of PDC/OGDC activity using E3BP-SBD*

The aim of this section was to investigate the inhibitory effects of the E3BP-SBD on the PDC/OGDC activity, and to determine if the E3BP-SBD had a selective inhibitory effect on PDC activity. E3BP-SBD (GST fusion protein) was over-expressed and purified as described in section 6.2.4.1.

#### 6.2.4.1 E3BP-SBD over-expression and purification

A human E3BP-SBD construct housed in pGEX-2T was already available in the laboratory (Smolle *et al.* 2006). The SBD of human E3BP comprised 65 residues (166-230 a.a. of E3BP). The plasmid was transformed into *E.coli* BL21 (DE3) pLysS. Over-expression was successfully

carried out at 30°C for 4 h and induced by the addition of 1mM IPTG as described in Materials and Methods, section 2.4.1.

SDS-PAGE analysis of samples taken at the time of induction and after 4 h demonstrated the presence of over-expressed E3BP-SBD. A major band at approx. 35 kDa was observed corresponding to the predicted $M_r$ value of the E3BP-SBD GST fusion protein (Fig. 6.5). The solubility of the expressed protein was analysed by the standard protocol (section 2.4.2) and resolved by SDS-PAGE indicating the E3BP-SBD was present in the soluble fraction (data not shown).

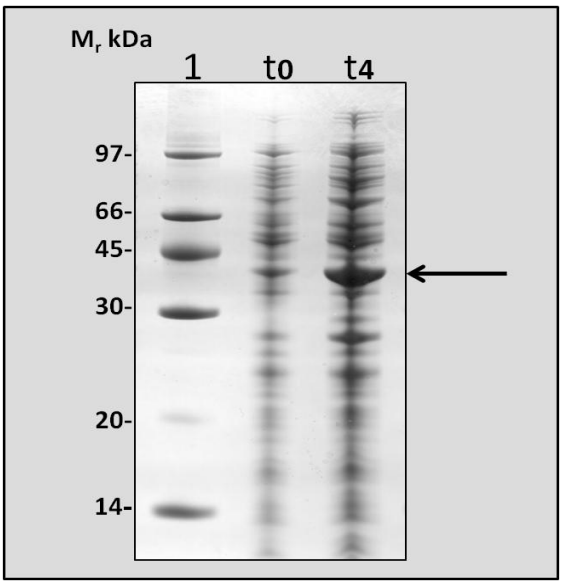


**Figure 6.5: Over-expression of human E3BP-SBD (GST fusion protein)**
E3BP-SBD was expressed over 4 h at 30°C in *E. coli* BL21 (DE3) pLysS. Cells were grown in LB media. Samples were taken at the time of induction (t0) and after 4 h (t4) and denatured in the presence of 150mM DTT at 100°C for 5min prior to resolution on a 10% SDS/polyacrylamide gel. Protein bands were visualised with Coomassie Brilliant Blue. Lane 1, molecular mass markers. The arrow on the right of the gel indicates over-expressed protein.

Purification of GST-tagged N-terminal E3BP-SBD required only a single purification step using a glutathione Sepharose 4B column (bed volume, 5ml). Figure 6.6 shows successful purification of E3BP-SBD producing high yields of pure protein (approx. 20-30 mg/l of culture).

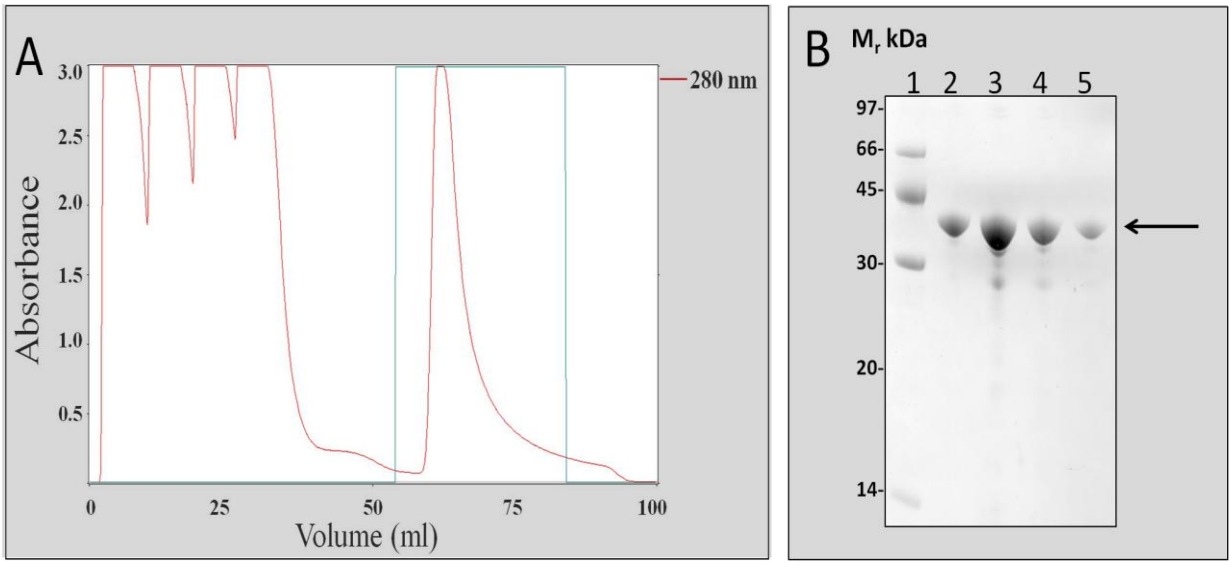


**Figure 6.6: Purification of E3BP-SBD (GST fusion protein)**
(A) Glutathione affinity chromatography of E3BP-SBD. Cell lysates (20ml) were applied to the column in 5ml aliquots (see section 2.4.4). Bound protein was eluted from the column using 5 CV elution buffer (20mM reduced glutathione, 50mM Tris-HCl, pH 8.0). The reduced glutathione buffer step used for elution is shown in green. Absorbance of eluted protein was measured at 280 nm (red line). Peak fractions (2ml) were collected and analysed by SDS-PAGE. (B) SDS-PAGE analysis of eluted protein fractions. Lane 1, molecular mass markers; lanes 2-5, purified E3BP-SBD elution fractions stained with Coomassie Brilliant Blue. The arrow on the right of the blot indicates purified protein.

### 6.2.4.2 Inhibitory effects of E3BP-SBD on PDC/OGDC activity

To investigate the effect of adding increasing amounts of E3BP-SBD (GST fusion protein) on PDC/OGDC activity, both complexes and E3BP-SBD were dialysed overnight against 50mM KPi buffer ($KH_2PO_4/K_2HPO_4$), pH 7.4 (see section 2.4.5). E3BP-SBD (GST fusion protein) at a concentrations of 124µM and 213µM were pre-incubated with 10µg PDC or 10µg OGDC at 30°C for 5 min. Enzymatic activity of PDC/OGDC was determined as described in Materials and Methods, section 2.4.6.4. Addition of the E3BP-SBD GST constructs induced a significant inhibitory effect (60-80%) on PDC activity compared to the control (120µM and 230µM, wild-type GST) that had little or no effect (Fig. 6.7).

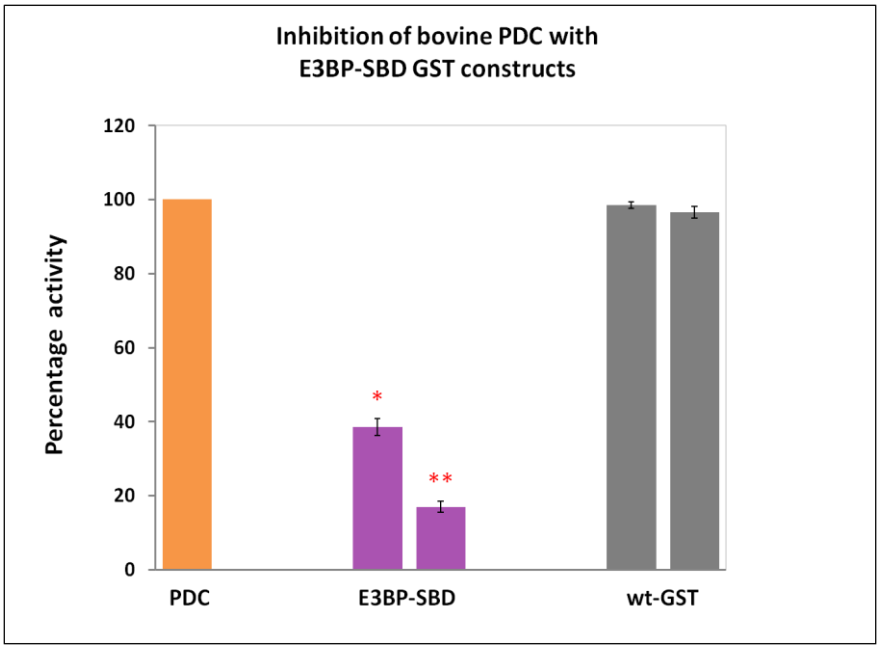


**Figure 6.7: Inhibition of bovine PDC activity using E3BP-SBD construct**
Histogram shows activity of bovine PDC with the following: E3BP-SBD (124µM and 213µM) purple bars. The gray bars represent wild-type GST as control (120µM and 230µM). The orange bar represents PDC as 100% activity (control). Samples were assayed in triplicate and error bars indicate extent of variation between triplicates. * $P < 0.05$ versus wt-GST (120 µM). ** $P < 0.01$ versus wt-GST (230 µM).

In the same manner, bovine OGDC incubated with the E3BP-SBD GST construct at concentrations of 124µM and 213µM retained 40-60% of control activity (Fig. 6.8).

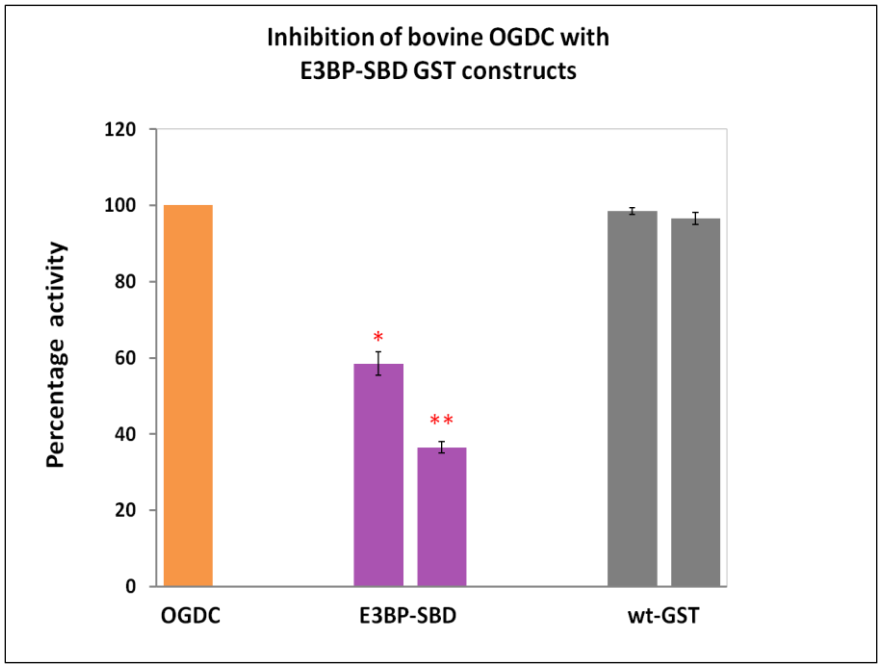


**Figure 6.8: Inhibition of bovine OGDC activity using E3BP-SBD construct**
Histogram shows activity of bovine OGDC with the following: E3BP-SBD (124µM and 213µM) purple bars. The gray bars represent wild-type GST as control (120µM and 230µM). The orange bar represents OGDC as 100% activity (control). Samples were assayed in triplicate and error bars indicate extent of variation between triplicates. * $P < 0.05$ versus wt-GST (120 µM). ** $P < 0.01$ versus wt-GST (230 µM).

These interaction studies on PDC/OGDC activity using E3BP-SBD as competitive inhibitors has shown that overall PDC activity was significantly decreased by adding excess E3BP-SBD, presumably due to displacement of the E3 enzyme as a consequence of specific binding occurring between free E3BP-SBD and E3. Interestingly, in this case, E3BP-SBD showed less inhibitory effect on OGDC than PDC suggesting that the mode of E3 interaction with PDC is distinct from its mode of binding to OGDC.

## 6.3 Discussion

The aim of this chapter was to test the hypothesis that N-terminal E1o constructs and E3BP-SBD could act as inhibitors of OGDC/PDC activity and to determine if they have a selective inhibitory action. In addition, the effect of NaCl on bovine OGDC/PDC activity was investigated as high ionic strength is well established to promote specific E3 dissociation leading to complex inactivation.

Treatment of bovine OGDC/PDC with NaCl in the range 0-1.0 M led to a gradual loss of activity that could be recovered by diluting out the salt as anticipated (Fig. 6.2). Approx. 85-95% inhibition was achieved with 0.5M NaCl for both complexes i.e. in the range required to promote E3 dissociation. These data are in agreement with our previous peptide array studies (Fig. 4.14) indicating that E3 binding is markedly reduced at elevated (300-500mM) NaCl levels. It is also apparent that the effects of NaCl treatment on bovine OGDC and PDC activity are readily reversible suggesting that E3 can re-attach to the core assembly in a kinetically-competent fashion.

Previous chapters (chapter 4 & 5) have shown that N-terminal region of E1o was important for maintaining the structural integrity of the OGDC. Here, the functional significance of its interaction with E3 was explored by using a series of N-terminal E1o fragments and E3BP-SBD, all produced as GST fusion proteins to act as competitive inhibitors of E3 binding to intact OGDC and PDC. Maximal inhibition of OGDC (50-70%) was achieved with the E1o-90 constructs (Ser1-Val90) whereas the E1o-60 fragment (Ser11-Ala70) was non-inhibitory (Fig. 6.3) in agreement with its previously observed inability to interact with E3 (see sections,

4.2.3.3 & 4.2.3.4). The longer E1o-153 fragment (Ser1-Phe153) produced only minor inhibition (Fig. 6.3) although it may bind to E3 with higher affinity as judged by ITC (Fig. 4.22). However, as discussed previously, this extended segment is highly susceptible to aggregation/proteolysis. Thus, the minimal inhibition observed may relate to the fact that intact monomeric E1o-153 (Ser1-Phe153) represents only a small percentage of the total population. A similar inhibition profile was observed with PDC although the E1o-90 construct was markedly less effective in this case indicating a degree of selectivity in the inhibition (Fig. 6.4).

A parallel study employing E3BP-SBD GST as a competitive inhibitor of E3 binding revealed that it could induce 40-60% and 60-80% inhibition of OGDC and PDC, respectively (Fig. 6.7 & 6.8) over a similar concentration range to those employed with the E1o N-terminal constructs. In this case, the E3BP-SBD displayed a small selective inhibitory effect on PDC again suggesting differences in the mode of E3 binding between OGDC and PDC.

In all cases, controls were performed with recombinant GST present at similar concentrations. No inhibitory effects were observed demonstrating that no non-specific inhibition was occurring owing the presence of high protein concentrations.

## 6.4 Summary

In this chapter, N-terminal E1o fragments and the E3BP-SBD were studied as potential inhibitors of native bovine OGDC/PDC activity. The effect of increasing ionic strength on bovine OGDC/PDC activity was also investigated. All treatments were expected to displace the E3 enzyme from its normal binding site on the relevant core assemblies. The data presented in this chapter can be summarized as follows:

- Increasing NaCl concentrations had a parallel inhibitory effect on both OGDC and PDC with 85-95% inhibition occurring by 0.5 M NaCl. The effect of NaCl treatment on OGDC/PDC activity was readily reversible.

- N-terminal E1o constructs had a preferential inhibitory effect on bovine OGDC as compared to PDC presumably via displacement of E3 from its normal binding site on the intact complex. These results confirmed the predicted functional role for the N-terminal E1o segment in mediating E3 binding.

- Conversely, the E3BP-SBD was slightly more effective at inhibiting PDC than OGDC suggesting that the mode of E3 binding differed significantly between the two complexes.

# Chapter 7

# General conclusions

The family of 2-oxoacid dehydrogenase complexes are multi-enzyme arrays composed of multiple protein subunits that assemble non-covalently in a highly-ordered fashion. Moreover, OGDC, PDC and BCOADC all have multiple copies of three separate enzymes: E1, E2 and E3. The E3 enzyme is common to PDC, OGDC and BCOADC. In addition, mammalian PDC has a fourth E2-related subunit termed E3BP that can partially replace E2.

Each of these complexes has a distinctive overall general morphology dictated by the presence of a 24-meric cubic or 60-meric icosahedral E2 core. In mammalian PDC, E1p binds to the E2p core via a specific SBD located on E2p, while E3BP mediates E3 binding to the core via a similar SBD. In mammalian BCOADC, both E1b and E3 are tethering to the E2b core by a single E2b-SBD. Mammalian OGDC differs in its overall design as E2o does not appear to provide the central scaffold responsible for E1o and E3 docking as it does not contain any an E3- or E1-SBD.

The principal area of research in this project related to defining the interactions between the human OGDC enzymes (E1o, E2o and E3) in order to understand complex organisation and mode of assembly. Our evidence implicates a pivotal role for the N-terminal region of E1o that is required for both co-translational integration with E2o and subsequent post-translational E3 binding, leading to formation of a stable complex.

Initial research was directed towards the cloning and expression of 9 short recombinant N-terminal human E1o constructs in various forms (His-tag, MBP and GST fusion proteins) and cloning/expression of mature human E1o in an *E. coli* BL21 host system. In addition, both His-tagged E2o and E3 were over-expressed and purified as described in chapter 3. The ability to purify large amounts of pure protein, in particular GST fusion proteins, enabled us to test the ability of this region to interact with E2o and E3 using a variety of biochemical and biophysical techniques. Unfortunately, although full-length E1o was successfully cloned and over-expressed in *E. coli*, it failed to produce soluble recombinant protein.

Detailed structural characterisation and a basic bio-informatics approach employing a diverse range of biochemical and biophysical techniques was conducted on the human E1o N-terminal region (chapter 4). These studies demonstrated that two short segments of the N-terminal region of human E1o have the ability to form α-helices whereas the majority of the N-terminal region is predicted to be highly dynamic and disordered. Interestingly, the N-terminal region of E1o showed a degree of structural similarity to E3BP-SBD as judged using the structural alignment software (TM-align). Both domains contain two parallel α-helices and two irregular loops as the most prominent structural features.

TM-align (Zhang and Skolnick 2005) is a structural alignment software program for identifying the best structural alignment between two proteins. Template modeling score or TM-score is a measure of similarity between two protein structures with different tertiary structures. Typically, TM-scores are scaled in the range (0 - 1) where values less than 0.2 indicates that there is no similarity between two structures and values more than 0.5

reflect the structures share the same fold. Figure 7.1 shows structural alignment of human N-terminal region of E1o (Ser1-Gln77) and crystal structure of human E3BP-SBD (Brautigam *et al.* 2006) that has been analysed by TM-align. The N-terminal E1o-77 and E3BP-SBD were provided in pdb format to http://zhanglab.ccmb.med.umich.edu/TM-align/, resulting in a TM-score of 0.44 suggesting that the both proteins share the same fold over 43 residues in aligned length.

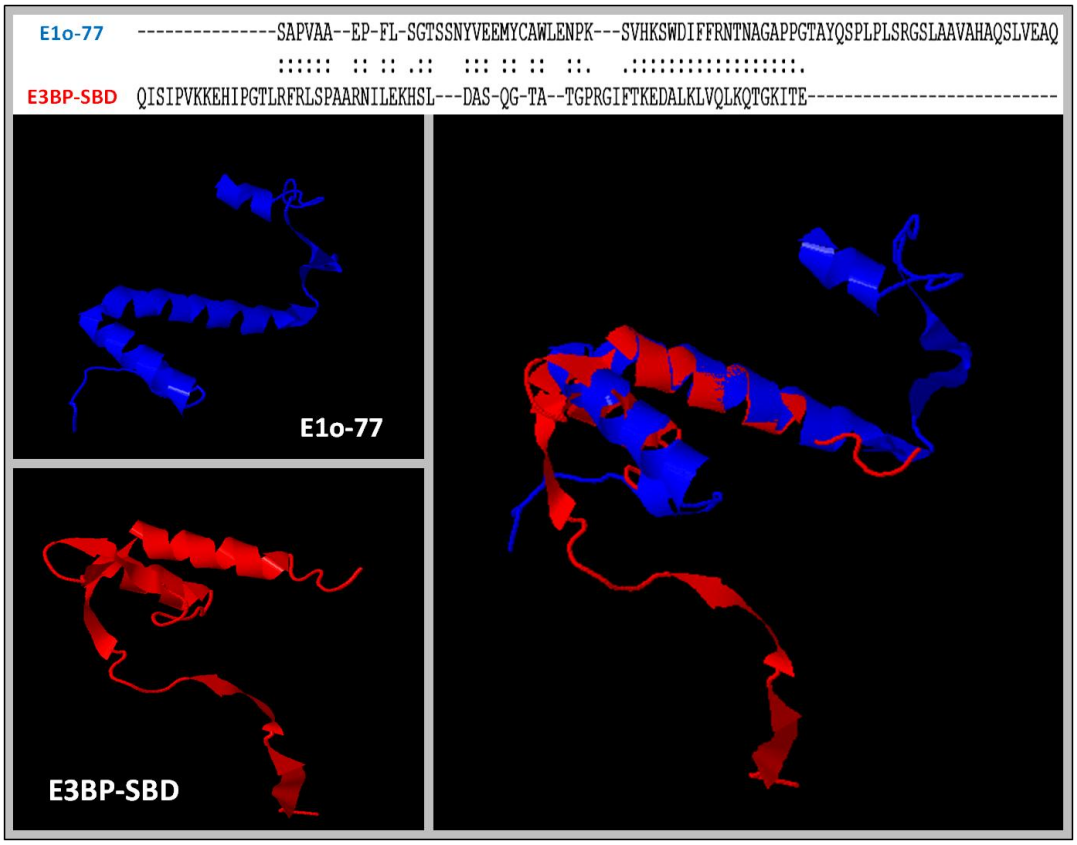


**Figure 7.1: Structure alignment of human N-terminal E1o and E3BP-SBD**
The structure alignment was carried out using the TM-align program (Zhang and Skolnick 2005). The 3-D structure for human N-terminal E1o-77 (blue) was predicted by I-TASSER (Zhang 2008). A crystal structure of human E3BP-SBD (Brautigam *et al.* 2006) was used (red). Human N-terminal E1o-77 showed structural similarity to human E3BP-SBD.

The main aim of chapter 4 was to investigate a potential interaction between N-terminal E1o and E3. This chapter provided direct evidence highlighting an important role of the N-terminal region of human E1o in promoting E3 binding in mammalian OGDC as judged by peptide array analysis, ala-scanning, ITC and affinity chromatography.

Chapter 5 focused on investigation of a possible interaction between the N-terminal region of human E1o and E2o, both post-translationally and co-translationally. The N-terminal region of human E1o failed to interact with E2o post-translationally as monitored by gel filtration or affinity chromatography. However, this region proved capable of integrating with E2o and forming a stable complex when the 2 polypeptides were co-expressed in the same bacterial cell.

In addition, no stable post-translation association was detected between E2o and E3. However, in co-translational binding studies, it was found that the E1o N-terminus is pivotal for mediating formation of a stable OGDC multienzyme assembly by directing self-integration with the E2o core and subsequently promoting high affinity E3 binding. A post-translation interaction between the E1o/E2o sub-complex and E3 was established using gel filtration where it was possible to detect complex formation between E1o-90 GST/E2o and E3. In summary, our current findings provide direct evidence that the N-terminal region of human E1o has a dual role in promoting stable OGDC organisation, namely mediating the co-translationally directed integration of E1o and E2o while also being responsible for the post-translational tethering of E3.

As a corollary to the previous results, parallel inhibition studies (chapter 6) on native bovine OGDC/PDC were conducted using N-terminal E1o and E3BP-SBD constructs showing that the N-terminal E1o constructs were functional and had a selective inhibitory effect on bovine OGDC presumably via displacement of E3 from its normal binding sites on the intact complex. Moreover, E3BP-SBD was slightly more effective at inhibiting PDC than OGDC suggesting that the mode of E3 binding differed significantly between the two complexes.

Further experiments are necessary to substantiate these results. In particular, it will be of great interest to produces soluble, recombinant full-length E1o. One possibility would be to use a low level *E. coli* expression system such as the pQE-9 vector and *E. coli* M15 strain that has proved successful in the production of the $\alpha_2\beta_2$ E1p heterotetramer. Moreover, further experiments using biophysical techniques including AUC, SAXS, and SANS are required to obtain more conclusive structural data on the morphology, organisation and stoichiometry of the E1o/E2o sub-complex.

Interestingly, Bunik and Degtyarev (2008a) have described 2 possible $Ca^{2+}$ binding motifs (ExDxDx and DxDxDx) within the N-terminal region of E1o. It will be of great interest to assess the functionality of these putative $Ca^{2+}$-binding sites in our E1o-153 fragment e.g. using ITC since $Ca^{2+}$-binding sites in proteins play a wide range of roles including stabilizing protein structures or acting as cofactors in catalytic and regulatory processes.

# Appendices

# Appendices

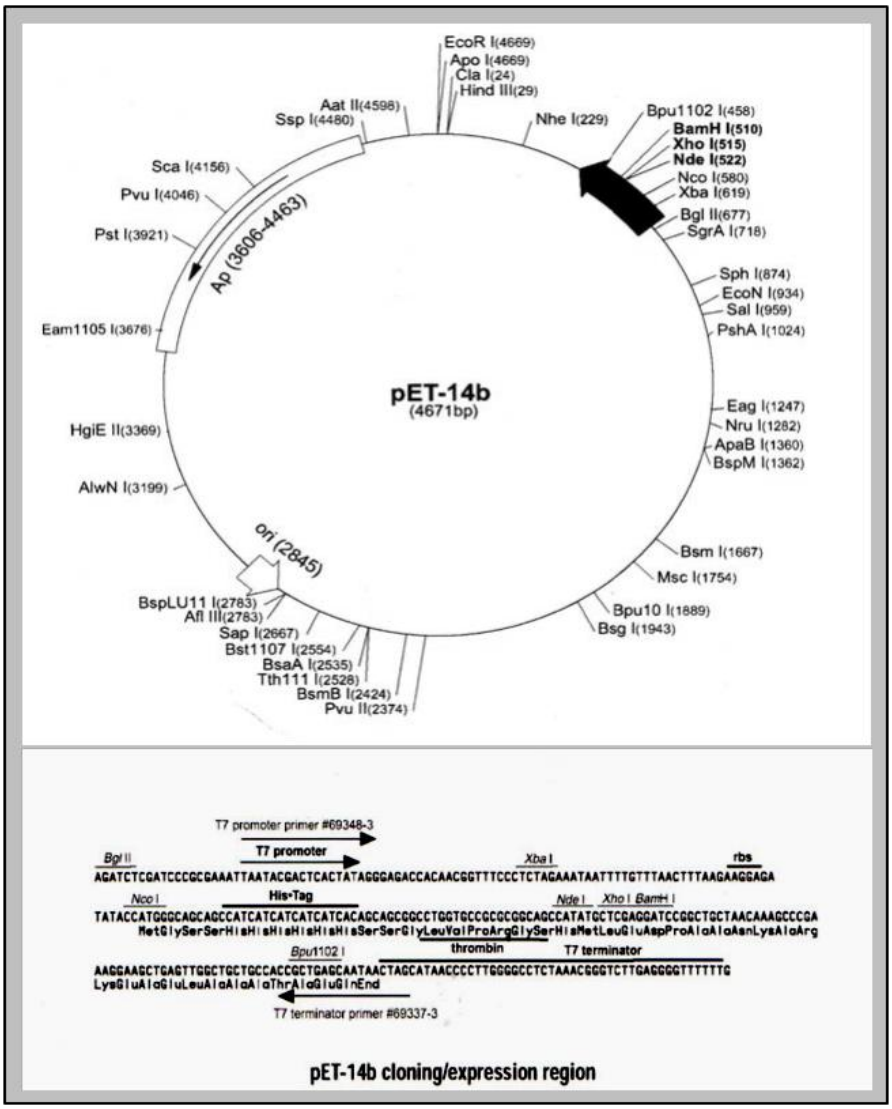


**Appendix 1: Plasmid map of the pET-14b cloning/expression vector**

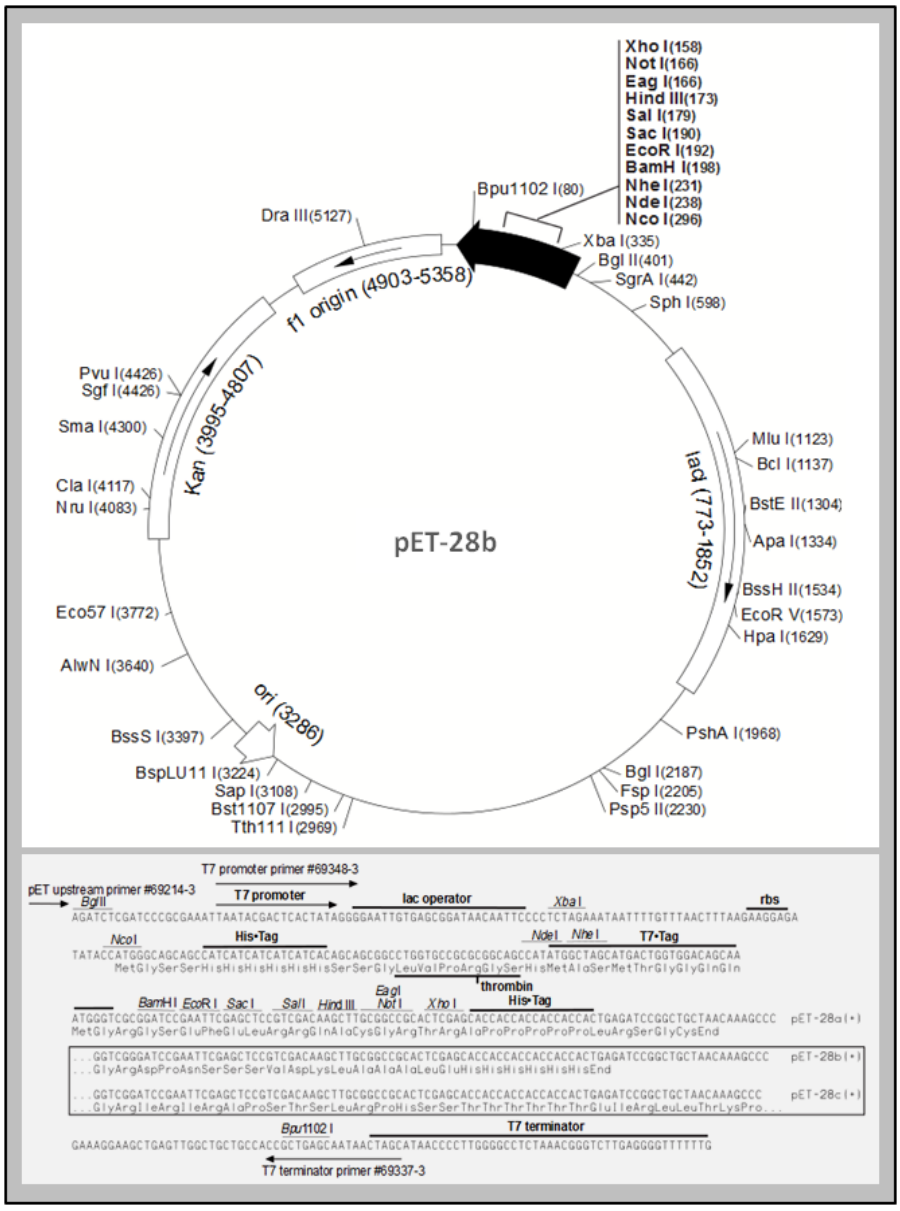


**Appendix 2: Plasmid map of the pET-28b cloning/expression vector**

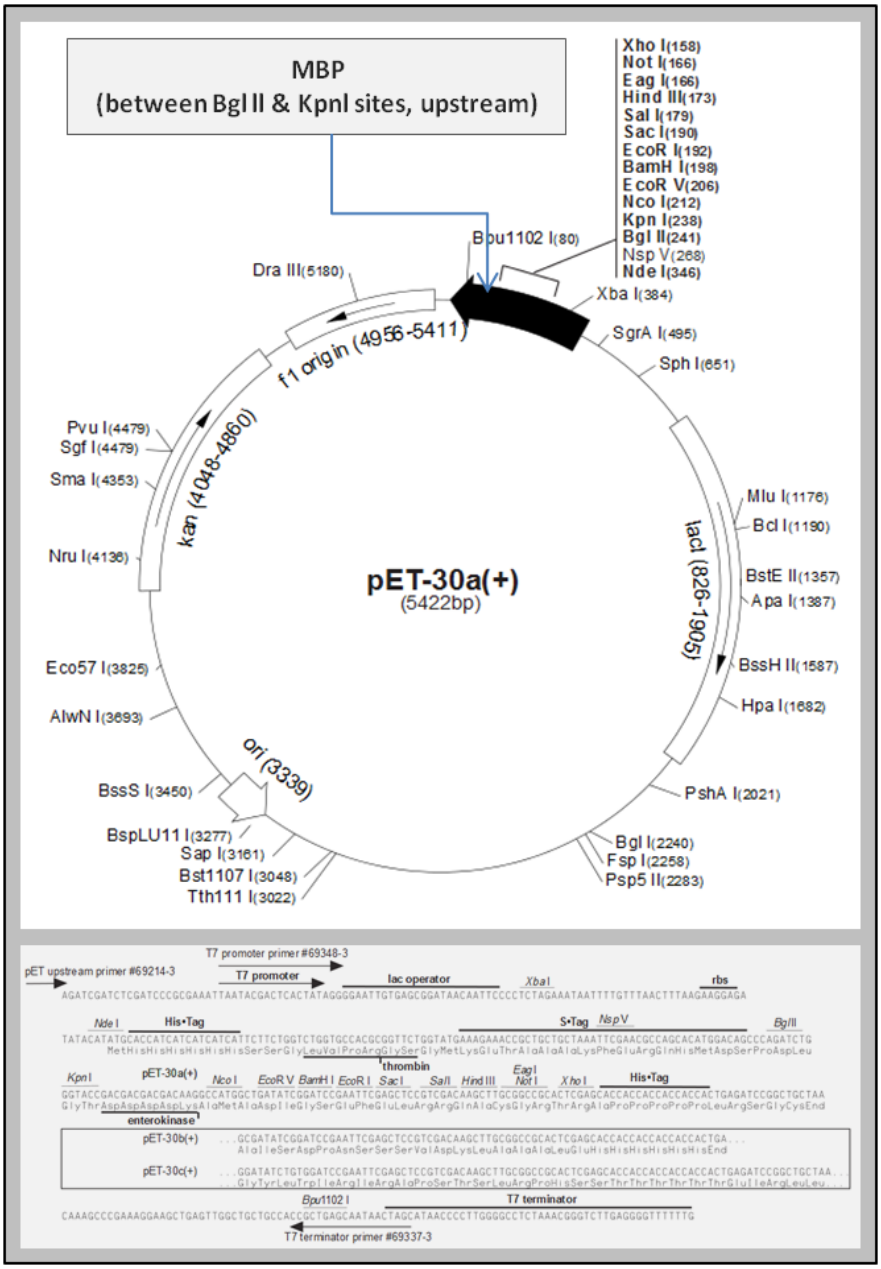


**Appendix 3: Plasmid map of the pET-30a cloning/expression vector**

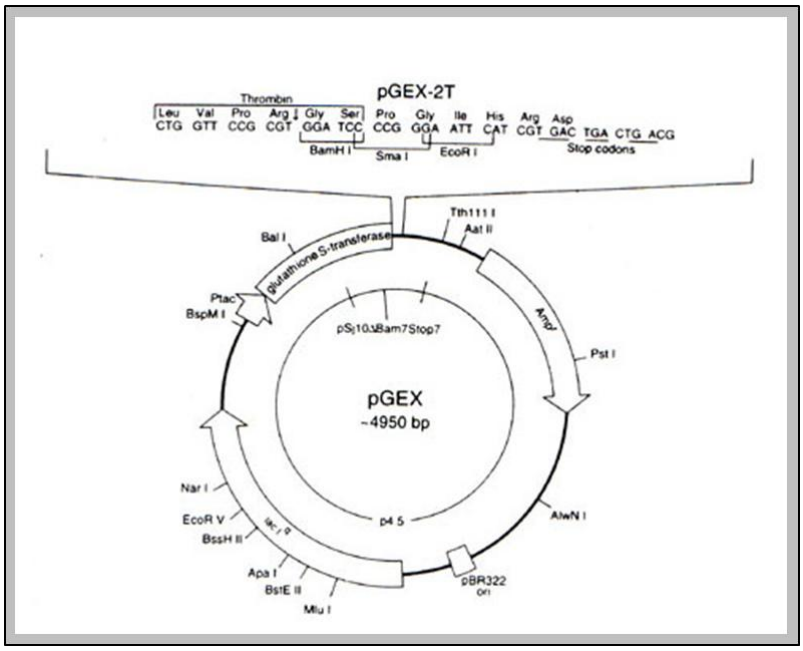


**Appendix 4: Map of the glutathione S-transferase fusion vector pGEX-2T**

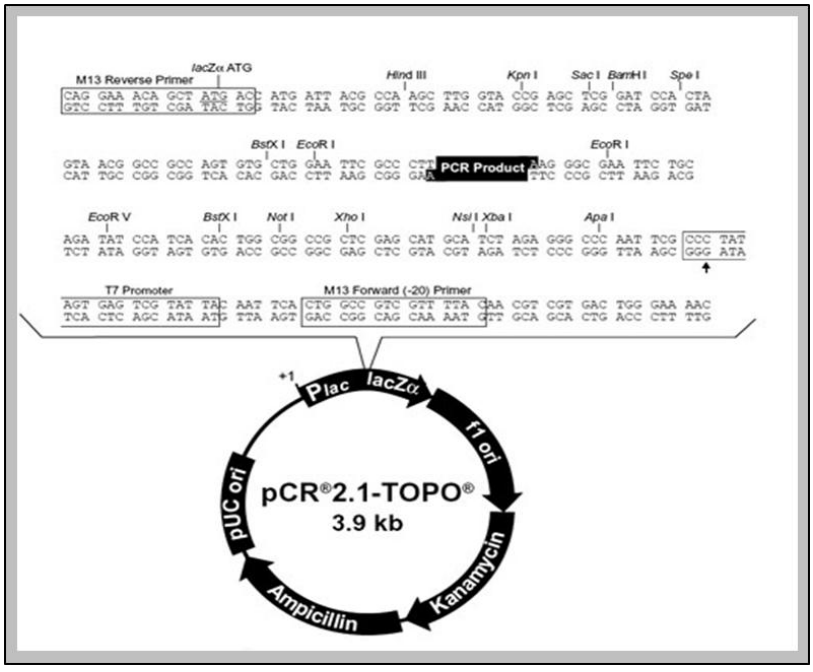


**Appendix 5: Map of the pCR 2.1-TOPO cloning vector**

# Bibliography

# Bibliography

Ævarsson, A., K. Seger, S. Turley, J. R. Sokatch and W. G. Hol (1999) Crystal structure of 2-oxoisovalerate dehydrogenase and the architecture of 2-oxo acid dehydrogenase multienzyme complexes. *Nat Struct Biol*. **6**, 785-92.

Arjunan, P., N. Nemeria, A. Brunskill, K. Chandrasekhar, M. Sax, Yan, F. Jordan, J. R. Guest and W. Furey (2002) Structure of the Pyruvate Dehydrogenase Multienzyme Complex E1 Component from *Escherichia coli*. *Biochemistry*. **41**, 5213-5221.

Arnold, K., L. Bordoli, J. r. Kopp and T. Schwede (2006) The SWISS-MODEL workspace: a web-based environment for protein structure homology modelling. *Bioinformatics*. **22**, 195-201.

Beddoe, T. and T. Lithgow (2002) Delivery of nascent polypeptides to the mitochondrial surface. *Biochim Biophys Acta*. **1592**, 35-9.

Behal, R. H., K. S. Browning, T. B. Hall and L. J. Reed (1989) Cloning and nucleotide sequence of the gene for protein X from *Saccharomyces cerevisiae. Proc Natl Acad Sci U S A*. **86**, 8732-6.

Behal, R. H., D. B. Buxton, J. G. Robertson and M. S. Olson (1993) Regulation of the pyruvate dehydrogenase multienzyme complex. *Annu Rev Nutr*. **13**, 497-520.

Bellomo, G. (1991) Cell damage by oxygen free radicals. *Cytotechnology*. **5**, 71-73.

Berg, A., O. Smits, A. de Kok and J. Vervoort (1995) Sequential 1H and 15N Nuclear Magnetic Resonance Assignments and Secondary Structure of the Lipoyl Domain of the 2-Oxoglutarate Dehydrogenase Complex from *Azotobacter Vinelandii. European Journal of Biochemistry*. **234**, 148-159.

Berg, A., A. H. Westphal, H. J. Bosma and A. De Kok (1998) Kinetics and specificity of reductive acylation of wild-type and mutated lipoyl domains of 2-oxo-acid dehydrogenase complexes from *Azotobacter vinelandii. European Journal of Biochemistry*. **252**, 45-50.

Blass, J. P. (1999) Mitochondria, neurodegenerative diseases, and selective neuronal vulnerability. *Ann N Y Acad Sci*. **893**, 434-9.

Bollag, D. M., M. D. Rozycki and S. J. and Edelstein (1996a) Gel electrophoresis under nondenaturing conditions *In Protein Methods. Wiley-Liss, New York,*, 155-172.

Bollag, D. M., M. D. Rozycki and S. J. and Edelstein (1996b) Concentrating protein solutions. *In Protein Methods. Wiley-Liss, New York,*, 83-106.

Bradford, A. P., A. Aitken, F. Beg, K. G. Cook and S. J. Yeaman (1987) Amino acid sequence surrounding the lipoic acid cofactor of bovine kidney 2-oxoglutarate dehydrogenase complex. *FEBS Letters*. **222**, 211-214.

Bradford, M. M. (1976) A rapid and sensitive method for the quantitation of microgram quantities of protein utilizing the principle of protein-dye binding. *Anal Biochem*. **72**, 248-54.

Brautigam, C. A., J. L. Chuang, D. R. Tomchick, M. Machius and D. T. Chuang (2005) Crystal Structure of Human Dihydrolipoamide Dehydrogenase: $NAD^+$/NADH Binding and the Structural Basis of Disease-causing Mutations. *Journal of Molecular Biology*. **350**, 543-552.

Brautigam, C. A., R. M. Wynn, J. L. Chuang, M. Machius, D. R. Tomchick and D. T. Chuang (2006) Structural insight into interactions between dihydrolipoamide dehydrogenase (E3) and E3 binding protein of human pyruvate dehydrogenase complex. *Structure*. **14**, 611-21.

Brown, J. P. and R. N. Perham (1976) Selective inactivation of the transacylase components of the 2-oxo acid dehydrogenase multienzyme complexes of *Escherichia coli. Biochem J*. **155**, 419-27.

Bubber, P., V. Haroutunian, G. Fisch, J. P. Blass and G. E. Gibson (2005) Mitochondrial abnormalities in Alzheimer brain: mechanistic implications. *Ann Neurol*. **57**, 695-703.

Bunik, V., T. Kaehne, D. Degtyarev, T. Shcherbakova and G. Reiser (2008b) Novel isoenzyme of 2-oxoglutarate dehydrogenase is identified in brain, but not in heart. *FEBS Journal*. **275**, 4990-5006.

Bunik, V., A. H. Westphal and A. de Kok (2000) Kinetic properties of the 2-oxoglutarate dehydrogenase complex from *Azotobacter vinelandii. European Journal of Biochemistry*. **267**, 3583-3591.

Bunik, V. I. (2003) 2-Oxo acid dehydrogenase complexes in redox regulation. *Eur J Biochem*. **270**, 1036-42.

Bunik, V. I. and D. Degtyarev (2008a) Structure–function relationships in the 2-oxo acid dehydrogenase family: Substrate-specific signatures and functional predictions for the 2-oxoglutarate dehydrogenase-like proteins. *Proteins: Structure, Function, and Bioinformatics*. **71**, 874-890.

Bunik, V. I. and A. R. Fernie (2009) Metabolic control exerted by the 2-oxoglutarate dehydrogenase reaction: a cross-kingdom comparison of the crossroad between energy production and nitrogen assimilation. *Biochem J*. **422**, 405-21.

Bunik, V. I. and C. Sievers (2002) Inactivation of the 2-oxo acid dehydrogenase complexes upon generation of intrinsic radical species. *European Journal of Biochemistry*. **269**, 5004-5015.

Burns, G., T. Brown, K. Hatter, J. M. Idriss and J. R. Sokatch (1988) Similarity of the E1 subunits of branched-chain-oxoacid dehydrogenase from Pseudomonas putida to the corresponding subunits of mammalian branched-chain-oxoacid and pyruvate dehydrogenases. *Eur J Biochem*. **176**, 311-7.

Cabiscol, E., E. Piulats, P. Echave, E. Herrero and J. Ros (2000) Oxidative stress promotes specific protein damage in *Saccharomyces cerevisiae. J Biol Chem*. **275**, 27393-8.

Cao, Z., A. W. Roszak, L. J. Gourlay, J. G. Lindsay and N. W. Isaacs (2005) Bovine Mitochondrial Peroxiredoxin III Forms a Two-Ring Catenane. *Structure*. **13**, 1661-1664.

Carothers, D. J., G. Pons and M. S. Patel (1989) Dihydrolipoamide dehydrogenase: Functional similarities and divergent evolution of the pyridine nucleotide-disulfide oxidoreductases. *Archives of Biochemistry and Biophysics*. **268**, 409-425.

Chinopoulos, C., L. Tretter and V. Adam-Vizi (1999) Depolarization of In Situ Mitochondria Due to Hydrogen Peroxide-Induced Oxidative Stress in Nerve Terminals. *Journal of Neurochemistry*. **73**, 220-228.

Ciszak, E., L. G. Korotchkina, Y. S. Hong, A. Joachimiak and M. S. Patel (2001) Crystallization and initial X-ray diffraction analysis of human pyruvate dehydrogenase. *Acta Crystallogr D Biol Crystallogr*. **57**, 465-8.

Ciszak, E. M., L. G. Korotchkina, P. M. Dominiak, S. Sidhu and M. S. Patel (2003) Structural basis for flip-flop action of thiamin pyrophosphate-dependent enzymes revealed by human pyruvate dehydrogenase. *J Biol Chem*. **278**, 21240-6.

Ciszak, E. M., A. Makal, Y. S. Hong, A. K. Vettaikkorumakankauv, L. G. Korotchkina and M. S. Patel (2006) How Dihydrolipoamide Dehydrogenase-binding Protein Binds Dihydrolipoamide Dehydrogenase in the Human Pyruvate Dehydrogenase Complex. *Journal of Biological Chemistry*. **281**, 648-655.

Clarkson, G. H. and J. G. Lindsay (1991) Immunology, biosynthesis and in vivo assembly of the branched-chain 2-oxoacid dehydrogenase complex from bovine kidney. *Eur J Biochem*. **196**, 95-100.

Cohen-Addad, C., M. Faure, M. Neuburger, R. Ober, L. Sieker, J. Bourguignon, D. Macherel and R. Douce (1997) Structural studies of the glycine decarboxylase complex from pea leaf mitochondria. *Biochimie*. **79**, 637-643.

Collins *et al* (2002) Generation and initial analysis of more than 15,000 full-length human and mouse cDNA sequences. *Proceedings of the National Academy of Sciences*. **99**, 16899-16903.

Conner, M., T. Krell and J. G. Lindsay (1996) Identification and purification of a distinct dihydrolipoamide dehydrogenase from pea chloroplasts. *Planta*. **200**, 195-202.

Culp, K. S., C. R. Fleming, J. Duffy, W. P. Baldus and E. R. Dickson (1982) Autoimmune associations in primary biliary cirrhosis. *Mayo Clin Proc*. **57**, 365-70.

Dahl, H. H., S. M. Hunt, W. M. Hutchison and G. K. Brown (1987) The human pyruvate dehydrogenase complex. Isolation of cDNA clones for the E1 alpha subunit, sequence analysis, and characterization of the mRNA. *J Biol Chem*. **262**, 7398-403.

Damuni, Z. and L. J. Reed (1987) Purification and properties of the catalytic subunit of the branched-chain alpha-keto acid dehydrogenase phosphatase from bovine kidney mitochondria. *J Biol Chem*. **262**, 5129-32.

Danhauser, K., SvenÂ W. Sauer, TobiasÂ B. Haack, T. Wieland, C. Staufner, E. Graf, J. Zschocke, TimÂ M. Strom, T. Traub, JÃrgenÂ G. Okun, T. Meitinger, GeorgÂ F. Hoffmann, H. Prokisch and S. KÃlker (2012) DHTKD1 Mutations Cause 2-Aminoadipic and 2-Oxoadipic Aciduria. *The American Journal of Human Genetics*. **91**, 1082-1087.

Danson, M. J., A. R. Fersht and R. N. Perham (1978) Rapid intramolecular coupling of active sites in the pyruvate dehydrogenase complex of *Escherichia coli*: mechanism for rate enhancement in a multimeric structure. *Proc Natl Acad Sci U S A*. **75**, 5386-90.

Danson, M. J., G. Hale, P. Johnson, R. N. Perham, J. Smith and P. Spragg (1979) Molecular weight and symmetry of the pyruvate dehydrogenase multienzyme complex of *Escherichia coli. J Mol Biol*. **129**, 603-17.

Dardel, F. d. r., A. L. Davis, E. D. Laue and R. N. Perham (1993) Three-dimensional Structure of the Lipoyl domain from *Bacillus stearothermophilus* Pyruvate Dehydrogenase Multienzyme Complex. *Journal of Molecular Biology*. **229**, 1037-1048.

Darlison, M. G., M. E. Spencer and J. R. Guest (1984) Nucleotide sequence of the sucA gene encoding the 2-oxoglutarate dehydrogenase of *Escherichia coli* K12. *European Journal of Biochemistry*. **141**, 351-359.

De Marcucci, O. and J. G. Lindsay (1985a) Component X. An immunologically distinct polypeptide associated with mammalian pyruvate dehydrogenase multi-enzyme complex. *Eur J Biochem*. **149**, 641-8.

De Marcucci, O. and J. G. Lindsay (1985b) Component X. *European Journal of Biochemistry*. **149**, 641-648.

Derosier, D. J., R. M. Oliver and L. J. Reed (1971) Crystallization and Preliminary Structural Analysis of Dihydrolipoyl Transsuccinylase, the Core of the 2-Oxoglutarate Dehydrogenase Complex. *Proceedings of the National Academy of Sciences*. **68**, 1135-1137.

Douce, R., J. Bourguignon, M. Neuburger and F. Rbeill (2001) The glycine decarboxylase system: a fascinating complex. *Trends in Plant Science*. **6**, 167-176.

Douglas, M. G., M. T. McCammon and A. Vassarotti (1986) Targeting proteins into mitochondria. *Microbiol Rev*. **50**, 166-78.

Drake, S. K., M. A. Zimmer, C. Kundrot and J. J. Falke (1997) Molecular Tuning of an EF-Hand-like Calcium Binding Loop. *The Journal of General Physiology*. **110**, 173-184.

Faure, M., J. Bourguignon, M. Neuburger, D. Macherel, L. Sieker, R. Ober, R. Kahn, C. Cohen-Addad and R. Douce (2000) Interaction between the lipoamide-containing H-protein and the lipoamide dehydrogenase (L-protein) of the glycine decarboxylase multienzyme system. *European Journal of Biochemistry*. **267**, 2890-2898.

Feigenbaum, A. S. and B. H. Robinson (1993) The Structure of the Human Dihydrolipoamide Dehydrogenase Gene (DLD) and Its Upstream Elements. *Genomics*. **17**, 376-381.

Finkel, L. H. (2000) Neuroengineering models of brain disease. *Annu Rev Biomed Eng*. **2**, 577-606.

Flaherty, K. M., C. DeLuca-Flaherty and D. B. McKay (1990) Three-dimensional structure of the ATPase fragment of a 70K heat-shock cognate protein. *Nature*. **346**, 623-628.

Floyd, R. A. (1999) Neuroinflammatory processes are important in neurodegenerative diseases: an hypothesis to explain the increased formation of reactive oxygen and nitrogen species as major factors involved in neurodegenerative disease development. *Free Radic Biol Med*. **26**, 1346-55.

Frank, R. A., J. V. Pratap, X. Y. Pei, R. N. Perham and B. F. Luisi (2005) The molecular origins of specificity in the assembly of a multienzyme complex. *Structure*. **13**, 1119-30.

Frank, R. A., C. M. Titman, J. V. Pratap, B. F. Luisi and R. N. Perham (2004) A molecular switch and proton wire synchronize the active sites in thiamine enzymes. *Science*. **306**, 872-6.

Frank, R. A. W., A. J. Price, F. D. Northrop, R. N. Perham and B. F. Luisi (2007) Crystal Structure of the E1 Component of the *Escherichia coli* 2-Oxoglutarate Dehydrogenase Multienzyme Complex. *Journal of Molecular Biology*. **368**, 639-651.

Freudenberg, W. and J. R. Andreesen (1989) Purification and partial characterization of the glycine decarboxylase multienzyme complex from *Eubacterium acidaminophilum*. *Journal of Bacteriology*. **171**, 2209-2215.

Fridovich, I. (1995) Superoxide radical and superoxide dismutases. *Annu Rev Biochem*. **64**, 97-112.

Fujiwara, K., K. Okamura-Ikeda and Y. Motokawa (1996) Lipoylation of acyltransferase components of alpha-ketoacid dehydrogenase complexes. *J Biol Chem*. **271**, 12932-6.

Fussey, S. P., M. F. Bassendine, D. Fittes, I. B. Turner, O. F. James and S. J. Yeaman (1989) The E1 alpha and beta subunits of the pyruvate dehydrogenase complex are M2'd' and M2'e' autoantigens in primary biliary cirrhosis. *Clin Sci (Lond)*. **77**, 365-8.

Fussey, S. P., J. R. Guest, O. F. James, M. F. Bassendine and S. J. Yeaman (1988) Identification and analysis of the major M2 autoantigens in primary biliary cirrhosis. *Proc Natl Acad Sci U S A*. **85**, 8654-8.

Fussey, S. P., J. G. Lindsay, C. Fuller, R. N. Perham, S. Dale, O. F. James, M. F. Bassendine and S. J. Yeaman (1991) Autoantibodies in primary biliary cirrhosis: analysis of reactivity against eukaryotic and prokaryotic 2-oxo acid dehydrogenase complexes. *Hepatology*. **13**, 467-74.

Gakh, O., P. Cavadini and G. Isaya (2002) Mitochondrial processing peptidases. *Biochimica et Biophysica Acta (BBA) - Molecular Cell Research*. **1592**, 63-77.

Gershwin, M. E., I. R. Mackay, A. Sturgess and R. L. Coppel (1987) Identification and specificity of a cDNA encoding the 70 kd mitochondrial antigen recognized in primary biliary cirrhosis. *The Journal of Immunology*. **138**, 3525-31.

Gibson, G. E., J. P. Blass, M. F. Beal and V. Bunik (2005) The alpha-ketoglutarate-dehydrogenase complex: a mediator between mitochondria and oxidative stress in neurodegeneration. *Mol Neurobiol*. **31**, 43-63.

Gibson, G. E., L. C. Park, K. F. Sheu, J. P. Blass and N. Y. Calingasan (2000) The alpha-ketoglutarate dehydrogenase complex in neurodegeneration. *Neurochem Int*. **36**, 97-112.

Gibson, G. E., K. F. R. Sheu and J. P. Blass (1998) Abnormalities of mitochondrial enzymes in Alzheimer disease. *Journal of Neural Transmission*. **105**, 855-870.

Goeddel, D. V., H. L. Heyneker, T. Hozumi, R. Arentzen, K. Itakura, D. G. Yansura, M. J. Ross, G. Miozzari, R. Crea and P. H. Seeburg (1979a) Direct expression in *Escherichia coli* of a DNA sequence coding for human growth hormone. *Nature*. **281**, 544-8.

Goeddel, D. V., D. G. Kleid, F. Bolivar, H. L. Heyneker, D. G. Yansura, R. Crea, T. Hirose, A. Kraszewski, K. Itakura and A. D. Riggs (1979b) Expression in *Escherichia coli* of chemically synthesized genes for human insulin. *Proc Natl Acad Sci U S A*. **76**, 106-10.

Gopalakrishnan, S., M. Rahmatullah, G. A. Radke, S. Powers-Greenwood and T. E. Roche (1989) Role of protein X in the function of the mammalian pyruvate dehydrogenase complex. *Biochemical and Biophysical Research Communications*. **160**, 715-721.

Graham, L. D., L. C. Packman and R. N. Perham (1989) Kinetics and specificity of reductive acylation of lipoyl domains from 2-oxo acid dehydrogenase multienzyme complexes. *Biochemistry*. **28**, 1574-81.

Graham, L. D. and R. N. Perham (1990) Interactions of lipoyl domains with the E1p subunits of the pyruvate dehydrogenase multienzyme complex from *Escherichia coli. FEBS Letters*. **262**, 241-244.

Green, J. D., R. N. Perham, S. J. Ullrich and E. Appella (1992) Conformational studies of the interdomain linker peptides in the dihydrolipoyl acetyltransferase component of the pyruvate dehydrogenase multienzyme complex of *Escherichia coli. Journal of Biological Chemistry*. **267**, 23484-8.

Griffin, T. A., K. S. Lau and D. T. Chuang (1988) Characterization and conservation of the inner E2 core domain structure of branched-chain alpha-keto acid dehydrogenase complex from bovine liver. Construction of a cDNA encoding the entire transacylase (E2b) precursor. *Journal of Biological Chemistry*. **263**, 14008-14014.

Guest, J. R. (1987) Functional implications of structural homologies between chloramphenicol acetyltransferase and dihydrolipoamide acetyltransferase. *FEMS Microbiology Letters*. **44**, 417-422.

Guex, N. and M. C. Peitsch (1997) SWISS-MODEL and the Swiss-PdbViewer: an environment for comparative protein modeling. *Electrophoresis*. **18**, 2714-23.

Gutteridge, J. M. C. (1994) Hydroxyl Radicals, Iron, Oxidative Stress, and Neurodegenerationa. *Annals of the New York Academy of Sciences*. **738**, 201-213.

Hackert, M. L., R. M. Oliver and L. J. Reed (1983) Evidence for a multiple random coupling mechanism in the alpha-ketoglutarate dehydrogenase multienzyme complex of *Escherichia coli*: a computer model analysis. *Proc Natl Acad Sci U S A*. **80**, 2226-30.

Hakozaki, M., K. Ono, T. Suzuki, H. Hata, T. Mori and H. Kochi (2002) Characterization of rainbow trout branched-chain alpha-keto acid dehydrogenase complex: inter-domain segments of the E2 component affect the overall activity. *Comparative Biochemistry and Physiology Part B: Biochemistry and Molecular Biology*. **132**, 433-442.

Halliwell, B. and J. M. C. Gutteridge (1985) The importance of free radicals and catalytic metal ions in human diseases. *Molecular Aspects of Medicine*. **8**, 89-193.

Hammond, B. and M. L. Hess (1985) The oxygen free radical system: Potential mediator of myocardial injury. *Journal of the American College of Cardiology*. **6**, 215-220.

Harris, R. A., M. M. Bowker-Kinley, B. Huang and P. Wu (2002) Regulation of the activity of the pyruvate dehydrogenase complex. *Adv Enzyme Regul*. **42**, 249-59.

Harris, R. A., J. W. Hawes, K. M. Popov, Y. Zhao, Y. Shimomura, J. Sato, J. Jaskiewicz and T. D. Hurley (1997) Studies on the regulation of the mitochondrial alpha-ketoacid dehydrogenase complexes and their kinases. *Adv Enzyme Regul*. **37**, 271-93.

Hasse, D., M. Hagemann, I. Andersson and H. Bauwe (2009) Crystallization and preliminary X-ray diffraction analyses of the homodimeric glycine decarboxylase (P-protein) from the *cyanobacterium Synechocystis* sp. PCC 6803. *Acta Crystallographica Section F*. **66**, 187-191.

Hawkins, C. F., A. Borges and R. N. Perham (1989) A common structural motif in thiamin pyrophosphate-binding enzymes. *FEBS Letters*. **255**, 77-82.

Hawkins, C. F., A. Borges and R. N. Perham (1990) Cloning and sequence analysis of the genes encoding the alpha and beta subunits of the E1 component of the pyruvate dehydrogenase multienzyme complex of *Bacillus stearothermophilus. Eur J Biochem*. **191**, 337-46.

Henderson, C. E. and R. N. Perham (1980) Purificaton of the pyruvate dehydrogenase multienzyme complex of *Bacillus stearothermophilus* and resolution of its four component polypeptides. *Biochem J*. **189**, 161-72.

Hipps, D. S., L. C. Packman, M. D. Allen, C. Fuller, K. Sakaguchi, E. Appella and R. N. Perham (1994) The peripheral subunit-binding domain of the dihydrolipoyl acetyltransferase component of the pyruvate dehydrogenase complex of *Bacillus stearothermophilus*: preparation and characterization of its binding to the dihydrolipoyl dehydrogenase component. *Biochem J*. **297**, 137-43.

Hiromasa, Y., T. Fujisawa, Y. Aso and T. E. Roche (2004) Organization of the Cores of the Mammalian Pyruvate Dehydrogenase Complex Formed by E2 and E2 Plus the E3-binding Protein and Their Capacities to Bind the E1 and E3 Components. *Journal of Biological Chemistry*. **279**, 6921-6933.

Holz, M., C. Otto, A. Kretzschmar, V. Yovkova, A. Aurich, M. Pötter, A. Marx and G. Barth (2011) Overexpression of alpha-ketoglutarate dehydrogenase in Yarrowia lipolytica and its effect on production of organic acids. *Applied Microbiology and Biotechnology*. **89**, 1519-1526.

Howard, M. J., H. J. Chauhan, G. J. Domingo, C. Fuller and R. N. Perham (2000) Protein-protein interaction revealed by NMR T2 relaxation experiments: the lipoyl domain and E1 component of the pyruvate dehydrogenase multienzyme complex of *Bacillus stearothermophilus. Journal of Molecular Biology*. **295**, 1023-1037.

Hoyer, S. (2000) Brain glucose and energy metabolism abnormalities in sporadic Alzheimer disease. Causes and consequences: an update. *Experimental Gerontology*. **35**, 1363-1372.

Huang, B., R. Gudi, P. Wu, R. A. Harris, J. Hamilton and K. M. Popov (1998) Isoenzymes of pyruvate dehydrogenase phosphatase. DNA-derived amino acid sequences, expression, and regulation. *J Biol Chem*. **273**, 17680-8.

Huang, B., P. Wu, K. M. Popov and R. A. Harris (2003) Starvation and diabetes reduce the amount of pyruvate dehydrogenase phosphatase in rat heart and kidney. *Diabetes*. **52**, 1371-6.

Hulett, J. M., F. Lueder, N. C. Chan, A. J. Perry, P. Wolynec, V. A. Liki, P. R. Gooley and T. Lithgow (2008) The Transmembrane Segment of Tom20 Is Recognized by Mim1 for Docking to the Mitochondrial TOM Complex. *Journal of Molecular Biology*. **376**, 694-704.

Hull, E. P., M. E. Spencer, D. Wood and J. R. Guest (1983) Nucleotide sequence of the promoter region of the citrate synthase gene (gltA) of *Escherichia coli. FEBS Letters*. **156**, 366-370.

Humphries, K. M. and L. I. Szweda (1998) Selective Inactivation of alpha-Ketoglutarate Dehydrogenase and Pyruvate Dehydrogenase: Reaction of Lipoic Acid with 4-Hydroxy-2-nonenal *Biochemistry*. **37**, 15835-15841.

Hunter, A. and J. G. Lindsay (1986) Immunological and biosynthetic studies on the mammalian 2-oxoglutarate dehydrogenase multienzyme complex. *European Journal of Biochemistry*. **155**, 103-109.

Hurt, E. C., N. Soltanifar, M. Goldschmidt-Clermont, J. D. Rochaix and G. Schatz (1986) The cleavable pre-sequence of an imported chloroplast protein directs attached polypeptides into yeast mitochondria. *EMBO J.* **5**, 1343-50.

Invernizzi, P., M. Miozzo, P. M. Battezzati, I. Bianchi, F. R. Grati, G. Simoni, C. Selmi, M. Watnik, M. E. Gershwin and M. Podda (2004) Frequency of monosomy X in women with primary biliary cirrhosis. *The Lancet*. **363**, 533-535.

Invernizzi, P., M. Miozzo, C. Selmi, L. Persani, P. M. Battezzati, M. Zuin, S. Lucchi, P. L. Meroni, B. Marasini, S. Zeni, M. Watnik, F. R. Grati, G. Simoni, M. E. Gershwin and M. Podda (2005) X Chromosome Monosomy: A Common Mechanism for Autoimmune Diseases. *The Journal of Immunology*. **175**, 575-578.

Ishikawa, E., R. M. Oliver and L. J. Reed (1966) Alpha-Keto acid dehydrogenase complexes, V. Macromolecular organization of pyruvate and alpha-ketoglutarate dehydrogenase complexes isolated from beef kidney mitochondria. *Proc Natl Acad Sci U S A*. **56**, 534-41.

Itakura, K., T. Hirose, R. Crea, A. D. Riggs, H. L. Heyneker, F. Bolivar and H. W. Boyer (1977) Expression in *Escherichia coli* of a chemically synthesized gene for the hormone somatostatin. *Science*. **198**, 1056-63.

Izard, T., A. Aevarsson, M. D. Allen, A. H. Westphal, R. N. Perham, A. de Kok and W. G. Hol (1999) Principles of quasi-equivalence and Euclidean geometry govern the assembly of cubic and dodecahedral cores of pyruvate dehydrogenase complexes. *Proc Natl Acad Sci U S A*. **96**, 1240-5.

Jones, D. D., H. J. Horne, P. A. Reche and R. N. Perham (2000) Structural determinants of post-translational modification and catalytic specificity for the lipoyl domains of the pyruvate dehydrogenase multienzyme complex of *Escherichia coli* . *J Mol Biol*. **295**, 289-306.

Jones, D. E. J. (2003) Pathogenesis of primary biliary cirrhosis. *Journal of Hepatology*. **39**, 639-648.

Joplin, R. and M. E. Gershwin (1997) Ductular expression of autoantigens in primary biliary cirrhosis. *Semin Liver Dis*. **17**, 97-103.

Jordan, F., E. Sergienko, N. Nemeria, Min Liu, Jue Wang, Fusheng Guo and W. F. Furey (2000) Structure-function studies in thiamin diphosphate-dependent 2-oxoacid decarboxylating enzymes. *VESTNIK MOSKOVSKOGO UNIVERSITETA. KHIMIYA.* **41**, 6.

Jung, H. I., S. J. Bowden, A. Cooper and R. N. Perham (2002) Thermodynamic analysis of the binding of component enzymes in the assembly of the pyruvate dehydrogenase multienzyme complex of *Bacillus stearothermophilus. Protein Sci*. **11**, 1091-100.

Kalia, Y. N., S. M. Brocklehurst, D. S. Hipps, E. Appella, K. Sakaguchi and R. N. Perham (1993) The High-resolution Structure of the Peripheral Subunit-binding Domain of Dihydrolipoamide Acetyltransferase from the Pyruvate Dehydrogenase Multienzyme Complex of *Bacillus stearothermophilus. Journal of Molecular Biology*. **230**, 323-341.

Kato, M., R. M. Wynn, J. L. Chuang, C. A. Brautigam, M. Custorio and D. T. Chuang (2006) A synchronized substrate-gating mechanism revealed by cubic-core structure of the bovine branched-chain alpha-ketoacid dehydrogenase complex. *EMBO J*. **25**, 5983-94.

Katzman, R. (1986) Alzheimer's Disease. *New England Journal of Medicine*. **314**, 964-973.

Kern, D., G. Kern, H. Neef, K. Tittmann, M. Killenberg-Jabs, C. Wikner, G. Schneider and G. Hubner (1997) How thiamine diphosphate is activated in enzymes. *Science*. **275**, 67-70.

Kirkinezos, I. G. and C. T. Moraes (2001) Reactive oxygen species and mitochondrial diseases. *Semin Cell Dev Biol*. **12**, 449-57.

Klivenyi, P., A. A. Starkov, N. Y. Calingasan, G. Gardian, S. E. Browne, L. Yang, P. Bubber, G. E. Gibson, M. S. Patel and M. F. Beal (2004) Mice deficient in dihydrolipoamide dehydrogenase show increased vulnerability to MPTP, malonate and 3-nitropropionic acid neurotoxicity. *Journal of Neurochemistry*. **88**, 1352-1360.

Knapp, J. E., D. Carroll, J. E. Lawson, S. R. Ernst, L. J. Reed and M. L. Hackert (2000) Expression, purification, and structural analysis of the trimeric form of the catalytic domain of the *Escherichia coli* dihydrolipoamide succinyltransferase. *Protein Sci*. **9**, 37-48.

Knapp, J. E., D. T. Mitchell, M. A. Yazdi, S. R. Ernst, L. J. Reed and M. L. Hackert (1998) Crystal structure of the truncated cubic core component of the *Escherichia coli* 2-oxoglutarate dehydrogenase multienzyme complex. *Journal of Molecular Biology*. **280**, 655-668.

Koike, K. (1995) The gene encoding human 2-oxoglutarate dehydrogenase: structural organization and mapping to chromosome 7p13-p14. *Gene*. **159**, 261-266.

Koike, K. (1998) Cloning, structure, chromosomal localization and promoter analysis of human 2-oxoglutarate dehydrogenase gene. *Biochimica et Biophysica Acta (BBA) - Protein Structure and Molecular Enzymology*. **1385**, 373-384.

Koike, K., M. Hamada, N. Tanaka, K.-I. Otsuka, K. Ogasahara and M. Koike (1974) Properties and Subunit Composition of the Pig Heart 2-Oxoglutarate Dehydrogenase. *Journal of Biological Chemistry*. **249**, 3836-3842.

Koike, K., T. Suematsu and M. Ehara (2000) Cloning, overexpression and mutagenesis of cDNA encoding dihydrolipoamide succinyltransferase component of the porcine 2-oxoglutarate dehydrogenase complex. *Eur J Biochem*. **267**, 3005-16.

Koike, K., Y. Urata and S. Goto (1992) Cloning and nucleotide sequence of the cDNA encoding human 2-oxoglutarate dehydrogenase (lipoamide). *Proc Natl Acad Sci U S A*. **89**, 1963-7.

Koike, M. and K. Koike (1976) Structure, assembly and function of mammalian alpha-keto acid dehydrogenase complexes. *Adv Biophys*, 187-227.

Kolobova, E., A. Tuganova, I. Boulatnikov and K. M. Popov (2001) Regulation of pyruvate dehydrogenase activity through phosphorylation at multiple sites. *Biochem J*. **358**, 69-77.

Korotchkina, L. G., M. M. Tucker, T. J. Thekkumkara, K. T. Madhusudhan, G. Pons, H. Kim and M. S. Patel (1995) Overexpression and characterization of human tetrameric pyruvate dehydrogenase and its individual subunits. *Protein Expr Purif*. **6**, 79-90.

Kresze, G. B., H. Ronft, B. Dietl and L. Steber (1981) Limited proteolysis of 2-oxoglutarate dehydrogenase multienzyme complex from bovine kidney. *FEBS Lett*. **127**, 157-60.

Laemmli, U. K. (1970) Cleavage of Structural Proteins during the Assembly of the Head of *Bacteriophage* T4. *Nature*. **227**, 680-685.

Lawlis, V. B. and T. E. Roche (1981) Regulation of bovine kidney alpha-ketoglutarate dehydrogenase complex by calcium ion and adenine nucleotides. Effects on $S_{0.5}$ for alpha-ketoglutarate. *Biochemistry*. **20**, 2512-2518.

Lennon, S. V., S. J. Martin and T. G. Cotter (1991) Dose-dependent induction of apoptosis in human tumour cell lines by widely diverging stimuli. *Cell Prolif.* **24**, 203-14.

Leslie, A. G., P. C. Moody and W. V. Shaw (1988) Structure of chloramphenicol acetyltransferase at 1.75 A resolution. *Proceedings of the National Academy of Sciences*. **85**, 4133-4137.

Lessard, I. A. and R. N. Perham (1995) Interaction of component enzymes with the peripheral subunit-binding domain of the pyruvate dehydrogenase multienzyme complex of *Bacillus stearothermophilus*: stoichiometry and specificity in self-assembly. *Biochem J.* **306**, 727-33.

Leung, P. S., T. Iwayama, R. L. Coppel and M. E. Gershwin (1990) Site-directed mutagenesis of lysine within the immunodominant autoepitope of PDC-E2. *Hepatology (Baltimore, Md.)*. **12**, 1321-1328.

Lindner, P., B. Guth, Wiilfing, C, Krebber, C, and B. Steipe, Miiller, F, and APliickthun,A. (1992) Purification of Native Proteins from the Cytoplasm and Periplasm of *Escherichia coli* Using IMAC and Histidine Tails: A Comparison of Proteins and Protocols. *METHODS: A Companion to Methods in Enzymology*. **4**, 41-56.

Lindor, K. D., M. E. Gershwin, R. Poupon, M. Kaplan, N. V. Bergasa and E. J. Heathcote (2009) Primary biliary cirrhosis. *Hepatology*. **50**, 291-308.

Lindsay, H., E. Beaumont, S. D. Richards, S. M. Kelly, S. J. Sanderson, N. C. Price and J. G. Lindsay (2000) FAD Insertion Is Essential for Attaining the Assembly Competence of the Dihydrolipoamide Dehydrogenase (E3) Monomer from *Escherichia coli*. *Journal of Biological Chemistry*. **275**, 36665-36670.

Lindsay, J. G. (1989) Targeting of 2-Oxo Acid Dehydrogenase Complexes to the Mitochondriona. *Annals of the New York Academy of Sciences*. **573**, 254-266.

Linn, T. C., J. W. Pelley, F. H. Pettit, F. Hucho, D. D. Randall and L. J. Reed (1972) alpha-Keto acid dehydrogenase complexes. XV. Purification and properties of the component enzymes of the pyruvate dehydrogenase complexes from bovine kidney and heart. *Arch Biochem Biophys*. **148**, 327-42.

Linn, T. C., F. H. Pettit, F. Hucho and L. J. Reed (1969) Alpha-keto acid dehydrogenase complexes. XI. Comparative studies of regulatory properties of the pyruvate dehydrogenase complexes from kidney, heart, and liver mitochondria. *Proc Natl Acad Sci U S A*. **64**, 227-34.

Long, S. A., J. Van de Water and M. E. Gershwin (2002) Antimitochondrial antibodies in primary biliary cirrhosis: the role of xenobiotics. *Autoimmunity Reviews*. **1**, 37-42.

Loumaye, E., R. Campbell and J. Salat-Baroux (1995) Human follicle-stimulating hormone produced by recombinant DNA technology: a review for clinicians. *Hum Reprod Update*. **1**, 188-99.

Lyubarev, A. E. and B. I. Kurganov (1989) Supramolecular organization of tricarboxylic acid cycle enzymes. *Biosystems*. **22**, 91-102.

Maas, E. and H. Bisswanger (1990) Localization of the 2-oxoacid dehydrogenase multienzyme complexes within the mitochondrion. *FEBS Letters*. **277**, 189-190.

Maj, M. C., J. M. Cameron and B. H. Robinson (2006) Pyruvate dehydrogenase phosphatase deficiency: Orphan disease or an under-diagnosed condition. *Molecular and Cellular Endocrinology*. **249**, 1-9.

Mande, S. S., S. Sarfaty, M. D. Allen, R. N. Perham and W. G. Hol (1996) Protein-protein interactions in the pyruvate dehydrogenase multienzyme complex: dihydro-lipoamide dehydrogenase complexed with the binding domain of dihydrolipoamide acetyltransferase. *Structure*. **4**, 277-86.

Maniatis, T., E. F. Fritsch and J. and Sambrook (1987a) Gel Electrophoresis. In *Molecular Cloning - a Laboratory Manual*. *Cold Spring Harbor Laboratory Press, Cold Spring Harbor,*, 149-186.

Maniatis, T., E. F. Fritsch and J. and Sambrook (1987b) Introduction of plasmid and bacteriophage DNA into *Escherichia coli*. In *Molecular cloning - a Laboratory Manual*. *Cold Spring Harbor Laboratory Press, Cold Spring Harbor,*, 247-268.

Mareck, A., H. Bessam, P. Delattre and B. Foucher (1986) Purification of the 2-oxoglutarate dehydrogenase and pyruvate dehydrogenase complexes of Neurospora crassa mitochondria. *Biochimie*. **68**, 1175-1180.

Markiewicz , J. and S. Strumiło (1995) Some regulatory properties of the 2-oxoglutarate dehydrogenase complex from European bison heart. *Acta Biochim Pol* **42(3)**, 339-46.

Matsushita, S., H. Arai, T. Yuzuriha, M. Kato, T. Matsui, K. Urakami and S. Higuchi (2001) No association between DLST gene and Alzheimers disease or Wernicke-Korsakoff syndrome. *Neurobiology of Aging*. **22**, 569-574.

Mattevi, A., A. De Kok and R. N. Perham (1992a) The pyruvate dehydrogenase multienzyme complex. *Current Opinion in Structural Biology*. **2**, 877-887.

Mattevi, A., G. Obmolova, K. H. Kalk, W. J. H. van Berkel and W. G. J. Hol (1993) Three-dimensional Structure of Lipoamide Dehydrogenase from *Pseudomonas fluorescens* at 2Â·8 Ã Resolution: Analysis of Redox and Thermostability Properties. *Journal of Molecular Biology*. **230**, 1200-1215.

Mattevi, A., G. Obmolova, E. Schulze, K. Kalk, A. Westphal, A. de Kok and W. Hol (1992c) Atomic structure of the cubic core of the pyruvate dehydrogenase multienzyme complex. *Science*. **255**, 1544-1550.

Mattevi, A., G. Obmolova, J. R. Sokatch, C. Betzel and W. G. Hol (1992b) The refined crystal structure of *Pseudomonas putida* lipoamide dehydrogenase complexed with $NAD^+$ at 2.45 A resolution. *Proteins*. **13**, 336-51.

Mattevi, A., A. J. Schierbeek and W. G. J. Hol (1991) Refined crystal structure of lipoamide dehydrogenase from *Azotobacter vinelandii* at 2.2 Ã resolution: A comparison with the structure of glutathione reductase. *Journal of Molecular Biology*. **220**, 975-994.

Matuda, S., K. Nakano, S. Ohta, T. Saheki, Y. Kawanishi and T. Miyata (1991) The alpha-ketoacid dehydrogenase complexes. Sequence similarity of rat pyruvate dehydrogenase with *Escherichia coli* and *Azotobacter vinelandii* alpha-ketoglutarate dehydrogenase. *Biochimica et biophysica acta*. **1089**, 1-7.

Matuda, S., K. Nakano, S. Ohta, M. Shimura, T. Yamanaka, S. Nakagawa, K. Titani and T. Miyata (1992) Molecular cloning of dihydrolipoamide acetyltransferase of the rat pyruvate dehydrogenase complex: sequence comparison and evolutionary relationship to other dihydrolipoamide acyltransferases. *Biochimica et Biophysica Acta (BBA) - Gene Structure and Expression*. **1131**, 114-118.

Mayers, R. M., R. J. Butlin, E. Kilgour, B. Leighton, D. Martin, J. Myatt, J. P. Orme and B. R. Holloway (2003) AZD7545, a novel inhibitor of pyruvate dehydrogenase kinase 2 (PDHK2), activates pyruvate dehydrogenase *in vivo* and improves blood glucose control in obese (fa/fa) Zucker rats. *Biochem Soc Trans*. **31**, 1165-7.

McCartney, R. G., J. E. Rice, S. J. Sanderson, V. Bunik, H. Lindsay and J. G. Lindsay (1998) Subunit interactions in the mammalian alpha-ketoglutarate dehydrogenase complex. Evidence for direct association of the alpha-ketoglutarate dehydrogenase and dihydrolipoamide dehydrogenase components. *J Biol Chem*. **273**, 24158-64.

McCartney, R. G., S. J. Sanderson and J. G. Lindsay (1997) Refolding and Reconstitution Studies on the Transacetylase Protein X (E2/X) Subcomplex of the Mammalian Pyruvate Dehydrogenase Complex: Evidence for Specific Binding of the Dihydrolipoamide Dehydrogenase Component to Sites on Reassembled E2 *Biochemistry*. **36**, 6819-6826.

Meixner-Monori, B., C. P. Kubicek, A. Habison, E. M. Kubicek-Pranz and M. Rhr (1985) Presence and regulation of the alpha-ketoglutarate dehydrogenase multienzyme complex in the filamentous fungus Aspergillus niger. *Journal of Bacteriology*. **161**, 265-271.

Millar, A. H., S. A. Hill and C. J. Leaver (1999) Plant mitochondrial 2-oxoglutarate dehydrogenase complex: purification and characterization in potato. *Biochem J*. **343**, 327-34.

Milne, J. L., D. Shi, P. B. Rosenthal, J. S. Sunshine, G. J. Domingo, X. Wu, B. R. Brooks, R. N. Perham, R. Henderson and S. Subramaniam (2002) Molecular architecture and mechanism of an icosahedral pyruvate dehydrogenase complex: a multifunctional catalytic machine. *EMBO J*. **21**, 5587-98.

Milne, J. L. S., X. Wu, M. J. Borgnia, J. S. Lengyel, B. R. Brooks, D. Shi, R. N. Perham and S. Subramaniam (2006) Molecular Structure of a 9-MDa Icosahedral Pyruvate Dehydrogenase Subcomplex Containing the E2 and E3 Enzymes Using Cryoelectron Microscopy. *Journal of Biological Chemistry*. **281**, 4364-4370.

Morris, T. W., K. E. Reed and J. E. Cronan (1994) Identification of the gene encoding lipoate-protein ligase A of *Escherichia coli*. Molecular cloning and characterization of the lplA gene and gene product. *Journal of Biological Chemistry*. **269**, 16091-100.

Moteki, S., P. S. Leung, E. R. Dickson, D. H. Van Thiel, C. Galperin, T. Buch, D. Alarcon-Segovia, D. Kershenobich, K. Kawano, R. L. Coppel and et al. (1996) Epitope mapping and reactivity of autoantibodies to the E2 component of 2-oxoglutarate dehydrogenase complex in primary biliary cirrhosis using recombinant 2-oxoglutarate dehydrogenase complex. *Hepatology*. **23**, 436-44.

Mukhopadhyay, A., C.-s. Yang, B. Wei and H. Weiner (2007) Precursor Protein Is Readily Degraded in Mitochondrial Matrix Space if the Leader Is Not Processed by Mitochondrial Processing Peptidase. *Journal of Biological Chemistry*. **282**, 37266-37275.

Murphy, G. E. and G. J. Jensen (2005) Electron Cryotomography of the *E. coli* Pyruvate and 2-Oxoglutarate Dehydrogenase Complexes. *Structure*. **13**, 1765-1773.

Nagase, T., K.-i. Ishikawa, R. Kikuno, M. Hirosawa, N. Nomura and O. Ohara (1999) Prediction of the Coding Sequences of Unidentified Human Genes.XV. The Complete Sequences of 100 New cDNA Clones from Brain Which Code for Large Proteins in vitro. *DNA Research*. **6**, 337-345.

Nagase, T., M. Nakayama, D. Nakajima, R. Kikuno and O. Ohara (2001) Prediction of the Coding Sequences of Unidentified Human Genes. XX. The Complete Sequences of 100 New cDNA Clones from Brain Which Code for Large Proteins in vitro. *DNA Research*. **8**, 85-95.

Najdi, T. S., G. W. Hatfield and E. D. Mjolsness (2010) A 'random steady-state' model for the pyruvate dehydrogenase and alpha-ketoglutarate dehydrogenase enzyme complexes. *Phys Biol*. **7**, 16016.

Nakai, T., S. Kuramitsu and N. Kamiya (2008) Structural bases for the specific interactions between the E2 and E3 components of the *Thermus thermophilus* 2-oxo acid dehydrogenase complexes. *Journal of Biochemistry*. **143**, 747-758.

Nakano, K., S. Matuda, T. Sakamoto, C. Takase, S. Nakagawa, S. Ohta, T. Ariyama, J. Inazawa, T. Abe and T. Miyata (1993) Human dihydrolipoamide succinyltransferase: cDNA cloning and localization on chromosome 14q24.2-q24.3. *Biochimica et Biophysica Acta (BBA) - Gene Structure and Expression*. **1216**, 360-368.

Nakano, K., S. Matuda, T. Yamanaka, H. Tsubouchi, S. Nakagawa, K. Titani, S. Ohta and T. Miyata (1991) Purification and molecular cloning of succinyltransferase of the rat alpha-ketoglutarate dehydrogenase complex. Absence of a sequence motif of the putative E3 and/or E1 binding site. *J Biol Chem*. **266**, 19013-7.

Nakano, K., S. Ohta, K. Nishimaki, T. Miki and S. Matuda (1997) Alzheimer's disease and DLST genotype. *The Lancet*. **350**, 1367-1368.

Nakano, K., C. Takase, T. Sakamoto, S. Nakagawa, J. Inazawa, S. Ohta and S. Matuda (1994) Isolation, Characterization and Structural Organization of the Gene and Pseudogene for the Dihydrolipoamide Succinyltransferase Component of the Human 2-Oxoglutarate Dehydrogenase Complex. *European Journal of Biochemistry*. **224**, 179-189.

Nath, K. A., V. E. Andreucci and L. G. Fine (1991) Reactive Oxygen Species and Renal Injury. *International Yearbook of Nephrology* pp 47-69, Springer US

Neagle, J. C. and J. G. Lindsay (1991) Selective proteolysis of the protein X subunit of the bovine heart pyruvate dehydrogenase complex. Effects on dihydrolipoamide dehydrogenase (E3) affinity and enzymic properties of the complex. *Biochem J.* **278** 423-7.

Neuburger, M., A. M. Polidori, E. Piètre, M. Faure, A. Jourdain, J. Bourguignon, B. Pucci and R. Douce (2000) Interaction between the lipoamide-containing H-protein and the lipoamide dehydrogenase (L-protein) of the glycine decarboxylase multienzyme system. *European Journal of Biochemistry*. **267**, 2882-2889.

Neupert, W. (1997) Protein import into mitochondria. *Annual Review of Biochemistry*. **66**, 863-917.

Nishio, A., E. B. Keeffe and M. E. Gershwin (2001) Primary biliary cirrhosis: lessons learned from an organ-specific disease. *Clinical and experimental medicine*. **1**, 165-178.

Oliver, D. J., M. Neuburger, J. Bourguignon and R. Douce (1990) Interaction between the Component Enzymes of the Glycine Decarboxylase Multienzyme Complex. *Plant Physiol*. **94**, 833-9.

Oliver, R. M. and L. J. Reed (1982) Multienzyme complexes. *Electron Microscopy of Proteins. J.R. Harris*. **2** 1-48.

Omura, T. (1998) Mitochondria-Targeting Sequence, a Multi-Role Sorting Sequence Recognized at All Steps of Protein Import into Mitochondria. *Journal of Biochemistry*. **123**, 1010-1016.

Packman, L. C. and R. N. Perham (1986) Chain folding in the dihydrolipoyl acyltransferase components of the 2-oxo-acid dehydrogenase complexes from *Escherichia coli*. Identification of a segment involved in binding the E3 subunit. *FEBS Lett*. **206**, 193-8.

Packman, L. C. and R. N. Perham (1987) Limited proteolysis and sequence analysis of the 2-oxo acid dehydrogenase complexes from *Escherichia coli*. Cleavage sites and domains in the dihydrolipoamide acyltransferase components. *Biochem J*. **242**, 531-8.

Palmer, J. M., D. E. Jones, J. Quinn, A. McHugh and S. J. Yeaman (1999) Characterization of the autoantibody responses to recombinant E3 binding protein (protein X) of pyruvate dehydrogenase in primary biliary cirrhosis. *Hepatology*. **30**, 21-6.

Palmer, J. M., O. F. J. M.F. Bassendine and a. S. J. Yeaman. (1993) Human pyruvate dehydrogenase complex as an autoantigen in primary biliary cirrhosis. *Clin Sci (Lond).* **85**, 289-93.

Panov, A. and A. Scarpa (1996) Independent modulation of the activity of alpha-ketoglutarate dehydrogenase complex by $Ca^{2+}$ and $Mg^{2+}$. *Biochemistry*. **35**, 427-32.

Park, S. J., G. Chao and R. P. Gunsalus (1997) Aerobic regulation of the sucABCD genes of *Escherichia coli*, which encode alpha-ketoglutarate dehydrogenase and succinyl coenzyme A synthetase: roles of ArcA, Fnr, and the upstream sdhCDAB promoter. *Journal of Bacteriology*. **179**, 4138-42.

Patel, K. P., T. W. O'Brien, S. H. Subramony, J. Shuster and P. W. Stacpoole (2011) The spectrum of pyruvate dehydrogenase complex deficiency: Clinical, biochemical and genetic features in 371 patients. *Molecular Genetics and Metabolism*. **105**, 34-43.

Patel, M. S. and R. A. Harris (1995) Mammalian alpha-keto acid dehydrogenase complexes: gene regulation and genetic defects. *FASEB J*. **9**, 1164-72.

Patel, M. S. and L. G. Korotchkina (2001) Regulation of mammalian pyruvate dehydrogenase complex by phosphorylation: complexity of multiple phosphorylation sites and kinases. *Exp Mol Med*. **33**, 191-7.

Patel, M. S. and T. E. Roche (1990) Molecular biology and biochemistry of pyruvate dehydrogenase complexes. *FASEB J*. **4**, 3224-33.

Perham, R. N. (1991) Domains, motifs, and linkers in 2-oxo acid dehydrogenase multienzyme complexes: a paradigm in the design of a multifunctional protein. *Biochemistry*. **30**, 8501-12.

Perham, R. N. (2000) Swinging arms and swinging domains in multifunctional enzymes: catalytic machines for multistep reactions. *Annu Rev Biochem*. **69**, 961-1004.

Perham, R. N., D. D. Jones, H. J. Chauhan and M. J. Howard (2002) Substrate channelling in 2-oxo acid dehydrogenase multienzyme complexes. *Biochem Soc Trans*. **30**, 47-51.

Pettit, F. H., L. Hamilton, P. Munk, G. Namihira, M. H. Eley, C. R. Willms and L. J. Reed (1973) Alpha-keto acid dehydrogenase complexes. Subunit structure of the *Escherichia coli* alpha-ketoglutarate dehydrogenase complex. *J Biol Chem*. **248**, 5282-90.

Pfanner, N. and K. N. Truscott (2002a) Powering mitochondrial protein import. *Nat Struct Biol*. **9**, 234-6.

Pfanner, N. and N. Wiedemann (2002b) Mitochondrial protein import: two membranes, three translocases. *Curr Opin Cell Biol*. **14**, 400-11.

Popov, K. M. (1997) Regulation of mammalian pyruvate dehydrogenase kinase. *FEBS Lett*. **419**, 197-200.

Poulsen, L. L. and R. T. Wedding (1970) Purification and properties of the alpha-ketoglutarate dehydrogenase complex of cauliflower mitochondria. *J Biol Chem*. **245**, 5709-17.

Poupon, R. (2010) Primary biliary cirrhosis: a 2010 update. *J Hepatol*. **52**, 745-58.

Prince, J. A., L. Feuk, S. L. Sawyer, J. Gottfries, A. Ricksten, K. Nagga, N. Bogdanovic, K. Blennow and A. J. Brookes (2001) Lack of replication of association findings in complex disease: an analysis of 15 polymorphisms in prior candidate genes for sporadic Alzheimer's disease. *Eur J Hum Genet*. **9**, 437-44.

Qi, F., R. K. Pradhan, R. K. Dash and D. A. Beard (2011) Detailed kinetics and regulation of mammalian 2-oxoglutarate dehydrogenase. *BMC biochemistry*. **12**, 53.

Quinn, J., A. G. Diamond, A. K. Masters, D. E. Brookfield, N. G. Wallis and S. J. Yeaman (1993) Expression and lipoylation in *Escherichia coli* of the inner lipoyl domain of the E2 component of the human pyruvate dehydrogenase complex. *Biochem J*. **289** 81-5.

Radford, S. E., E. D. Laue, R. N. Perham, S. R. Martin and E. Appella (1989) Conformational flexibility and folding of synthetic peptides representing an interdomain segment of polypeptide chain in the pyruvate dehydrogenase multienzyme complex of *Escherichia coli*. *Journal of Biological Chemistry*. **264**, 767-775.

Radford, S. E., E. D. Laue, R. N. Perham, J. S. Miles and J. R. Guest (1987) Segmental structure and protein domains in the pyruvate dehydrogenase multienzyme complex of *Escherichia coli*. Genetic reconstruction in vitro and 1H-n.m.r. spectroscopy. *Biochem J*. **247**, 641-9.

Rahmatullah, M., S. Gopalakrishnan, P. C. Andrews, C. L. Chang, G. A. Radke and T. E. Roche (1989) Subunit associations in the mammalian pyruvate dehydrogenase complex. Structure and role of protein X and the pyruvate dehydrogenase component binding domain of the dihydrolipoyl transacetylase component. *J Biol Chem*. **264**, 2221-7.

Randle, P. J. (1983) Mitochondrial 2-oxoacid dehydrogenase complexes of animal tissues. *Philos Trans R Soc Lond B Biol Sci*. **302**, 47-57.

Rashed, H. M., F. M. Waller and T. B. Patel (1988) Hormonal regulation of the alpha-ketoglutarate dehydrogenase complex in the isolated perfused rat liver. *J Biol Chem*. **263**, 5700-6.

Reed, L. and M. Hackert (1990) Structure-function relationships in dihydrolipoamide acyltransferases. *J. Biol. Chem.* **265**, 8971-8974.

Reed, L. J. (1974) Multienzyme complexses. *Acc. Chem. Res.* **7**, 40-56.

Reed, L. J. (2001) A trail of research from lipoic acid to alpha-keto acid dehydrogenase complexes. *J Biol Chem*. **276**, 38329-36.

Reed, L. J. and R. M. Oliver (1968) The multienzyme alpha-keto acid dehydrogenase complexes. *Brookhaven Symp Biol*. **21**, 397-412.

Reed, L. J., F. H. Pettit, M. H. Eley, L. Hamilton, J. H. Collins and R. M. Oliver (1975) Reconstitution of the *Escherichia coli* pyruvate dehydrogenase complex. *Proceedings of the National Academy of Sciences*. **72**, 3068-3072.

Repetto, B. and A. Tzagoloff (1989) Structure and regulation of KGD1, the structural gene for yeast alpha-ketoglutarate dehydrogenase. *Molecular and Cellular Biology*. **9**, 2695-2705.

Repetto, B. and A. Tzagoloff (1991) In vivo assembly of yeast mitochondrial alpha-ketoglutarate dehydrogenase complex. *Molecular and Cellular Biology*. **11**, 3931-3939.

Ricaud, P. M., M. J. Howard, E. L. Roberts, R. W. Broadhurst and R. N. Perham (1996) Three-dimensional Structure of the Lipoyl Domain from the Dihydrolipoyl Succinyltransferase Component of the 2-Oxoglutarate Dehydrogenase Multienzyme Complex of *Escherichia coli*. *Journal of Molecular Biology*. **264**, 179-190.

Rice, J. E., B. Dunbar and J. G. Lindsay (1992) Sequences directing dihydrolipoamide dehydrogenase (E3) binding are located on the 2-oxoglutarate dehydrogenase (E1) component of the mammalian 2-oxoglutarate dehydrogenase multienzyme complex. *The EMBO journal*. **11**, 3229-35.

Rice, J. E. and J. G. Lindsay (1991) Evidence for a protein X-like domain at the N-terminus of the E1 component of the mammalian 2-oxoglutarate dehydrogenase complex. *Biochem Soc Trans*. **19**, 403S.

Rigden, D. J. and M. Y. Galperin (2004) The DxDxDG Motif for Calcium Binding: Multiple Structural Contexts and Implications for Evolution. *Journal of Molecular Biology*. **343**, 971-984.

Robien, M. A., G. M. Clore, J. G. Omichinski, R. N. Perham, E. Appella, K. Sakaguchi and A. M. Gronenborn (1992) Three-dimensional solution structure of the E3-binding domain of the dihydrolipoamide succinyltransferase core from the 2-oxoglutarate dehydrogenase multienzyme complex of *Escherichia coli*. *Biochemistry*. **31**, 3463-71.

Roche, T. E. and R. L. Cate (1976) Evidence for lipoic acid mediated NADH and acetyl-CoA stimulation of liver and kidney pyruvate dehydrogenase kinase. *Biochem Biophys Res Commun*. **72**, 1375-83.

Roche, T. E. and R. L. Cate (1977) Purification of porcine liver pyruvate dehydrogenase complex and characterization of its catalytic and regulatory properties. *Arch Biochem Biophys*. **183**, 664-77.

Roche, T. E., Y. Hiromasa, A. Turkan, X. Gong, T. Peng, X. Yan, S. A. Kasten, H. Bao and J. Dong (2003) Essential roles of lipoyl domains in the activated function and control of pyruvate dehydrogenase kinases and phosphatase isoform 1. *Eur J Biochem*. **270**, 1050-6.

Roche, T. E. and V. B. Lawlis (1982) Structure and regulation of α-ketoglutarate dehydrogenase of bovine kidney. *Annals of the New York Academy of Sciences*. **378**, 236-249.

Roise, D. and G. Schatz (1988) Mitochondrial presequences. *Journal of Biological Chemistry*. **263**, 4509-4511.

Russell, G. C. and J. R. Guest (1991) Sequence similarities within the family of dihydrolipoamide acyltransferases and discovery of a previously unidentified fungal enzyme. *Biochimica et Biophysica Acta (BBA) - Protein Structure and Molecular Enzymology*. **1076**, 225-232.

Rutter, G. A. and R. M. Denton (1989) The binding of $Ca^{2+}$ ions to pig heart $NAD^{+}$-isocitrate dehydrogenase and the 2-oxoglutarate dehydrogenase complex. *Biochem J*. **263**, 453-62.

Sale, G. J. and P. J. Randle (1981) Analysis of Site Occupancies in [32P] Phosphorylated Pyruvate Dehydrogenase Complexes by Aspartyl-Prolyl Cleavage of Tryptic Phosphopeptides. *European Journal of Biochemistry*. **120**, 535-540.

Sambrook, J. and D. Russell (2001) Molecular cloning. a laboratory manual. 3ed. edition. *Cold Spring Harbour Laboratory Press*. **New York**.

Sanderson, S. J., S. S. Khan, R. G. McCartney, C. Miller and J. G. Lindsay (1996a) Reconstitution of mammalian pyruvate dehydrogenase and 2-oxoglutarate dehydrogenase complexes: analysis of protein X involvement and interaction of homologous and heterologous dihydrolipoamide dehydrogenases. *Biochem J*. **319** 109-16.

Sanderson, S. J., C. Miller and J. G. Lindsay (1996b) Stoichiometry, organisation and catalytic function of protein X of the pyruvate dehydrogenase complex from bovine heart. *Eur J Biochem*. **236**, 68-77.

Scaduto, R. C. (1994) Calcium and 2-oxoglutarate-mediated control of aspartate formation by rat heart mitochondria. *European Journal of Biochemistry*. **223**, 751-758.

Schellenberg, G., T. Bird, E. Wijsman, H. Orr, L. Anderson, E. Nemens, J. White, L. Bonnycastle, J. Weber, M. Alonso and a. et (1992) Genetic linkage evidence for a familial Alzheimer's disease locus on chromosome 14. *Science*. **258**, 668-671.

Schierbeek, A. J., M. B. Swarte, B. W. Dijkstra, G. Vriend, R. J. Read, W. G. Hol, J. Drenth and C. Betzel (1989) X-ray structure of lipoamide dehydrogenase from *Azotobacter vinelandii* determined by a combination of molecular and isomorphous replacement techniques. *J Mol Biol*. **206**, 365-79.

Schleyer, M., B. Schmidt and W. Neupert (1982) Requirement of a Membrane Potential for the Post-translational Transfer of Proteins into Mitochondsria. *European Journal of Biochemistry*. **125**, 109-116.

Schwartz, E. R. and L. J. Reed (1970) Regulation of the activity of the pyruvate dehydrogenase complex of *Escherichia coli*. . *Biochemistry*. **9**, 1434-9.

Schwede, T., J. r. Kopp, N. Guex and M. C. Peitsch (2003) SWISS-MODEL: an automated protein homology-modeling server. *Nucleic acids research*. **31**, 3381-3385.

Seyda, A., G. McEachern, R. Haas and B. H. Robinson (2000) Sequential deletion of C-terminal amino acids of the E1p component of the pyruvate dehydrogenase (PDH) complex leads to reduced steady-state levels of functional E1 $\alpha_2$ $\beta_2$ tetramers: implications for patients with PDH deficiency. *Human Molecular Genetics*. **9**, 1041-1048.

Sheu, K.-F. and J. P. Blass (1999a) The α-Ketoglutarate Dehydrogenase Complex. *Annals of the New York Academy of Sciences*. **893**, 61-78.

Sheu, K.-F. R., A. M. Brown, B. S. Kristal, R. N. Kalaria, L. Lilius, L. Lannfelt and J. P. Blass (1999b) A DLST genotype associated with reduced risk for Alzheimer's disease. *Neurology*. **52**, 1505.

Sheu, K. F., A. J. Cooper, K. Koike, M. Koike, J. G. Lindsay and J. P. Blass (1994) Abnormality of the alpha-ketoglutarate dehydrogenase complex in fibroblasts from familial Alzheimer's disease. *Ann Neurol*. **35**, 312-8.

Shi, Q., H.-L. Chen, H. Xu and G. E. Gibson (2005) Reduction in the E2k Subunit of the alpha-Ketoglutarate Dehydrogenase Complex Has Effects Independent of Complex Activity. *Journal of Biological Chemistry*. **280**, 10888-10896.

Shi, Q., H. Xu, H. Yu, N. Zhang, Y. Ye, A. G. Estevez, H. Deng and G. E. Gibson (2011) Inactivation and reactivation of the mitochondrial alpha-ketoglutarate dehydrogenase complex. *J Biol Chem*. **286**, 17640-8.

Shim, D. J., N. S. Nemeria, A. Balakrishnan, H. Patel, J. Song, J. Wang, F. Jordan and E. T. Farinas (2011) Assignment of Function to Histidines 260 and 298 by Engineering the E1 Component of the *Escherichia coli* 2-Oxoglutarate Dehydrogenase Complex; Substitutions That Lead to Acceptance of Substrates Lacking the 5-Carboxyl Group. *Biochemistry*. **50**, 7705-7709.

Shoffner, J. M. (1997) Oxidative phosphorylation defects and Alzheimer's disease. *Neurogenetics*. **1**, 13-9.

Siesjo, B. K., Q. Zhao, K. Pahlmark, P. Siesj, K.-i. Katsura and J. Folbergrov (1995) Glutamate, calcium, and free radicals as mediators of ischemic brain damage. *The Annals of Thoracic Surgery*. **59**, 1316-1320.

Sims, N. R., M. F. Anderson, L. M. Hobbs, J. Y. Kong, S. Phillips, J. A. Powell and E. Zaidan (2000) Impairment of brain mitochondrial function by hydrogen peroxide. *Molecular Brain Research*. **77**, 176-184.

Singh, G. (2008) Analysis of genetic mutations using a recombinant model of the mammalian pyruvate dehydrogenase complex, University of Glasgow, PhD thesis.

Smith, M. W. and F. C. Neidhardt (1983) 2-Oxoacid dehydrogenase complexes of *Escherichia coli*: cellular amounts and patterns of synthesis. *J Bacteriol*. **156**, 81-8.

Smolle, M., A. E. Prior, A. E. Brown, A. Cooper, O. Byron and J. G. Lindsay (2006) A New Level of Architectural Complexity in the Human Pyruvate Dehydrogenase Complex. *Journal of Biological Chemistry*. **281**, 19772-19780.

Spector, S., B. Kuhlman, R. Fairman, E. Wong, J. A. Boice and D. P. Raleigh (1998) Cooperative folding of a protein mini domain: the peripheral subunit-binding domain of the pyruvate dehydrogenase multienzyme complex. *J Mol Biol*. **276**, 479-89.

Spencer, M. E., M. G. Darlison, P. E. Stephens, I. K. Duckenfield and J. R. Guest (1984) Nucleotide sequence of the sucB gene encoding the dihydrolipoamide succinyltransferase of Escherichia coli K12 and homology with the corresponding acetyltransferase. *European Journal of Biochemistry*. **141**, 361-374.

Stanley, C. J. and R. N. Perham (1980) Purification of 2-oxo acid dehydrogenase multienzyme complexes from ox heart by a new method. *Biochem J*. **191**, 147-54.

Starkov, A. A., G. Fiskum, C. Chinopoulos, B. J. Lorenzo, S. E. Browne, M. S. Patel and M. F. Beal (2004) Mitochondrial alpha-ketoglutarate dehydrogenase complex generates reactive oxygen species. *J Neurosci*. **24**, 7779-88.

Stephens, P. E., M. G. Darlison, H. M. Lewis and J. R. Guest (1983) The Pyruvate Dehydrogenase Complex of *Escherichia coli* K12. *European Journal of Biochemistry*. **133**, 155-162.

Stoops, J. K., T. S. Baker, J. P. Schroeter, S. J. Kolodziej, X. D. Niu and L. J. Reed (1992) Three-dimensional structure of the truncated core of the *Saccharomyces cerevisiae* pyruvate dehydrogenase complex determined from negative stain and cryoelectron microscopy images. *Journal of Biological Chemistry*. **267**, 24769-24775.

Stoops, J. K., R. H. Cheng, M. A. Yazdi, C.-Y. Maeng, J. P. Schroeter, U. Klueppelberg, S. J. Kolodziej, T. S. Baker and L. J. Reed (1997) On the Unique Structural Organization of the *Saccharomyces cerevisiae* Pyruvate Dehydrogenase Complex. *Journal of Biological Chemistry*. **272**, 5757-5764.

Strumito, S., M. Czygier, J. Kondracikowska, P. Dobrzyn and J. Czerniecki (2002) Kinetic and spectral investigation of allosteric interaction of co-enzymes with 2-oxo acid dehydrogenase complexes. *Journal of Molecular Structure*. **614**, 221-226.

Sugden, M. C. and M. J. Holness (2003) Recent advances in mechanisms regulating glucose oxidation at the level of the pyruvate dehydrogenase complex by PDKs. *American Journal of Physiology - Endocrinology And Metabolism*. **284**, E855-E862.

Surh, C. D., T. E. Roche, D. J. Danner, A. Ansari, R. L. Coppel, T. Prindiville, E. R. Dickson and M. E. Gershwin (1989) Antimitochondrial autoantibodies in primary biliary cirrhosis recognize cross-reactive epitope(s) on protein X and dihydrolipoamide acetyltransferase of pyruvate dehydrogenase complex. *Hepatology (Baltimore, Md.)*. **10**, 127-133.

Suzuki, K., W. Adachi, N. Yamada, M. Tsunoda, K. Koike, M. Koike, T. Sekiguchi and A. Takenaka (2002) Crystallization and preliminary X-ray analysis of the full-size cubic core of pig 2-oxoglutarate dehydrogenase complex. *Acta Crystallogr D Biol Crystallogr*. **58**, 833-5.

Sweetlove, L. J., J. L. Heazlewood, V. Herald, R. Holtzapffel, D. A. Day, C. J. Leaver and A. H. Millar (2002) The impact of oxidative stress on *Arabidopsis* mitochondria. *Plant J.* **32**, 891-904.

Szabo, P., X. Cai, G. Ali and J. P. Blass (1994) Localization of the Gene (OGDH) Coding for the E1k Component of the alpha-Ketoglutarate Dehydrogenase Complex to Chromosome 7p13-p11.2. *Genomics*. **20**, 324-326.

Szutowicz, A., H. Bielarczyk, S. Gul, A. Ronowska, T. Pawełczyk and A. Jankowska-Kulawy (2006) Phenotype-dependent susceptibility of cholinergic neuroblastoma cells to neurotoxic inputs. *Metabolic Brain Disease*. **21**, 143-155.

Takenaka, A., K. Kizawa, T. Hata, S. Sato, E.-i. Misaka, C. Tamura and Y. Sasada (1988) X-Ray Study of Baker's Yeast Lipoamide Dehydrogenase at 4.5 Ã Resolution by Molecular Replacement Method. *Journal of Biochemistry*. **103**, 463-469.

Tamarit, J., E. Cabiscol and J. Ros (1998) Identification of the Major Oxidatively Damaged Proteins in *Escherichia coli* Cells Exposed to Oxidative Stress. *Journal of Biological Chemistry*. **273**, 3027-3032.

Tanaka, N., K. Koike, M. Hamada, K. I. Otsuka, T. Suematsu and M. Koike (1972) Mammalian -keto acid dehydrogenase complexes. VII. Resolution and reconstitution of the pig heart 2-oxoglutarate dehydrogenase complex. *J Biol Chem*. **247**, 4043-9.

Tanaka, N., K. Koike, K. I. Otsuka, M. Hamada, K. Ogasahara and M. Koike (1974) Mammalian alpha-Keto Acid Dehydrogenase Complexes. *Journal of Biological Chemistry*. **249**, 191-198.

Team, M. G. C. P. (2002) Generation and initial analysis of more than 15,000 full-length human and mouse cDNA sequences. *Proceedings of the National Academy of Sciences*. **99**, 16899-16903.

Thekkumkara, T. J., L. Ho, I. D. Wexler, G. Pons, L. Te-Chung and M. S. Patel (1988) Nucleotide sequence of a cDNA for the dihydrolipoamide acetyltransferase component of human pyruvate dehydrogenase complex. *FEBS Letters*. **240**, 45-48.

Toyoda, T., R. Kobayashi, T. Sekiguchi, K. Koike, M. Koike and A. Takenaka (1998) Crystallization and preliminary X-ray analysis of pig E3, lipoamide dehydrogenase. *Acta Crystallogr D Biol Crystallogr*. **54**, 982-5.

Tretter, L. and V. Adam-Vizi (2000) Inhibition of Krebs cycle enzymes by hydrogen peroxide: A key role of alpha-ketoglutarate dehydrogenase in limiting NADH production under oxidative stress. *J Neurosci*. **20**, 8972-9.

Tretter, L. and V. Adam-Vizi (2005) Alpha-ketoglutarate dehydrogenase: a target and generator of oxidative stress. *Philos Trans R Soc Lond B Biol Sci*. **360**, 2335-45.

Turrens, J. F. (1997) Superoxide production by the mitochondrial respiratory chain. *Biosci Rep*. **17**, 3-8.

Valko, M., H. Morris and M. T. Cronin (2005) Metals, toxicity and oxidative stress. *Curr Med Chem*. **12**, 1161-208.

Vijayakrishnan, S., S. M. Kelly, R. J. C. Gilbert, P. Callow, D. Bhella, T. Forsyth, J. G. Lindsay and O. Byron (2010) Solution Structure and Characterisation of the Human Pyruvate Dehydrogenase Complex Core Assembly. *Journal of Molecular Biology*. **399**, 71-93.

Voos, W. and K. Rottgers (2002) Molecular chaperones as essential mediators of mitochondrial biogenesis. *Biochimica et Biophysica Acta (BBA) - Molecular Cell Research*. **1592**, 51-62.

Wagenknecht, T., R. Grassucci and D. Schaak (1990) Cryoelectron microscopy of frozen-hydrated alpha-ketoacid dehydrogenase complexes from *Escherichia coli*. *J Biol Chem*. **265**, 22402-8.

Wagner, T., M. Bellinzoni, A. Wehenkel, HelenÂ M. O'Hare and PedroÂ M. Alzari (2011) Functional Plasticity and Allosteric Regulation of alpha-Ketoglutarate Decarboxylase in Central Mycobacterial Metabolism. *Chemistry & Biology*. **18**, 1011-1020.

Waldemar, G., B. Dubois, M. Emre, J. Georges, I. G. McKeith, M. Rossor, P. Scheltens, P. Tariska and B. Winblad (2007) Recommendations for the diagnosis and management of Alzheimer's disease and other disorders associated with dementia: EFNS guideline. *European Journal of Neurology*. **14**, e1-e26.

Walker, J. and D. Oliver (1986) Glycine decarboxylase multienzyme complex. Purification and partial characterization from pea leaf mitochondria. *J. Biol. Chem.* **261**, 2214-2221.

Wallis, N. G., M. D. Allen, R. W. Broadhurst, I. A. Lessard and R. N. Perham (1996) Recognition of a surface loop of the lipoyl domain underlies substrate channelling in the pyruvate dehydrogenase multienzyme complex. *J Mol Biol*. **263**, 463-74.

Wallis, N. G. and R. N. Perham (1994) Structural Dependence of Post-translational Modification and Reductive Acetylation of the Lipoyl Domain of the Pyruvate Dehydrogenase Multienzyme Complex. *Journal of Molecular Biology*. **236**, 209-216.

Wang, L., S. Kaneko, M. Kagaya, H. Ohno, M. Honda and K. Kobayashi (2002) Molecular cloning, characterization and expression of dihydrolipoamide acetyltransferase component of murine pyruvate dehydrogenase complex in bile duct cancer cells. *Journal of Gastroenterology*. **37**, 449-454.

Westphal, A. H. and A. de Kok (1990) The 2-oxoglutarate dehydrogenase complex from *Azotobacter vinelandii. European Journal of Biochemistry*. **187**, 235-239.

Wieland, O. H. (1983) The mammalian pyruvate dehydrogenase complex: structure and regulation. *Rev Physiol Biochem Pharmacol*. **96**, 123-70.

Yang, H. C., J. F. Hainfeld, J. S. Wall and P. A. Frey (1985) Quaternary structure of pyruvate dehydrogenase complex from *Escherichia coli. J Biol Chem*. **260**, 16049-51.

Yeaman, S. J. (1986) The mammalian 2-oxoacid dehydrogenases: a complex family. *Trends in Biochemical Sciences*. **11**, 293-296.

Yeaman, S. J. (1989) The 2-oxo acid dehydrogenase complexes: recent advances. *Biochem J*. **257**, 625-32.

Yeaman, S. J., D. J. Danner, D. J. Mutimer, S. P. M. Fussey, O. F. W. James and M. F. Bassendine (1988) Primary bilIary cirrhosis: identIfication of two major M2 mitochondrial autoantigens. *The Lancet*. **331**, 1067-1070.

Yeaman, S. J., E. T. Hutcheson, T. E. Roche, F. H. Pettit, J. R. Brown, L. J. Reed, D. C. Watson and G. H. Dixon (1978) Sites of phosphorylation on pyruvate dehydrogenase from bovine kidney and heart. *Biochemistry*. **17**, 2364-70.

Yeaman, S. J., J. A. Kirby and D. E. J. Jones (2000) Autoreactive responses to pyruvate dehydrogenase complex in the pathogenesis of primary biliary cirrhosis. *Immunological Reviews*. **174**, 238-249.

Zavala, g., J. P. Pardo and R. Moreno-SÃ¡nchez (2000) Modulation of 2-Oxoglutarate Dehydrogenase Complex by Inorganic Phosphate, $Mg^{2+}$, and Other Effectors. *Archives of Biochemistry and Biophysics*. **379**, 78-84.

Zeilstra-Ryalls, J., O. Fayet and C. Georgopoulos (1991) The universally conserved GroE (Hsp60) chaperonins. *Annu Rev Microbiol*. **45**, 301-25.

Zhang, Y. (2008) I-TASSER server for protein 3D structure prediction. *BMC Bioinformatics*. **9**, 40.

Zhang, Y. and J. Skolnick (2005) TM-align: a protein structure alignment algorithm based on the TM-score. *Nucleic Acids Res*. **33**, 2302-9.

Zhang, Y., L. Taiming and J. Liu (2003) Low temperature and glucose enhanced T7 RNA polymerase-based plasmid stability for increasing expression of glucagon-like peptide-2 in *Escherichia coli*. *Protein Expression and Purification*. **29**, 132-139.

Zhao, X., J. R. Miller, Y. Jiang, M. A. Marletta and J. E. Cronan (2003) Assembly of the Covalent Linkage between Lipoic Acid and Its Cognate Enzymes. *Chemistry & Biology*. **10**, 1293-1302.

Zhou, Y., W. Yang, M. Kirberger, H.-W. Lee, G. Ayalasomayajula and J. J. Yang (2006) Prediction of EF-hand calcium-binding proteins and analysis of bacterial EF-hand proteins. *Proteins: Structure, Function, and Bioinformatics*. **65**, 643-655.

Zhou, Z. H., D. B. McCarthy, C. M. O'Connor, L. J. Reed and J. K. Stoops (2001) The remarkable structural and functional organization of the eukaryotic pyruvate dehydrogenase complexes. *Proceedings of the National Academy of Sciences*. **98**, 14802-14807.

Zinn, A. R. (2001) The X chromosome and the ovary. *J Soc Gynecol Investig*. **8**, S34-6.